University of Stavanger

Faculty of Science and Technology

MASTER'S THESIS

Study program/ Specialization: Petroleum Geosciences Engineering	Spring semester, 2017 Open access
Writer: Sigrid Øxnevad	………………………………………… (Writer's signature)
Faculty supervisor: Udo Zimmermann	
Thesis title: High-resolution heavy mineral studies on "black sands" from the Nama Group (Fish River Subgroup) in Namibia – Part I	
Credits (ECTS): 30	
Key words: Nama Group (Fish River Subgroup) Heavy minerals Placer deposits/black sands Provenance Scanning Electron Microscope (SEM) X-Ray Diffractometer (XRD) Mineral Liberation Analyser (MLA) Electron Microprobe Analyser (EMPA)	Pages: 97 + enclosure: 103 Stavanger, 11.07.17

High-resolution heavy mineral studies on ”black sands” from the Nama Group (Fish River Subgroup) in Namibia – Part I

by

Sigrid Øxnevad

MSc Thesis
Petroleum Geosciences Engineering
Presented to the Faculty of Science and Technology
University of Stavanger
Norway

University of Stavanger
July 2017

Acknowledgements

Firstly, I would like to express my sincerest gratitude to my supervisor, Dr. Udo Zimmermann, for the opportunity to conduct and complete this thesis. Your continuous guidance, engagement and encouragement have been very much appreciated. Your dedication to geology has deeply inspired me. Thank you for sharing your knowledge!

I want to express my appreciation to PhD candidate Mona Wetrhus Minde for assistance with the FE-SEM. Thank you for sharing your enthusiasm of working in the laboratory and for providing good guidance and support. I would like to thank Mari Kristjansdottir for help with CL-images of detrital zircons, and Caroline Ruud for assistance and guidance with mounting and other sample preparations. I would also like to thank PhD candidate Emanuela Iedidia Kallesten for insights in the XRD process and for completion of the XRD analyses.

I would like to thank the staff at the laboratory at TU Bergakademie Freiberg for all their support and guidance, and for giving me the opportunity to use their MLA and EMPA. I would like to express my gratitude to Sabine Haser for assistance with the MLA and for helping me with the analyses. I would also like to thank Professor Dr. Bernhard Schulz for completing the analyses with EMPA when time was to short for me to finish.

I want to express my gratitude to the Norwegian Oil Fund for funding the traveling costs in this study.

Thanks to my fellow students for all your support and for all the fun times we have had the last five years. A special thanks to Alexandra Elisabeth Myhre and André Solvang for shearing your knowledge and motivation. Thank you for the long hours in the lab, the breaks, and the laughs.

Finally, I want to thank my family and friends for the support and encouragement throughout the completion of my Master´s Degree in Petroleum Geosciences Engineering at the University of Stavanger.

Abstract

A detailed high-resolution study is applied on selected samples to decipher the provenance for these deposits. The samples analysed in the project are placer deposits ("black sands") from the Nama Group (Fish River Subgroup) in Namibia. The samples come from heavy mineral layers in red sandstones from the Rosenhof Mb (Gross Aub Fm) and the Haribes Mb (Nababis Fm). Heavy minerals in the samples are identified and quantified based on results from several analytical methods: Field Emission Scanning Electron Microscopy (FE-SEM) with Energy Dispersive Spectroscopy (EDS) detector, X-Ray Diffractometer (XRD), Mineral Liberation Analyser (MLA), and Electron Microprobe Analyser (EMPA). All samples contain chamosite, amphibole, tourmaline, garnet (almandine and grossular), magnetite, ilmenite, rutile, titanite, zircon and apatite. Grain shape, sorting and particle size distributions indicate that the sediments were accumulated in a river, and the energy of the water flow caused a selective settling of the heavy minerals based on grain size and grain density. The main differences between the samples is that the one from the Haribes Mb contains larger amounts of grossular and tourmaline, and less amounts of almandine, compared to the ones from the Rosenhof Mb. Also the grains in the samples from the Haribes Mb have a smaller grain size than the samples from the Rosenhof Mb, which means that they have lower grain settling velocities. The chemical composition of the heavy minerals indicates that the sediments derived from several provenances. Most almandines are interpreted to derive from metasediments (including amphibolite facies), from high-grade metamorphic rocks or acidic to intermediate gneisses and granites. Some of the almandines probably derived from high-grade mafic and ultramafic gneisses, and the grossular grains from contact or thermally metamorphosed calcareous sediments or associated metasomatic skarns. Titanites are interpreted to derive from mafic igneous source rocks, and tourmalines from Li-poor granitoid, pegmatite or aplite, and aluminous, Ca-poor metapelite or metapsammite. The detrital heavy mineral records of the deposits of the Fish River Subgroup indicate a complex source region composed of high-grade metamorphic, felsic and mafic rocks. The heavy mineral grains are generally not well rounded, they are probably river deposits, and therefore they are not likely to have been transported hundreds of kilometers. The source rocks appears to be close. The Namaqua Belt is located next to and south of the sampling area and consists of mafic and felsic rocks metamorphosed to greenschist or amphibolite facies. The Namaqua Belt is interpreted to be the main source area for the heavy minerals in the samples.

TABLE OF CONTENTS

List of tables and figures

List of commonly used abbreviations

10×eV	10×Electron-volts (=keV)
Af	Apatite fraction
at%	Atomic percent
BSE	Back-Scattered Electron
CL	Cathodoluminescence
EDS	Energy Dispersive Spectroscopy
EMPA	Electron Microprobe Analyser
FE	Field Emission
Fm	Formation
HM	Heavy minerals
ICP	Inductively Coupled Plasma
kcps	Kilo counts per second
keV	Kilo electron-volts
LA	Laser Ablation
Ma	Million years ago
mA	Milliampere
Mb	Member
MC	Multi-Collector
Mf	Magnetic fraction
MLA	Mineral Liberation Analyser
MS	Mass Spectrometry
ms	Millisecond
NNMP	Namaqua-Natal Metamorphic Province
SE	Secondary Electron
SEM	Scanning Electron Microscope
sp.	Species
TU Bergakademie Freiberg	Technische Universität Bergakademie Freiberg
UiS	University of Stavanger
µm	Micrometer
WD	Working distance
WDS	Wavelength Dispersive Spectrometer
wt%	Weight percent
XRD	X-Ray Diffractometer
Z	Atomic number
Zf	Zircon fraction
Zc	Zircon concentrate

1 INTRODUCTION

A detailed high-resolution study is applied on selected samples to decipher the major source areas for these deposits. The thesis describes a strategy for discrimination and provenance evaluation of placer deposits (“black sands”). It is an integrated study of heavy mineral analysis, mineral chemistry and zircon age dating. Differences between heavy mineral populations are reinforced by single-grain mineral analysis, which also provides further information about the nature of the source terrains. The value of this integrated approach is illustrated in this thesis by a case study of sandstones (placer deposits) from the Nama Group (Fish River Subgroup) in Namibia.

1.1 Objectives of the study

The main objective of the thesis is to interpret and get a better understanding of the provenance of placer deposits of the Nama Group (Fish River Subgroup). The major goal is identification and quantification of the different provenance components found in the sampled rocks. The samples will be studied using different analytical methods: Field emission Scanning Electron Microscopy (FE-SEM) with Back-Scattered Electron (BSE) detector, Cathodoluminescence (CL) detector and Energy Dispersive Spectroscopy (EDS) detector, X-Ray Diffractometer (XRD), Mineral Liberation Analyser (MLA), Electron Microprobe Analyser (EMPA), and Inductively Coupled Plasma Mass Spectrometry with Laser Ablation and Multi-Collector (ICP-MS-LA-MC).

The results will be interpreted and combined in order to understand the provenance of the minerals for further interpretation of the rocks in terms of their depositional environment and tectonic setting, and identify the regional and paleotectonic constraints on provenance. The sorting and particle size distribution as an effect of transport and flow velocity will be evaluated. The settling velocity for the grains will be estimated based on size and density of the grains. Further, the effect of the heavy mineral placer formation for provenance will be studied and compared with data from the literature of samples of the same succession, which are not placers. Finally, the application and attractiveness of this methodological approach for the hydrocarbon industry will be evaluated.

1.2 Provenance studies

The chemical composition of the provenance is the major control on chemistry of sedimentary rocks, although subsequent processes can alter the rock. The main processes that control the chemical composition of sedimentary rocks are the tectonic setting, weathering, transport, deposition and diagenesis (*Figure 1.1*). The composition of the provenance is related to the tectonic setting. Weathering may alter the sedimentary rock and leave a signature in the resultant sediment. Major element studies may provide information about the former weathering conditions from the chemistry of the sediments (Rollinson, 1993). Transport and abrasion can impact the chemical composition (Morton et al., 2005). For example trace elements can become more concentrated in the clay components or in the heavy mineral fraction, while others are diluted in the quartz fraction. During deposition the chemical changes depend on the deposition environment and the subsidence rate. Diagenetic processes, diagenetic fluids, temperature, geothermal gradient and burial history are also important factors that can effect the chemical composition of the rock (Rollinson, 1993).

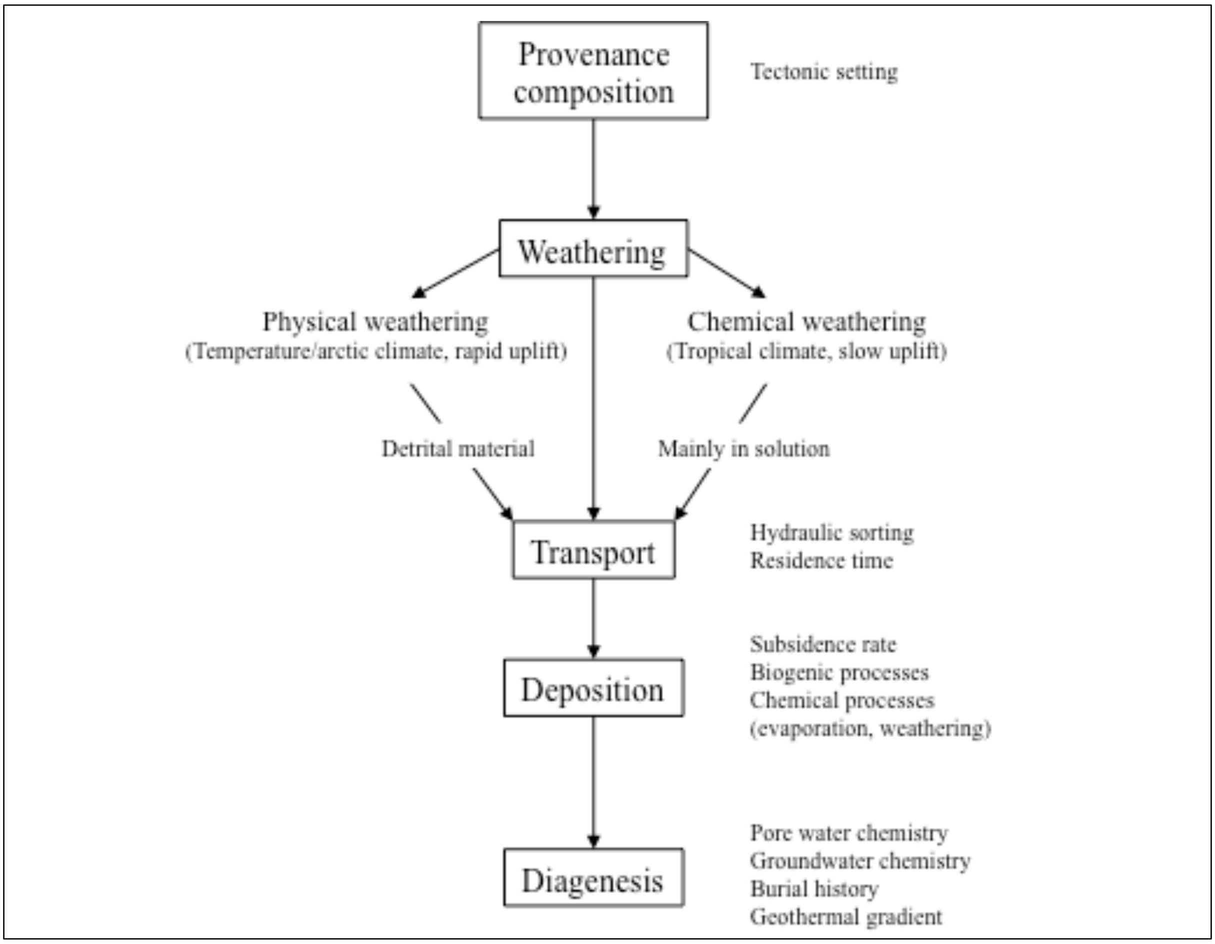

Figure 1.1: The main processes that control the chemical composition of sedimentary rocks are tectonic setting, weathering, transport, deposition and diagenesis (modified after Rollinson (1993)).

1.3 Placer deposits ("black sands")

A heavy mineral placer is a sedimentary deposit. It is a natural concentration of heavy minerals and it is formed by mechanical concentration of minerals as an effect of gravity (Leeder, 2011). Heavy mineral placer deposits in sandstones are often referred to as "black sands". Grains of heavy minerals in sediments have different hydrodynamic properties compared to light minerals (e.g. quartz and feldspar). The heavy minerals have a higher density, and the grain size and shape may also be different. Generally the heavy minerals are more difficult to transport by flowing water compared to the lighter minerals. The higher density of the heavy minerals lead to a higher settling velocity, compared to the lighter minerals, and the transport will take place closer to the bottom where the velocity of the current are lower. When the light minerals are selectively transported away it can lead to the formation of a lag deposit of concentrated heavy minerals (*Figure 1.2 and 1.3*) (Komar, 2007).

Heavy mineral placers are mechanically concentrated by fluvial or shallow marine processes. They occur in coastal areas where the heavy minerals derive from local bedrocks or from rocks of inland drainage basins that supply the coastal zone. Heavy minerals are transported from a rock source to a fluvial or coastal environment where they may be concentrated by tides, waves or other nearshore currents. Fluvial placers have been transported by high energy stream flows and deposited among alluvial deposits or river channel deposits (Osterkamp and Morton, 2005). Heavy mineral placers have been discovered in alluvial, marine, lacustrine and aeolian deposits (Komar, 2007).

Placer deposits are sensitive indicators of sediment provenance. Processes that operate during the sedimentary cycle (weathering, transport, deposition and diagenesis) may affect the original provenance signal of the heavy minerals. The two processes with most effect on heavy mineral assemblages are hydrodynamic fractionation and burial diagenesis. Hydrodynamic processes occur during transport and deposition. It can affect the relative abundances of minerals with different hydraulic behavior and it is controlled by grain size, density and shape of the mineral grains. Burial diagenesis selectively removes the unstable minerals and this is done by circulation of pore waters with elevated temperate (Morton et al., 2005). Some minerals are more resistant than others (e.g. zircon) and these grains can retain their size and shape inherited from the primary rock source (Komar, 2007). Grain abrasion and rounding of grains are greater on beaches than in rivers (Clemens and Komar, 1988).

Figure 1.2: Placer deposits ("black sands") from an outcrop in Namibia, close to the sampling area (photo by Udo Zimmermann).

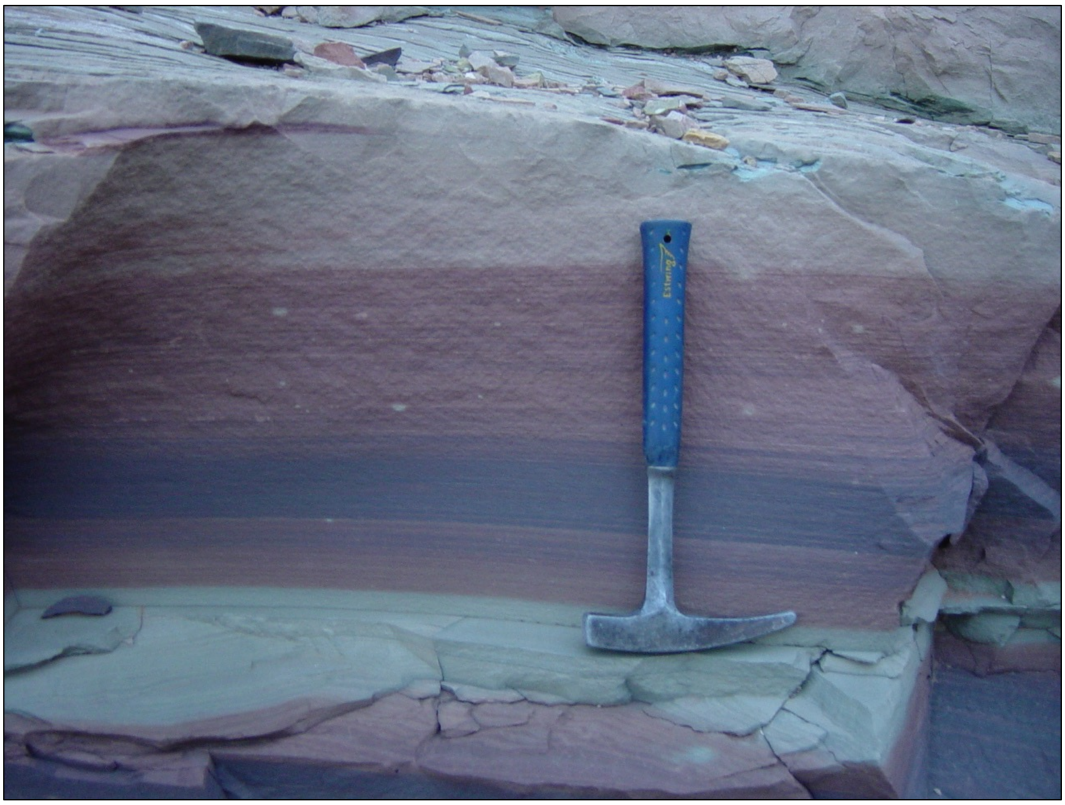

Figure 1.3: "Black sand" layers of placer deposits in between red sandstone layers (photo by Udo Zimmermann).

1.4 Sampling area

The sampling area is located in the southern part of Namibia. Samples have been collected from two outcrops. The first outcrop has GPS locality 26°36'29.30"S 19°13'56.40"E (marked with green triangle on *Figure 1.4*) and the second outcrop has GPS locality 26°55'04.20"S 18°36'15.90"E (marked with green circle on *Figure 1.4*). Both outcrops were visited by Dr. Udo Zimmermann (supervisor for the thesis project). Photos from the first outcrop can be seen in *Figure 1.5* and *1.6*, and photos from the second outcrop can be seen in *Figure 1.7* and *1.8*.

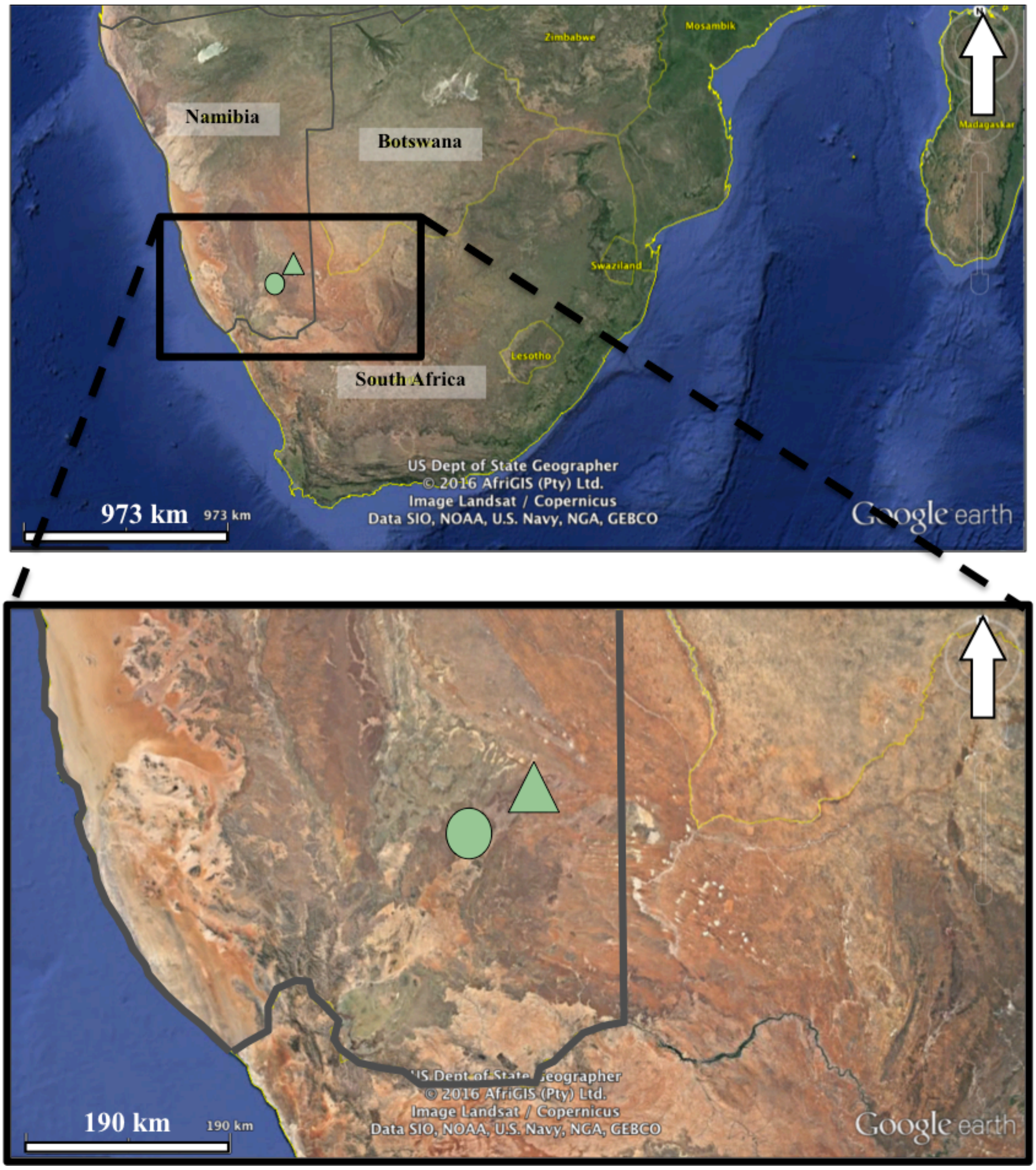

Figure 1.4: Location of the sampling areas in the southern part of Namibia. The green triangle and circle mark the two sampling areas (modified after Google earth (May 15, 2017)).

Figure 1.5: The first outcrop with GPS locality 26°36'29.30"S 19°13'56.40"E (photo by Udo Zimmermann).

Figure 1.6: The first outcrop with red sandstones from the Rosenhof Member (photo by Udo Zimmermann).

Figure 1.7: The second outcrop with GPS locality 26°55'04.20"S 18°36'15.90"E (photo by Udo Zimmermann).

Figure 1.8: The second outcrop with layers of placer deposits ("black sands") in sandstones from the Haribes Member (photo by Udo Zimmermann).

1.5 Geological setting

Namibia today consists of parts of the Kalahari Craton and the Congo Craton (*Figure 1.9*). The Kalahari Carton is surrounded by several Neoproterozoic to Early Paleozoic orogenic belts. The Namaqua Belt/Namaqua-Natal Metamorphic Province is located along the southern margin of the Kalahari Craton, and the Damara Belt is located to the north of the Kalahari Craton (Hofmann et al., 2013). These belts have been formed through different phases of continental rifting and spreading, then reversed plate motion, and further subduction and continental collision (Frimmel et al., 2011; Jacobs et al., 2008). The Kalahari Craton was affected by at least two supercontinental cycles forming the two supercontinents Rodinia and Gondwana (Hofmann et al., 2013).

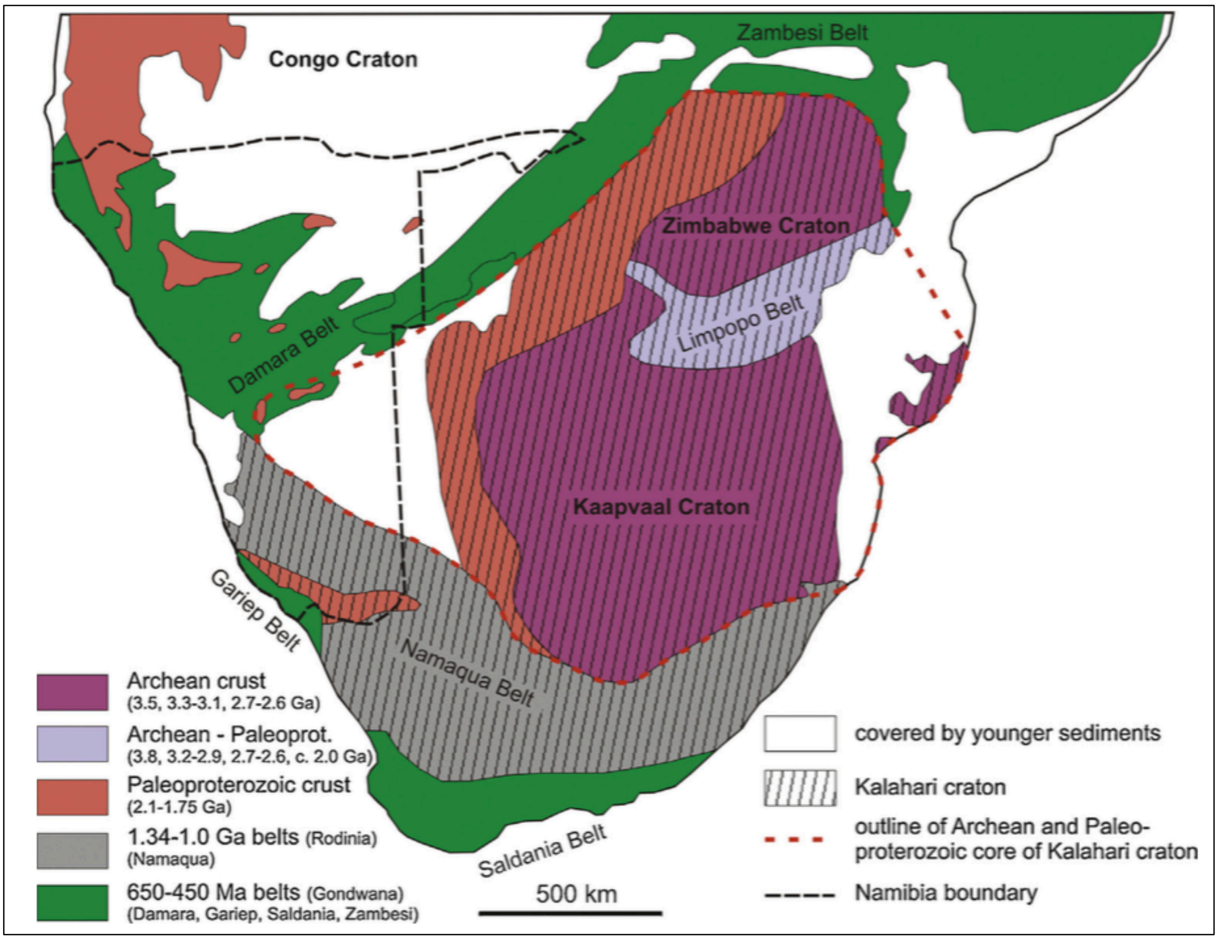

Figure 1.9: Map of the Kalahari craton in southern Africa (Hofmann et al. (2013) modified after Jacobs et al. (2008)). The Archean to Paleoproterozoic core of the Kalahari craton is surrounded by upper Neoproterozoic to lower Paleoproterozoic mobile belts (Damara, Gariep and Saldania Belt). The Namaqua Belt is a result of the formation of Rodinia supercontinent, and the younger belts are related to the formation of Gondwana. Ages for each belt are based on data from Jacobs et al. (2008) and Trompette (1994).

1.5.1 Supercontinents: Rodinia and Gondwana

At around 1.2-1.0 Ga there was a continent-continent collision forming the supercontinent Rodinia (Gaucher et al., 2010). The composition of the cratons and terranes within Rodinia is still under discussion and the result is different reconstructions of the continents and their locations (e.g. Evans (2009); Li et al. (2008); Pisarevsky et al. (2003); Frimmel et al. (2011)). Several reconstructions of Rodinia exist, with different positions for the Kalahari Craton in the Mesoproterozoic and Neoproterozoic times. Two of these positions are more reasonable stated by several scientists. According to Evans (2009) and Pisarevsky et al. (2003) there was a collision of Mawsonland (attached to Australia) and the Kalahari Craton at ~1.2-1.0 Ma. According to Li et al. (2008) the Kalahari Craton was located next to the Congo-Sao Francisco and the Rio the la Plata Cratons. This reconstruction is also preferred by Frimmel et al. (2011) and Gaucher et al. (2010). During the accretion and collisions of the supercontinent Rodinia the Namaqua Belt/Namaqua-Natal Metamorphic Province was formed (Evans et al., 2007).

The supercontinent Rodinia was not a stable construct, and rifting started around ~850 Ma (Early Cryogenian) in the western Kalahari Craton (*Figure 1.10*). The break-up of Rodinia was result of Early Cryogenian rifting, followed by a second event of rifting at around 630-600 Ma (Early Ediacaran) (Gaucher et al., 2010). The second rifting reflects the movement of the Kalahari Craton away from Australia/Mawsonland (according to Evans (2009) and Pisarevsky et al. (2003)) or the movement of the Rio de la Plata Craton away from the Kalahari Craton (according to Li et al. (2008), Frimmel et al. (2011) and Gaucher et al. (2010)). An ocean, the Adamastor Ocean, was formed along the western side of the Kalahari Craton as a result of the two events of rifting (Hofmann et al., 2013). Magmatism related to the rifting started ~830 Ma and lasted until ~740 Ma according to Gaucher et al. (2010). There are several theories for where the Kalahari Craton drifted when Rodinia broke apart, but scientists agree on the position of the Kalahari and Rio de la Plata Cratons within in supercontinent Gondwana. The Adamastor Ocean was closed when the Kalahari and Rio de la Plata Cratons drifted towards each other. They collided around 530 Ma and became part of the Gondwana configuration (Hofmann et al., 2013). During the collision forming the Gondwana supercontinent the Damara Orogenic Belt was formed (Miller, 1983).

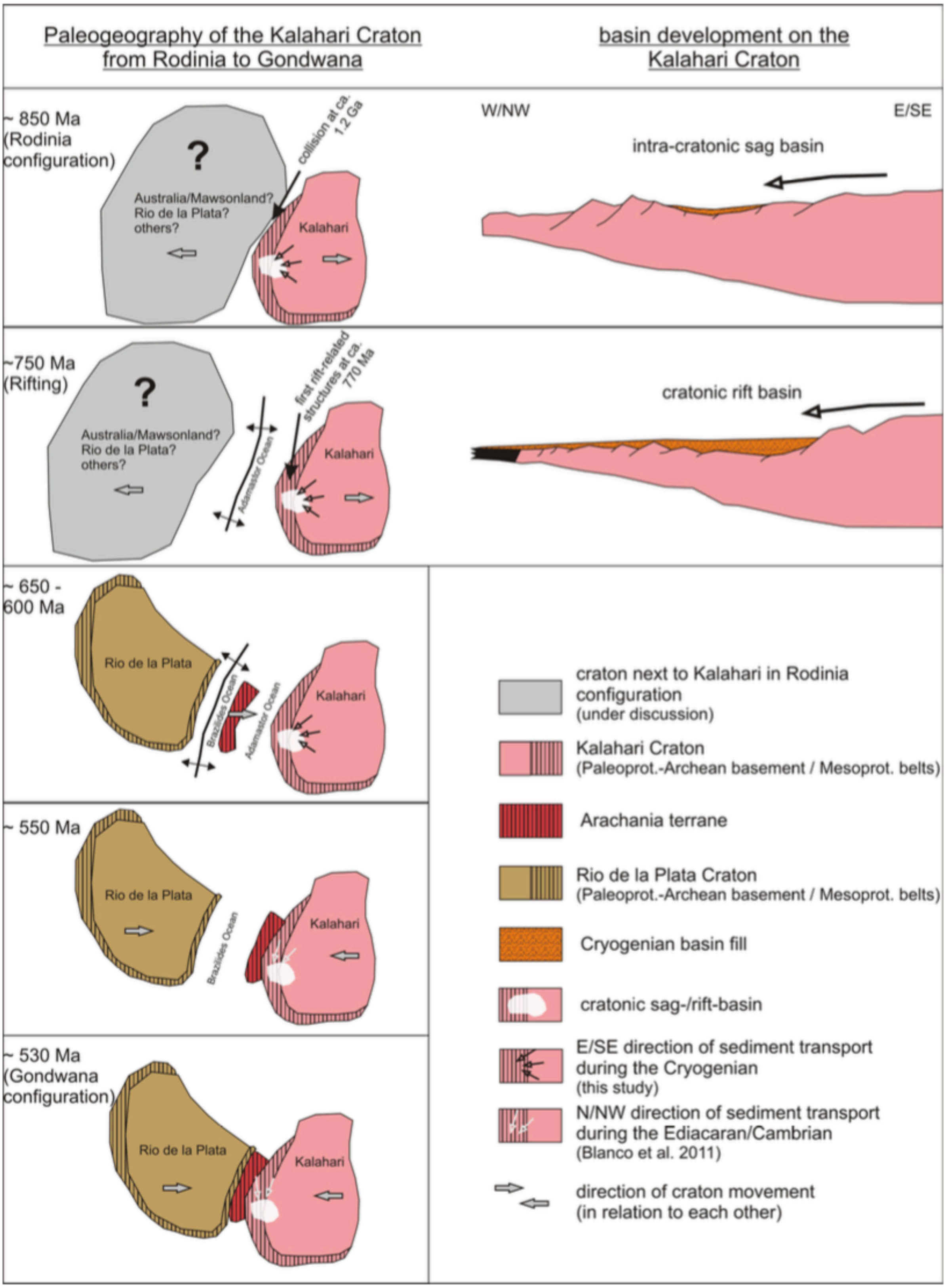

Figure 1.10: Paleogeography of the Kalahari Craton from the time of configuration of Rodinia to the configuration of supercontinent Gondwana (Hofmann et al., 2013). Sizes of cratons are not to scale.

1.5.2 The Nama Basin and the Nama Group

The Nama Basin is the foreland basin of the Damara Orogenic Belt located on the Kalahari Craton (*Figure 1.11*). The Damara Orogen consists of the Kaoko, Gariep and Damara Belts. It is a collisional triple junction of the Damara Orogen with a history of deformation and metamorphism (Miller, 1983; Germs, 1995). The Neoproterozoic to Lower Paleozoic sedimentary rocks of the Nama Basin were deposited as a result of rifting and break-up of the supercontinent Rodinia and further subduction and collision of Kalahari, Congo, Rio de la Plata and Malvinas plates (forming the supercontinent Gondwana) during the Ediacaran and Lower Cambrian (Miller, 1983; Gresse, 1986; Gray et al., 2006).

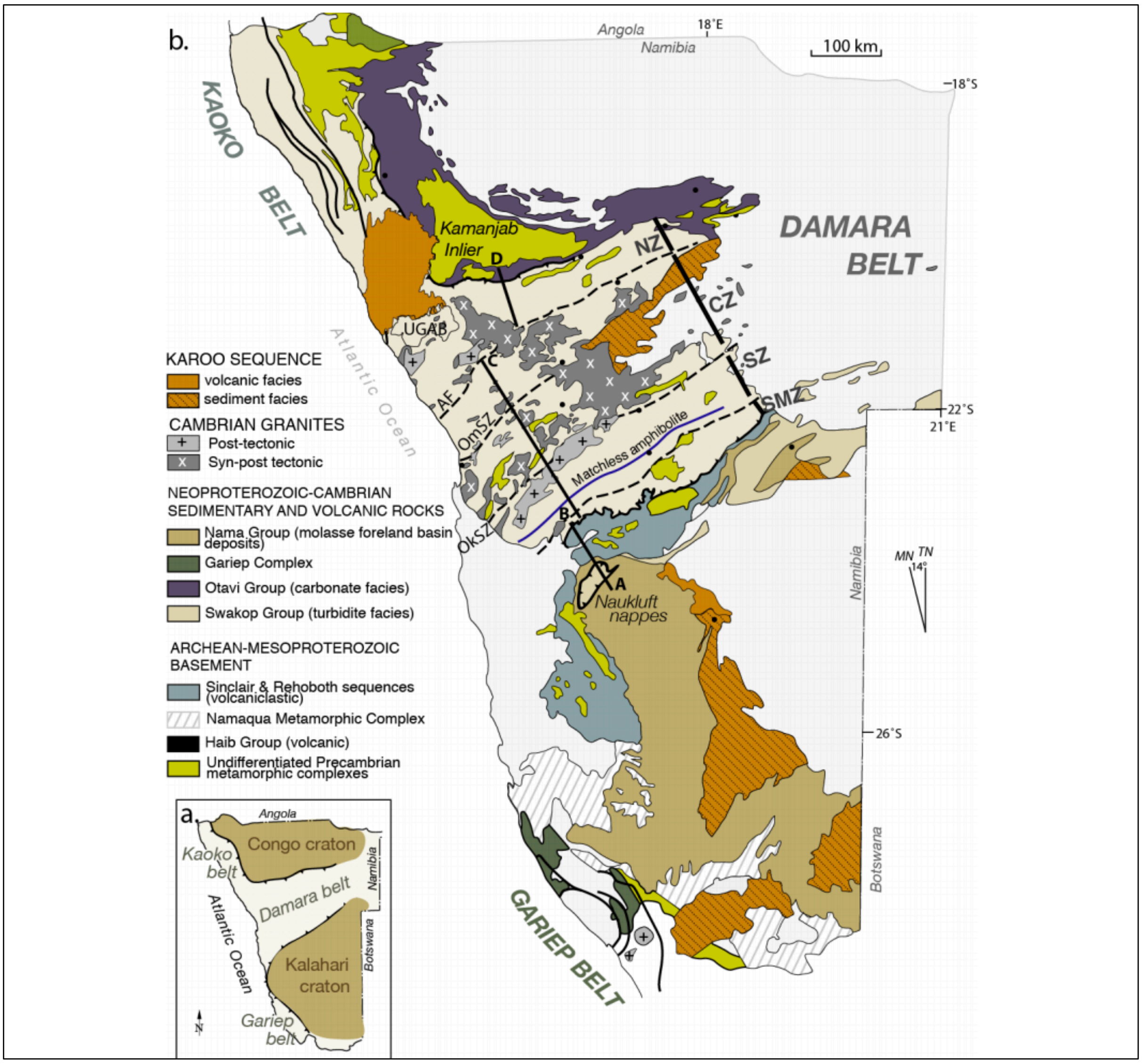

Figure 1.11: Simplified geological map of Namibia (Foster and Goscombe (2013) modified after Gray et al. (2006)). a) Arms and belts that define the collisional triple junction of the Damara Orogen. b) Geological map with the main geological units. The Nama Group is marked with light brown color and extends from the southern rim of the Damara belt (marked with SMZ) towards the Namaqua Belt (marked with stripes on white).

The Nama Group is a major lithostratigraphic unit in southeast Namibia and northwestern South Africa (*Figure 1.12*). It extends from the southern rim of the Damara Belt to the Vanrhynsdorp Basin (in South Africa), covering a distance of over 1000 km. The sediments of the Nama Group started to be deposited at ~550 Ma (Grotzinger et al., 1995) and were deposited in an area of more than 350 000 km^2 (Germs, 1983). The Nama Group consists of three lithostratigraphic units: Kuibis, Schwarzrand and Fish River Subgroups (SACS, 1980).

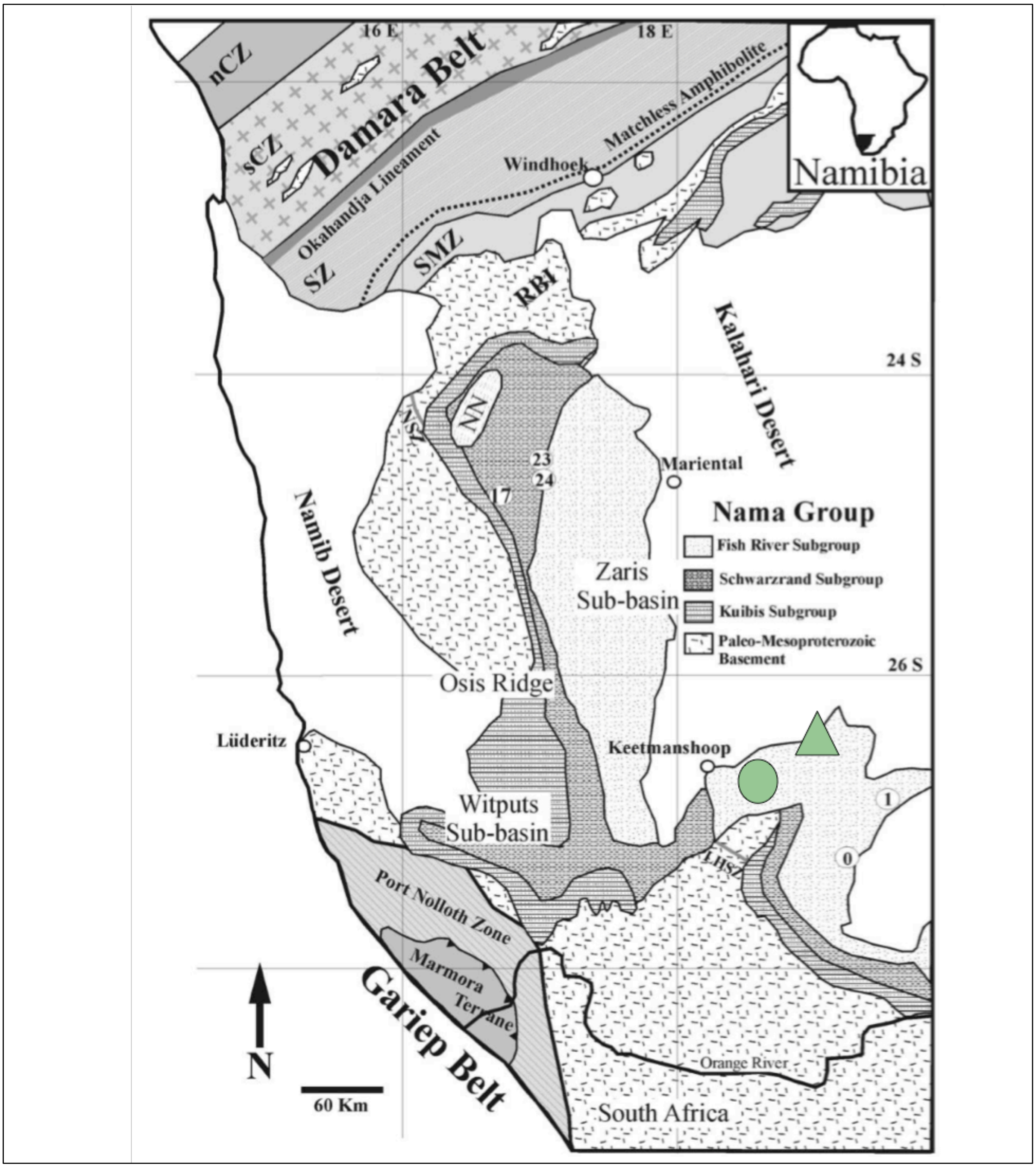

Figure 1.12: Regional map of Namibia displaying the location of the Nama Group and its subgroups Fish River, Schwarzrand and Kuibis (modified after Blanco et al. (2009) modified after Saylor et al. (1995)). The two outcrops where the samples in this project are from are marked with green triangle and circle.

Deposition of the lower Nama Group (Kuibis and lower Schwarzrand Subgroups) occurred in the foreland basin of the Damara Belt, which at the time consisted of three sub-basins (Zaris and Witputs located in Namibia, and Vanrhynsdorp located in South Africa; *Figure 1.12*) divided by two forebulges (Osis arch in the north and Kamieskroon arch in the south) (Germs, 1974, 1983). The lower part of the Nama Group received sediments mostly from the eastern Kalahari Craton (Germs, 1983). The upper part of the Nama Group (Fish River Subgroup) received sediments mostly from northern sources (*Figure 1.13 and 1.14*), and during this time the arches lost their importance and the sediments were deposited into one large foreland basin (Germs and Gresse, 1991). Paleocurrents of the Fish River Subgroup show that its detrital sediments came mostly from north-northwest to north-northeast (Blanco et al., 2011).

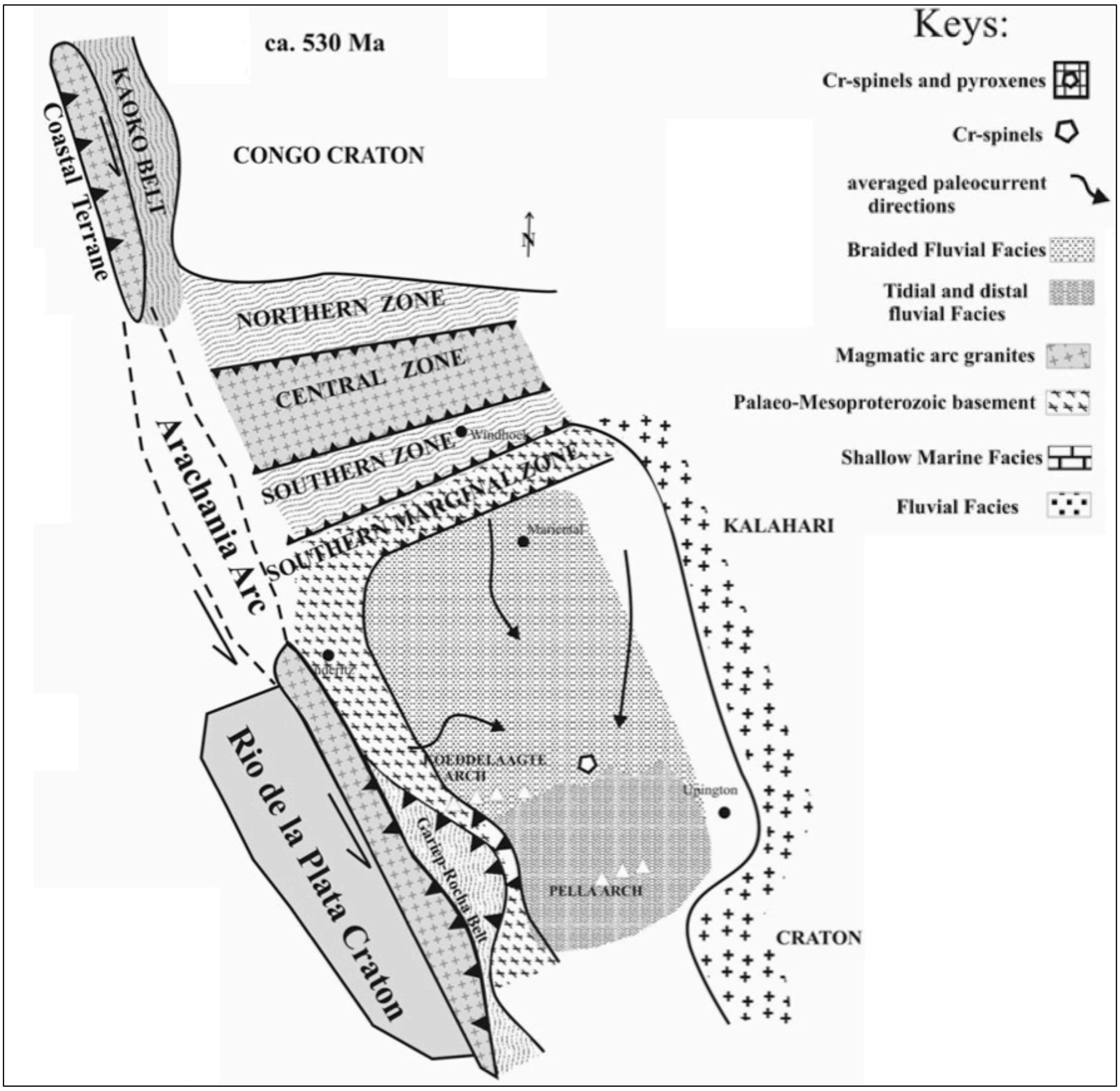

Figure 1.13: Paleogeographic reconstruction of the Nama Foreland Basin during deposition of the Fish River Subgroup (modified after Blanco et al. (2011) modified from Germs (1983) and Gresse and Germs (1993)).

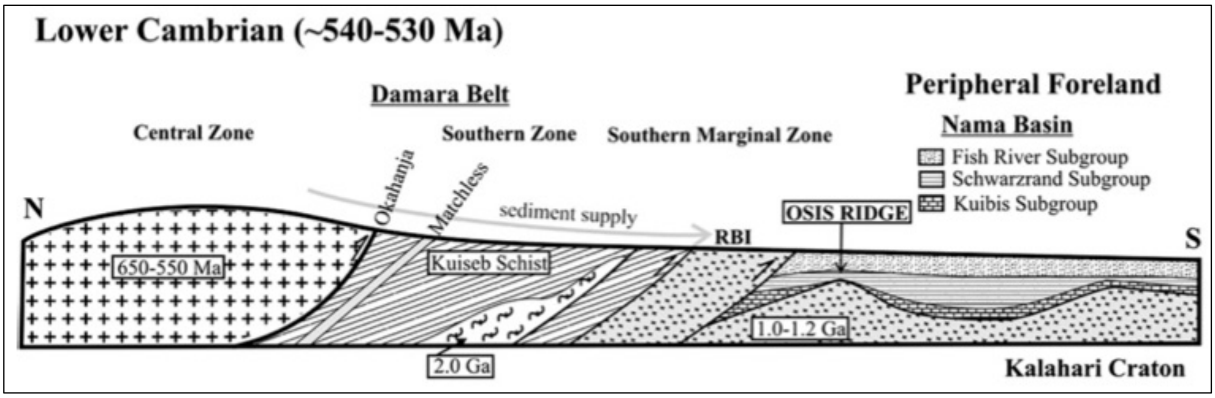

Figure 1.14: North-south cross section of the Damara Belt with the Nama Basin located in the peripheral foreland. The main sediment supply for the upper Nama Group was in the north (Blanco et al., 2009).

1.6 Stratigraphy and sedimentology

The sediments of the Nama Group was mostly accumulated in a braided fluvial to shallow marine environment (Germs, 1983; Geyer, 2005). Moving stratigraphically upward in the Nama Group, from Kuibis to Schwarzrand to Fish River Subgroups (*Figure 1.15*), the reddish sediments from the braided fluvial environment becomes more abundant and carbonates become more absent. The Haribes Member consists of red beds deposited mostly in a braided fluvial environment. The Rosenhof Member, overlying the Haribes Member, consist of mudrocks deposited in a braided fluvial to shallow marine environment (Germs, 1983).

Sandstones from both Rosenhof and Haribes members are mainly arkoses, and they are fine to medium grained and moderately well sorted (Blanco et al., 2006). Intercalated within the Haribes and Rosenhof members there are thin layers (typically 0.5-1.5 cm) of black sands, which have a large abundance of heavy minerals and are placer deposits (Blanco et al., 2006). The base of the Fish River Subgroup deposits show paleocurrent patterns derived from the west, and the top of the Fish River Subgroup show paleocurrent patterns derived from the north (*Figure 1.15*) (Germs, 1983).

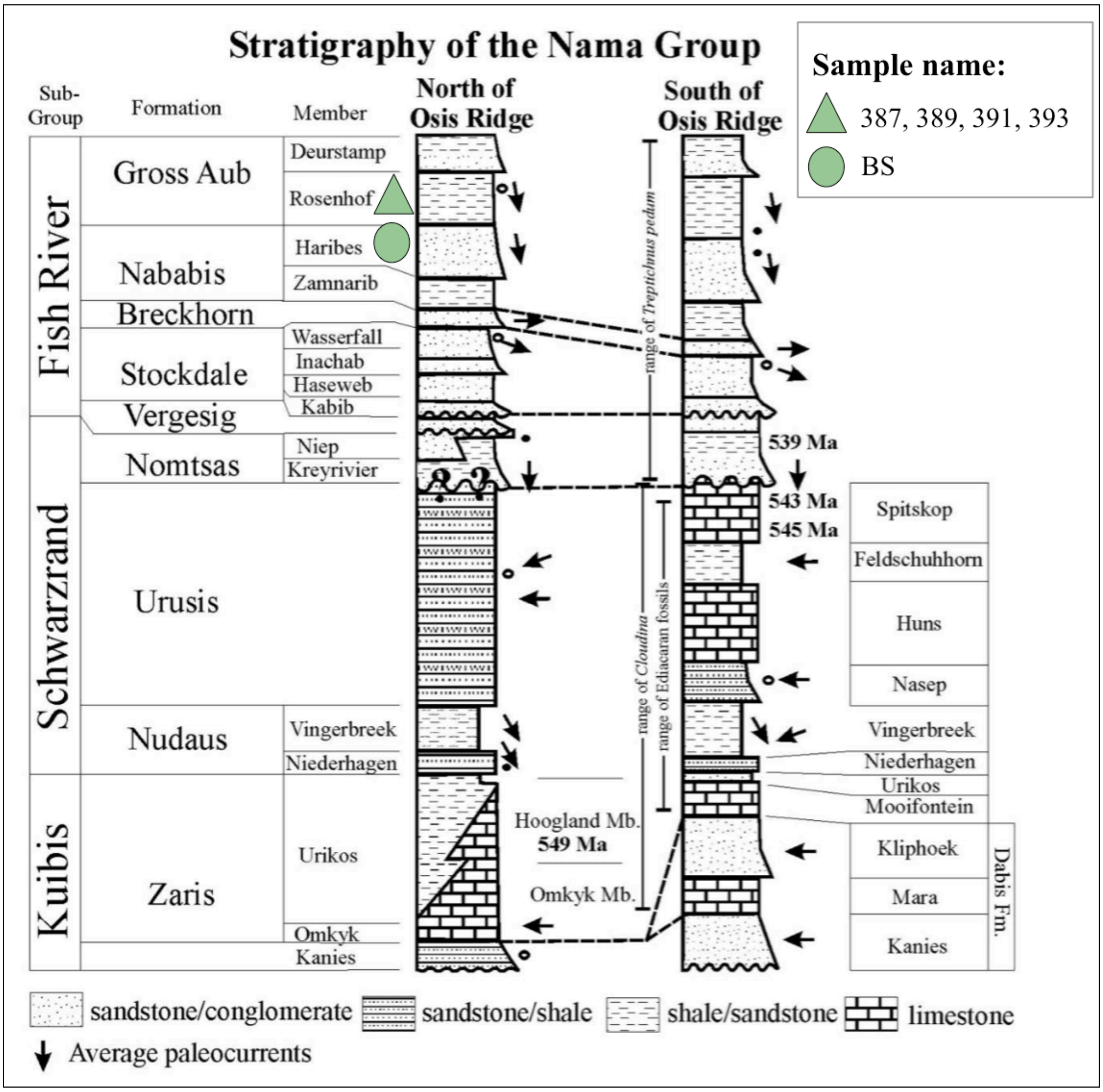

Figure 1.15: Stratigraphic column of the Nama Group (modified after Blanco et al. (2009) modified after Germs (1983)). Ages represent tuff layers after Grotzinger et al. (1995) and paleontological data is after Germs (1983, 1995). Green triangle and circle indicate where the samples in this study are from: four samples are from the Rosenhof Member (Gross Aub Formation) and one sample is from the Haribes Member (Nababis Formation).

1.7 Previous studies

The Nama Group has been analysed by several scientists (see compilation in e.g. Germs, 1995; Blanco et al., 2009). It can be divided into three subgroups, and the two lower ones have been examined the most. The upper one, the Fish River Subgroup, has received less attention in comparison. The five samples that are analysed in this project are from the Fish River Subgroup.

1.7.1 Paleontology and age

A lot of work has been completed on paleontology and fossils. Several scientists have analysed different parts of the Nama Group in different areas, and the work has been summarized by Germs (1995). The information about the fossils has helped to get a better understanding of the age when the different formations were formed. The lower Nama Group (below Nomtsas Formation) (*Figure 1.15*) contains *Cloudina* sp. and some trace fossils of Ediacaran age (Germs, 1983). These successions are estimated to have been formed ~590-540 Ma by Jenkins (1984), 590-570 Ma by Harland et al. (1990) and ~620-530 Ma by Conway Morris (1990). The upper Schwarzrand Subgroup (Nomtsas Formation) contains no Ediacaran fossils that have been possible to date, but it contains the trace fossil *Phycodes pedum* and maybe *Cloudina* sp. (Germs, 1983). The Fish River Subgroup, where the samples for this thesis project are from, consists mostly of red beds containing two types of trace fossils: *Phycodes pedum* and *Skolithos* (Germs, 1983). As a summary the boundary between Neoproterozoic and Cambrian occurs between the Nomtsas Formation and the lower Nama formations (Germs, 1995). Hence, the Fish River Subgroup can be allocated in the Lower Cambrian.

1.7.2 Zircons and age

Detrital zircons from the Nama Group and Fish River Subgroup have been dated and they display major peaks of Neoproterozoic and Mesoproterozoic age. This indicates a provenance from the Damara or Gariep Belts and their basements. Zircons from the Wasserfall Member (lower part of Fish River Subgroup) have been dated and they indicate an age of Neoproterozoic to Lower Cambrian. 76 % of the dated zircons have peaks at 637, 591 and 546 Ma, and the maximum age of sedimentation is the youngest zircon formed 531±9 Ma.

Zircons from the Haribes Member have an age distribution that is bimodal and with two main populations. The early Neoproterozoic to late Mesoproterozoic populations have peaks at 1171, 1055 and 980 Ma. The Neoproterozoic populations have a well-defined peak at 592 Ma. Zircons from the Rosenhof Member have an age distribution that is bimodal and with peaks at 626, 569 and 547 Ma (Blanco, 2008; Blanco et al., 2011).

U-Pb geochronology of ash beds have been done using separated zircons from a 1000 m section in the Nama Group. Zircons separated from four volcanic ashes (lower Hoogland Member, lower Spitskopf Member, upper Spitskopf Member and basal Nomtsas Formation) showed consistent age data results. According to the results the Precambrian/Neoproterozoic-Cambrian boundary in Namibia is younger than 543.3±1 Ma and older than 539.4±1 Ma (Grotzinger et al., 1995).

1.7.3 Lithostratigraphy

According to Geyer (2005) the only complete record of the Fish River Subgroup comes from a borehole (Tses 1-borehole). The core provides detailed information about lithostratigraphy, thickness and facies of the central part of the Nama Group, including the Fish River Subgroup. The Haribes Member (Nababis Formation) is dominated by sandstone with cross-bedding and minor shale intercalations. The unit was deposited mostly in a fluvial regime in braided river systems (Germs, 1983; Geyer, 2005). The Rosenhof Member (Gross Aub Formation) is dominated by thin layers of fine-grained sandstones and is regularly alternating with shales. Most of the unit contains rocks deposited in a shallow to shallowest marine environment, but the unit also contains asymmetric ripples and current lineation in some parts indicating deposition in a distal fluvial environment. The laminated shales in the unit have heterolithic rhythmites and were probably deposited in tidal channels (Germs, 1983; Geyer, 2005).

1.7.4 Chromian spinels

Chromian spinel is a mineral often occurring in mafic and ultramafic rocks. The chemical composition of the chromian spinel is affected by the tectonic setting where it was formed. Chromian spinels from different tectonic settings will therefore have different chemical composition (Irvine, 1967). Detrital chromian spinels have a chemical and mechanical resistance, and will often preserve the compositional fingerprint after burial in a sedimentary succession (Garzanti et al., 2000).

Chemical composition and tectonic setting of chromian spinels from the Nama Group (Schwarzrand Subgroup and upper Fish River Subgroup) have been analysed by Blanco et al. (2009). The detrital chromian spinels were analysed with an electron microprobe, and the result indicates that there are several groups of chromian spinals. For the Haribes and Rosenhof members the chromian spinels indicate two groups with different provenance (Blanco et al., 2009). One group has characteristics of a mid-ocean ridge basalt (MORB) source, and the other group has characteristics of suprasubduction peridotites or modern back-arc setting, according to diagrams by Kamenetsky et al. (2001).

Chromian spinels from the Haribes and Rosenhof members display conchoidal fractures along the margins. This can imply that the chromian spinels were exposed to mechanical breakage, indicating that the source area was not located close to the depositional area. Paleocurrents of the chromian spinel-bearing sandstones of the Nama Basin was also analysed, and the results indicate a source area located in the Damara Belt. A provenance in the Damara Belt supports the tectonic models that claim there was an active continental margin on the northern and western borders of the Kalahari Craton (Blanco et al., 2009).

1.8 Samples

The samples that are analysed in this thesis project are five rock samples collected in Namibia in 2004-2005 by Dr. Udo Zimmermann (supervisor for the thesis project). The samples are placer deposits ("black sands") from the Fish River Subgroup (Nama Group).

The five samples are named 387, 389, 391, 393 and BS. Four samples are from the Rosenhof Member (Gross Aub Formation) and one sample is from the Haribes Member (Nababis Formation). The five samples are heavy mineral sands that have been separated into fractions (more details in *Table 1.1*). The heavy minerals have been separated into a:

(i) magnetic fraction (>2.95 g/cm^3);
(ii) non-magnetic apatite fraction (2.95 - 3.3 g/cm^3);
(iii) non-magnetic zircon fraction (>3.3 g/cm^3); and
(iv) zircon concentrate (a fraction nearly only composed of detrital zircons).

Table 1.1: List of samples including sample name, GPS locality, fraction type, formation and member name.

#	Sample name	GPS locality	Fraction type	Formation	Member
1 2 3 4	387	26°36'29.30"S, 19°13'56.40"E	Magnetic fraction Apatite fraction Zircon fraction Zircon concentrate	Gross Aub	Rosenhof
5	389	26°36'29.30"S, 19°13'56.40"E	Magnetic fraction	Gross Aub	Rosenhof
6 7 8 9	391	26°36'29.30"S, 19°13'56.40"E	Magnetic fraction Apatite fraction Zircon fraction Zircon concentrate	Gross Aub	Rosenhof
10	393	26°36'29.30"S, 19°13'56.40"E	Magnetic fraction	Gross Aub	Rosenhof
11 12 13 14	BS	26°55'04.20"S, 18°36'15.90"E	Magnetic fraction Apatite fraction Zircon fraction Zircon concentrate	Nababis	Haribes

2 METHODOLOGY

Samples were prepared for laboratory work before several analytical methods were applied. The analytical methods applied on each sample are listed in *Table 2.1*. The analytical methods FE-SEM and XRD were carried out at the University of Stavanger (UiS). Analyses with MLA and EMPA were carried out at TU Bergakademie Freiberg in Germany. ICP-MS analyses were out-sourced to a laboratory in Brazil. After all the laboratory work was done, the results were summarized and combined. The results from each analysis were interpreted to reach the given goals.

Table 2.1: List of analytical methods applied on each sample and fraction. *Analytical methods have been applied to these samples, but the results were delayed and are therefore not included in this thesis project.

#	Sample name	Fraction type	FE-SEM			XRD	MLA	EMPA	ICP-MS
			BSE	CL	EDS				
1	387	Magnetic fraction	×		×	×	×	×	
2		Apatite fraction	×		×	×	×	×*	
3		Zircon fraction	×		×	×	×	×	
4		Zircon concentrate		×		×			×*
5	389	Magnetic fraction	×		×	×	×	×*	
6	391	Magnetic fraction	×		×	×	×	×	
7		Apatite fraction	×		×	×	×	×*	
8		Zircon fraction	×		×	×	×	×	
9		Zircon concentrate		×		×			×*
10	393	Magnetic fraction	×		×	×	×	×*	
11	BS	Magnetic fraction	×		×	×	×	×	
12		Apatite fraction	×		×	×	×	×*	
13		Zircon fraction	×		×	×	×	×	
14		Zircon concentrate		×		×			×*

2.1 Single grain analyses

The samples are already separated into fractions, which means that all methods will be applied on single grains. Single grain analyses of the heavy mineral fraction allow a more detailed characterization of the source components, in comparison to whole-rock geochemistry. Analyses of single grains as chemistry may indicate the tectonic setting of the protolith, and fitting all together we may find the setting for the sediment in which all these grains are unified.

2.2 Sample preparations

The samples are already divided into fractions using Frantz separation. For analyses with the XRD the fractions were milled. For the rest of the analytical methods (FE-SEM, MLA, EMPA and ICP-MS) the grains were placed in mounds, meaning that single grains were placed in a mounting material in order to give them a shape that can be used for further analysing. The mounds were later coated with carbon.

2.2.1 Frantz separation

The samples have been separated with a Frantz machine. The Frantz separation process was performed by Geotrack International in Australia. The grains were separated using conventional heavy liquid electromagnetic separation techniques. The samples were separated into 4 fractions: magnetic fraction (Mf), apatite fraction (Af), zircon fraction (Zf) and zircon concentrate (Zc). The zircon fractions have grains that are >3.3 g/cm^3 and non-magnetic. The Zc is the concentrate and should be the purest non-magnetic material, nearly only composed of detrital zircons. Zf is the fraction and is often more impure and contains darker more magnetic zircons. They are both separated with a 25° forward slope and 2° side angle and full scale on the Frantz machine. If rutile is present it will likely be in the Zc and possibly in the Zf. The Af contains grains that are between 2.95 g/cm^3 and 3.3 g/cm^3 and non-magnetic. It contains apatite if present, and may also contain aluminum silicates and other composites. The Mf contains grains that are >2.95 g/cm^3. The Mf contains, if present, sphene/titanite, garnet, monazite and other composites.

2.2.2 Milling

Before the XRD analyses the grains from each fraction were milled. The grains were crushed into powder using an agate mortar. This was done to less than 1 g of each magnetic fraction, apatite fraction, zircon fraction and zircon concentrate.

2.2.3 Mounting

A random selection of grains from each sample and fraction were placed on a sticky tape (*Figure 2.1*). The grains from one sample and fraction were handpicked and placed next to each other on a line on a sticky tape using a needle. Approximately 200-500 grains were placed on each line. On the mound with zircon concentrates there were also placed some zircon standards. A polymer/epoxy resin was poured on top of the grains creating the mound. The mound was put aside to dry for 48 hours and was then polished. Each mound has a diameter of 1 inch (~2.5 cm). In total, 7 mounds were created with different samples/fractions on each line (see *Table 2.2* for more details). A map for each mound can be seen in *Figure 2.2*. The mounds were first polished by hand using grinding paper, and then a machine called Struers Tegra was used to polish/smooth the surface. The machine polished the mounds using two cloths with diamond suspensions. "Nap" polished the samples with diamonds of 3 µm, and "Dac" polished with diamonds of 1 µm. Samples were polished for ~5 minutes with each.

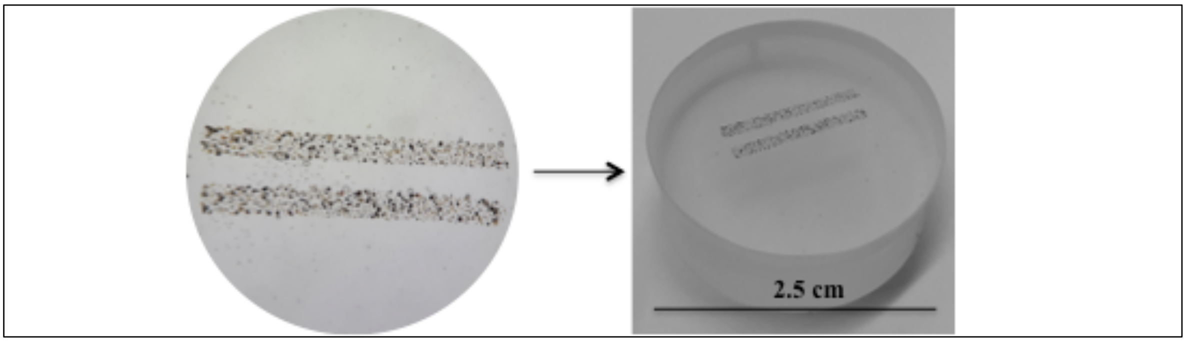

Figure 2.1: The mounting process: grains were placed on a sticky tape, a polymer/epoxy resin was poured on top to create the mound, and then the mound was polished.

Table 2.2: List with name of each mound and number of lines with the corresponding sample and fraction type.

Mound name	Line name	Sample name	Fraction type	Number of grains
Mound 11	D	391	Zircon concentrate	~ 400
	C	387	Zircon concentrate	~ 350
	A	BS	Zircon concentrate	~ 480
Mound A	Line 1	387	Magnetic fraction	~ 200
	Line 2	387	Magnetic fraction	~ 270
	Line 3	387	Magnetic fraction	~ 310
	Line 4	BS	Magnetic fraction	~ 460
	Line 5	BS	Magnetic fraction	~ 380
	Line 6	BS	Magnetic fraction	~ 260
Mound B	Line 1	BS	Apatite fraction	~ 330
	Line 2	387	Apatite fraction	~ 240
	Line 3	391	Apatite fraction	~ 350
Mound C	Line 1	387	Zircon fraction	~ 230
	Line 2	387	Zircon fraction	~ 270
	Line 3	BS	Zircon fraction	~ 500
	Line 4	391	Zircon fraction	~ 380
	Line 5	391	Zircon fraction	~ 300
Mound D	Line1	389	Magnetic fraction	~ 460
	Line2	389	Magnetic fraction	~ 450
Mound E	Line1	391	Magnetic fraction	~ 390
	Line2	391	Magnetic fraction	~ 450
Mound F	Line1	393	Magnetic fraction	~ 310
	Line2	393	Magnetic fraction	~ 400

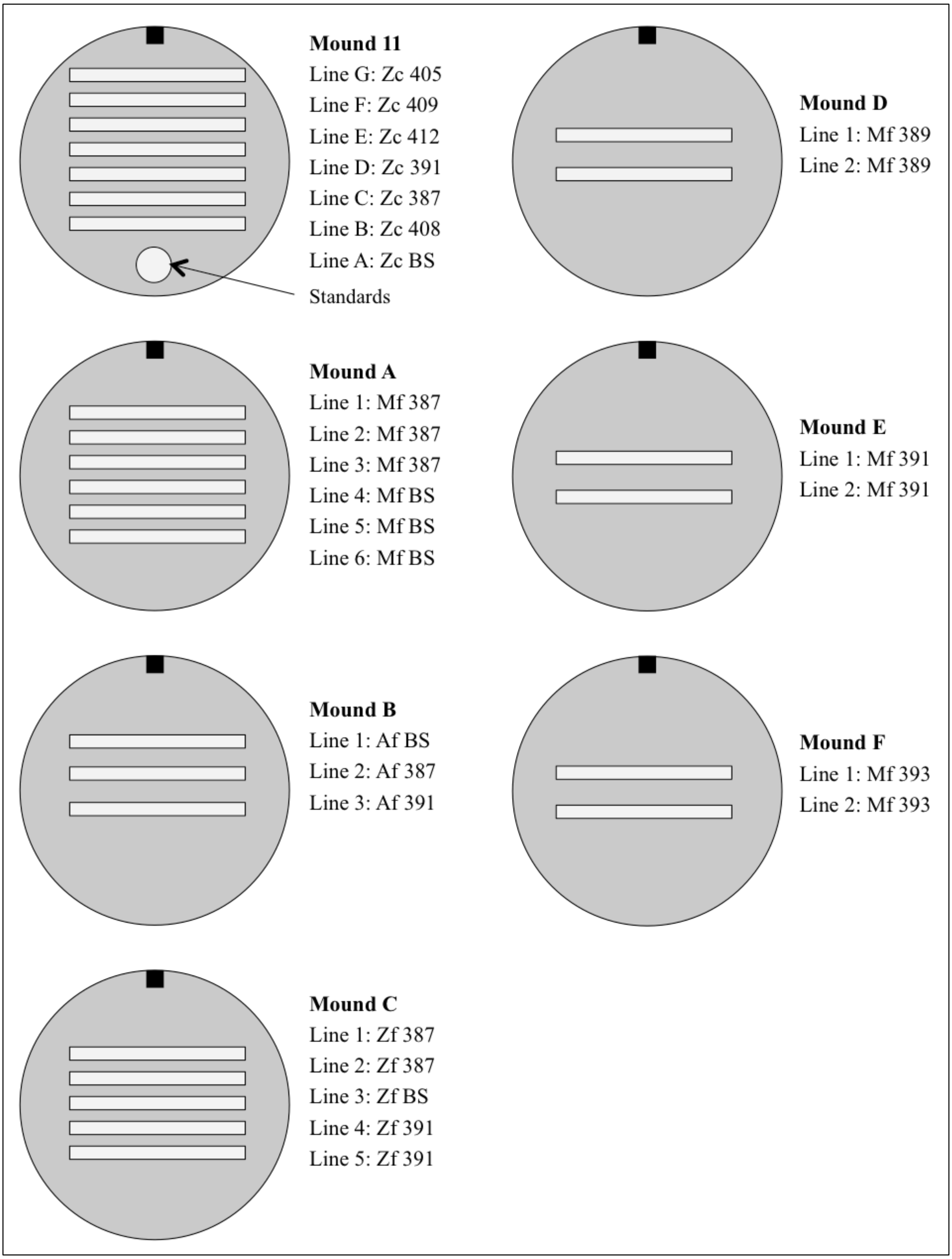

Figure 2.2: Map of the mounds with sample name and fraction type on each line (Mf = magnetic fraction, Af = apatite fraction, Zf = zircon fraction, Zc = zircon concentrate).

2.2.4 Coating

For all the analytical methods the sample/mound has to be coated with an electrically conductive material, for example carbon, palladium or gold. This allows a steady electron flux and it avoids surface charging. Surface charging can cause SEM image distortions. The samples/mounds in this project were coated with a thin layer of carbon before analysing them with SEM, MLA and EMPA. The carbon coating has less affect on the X-rays generated, compared to palladium or gold. Carbon will absorb few of the X-rays produced in the specimen. The carbon will generate its own characteristic peak, but it can be ignored when analysing the spectrum.

The coating machine used for the mounds before FE-SEM analyses is called Emitech K550 Sputter Coater (*Figure 2.3*). The sample was placed in a vacuum chamber. In the chamber was a carbon evaporation source consisting of two pointed carbon rods (3-6 mm in diameter) in contact with a carbon tread in between. A current was passed through the rods for some seconds causing the carbon to evaporate. The carbon evaporated from the region where the rods were in contact to the top of the mound/sample. The same mounds were later cleaned with alcohol and coated again with carbon before analyses with MLA and EMPA. The coating-machine used for the second coating is called Leica EM MED020 (*Figure 2.3*).

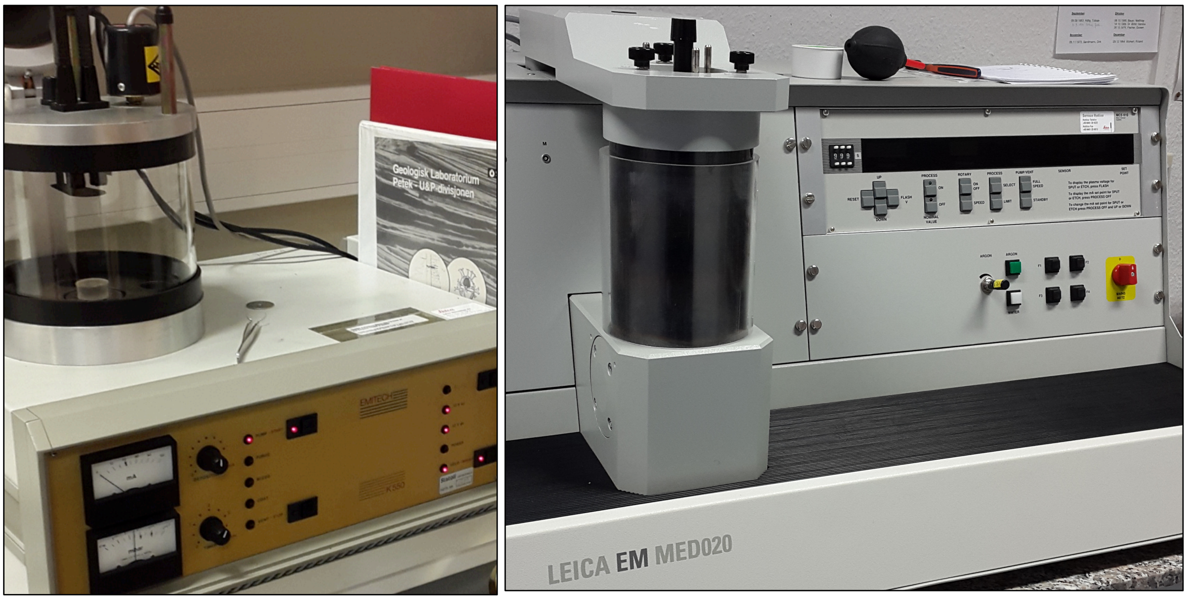

Figure 2.3: Carbon coating machines: Emitech K550 Sputter Coater used for coating the mounds with carbon before FE-SEM analyses, and Leica EM MED020 used for coating the mounds with carbon before analyses with MLA and EMPA.

2.3 Field Emission Scanning Electron Microscope (FE-SEM)

2.3.1 Theoretical background

2.3.1.1 Scanning electron microscopy

The Scanning Electron Microscope (SEM) is the most commonly used electron microscope. This type of microscope does not use visual light, but instead it image how electrons interact with the surface of a sample. The SEM is a close relative to the electron microprobe analyser (EMPA), but it is designed primarily for imaging rather than analyses. It can be used to look at microscopic structures with a very high resolution and a great depth of field. A SEM system can be connected to several detectors, which uses various techniques for analysing a sample (Reed, 2005).

2.3.1.2 Instrumentation

A SEM consists of an electron gun, several electromagnetic lenses (condenser lenses and objective lens) and apertures, a detector and an amplifier (*Figure 2.4*). There are two types of electron guns: thermionic and field emission (Leng, 2013). The field emission gun uses a very high electric field on a metal surface to pull out the electrons. The result is a tunneling effect, where the metal electrons can cross a surface barrier. The field emission gun produces the highest intensity electron beam, meaning that the beam brightness is very high and this will provide a better image quality of the sample/specimen. From the electron gun an electron beam is emitted. The electron beam is condensed to a fine probe and is used for scanning the surface of the sample. Before the electron beam reaches the surface of the sample it has to go through several electromagnetic lenses and apertures. Usually there are two condenser lenses and they reduce the crossover diameter of the electron beam. The objective lens focuses the electron beam and the result is a beam with a diameter of nanometer scale. A deflection system moves the electron beam over the surface of the sample/specimen, it is controlled by scan coils and it scans the surface in a systematic order. When the electron beam hits the surface of the sample signal electrons will be emitted and detected. The signals are amplified and used to reconstruct an image (Leng, 2013).

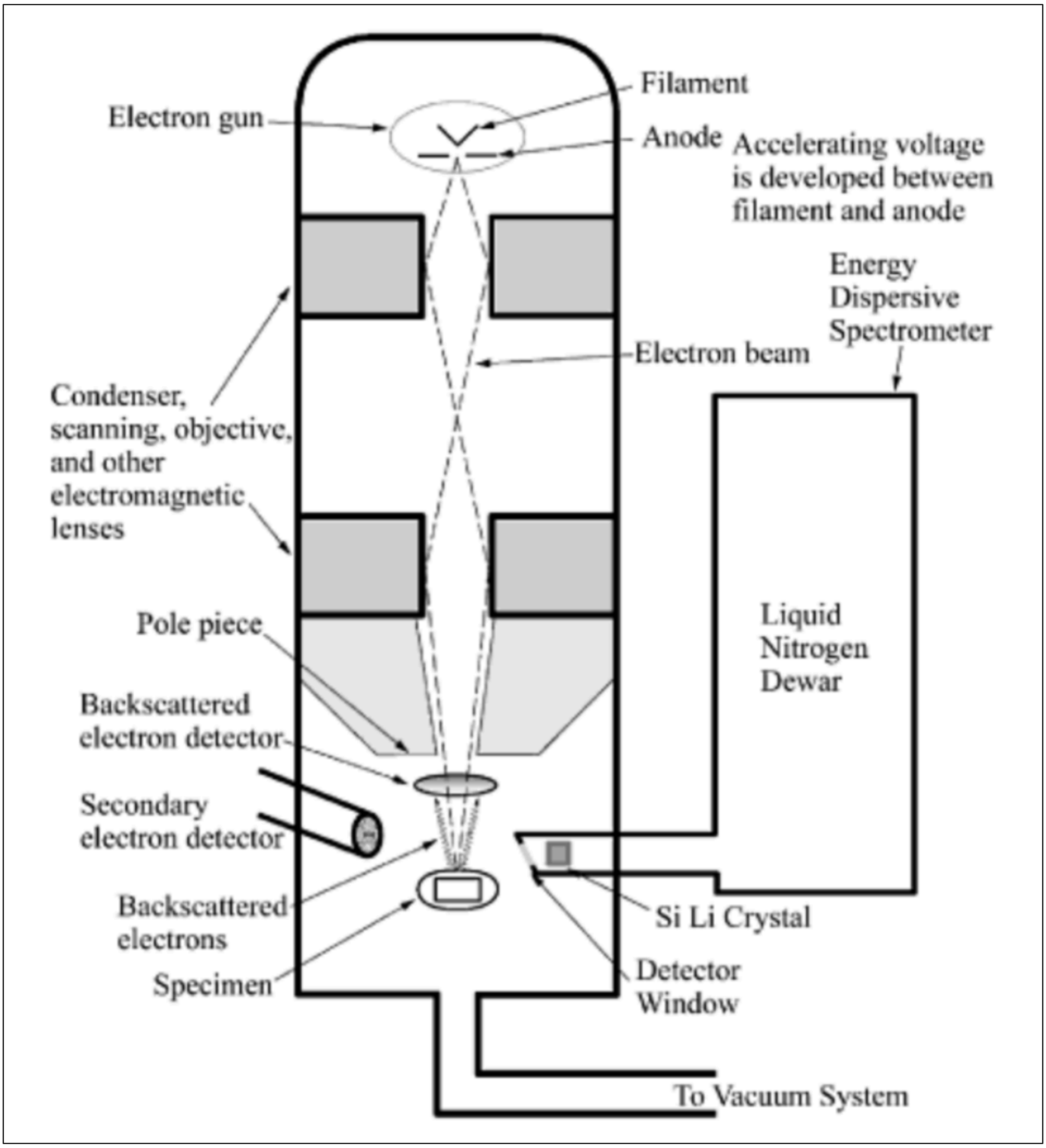

Figure 2.4: Arrangement of a SEM with EDS (Severin, 2004).

2.3.1.3 Magnification and resolution

The magnification possible using a SEM depends on the ratio of the linear size of the display screen and the linear size of the scanned sample area. The size of the scanned area can vary, and therefore the image magnification provided by the SEM will also change. The magnification can be from 20x to more than 100 000x. The image resolution of a SEM depends on the cross sectional diameter of the electron beam scanning the sample (*Figure*

2.5). High resolution can be obtained by minimizing the diameter size of the electron beam. The diameter can be expressed as d (Leng, 2013):

$$d = (\frac{4 \times i}{\beta \times \pi^2 \times \alpha^2})^{1/2} \tag{2.1}$$

i is the electron beam/probe current, β is the brightness of the beam controlled by the electron source and α is the convergence angle of the beam. α depends on the final aperture diameter and the working distance (Leng, 2013).

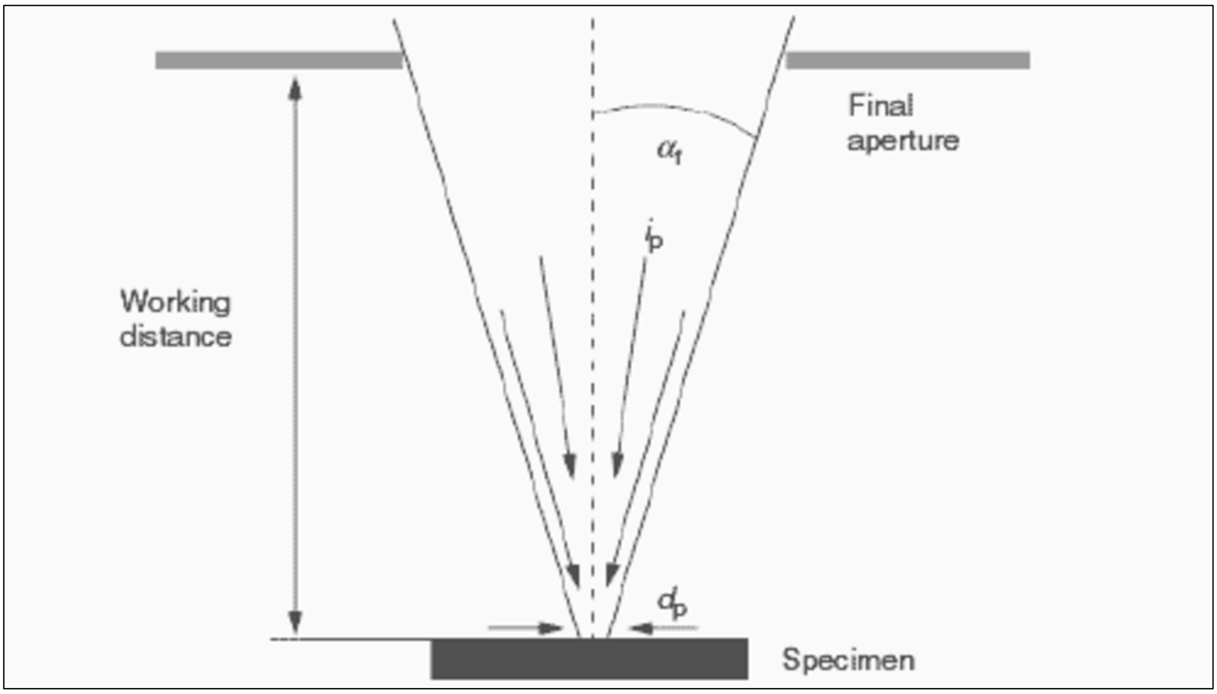

Figure 2.5: Illustration of the relationship between the diameter of the electron beam, convergence angle of the beam, aperture diameter and working distance (Leng, 2013).

2.3.1.4 Signal detection

There are several signals emitted when the electron beam hits the surface of the sample: black-scattered electrons, secondary electrons, auger electrons, characteristic x-rays, continuous x-rays and cathodoluminescence/light (*Figure 2.6*). Detectors can collect the different signals. The secondary electrons are detected by a Secondary Electron (SE) detector and the back-scattered electrons are detected by a Back-Scattered Electron (BSE) detector. The cathodoluminescence/light are detected by the Cathodoluminescence (CL) detector and the characteristic x-rays are detected by an Energy Dispersive Spectroscopy (EDS) detector (Hjelen, 1986).

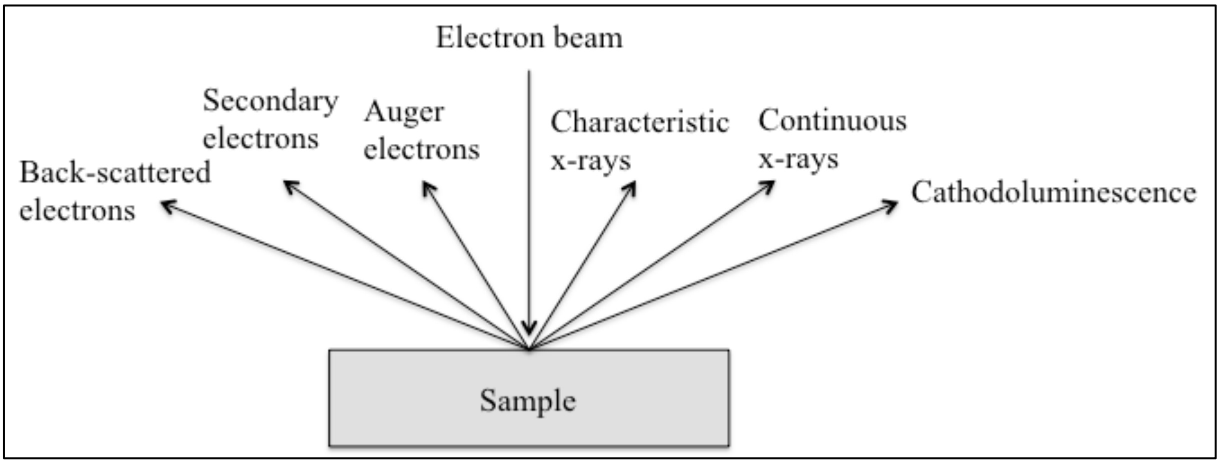

Figure 2.6: Signals emitted when an electron beam hits the surface of a sample are back-scattered electrons, secondary electrons, auger electrons, characteristic x-rays, continuous x-rays and cathodoluminescence/light (modified after Hjelen (1986)).

2.3.1.5 Back-Scattered Electron (BSE) detector

The Back-Scattered Electron (BSE) detector collects back-scattered electrons. When high-energy electrons strike the sample they will produce elastic scattering or inelastic scattering. It is the elastic scattering that produces the BSEs. These electrons are deflected from the sample at large angles and they loose little energy. The fraction of BSEs has a relation to the atomic number of the element that has been scanned (Leng, 2013). Larger atoms (with a high atomic number) have a higher probability of producing elastic scattering. Consequently the number of back-scattered electrons reaching the BSE detector is proportional to the mean atomic number of the sample. Brighter areas on the sample correlate with a greater average atomic number and darker areas correlate with lower average atomic number (Hjelen, 1986).

2.3.1.6 Cathodoluminescence (CL) detector

The Cathodoluminescence (CL) detector collects cathodoluminescence/light. CL is the emission of characteristic visible luminescence/light by a material that is bombarded with electrons, and the source of the electrons is a cathode. Combining the FE-SEM with the CL detector can generate high resolution and high magnification CL-images (Boggs and Krinsley, 2006). CL-images can display growth zoning in minerals (e.g. zircons), it can reveal alterations and deformations of the minerals, and it can help to distinguish between detrital/primary minerals and secondary minerals (Boggs and Krinsley, 2006; Götze et al., 2013). Minerals that exhibit CL are for example zircon, diamond, quartz, rutile, spinel, calcite, apatite, barite, feldspar, jadeite and diopside (Reed, 2005).

2.3.1.7 Energy Dispersive Spectroscopy (EDS) detector

The Energy Dispersive Spectroscopy (EDS) detector collects characteristic x-rays. It is also called Energy Dispersive Spectrometer (EDS) or Energy Dispersive X-ray (EDX) system. EDS can help to analyse samples since it can give the chemical composition of a point or an area. It determines the presence and quantity of chemical elements by detecting the characteristic x-rays emitted from atoms in a point on the sample. A beam that is approximately 2 μm wide defines the point. The EDS detector identifies chemical elements based on their x-ray energy. The x-ray energy is the energy difference between two electrons in different shells, and it is dependent on the atomic number of the atom (Leng, 2013). The EDS produces an x-ray spectrum that ranges from 0 to 10s of keV. The spectrums can be compared to other known spectrums of minerals or a standard. The accuracy of this detector varies because of several factors. Lighter elements, such as carbon, fluorine and oxygen, are difficult to measure accurately (Reed, 2005).

2.3.2 Purpose of the method

The FE-SEM with its detectors will help to identify and characterize minerals. It can give information about their structure, grain size, grain shape, fractures, inclusions and phases within one grain. The BSE detector can map elements on the surface of the sample. It can create elemental composition contrast images. The CL detector can provide high-resolution images of the separated detrital zircons displaying the different zonations. The EDS detector can be used for identification and semi-quantification of heavy minerals. It provides weight percent (wt%) and atomic percent (at%) for each element in the analysed mineral.

2.3.3 Technical specifications

A Field Emission Scanning Electron Microscope (FE-SEM) located at University of Stavanger (UiS) was used for this project. It is a Zeiss Supra 35VP FE-SEM, and it has a Field Emission (FE) gun, a Back-Scattered Electron (BSE) detector, a Cathodoluminescence (CL) detector and an Energy Dispersive Spectroscopy (EDS) detector (*Figure 2.7*). The EDS detector is of the type EDAX. The mounds (with carbon coating) were placed on sample holders and a tape of carbon was placed on both sides of the mound to avoid over-charging. One or two mounds were then placed inside the FE-SEM under vacuum.

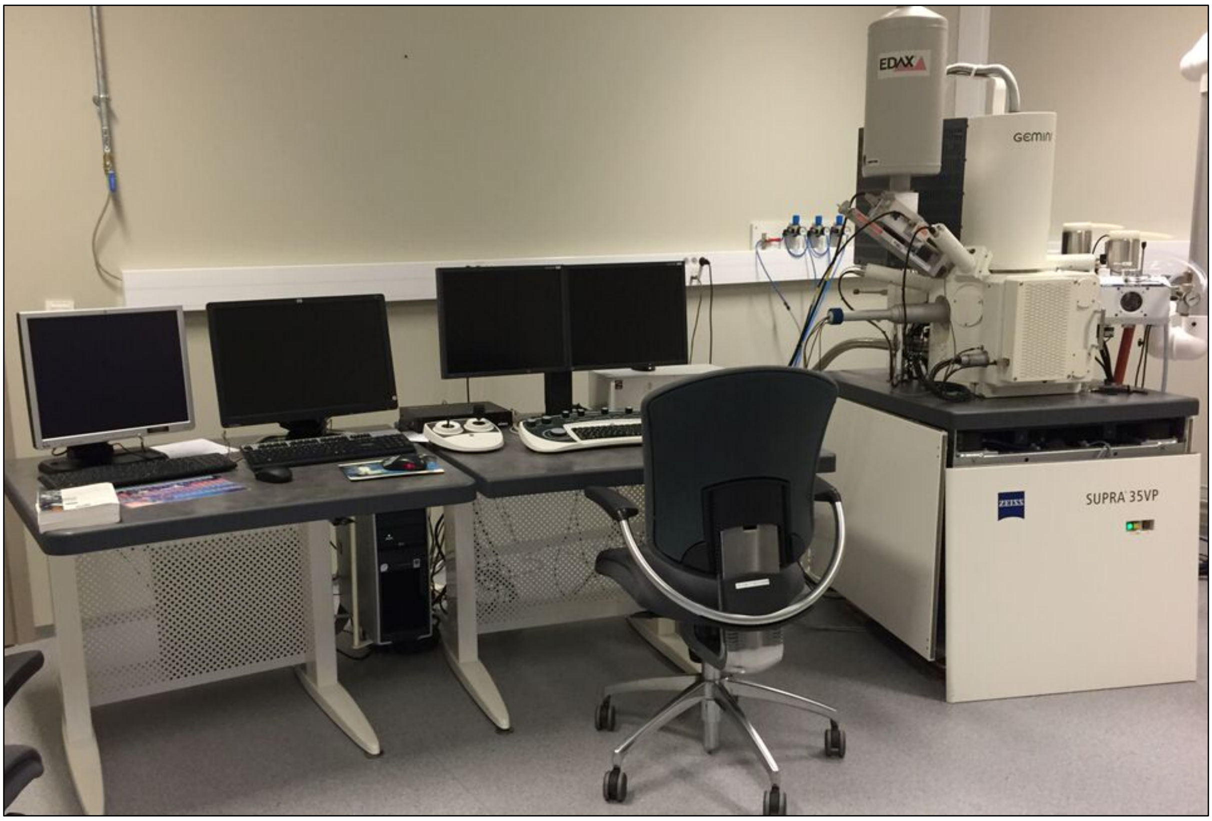

Figure 2.7: Zeiss Supra 35VP FE-SEM located at UiS.

The BSE detector was used to view the grains. The working distance (WD) was set to be 10-12 mm and focus was adjusted. Aperture size was set to 30 µm, and acceleration voltage to 20-25 kV. Brightness, contrast and magnification were adjusted for each sample. The EDS detector with the software EDAX Genesis collected spectrums from grains/phases in the samples. Spectrums of the different grains, or phases within the grains, were then compared to known literature of minerals and their spectrums, e.g. Severin (2004) and Reed (2005). The CL detector took high-resolution images of the zircon concentrates. When using the CL detector the WD was set to ~10 mm, aperture size to 300 µm, and acceleration voltage to 15 kV. These images were further used for ICP-MS analysis.

New measurements with the EDS detector were applied on identified garnets, but this time they were compared to a standard. The parameters that were used are based on results from a bachelor study by Bekkum and Egeland (2016). These parameters are best for measuring garnets in combination with a standard, according to Bekkum and Egeland (2016), and were therefore used in this analysis: magnification was set to 1500x, aperture size to 30 µm, acceleration voltage to 15 kV, working distance to 10-11 mm, and scan speed to 3.

2.4 X-Ray Diffractometer (XRD)

2.4.1 Theoretical background

2.4.1.1 X-ray diffraction methods

Discovering the x-rays made it possible to “see inside” the crystals and further to determine crystal structure and cell size. William Henry Bragg started using x-rays as a crystallographic tool and described very simple structures using x-ray diffraction. Further analyses of the intensities of x-rays reflected by crystals made it possible to relate it to the concept of chemical bonding and Niels Bohr´s atomic model (Hessenbruch, 2002). X-ray diffraction methods are often divided into two types: spectroscopic and photographic. For this project the spectroscopic method will be used. The spectroscopic method is also known as x-ray powder diffractometry or x-ray diffractometry (Leng, 2013).

2.4.1.2 Generation of x-rays

X-rays are electromagnetic waves with short wavelength and high energy. They are produced when electrons accelerate with high speed, because of a high voltage field, and then collide with a metal target (*Figure 2.8*). When the electrons collide with the target they decelerate rapidly and the kinetic energy of electrons is converted to the energy of x-ray radiation. Inside the x-ray tube (*Figure 2.8*) there is high vacuum, a source of electrons and two electrodes. There is high voltage across the two electrodes and the voltage makes the electrons drawn to the anode/target. When the electrons collide with the target, surface x-rays are produced. The x-rays are then guided out of the tube (Leng, 2013).

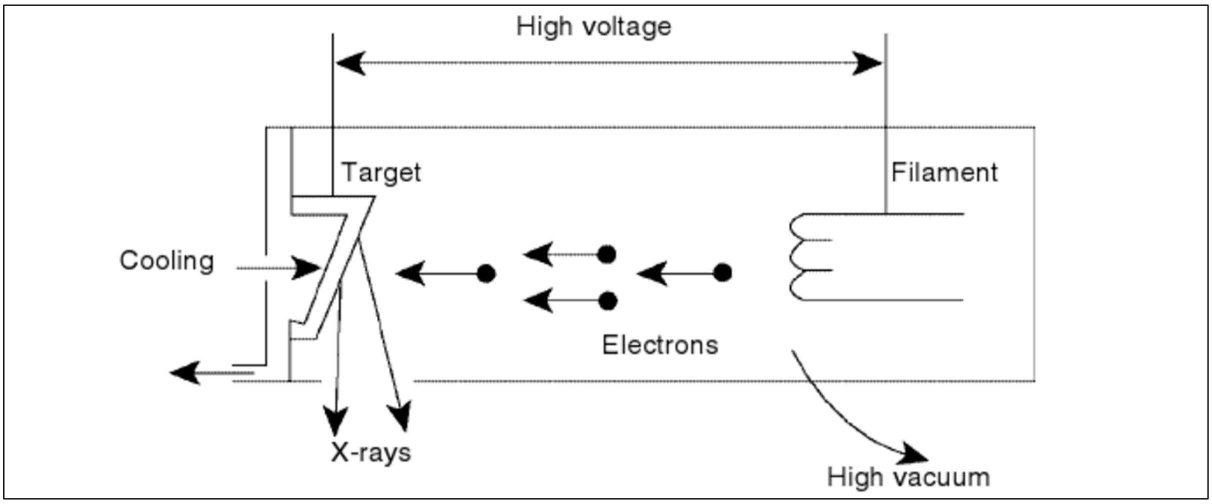

Figure 2.8: Illustration of an x-ray tube structure (Leng, 2013).

The x-rays generated in the tube contain a range of wavelengths (*Figure 2.9*). The minimum wavelength will appear as the background of the radiation spectrum and is called continuous x-rays. The minimum wavelength with maximum radiation energy (x-ray intensity) of continuous x-rays depends on the maximum acceleration voltage of electrons, and they are called characteristic x-rays (Leng, 2013).

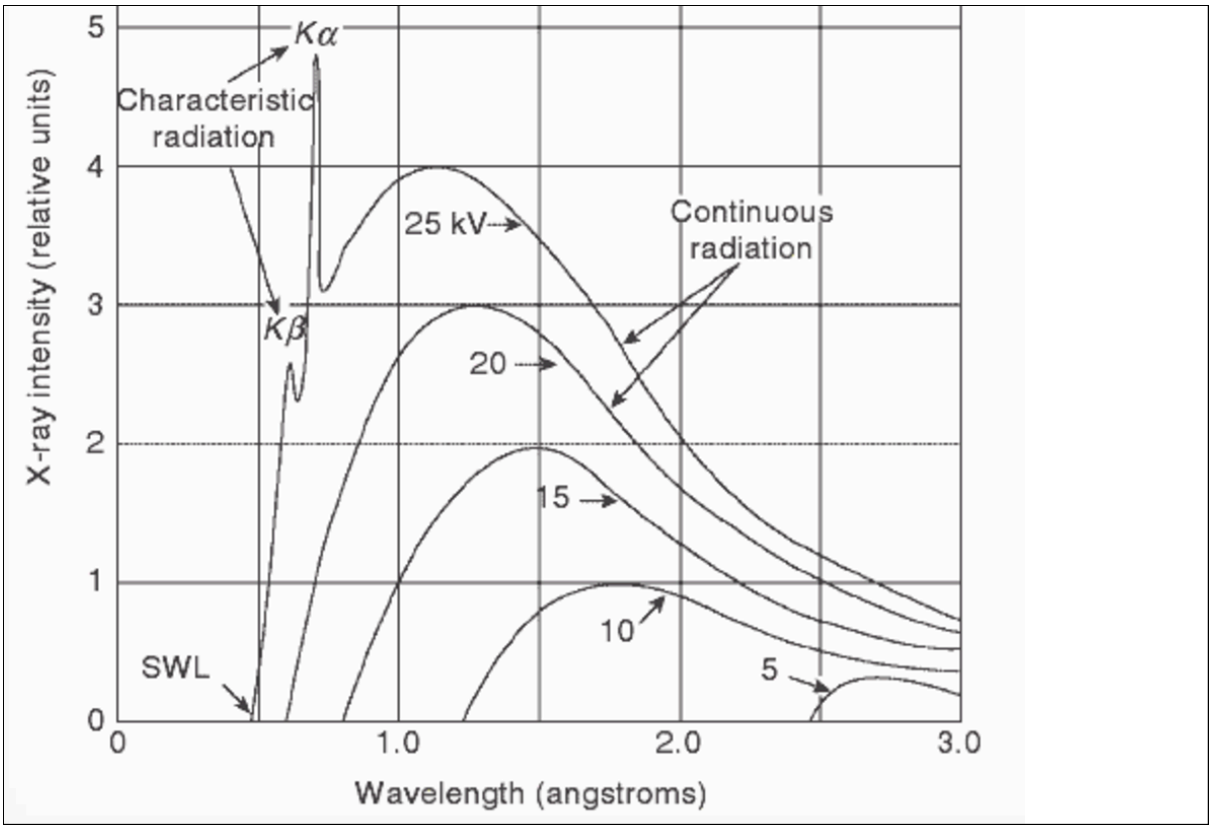

Figure 2.9: X-ray spectrum depends on the intensity and wavelength of the x-rays. SWL = short wavelength limit (Leng, 2013).

2.4.1.3 Bragg´s law

X-ray diffraction methods are based on how waves interfere. X-rays are electromagnetic waves, same as visible light. The difference is that x-rays have a much shorter wavelength. X-ray beams incident on a solid crystal will be diffracted, and the diffraction depends on the crystallographic planes of the solid crystal. *Figure 2.10* illustrates an example where two incident waves (incident beam 1 and 2) are deflected by two crystal planes (crystal plane A and B). The two deflected waves (diffracted beam 1´and 2´) will only be inphase when this relationship is fulfilled (Leng, 2013):

$$n\lambda = 2 \times d \times \sin(\theta) \qquad (2.2)$$

This equation is called Bragg´s law. Factor $n\lambda$ is the phase difference, n is an integer, θ is the incident angle and d is the spacing between the parallel crystal planes. The spacing between the atomic planes of a crystal can be obtained by detecting the constructive interference at a particular incident angle and wavelength of the incident beam. If the spacing of the atomic planes of a crystal is known, it is possible to identify the crystal structure of the material (Leng, 2013).

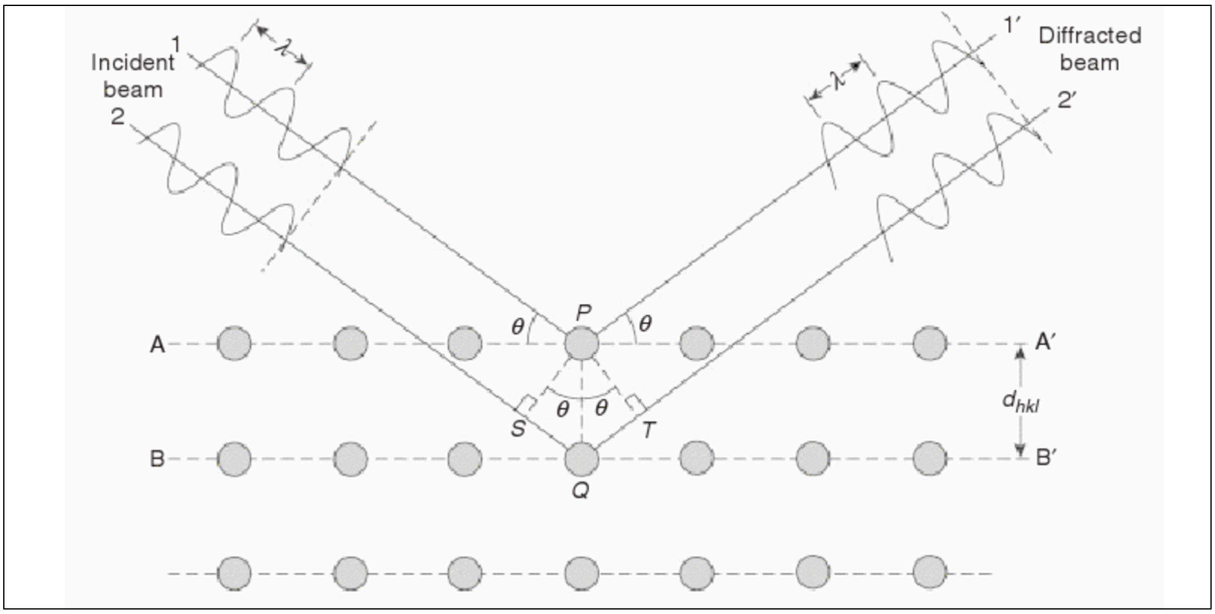

Figure 2.10: Bragg diffraction on crystal planes. Two incident waves are deflected by two crystal planes. The two deflected waves are inphase when the relationship nλ=2×d×sin(θ) is fulfilled (Leng, 2013).

2.4.1.4 Instrumentation

X-ray diffractometry is the most common x-ray diffraction method for characterization of materials, for example crystal structures. The instrument used for these analyses is called an X-Ray Diffractometer (XRD). In the XRD an x-ray beam with one wavelength is used, but the incident angle of the beam changes constantly. A spectrum registers the diffraction intensity versus the angle between the incident and diffraction beam. Diffractometry makes it possible to identify the crystal structure of the material by comparing the spectrum with a database containing thousands of diffraction spectrums of known crystalline materials (Leng, 2013).

The main task for the XRD is to detect x-ray diffraction from materials and the intensity of the diffraction in the range of the diffraction angle (2θ). An XRD consist of an x-ray source, a sample and a detector (*Figure 2.11*). The x-rays generated by the x-ray tube travels through soller slits. The soller slits make sure that the x-ray beam is parallel and straight and it makes sure that the beam does not diverge in the direction perpendicular to the figure plane. The x-ray beam strikes the sample and the x-rays are diffracted. The diffracted x-rays form a convergent beam at the receiving slit and finally they arrive at the detector. The diffracted x-rays also need to go through a monochromatic filter (monochromator) before they are detected. This filter helps to decrease the background radiation coming from within the sample (Leng, 2013).

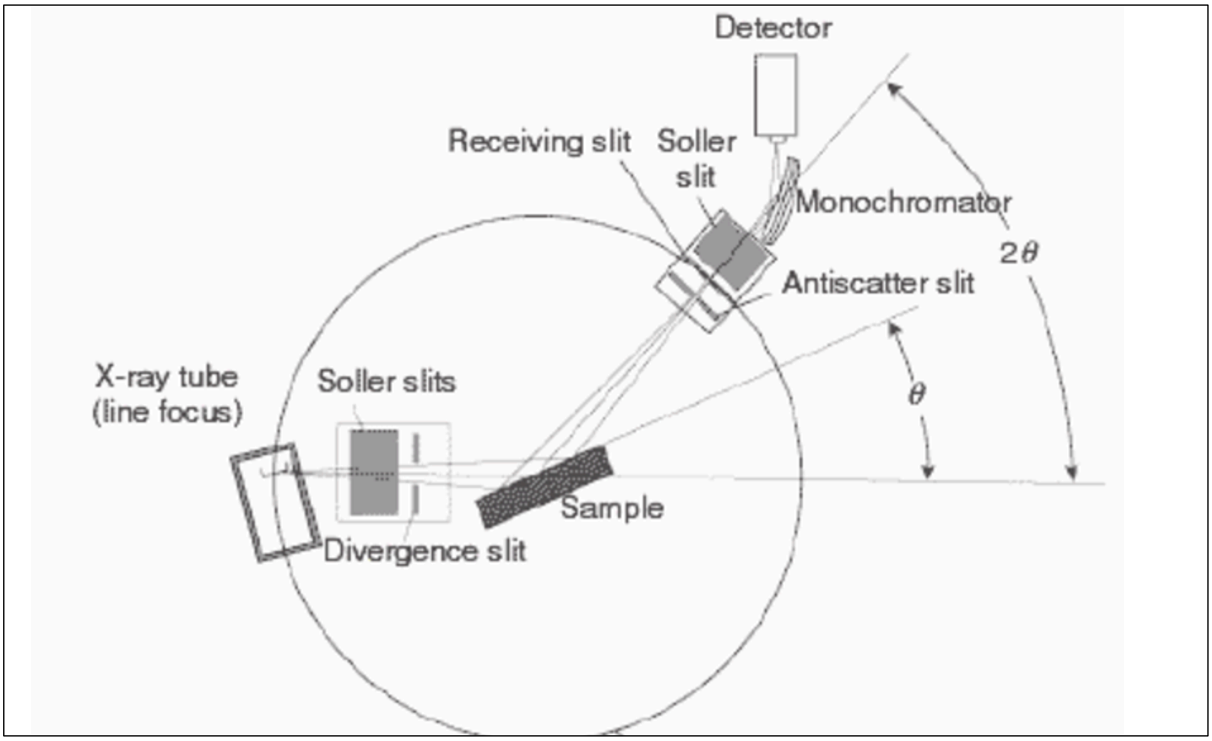

Figure 2.11: Illustration of an X-Ray Diffractometer (XRD) with x-ray source/tube, sample, soller slit and detector (Leng, 2013).

2.4.2 Purpose of the method

X-ray diffraction methods are very effective for determining the crystal and crystal structure of different materials. The diffraction methods can identify minerals based on their crystalline structure. It is therefore possible to identify minerals with the same element composition, but that have different crystal structure (Leng, 2013). These minerals are called polymorphic minerals. Minerals with the element composition TiO_2 are often referred to as rutile, but it can also be two other polymorphs of TiO_2 named anatase and brookite (Landmann et al., 2012). The three polymorphs of TiO_2 have different point groups, crystal systems and space groups (Leng, 2013).

2.4.3 Technical specifications

An X-Ray Diffractometer (XRD) located at University of Stavanger was used in this project. It is a Bruker D8 Advance ECO XRD (*Figure 2.12*). PhD student Emanuela Iedidia Kallesten and her assistants at UiS performed the analyses. The following scan parameters were used: voltage was set to 40 kV, current to 25 mA, increment to 0.010, time to 0.2 seconds/step, slit to 0.6 mm, and the diffraction angle range 2θ to 4-70°. CuK(alpha) radiation was used. The data were processed using the software Diffrac.Suite.Eva 4.0 by Bruker. The software contains a database of minerals and their spectrums and it was used to identify the different peaks in the spectrums provided from the XRD analyses.

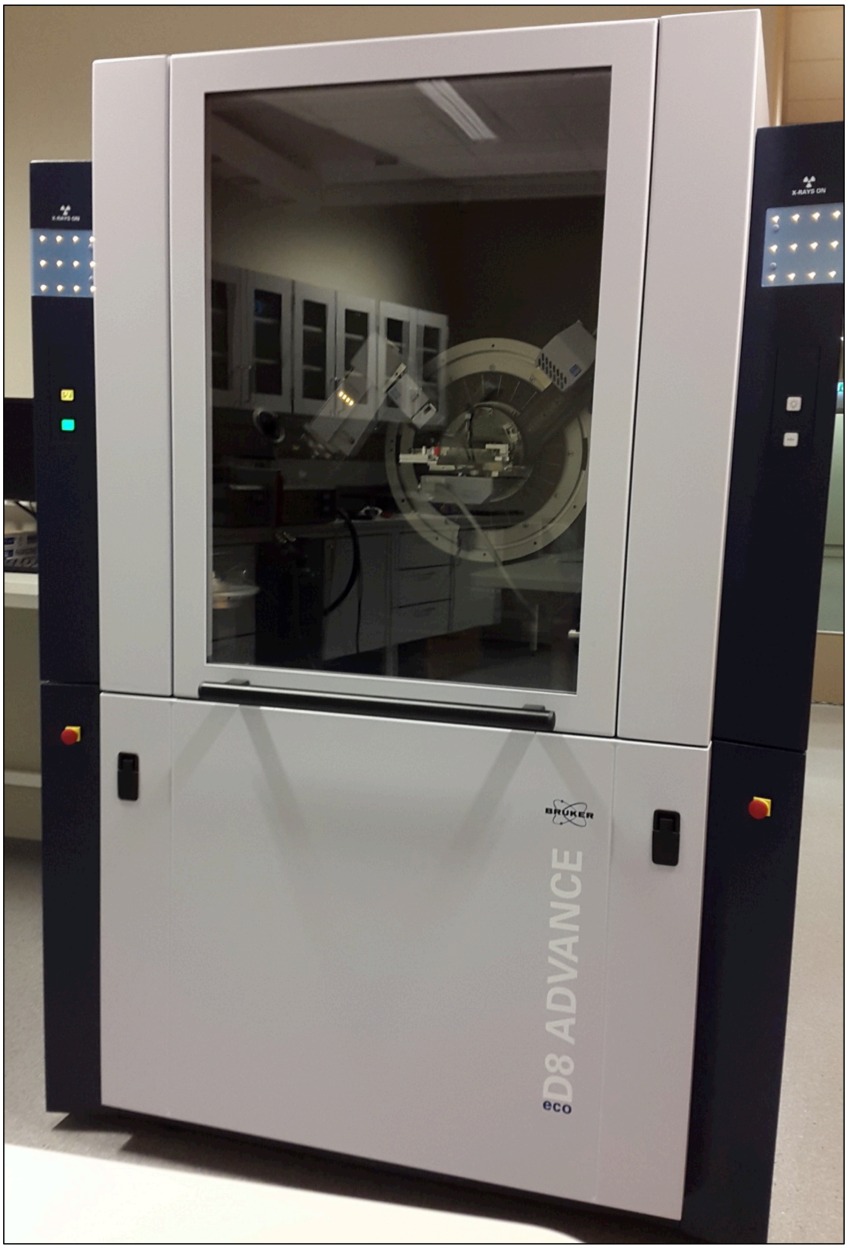

Figure 2.12: Bruker D8 Advance ECO XRD located at UiS.

2.5 Mineral Liberation Analyser (MLA)

2.5.1 Theoretical background

2.5.1.1 The MLA system

The Mineral Liberation Analyser (MLA) is used for quantitative chemical analyses of minerals. The MLA is a combination of an automated SEM and a collection of EDS detectors with automated quantitative mineralogy software. BSE-images are used for determining the grain boundaries and locations for the x-ray spectral acquisition (Sylvester, 2012). When identifying minerals using x-ray spectrums a library of mineral standards is required. The library has to be constructed before the automated run and it contains a collection of high quality reference x-ray spectra for each mineral in the sample (Fandrich et al., 2007; Sylvester, 2012).

The first MLA system was focused on mineralogy and metallurgical processing, especially on determining the degree of liberation of ore minerals from gangue (Fandrich et al., 2007), hence the name of the instrument: "mineral liberation analyser". Lately the potential for the MLA has been expanded and it is used for several applications, for example for studying the provenance of heavy minerals in sediments and sedimentary rocks. MLA can give much information about a variety of mineral properties such as mineral abundance, grain size, grain shape, mineral texture, mineral surface, mineral associations and degree of liberation (Sylvester, 2012).

2.5.1.2 Instrumentation

In the SEM a beam of electrons is generated and focused through a series of electromagnetic lenses and apertures (more details in chapter 2.3.1). The electron beam is scanned in a raster pattern on an area on the surface of the sample. The BSEs reflected from the sample are collected with the BSE detector and are used to produce an image of the sample. X-rays generated when the electron beam hits the surface of the sample are also detected with the EDS. The x-rays have energy levels that are characteristic for each element present in the sample. The software of the MLA will automatically integrate the images and x-rays to identify the minerals and map their distribution. This process is repeated until the entire sample is mapped and all minerals are identified (Sylvester, 2012).

2.5.1.3 Advantages and disadvantages with MLA

The MLA replaces time-consuming and tedious manual analyses with a systematic computer automated analyses. It reduces the potential for human errors. The MLA analyses much faster, so the number of grains examined will be more statistically representative for the sample. It can distinguish fine-grained samples and complex intergrowth of minerals down to micrometer scale (Sylvester, 2012).

The MLA has difficulties distinguishing between very similar components (e.g. gypsum and anhydrite) and it is not capable to distinguish between polymorphs (e.g. rutile, anatase and brookite). If there is a lack of available standard materials and therefore lack of reference x-ray spectra, it can influence the accuracy of the results (Sylvester, 2012).

2.5.2 Purpose of the method

The MLA can be used to identify and quantify heavy minerals on mounds. It can provide information about mineral characteristics such as grain shape, grain size, mineral structure and texture. It can calculate grain size distributions based on type of mineral, group or sample. The MLA can provide high-resolution BSE-images of the elemental composition of a sample, grain or phases within a grain. The results from the MLA can include wt% of each mineral type in the sample, area%, area (micron), particle count and grain count.

2.5.3 Technical specifications

A Mineral Liberation Analyser (MLA) at Technische Universität Bergakademie Freiberg (TU Bergakademie Freiberg) in Germany was used in this project. It is a SEM FEI Quanta 650 MLA-FEG, and it is equipped with two parallel Bruker X-Flash 6130 EDS detectors and the software version of the MLA 3.1 program by FEI (*Figure 2.13*). The two EDS detectors make it possible to double the amount on measurements on the same time. The mounds with carbon coating were placed in a sample holder, and a tape of copper was placed between the mounds to avoid over-charging. The sample holder was then placed in the SEM under vacuum.

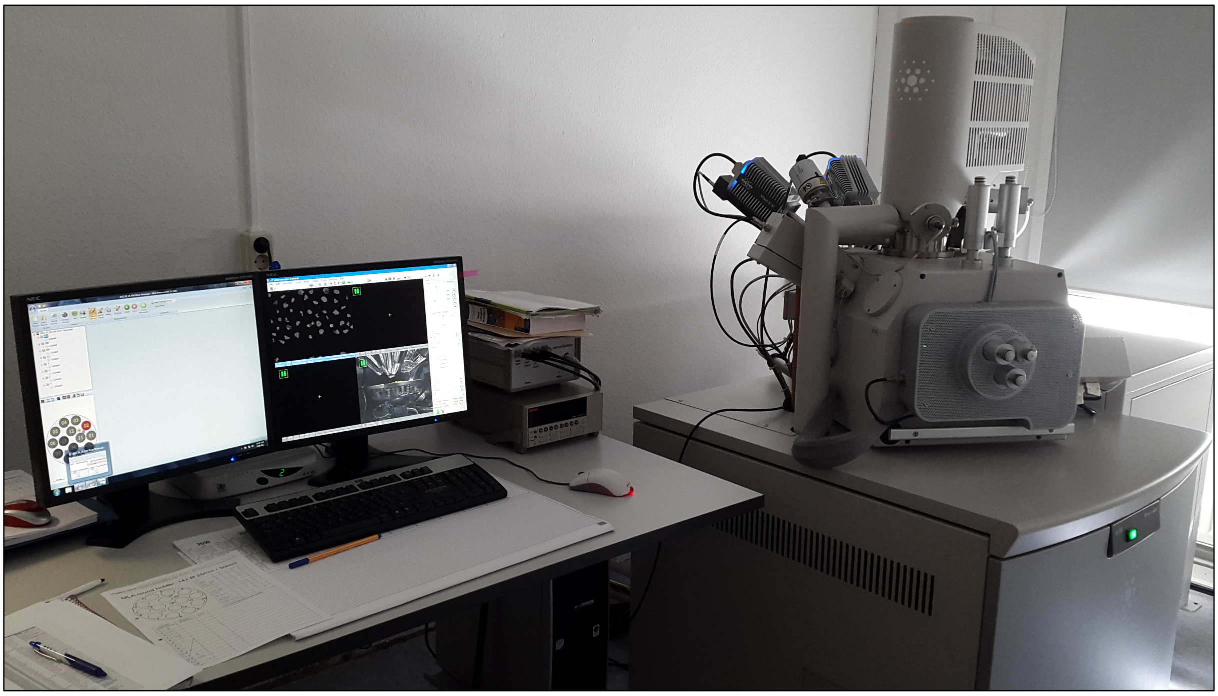

Figure 2.13: SEM FEI Quanta 650 MLA-FEG with two parallel Bruker X-Flash 6130 EDS detectors and the software version of the MLA 3.1 program by FEI located at TU Bergakademie Freiberg.

The BSE-images taken with the SEM are in grey-scale. Bright areas are minerals with high density (e.g. zircon, monazite, barite) and the darker areas are minerals with lower density (e.g. feldspar, quartz). The MLA was set to distinguish between different phases based on BSE-values for different areas on one grain. The epoxy resin that forms the mounds was measured with the EDS detectors, the spectrum was collected and it was classified as background. BSE-images were taken with a lower boundary to exclude measurements from the epoxy resin. The epoxy resin has a density of 25-30, and therefore the lower boundary for measurements was set to be 30.

The EDS detectors were used to collect spectrums from minerals in the samples. The data program “MLA Measurement 3.1” was used for measuring the samples and collecting an x-ray spectrum. “Bruker Esprit” was used for analysing the x-ray spectrums and identifying the mineral type. This program has a database of minerals with typical wt% of each element. Each mineral identified was saved into a standard spectra list, so the standard spectra list was collected and specified from the samples. “MLA Mineral Reference Editor 3.1” was used for creating and editing the standard spectra list. When several different minerals were collected and saved to the spectra list a quick automated scan was applied. The minerals not identified in this first scan were placed in a group called unknown. The EDS detector and the data programs were used again to identify the unknown minerals. When all unknown minerals were identified a high-resolution automated scan was applied to the samples using the updated standard spectra list of minerals. During the automated scan spectrums from grains/phases were compared to the standard spectra list.

Before starting the high-resolution scan several calibrations were performed. On the sample holder there was standards of gold, silver, copper and quartz. For every new run/scan the gold standard was measured and it was calibrated for brightness and contrast. The gold was used to calibrate the grey levels, because gold has the highest brightness. The grey level was set to 254. Every week it is also calibrated for silver, copper and quartz. The working distance (WD) was set to be 12 mm and the focus adjusted. The acceleration voltage was set to 25 kV, and current to 10 ampere. GXMAP mode was applied because then the MLA will classify different phases in one grain. Acquisition time was set to 9 ms, counts to 340 kcps, and dead time to 10 %.

After the high-resolution scan was finished the measurements are processed with "MLA Mineral Editor 3.1". The measured grains were displayed on images with colors, where each color represents one mineral. There was also one color for unknown minerals, low counts and no x-ray areas. Some unknown minerals appeared because grains can contain several phases of different minerals and then there can be areas with mixed spectra, which the MLA cannot identify. Scripts were created in the "MLA Mineral Editor 3.1" to edit the unknown minerals. Small areas classified as unknown were set to change into the host mineral. Another script was created to adjust for cuts in the grains from when the stage shifted position. Low-counts measured values are often dust and were therefore set to be background. Areas where no x-ray spectra has been measured was also set to be background. If grains were lying close to each other a thin line of background was added in between so the software recognizes it as two separate grains.

"MLA Data Viewer 3.1" was used to view the measurements and data and to display and plot the results in diagrams or tables. The program can visualize the modal mineralogy, grain sizes, mineral liberation characteristics, mineral density distribution, frame views and grain and particle line-ups. It can also compare or combine different samples.

2.6 Electron Microprobe Analyser (EMPA)

2.6.1 Theoretical background

2.6.1.1 Instrumentation

Electron Microprobe Analyser (EMPA) is an analytical method and technique for chemical analyses of small areas on samples of solid material. The method is also referred to as only microprobe, electron microprobe (EMP) or electron probe microanalyser (EPMA). The EMPA have much in common with the SEM: electron gun (the source of electrons), electron lenses, vacuum system and specimen stage. The EMPA also have an optical microscope, which the SEM usually does not. An electron beam is focused on the sample and x-rays are excited. The x-ray spectrum contain lines characteristic for each element present in the sample. The x-ray intensities can also be compared to standard samples (pure elements/compounds of known composition) and it can be used to determine the concentrations of the elements quantitatively (Reed, 2005).

2.6.1.3 Wavelength Dispersive Spectrometer (WDS)

A system called Wavelength Dispersive Spectrometer (WDS) is connected to the EMPA. In the WDS the x-rays are dispersed according to their wavelength by Bragg reflection. The WDS system contains an analysing crystal and an x-ray detector (*Figure 2.14*). The crystal is used to detect characteristic wavelengths emitted from the sample (Leng, 2013). The WDS can give high spectral resolution, but usually the intensity for a given beam current is lower than for the EDS. Values obtained with the WDS can range from hundreds to over thousand (for pure elements) and this is often ten times higher than for the EDS, meaning that the WDS has lower elemental detection limits (Reed, 2005).

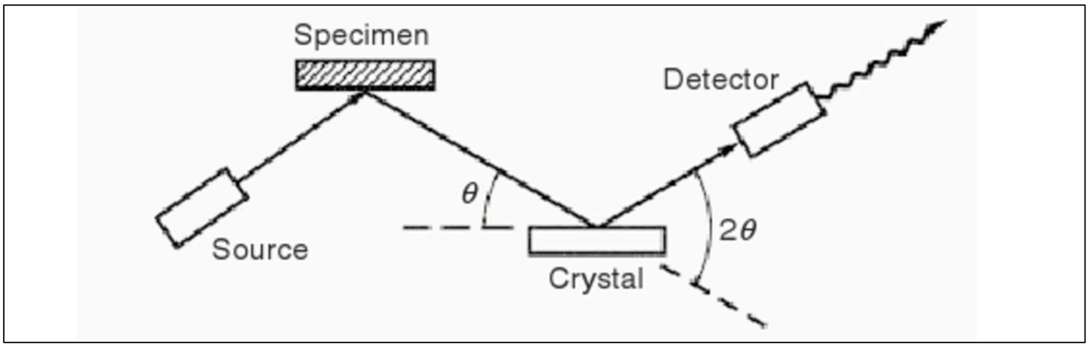

Figure 2.14: Wavelength Dispersive Spectrometer (WDS) with analysing crystal and an x-ray detector (Leng, 2013).

2.6.1.4 Advantages with EMPA

There are several advantages using the EMPA. It is a method that is non-destructive. The accuracy of the quantitative elemental analyses is usually ±1 % for the major elements (Reed, 2005). Sample preparation is minimal, but a well-polished surface is essential for accurate analysis. The detection limits are very low and therefore also minor and trace elements can be detected. The time it takes to analyse each sample is very short, often between 1 and 5 minutes, and the time it takes to switch between samples is also quite short. The spatial resolution is very good (is the order of 1 µm) and allows for most features to be resolved. The EMPA can also determine all elements above atomic number 3 (Reed, 2005).

2.6.2 Purpose of the method

The EMPA can assist with compositional information in mineral identification. Dating of minerals containing Pb, such as monazite, is possible with EMPA. Zoning within mineral grains can also be studied because of the high spatial resolution. EMPA can be used to identify small amounts of an element, it can detect elements with a low atomic number, and it can therefore separate between different types of apatite (e.g. chlorapatite, fluorapatite and hydroxyapatite).

2.6.3 Technical specifications

An Electron Microprobe Analyser (EMPA) at Technische Universität Bergakademie Freiberg (TU Bergakademie Freiberg) in Germany was used in this project. It is a JEOL microprobe JXA 8900 (*Figure 2.15)*. Professor Dr. Bernhard Schulz and Sabine Haser at TU Bergakademie Freiberg performed the analyses. The EMPA was be applied to the magnetic, apatite and zircon fractions of sample 387, 391 and BS for the following minerals: amphibole, tourmaline, garnet, magnetite, ilmenite, rutile, apatite, titanite, chromite and monazite. Several measurements were done on each grain in order to get more correct results.

Figure 2.15: JEOL microprobe JXA 8900 located at TU Bergakademie Freiberg (photo by Sabine Haser).

2.7 Inductively Coupled Plasma Mass Spectrometry (ICP-MS)

2.7.1 Theoretical background

The methodological background for Inductively Coupled Plasma Mass Spectrometry (ICP-MS) with Laser Ablation (LA) and Multi-Collector (MC) is rather wide, but the analytical technique is given in a relatively short section below.

2.7.1.1 Mass spectrometer

The mass spectrometer is used for determination of element concentrations, for surface and isotope analyses and much more. It is a very useful analytical technique because it has a high sensitivity, low detection limits and it can analyse very small volumes of sample material (Becker, 2007). The mass spectrometer consists of a sample introduction system, an ion source, a mass analyser/ion separator, an ion detector and a data processing system (*Figure 2.16*) (Becker, 2007; Westman-Brinkmalm and Brinkmalm, 2008).

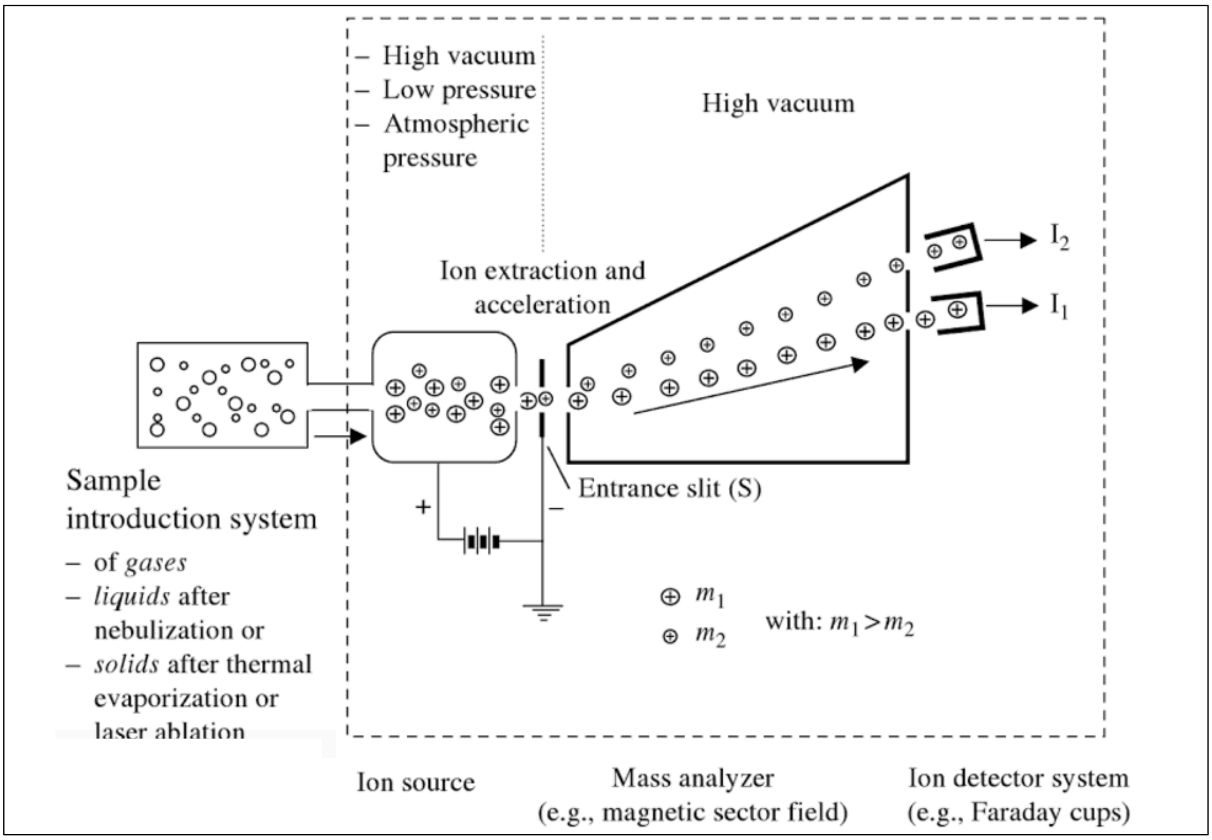

Figure 2.16: Illustration of the components in an ICP-MS-LA-MC (modified after Becker, 2007). First the sample will be in the sample introduction system (e.g. laser ablation), then it will move into the ion source (e.g. inductively coupled plasma), and further it enters the mass analyser/spectrometer, and finally it is detected in the ion detector system (e.g. multi-collector).

2.7.1.2 Sample introduction system: Laser Ablation (LA)

There are several sample introduction methods that can be used in combination with an ion source, e.g. laser ablation (LA). The sample is placed into a chamber, the ablation cell. A laser beam is focused on the sample surface to generate fine particles. Argon gas with atmospheric pressure flows through the ablated sample material, and the sample material is transported with the argon gas to the ion source (Westman-Brinkmalm and Brinkmalm, 2008).

2.7.1.3 Ion source: Inductively Coupled Plasma (ICP)

The ion source in the mass spectrometer generates gas phase ions. There exist several ion sources, e.g. inductively coupled plasma (ICP). It is a plasma source with atomic ions. The ICP-MS is the most used spectrometric technique for analysing inorganic samples. It can be used for measuring isotope ratios and for trace element analyses (Westman-Brinkmalm and Brinkmalm, 2008). The ICP source is build up of a torch and load coil. The sample enters the torch and load coil, and is vaporized, atomized and ionized. Radio frequency energy is applied to the load coil and this is how the plasma gets its energy. The energy is transferred by an electromagnetic field to the outer part of the plasma. The sample is transported with an argon gas flow, and then transferred from the plasma with atmospheric pressure to the mass spectrometer/mass analyser with low pressure (*Figure 2.16*). The gas will expand when entering the mass spectrometer, and ions will be extracted and accelerated. A multi-collector will further detect the ions (Becker, 2007; Westman-Brinkmalm and Brinkmalm, 2008).

2.7.2 Purpose of the method

The ICP-MS can give elemental isotopic ratios and the abundance of isotopes. Zircons have U-Pb isotopes, and these can further be used to date the zircon. Different ages on the different zones/rims in one zircon can indicate several metamorphic events.

2.7.3 Technical specifications

The ICP-MS analyses have been carried out by a laboratory in Porto Alegre in Brazil and are here treated as being out-sourced. U-Pb and Lu-Hf isotope geochemistry using ICP-MS-LA-MC was executed parallel to the other studies based on CL-images of the separated detrital zircon samples. The CL-images show zones/rims in the zircons and these different rims were analysed with isotope geochemistry.

3 RESULTS

The results are divided into the four analytical methods: FE-SEM, XRD, MLA and EMPA. The results are combined and interpreted in chapter 4 “Discussion and implications of the results”. The results from the ICP-MS analyses were delayed and are therefore not included in this thesis (see more in chapter 6 “Further work”).

3.1 Results from FE-SEM

3.1.1 Identification and semi-quantification of heavy minerals

Minerals are identified based on spectrums in *Appendix A*. Heavy minerals identified with the FE-SEM are chamosite, amphibole, tourmaline, garnet (almandine and grossular), magnetite, ilmenite, rutile, titanite, zircon, apatite, barite and monazite. *Table 3.1* contains each mineral type identified and the % of each heavy mineral in each fraction. A table containing all values including non-heavy minerals (minerals with density less than 2.9 g/cm^3, e.g. quartz, feldspar) can be seen in *Appendix B.* Percentages are based on manual spot analysis of 100-300 grains/phases from each fraction. The number of analysed grains/phases can also be seen in *Appendix B*.

Table 3.1: Heavy minerals identified with FE-SEM and EDS detector. Values are in % and represent only % of HM in the sample (minerals with density less than 2.9 g/cm^3 are not included, but can be seen in Appendix B).

			Magnetic fractions					Apatite fractions			Zircon fractions		
#	Color code	Mineral	387	389	391	393	BS	387	391	BS	387	391	BS
5		Chamosite	5,42	20,98	11,64	10,14	3,08				2,33	0,48	
7		Amphibole	0,72	1,40	2,74		1,03						
8		Tourmaline					1,03						
9		Almandine-Mn	3,61	0,70	0,68	4,35	0,51				0,47		
10		Almandine	20,22	30,07	23,97	26,81	6,67		1,92		2,33		
11		Grossular	5,42	2,10	2,05	1,45	13,85						
12		Magnetite	0,36		2,05	0,72	2,05						
13		Magnetite-Ti	5,78	6,99	17,81	13,77	8,21						
14		Ilmenite	0,36	3,50	1,37	3,62	2,56						
15		Rutile	4,33	9,09	4,79	4,35	1,54	0,70			23,72	11,43	4,39
16		Titanite	46,93	21,68	28,08	30,43	42,56	2,10	7,69	2,05	33,49	10,95	53,17
17		Titanite-Fe	0,72	2,10	0,68	3,62	2,56						
18		Zircon	2,53	0,70	1,37		5,13	0,70			32,09	73,81	21,95
19		Apatite-Cl	1,08		0,68		3,08	29,37	25,00	28,08	0,93	1,90	4,39
20		Apatite-F	1,81	0,70			3,59	59,44	63,46	57,53	2,79	1,43	10,24
21		Apatite-OH				0,72	2,56	6,99	1,92	12,33	1,40		5,85
22		Barite	0,72		1,37			0,70			0,47		
23		Monazite-Ce			0,68								
		Total:	100,00	100,00	100,00	100,00	100,00	100,00	100,00	100,00	100,00	100,00	100,00

The five magnetic fractions analysed contain similar minerals. The magnetic fractions contain mostly titanite, almandine, grossular, magnetite, rutile, ilmenite and chamosite (*Table 3.1*). Sample 387, 389, 391 and 393 contain more almandine than grossular. Sample BS contain more grossular than almandine. The apatite fractions contain mostly apatite and small amounts of titanite. The apatites vary in composition, containing chlorine, fluorine or hydroxide. The apatite fractions are quite similar. They contain mostly fluorapatite, some chlorapatite, and less hydroxyapatite. The zircon fractions contain mostly zircon, titanite and rutile. Sample 391 contain mostly zircon, and less titanite, compared to the other two samples 387 and BS.

3.1.2 Garnet measurements with standard

Garnets (almandine and grossular) identified with the FE-SEM and EDS detector were measured one more time with the EDS detector and a standard. Example of an almandine grain and settings used for measuring can be seen in *Figure 3.1*. A small area on the grain were analysed for its chemical composition and compared to a standard, providing more exact results.

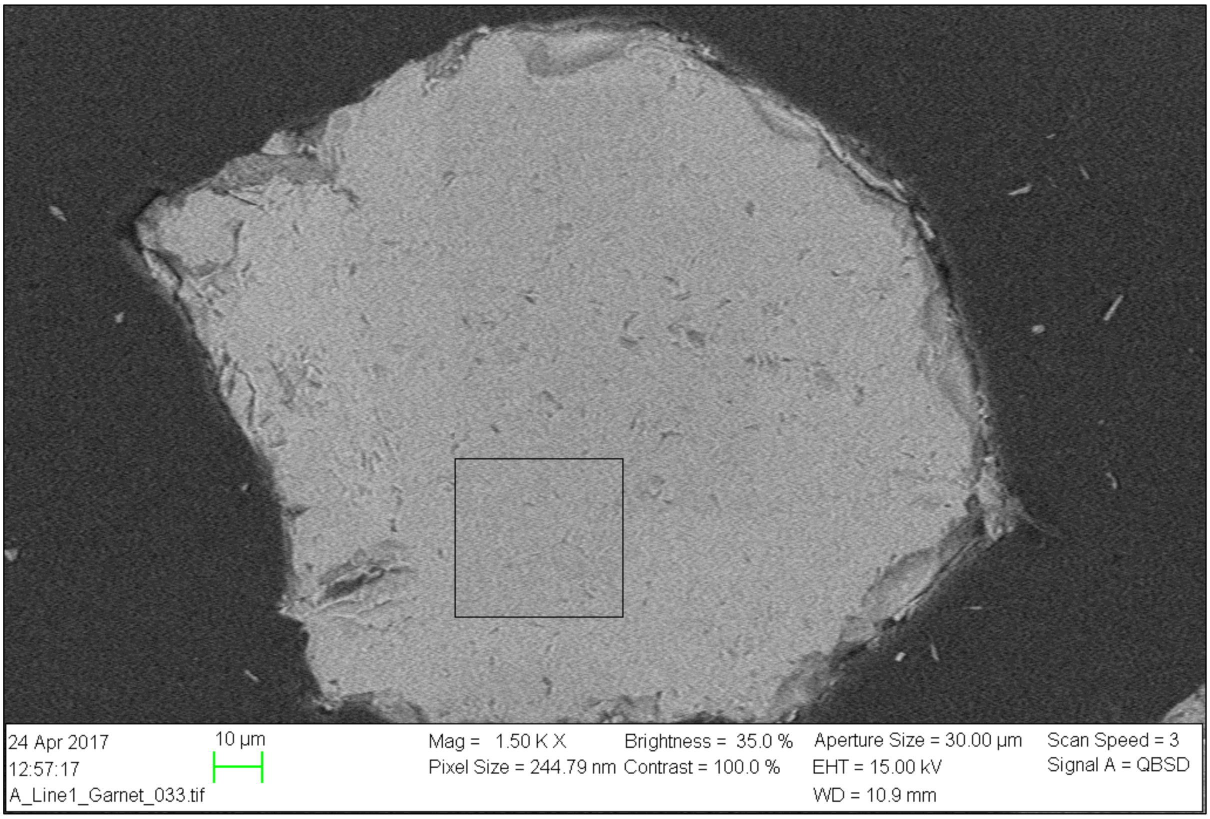

Figure 3.1: Example of an almandine grain (image taken with BSE detector). Settings used for measuring all garnets are: magnification = 1.50 KX, aperture size = 30, EHT = 15.00 kV, WD = 10-11 mm, scan speed = 3.

The ternary plot with garnet measurements in *Figure 3.2* is based on chemical composition values for several garnets analysed with the EDS. All values from the EDS measurements can be seen in *Appendix C*. The garnets analysed are from the magnetic fractions of sample 387, 389, 391, 393 and BS. The garnets are located in two main areas in the ternary plot. Garnets located in one area contain high wt% of iron and manganese, and little magnesium and calcium, and has been classified as almandine. Garnets located in the second area contain high wt% of calcium, some iron and manganese, and no magnesium, and has been classified as grossular.

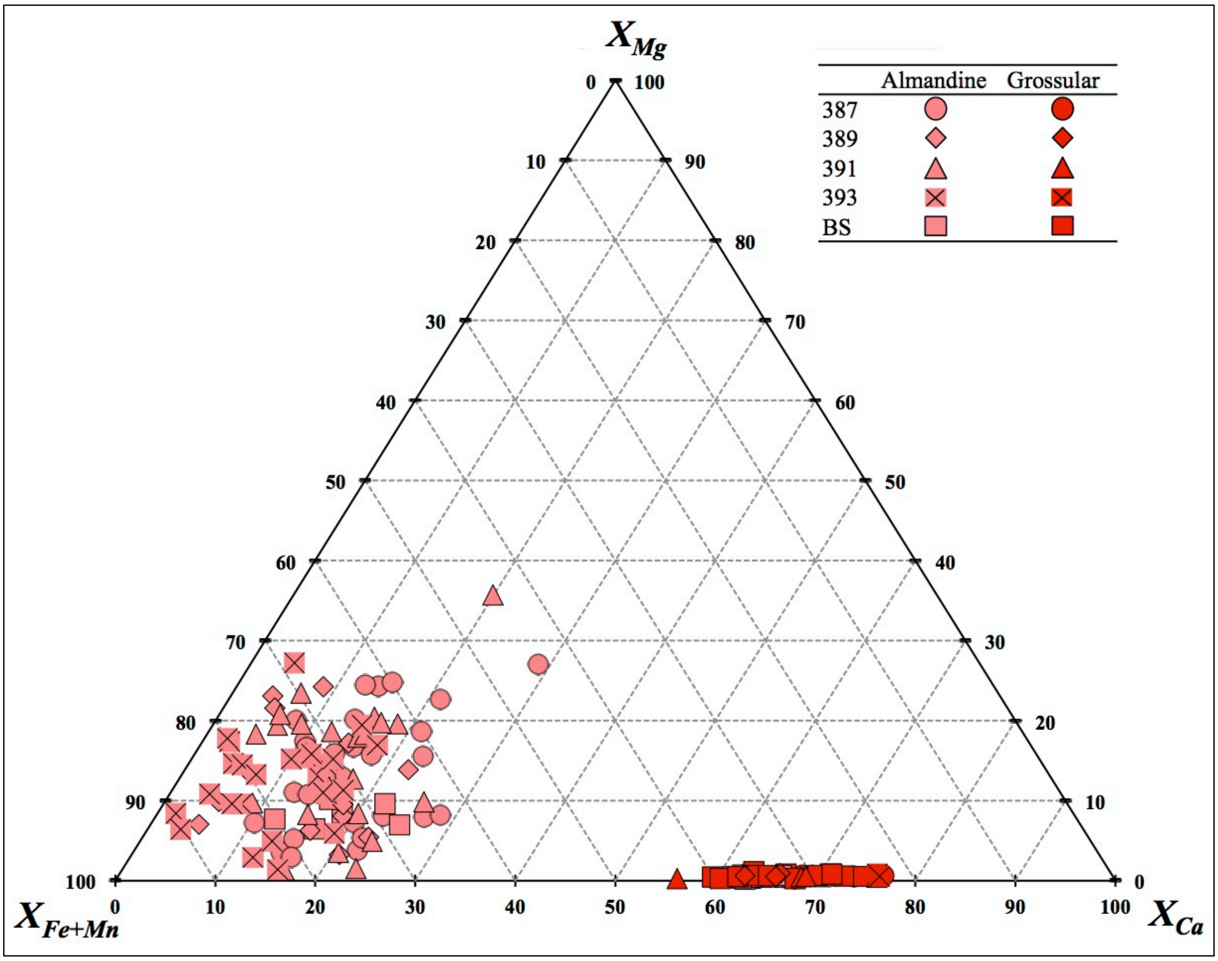

Figure 3.2: Ternary plot of typical garnet assemblages for the five samples. XMg, XCa, XFe+Mn = molecular values of Mg, Ca and Fe+Mn respectively, calculated on the basis of wt% values from the EDS analyses. Values used for this plot can be seen in Appendix C.

3.2 Results from XRD

Heavy minerals identified with the XRD are chamosite, garnet (almandine and grossular), magnetite, rutile, titanite, zircon and fluorapatite (*Table 3.2*). Spectrums from the XRD analyses for each sample and fraction can be seen in *Appendix D*. One example can be seen in *Figure 3.3* (magnetic fraction of sample 387). According to XRD results there is rutile in the samples, and no other polymorphic minerals with the same elemental composition of TiO_2. XRD results also indicate that the sample contain magnetite, and not hematite or other minerals containing only iron and oxygen.

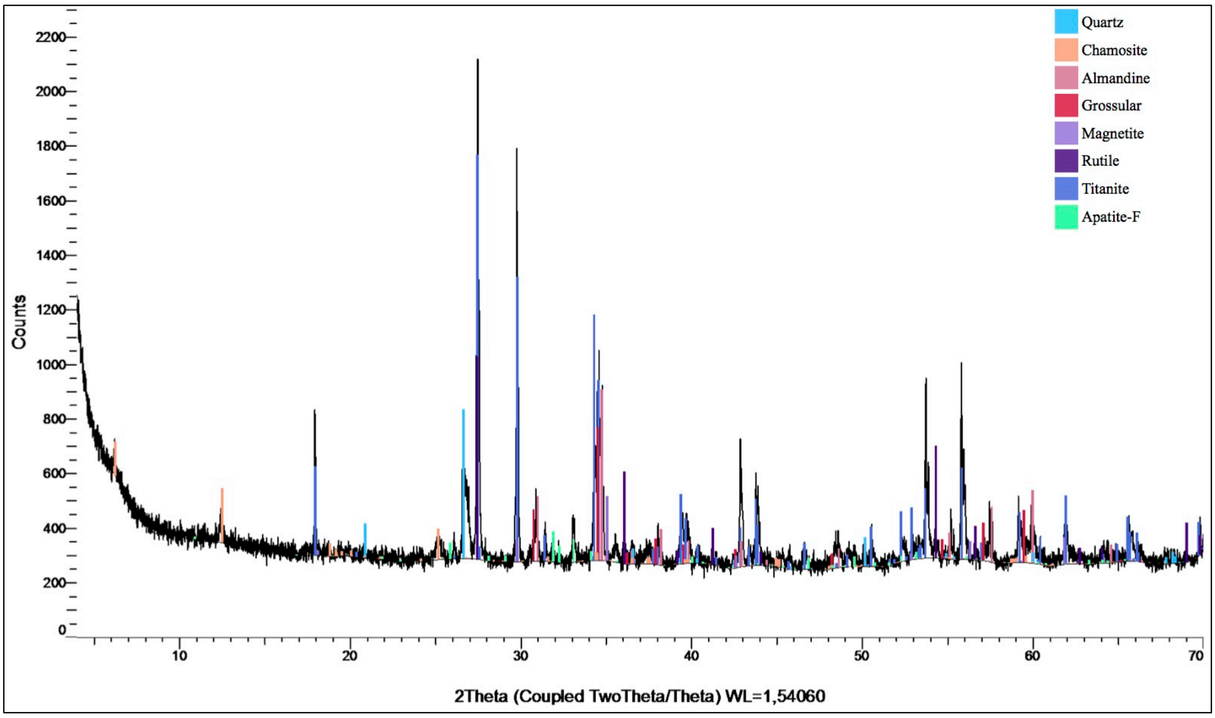

Figure 3.3: XRD spectrum for magnetic fraction of sample 387.

Table 3.2: Minerals identified with the XRD in each sample and fraction.

			Magnetic fractions					Apatite fractions			Zircon fractions			Zircon concentrates		
#	Color code	Mineral	387	389	391	393	BS	387	391	BS	387	391	BS	387	391	BS
1		Quartz	x	x	x	x	x		x							
2		Albite					x									
3		Chamosite	x	x	x	x	x									
4		Muscovite					x									
5		Almandine	x	x	x	x	x									
6		Grossular	x	x		x	x									
7		Magnetite	x	x	x	x	x									
8		Rutile	x	x	x	x					x					
9		Titanite	x	x	x	x	x				x		x			
10		Zircon		x	x		x				x	x	x	x	x	x
11		Apatite-F	x				x	x	x	x			x			x

3.3 Results from MLA

3.3.1 Identified heavy minerals

Minerals are classified based on the mineral list/reference list in *Table 3.3*. Heavy minerals identified with the MLA are chamosite, amphibole, tourmaline, garnet (almandine and grossular), magnetite, ilmenite, rutile, titanite, zircon and apatite. Complete list of all minerals, including minerals with density less than 2.9 g/cm^3 (e.g. quartz, feldspar) and minerals with ~0 wt% can be seen in *Appendix E*. Spectrums were collected for the minerals in the reference list and were compared to measurements of grains in the samples and fractions. Spectrums for the minerals in the reference list can be seen in *Appendix F*.

Table 3.3: Minerals used for the mineral list/reference list for analyses with MLA. Minerals with density less than 2.9 g/cm^3 are not included in this table, and yoderite, spessartine, chromite, barite and monazite has not been included in this table because they are ~0 wt%. The complete table can be seen in Appendix E.

#	Color code	Mineral	Abbreviation	Mineral group	Chemical formula	Density (g/cm3)	Z
5		Chamosite	Chm	Mica	(Fe2+,Mg,Fe3+)5Al(AlSi3)O10(OH,O)8	3,20	14,85
7		Amphibole	Amp	Amphibole	(Na0.5(Na,K)0.5)(Ca(Ca,Na))((Fe2+,Mg)3.5(Fe2+,Mg, Fe3+)Fe3+0.5)(Si5.5Al1.5(Si,Al))O22(OH,F,Cl)2	3,33	15,39
9		Tourmaline	Tur	Tourmaline	NaMg3Al6(BO3)3Si6O18(OH)4	3,10	11,66
10		Almandine-Mn	Alm	Garnet	Fe2+3Al2(SiO4)3	4,20	15,45
11		Almandine-Ca1	Alm	Garnet	Fe2+3Al2(SiO4)3	4,20	14,71
12		Almandine-Ca4	Alm	Garnet	Fe2+3Al2(SiO4)3	4,20	14,75
13		Almandine-Ca5	Alm	Garnet	Fe2+3Al2(SiO4)3	4,20	14,18
14		Almandine-Ca9	Alm	Garnet	Fe2+3Al2(SiO4)3	4,20	13,26
15		Grossular-Fe	Grs	Garnet	Ca3Al2(SiO4)3	3,57	13,80
16		Grossular	Grs	Garnet	Ca3Al2(SiO4)3	3,57	13,39
20		Magnetite	Mag	Spinel	FeO	5,00	21,22
21		Magnetite-Ti	Mag	Spinel	Fe3+2Fe2+O4	5,15	20,67
22		Ilmenite	Ilm	Oxide	Fe2+TiO3	4,72	17,51
23		Rutile	Rt	Oxide	TiO2	4,25	16,16
26		Titanite	Ttn	Neosilicate	CaTiSiO5	3,48	13,81
27		Titanite-Fe	Ttn	Neosilicate	CaTiSiO5	3,48	16,44
28		Zircon	Zrn	Silicate	ZrSiO4	4,65	24,84
29		Apatite	Ap	Phosphate	Ca5(PO4)(F,Cl,OH)	3,19	14,61

Minerals identified with MLA have compositions similar to the compositions of the minerals in the reference list (*Appendix E*). Amphibole has 11.98 wt% Al, 11.32 wt% Ca, 24.51 wt% Fe, 0.82 wt% Mn, 36.60 wt% O, and 14.77 wt% Si. Tourmaline has 21.28 wt% Al, 0.70 wt% Ca, 7.04 wt% Fe, 5.11 wt% Mg, 2.09 wt% Na, 48.17 wt% O, 15.10 wt% Si, and 0.51 wt% Ti.

Almandine garnet has 13.27-14.31 wt% Al, 0.89-9.29 wt% Ca, 11.57-27.68 wt% Fe, 2.36-8.39 wt% Mg, 0.10-2.48 wt% Mn, 35.82-39.72 wt% O, and 15.28-16.62 wt% Si. Grossular garnet has 14.24-16.19 wt% Al, 19.69-19.88 wt% Ca, 7.10-10.00 wt% Fe, 40.77-41.31 wt% O, and 15.11-15.71 wt% Si. The values for the almandine and grossular garnets have been plotted in a ternary plot to better illustrate the differences (*Figure 3.4*). The values used for the ternary plot can be seen in *Appendix G*. The main difference between the almandine and grossular is the amount of calcium compared to the amount of iron and manganese.

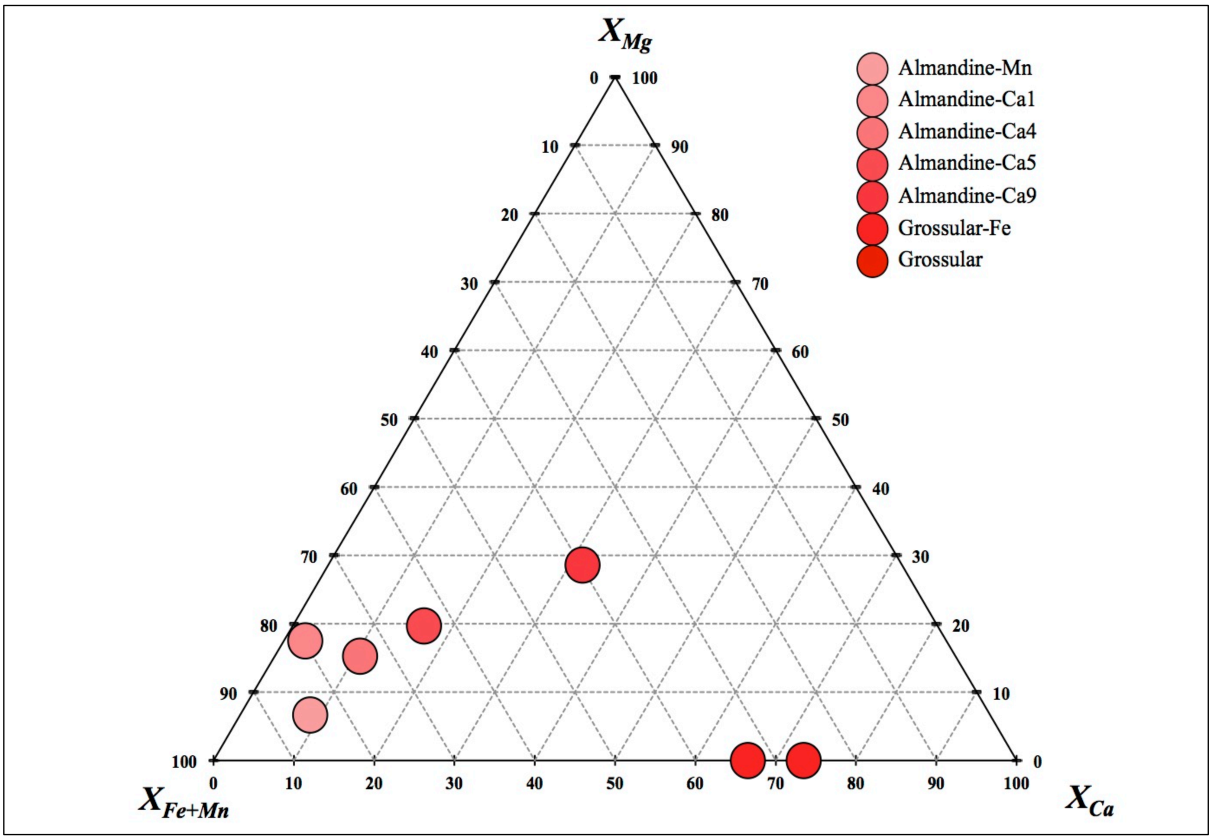

Figure 3.4: Ternary plot of the almandine and grossular garnets in the reference list. XMg, XCa, XFe+Mn = molecular values of Mg, Ca and Fe+Mn respectively, calculated on the basis of wt% values from the MLA analyses. Values used for this plot can be seen in Appendix G.

Magnetite has 65.76-73-21 wt% Fe, 0.00-0.26 wt% Mn, 26.53-28.32 wt% O, and 0.00-5.92 wt% Ti. Ilmenite has 25.26 wt% Fe, 39.30 wt% O, and 35.44 wt% Ti. Rutile has 0.95 wt% Ca, 0.22 wt% Fe, 41.57 wt% O, 0.15 wt% Si, and 57.11 wt% Ti. Titanite has 1.03-2.72 wt% Al, 16.74-19.26 wt% Ca, 1.41-18.15 wt% Fe, 37.09-39.65 wt% O, 0.00-3.64 wt% RE, 8.34-14.20 wt% Si, and 18.16-18.65 wt% Ti. Zircon has 34.91 wt% O, 15.32 wt% Si, and 49.76 wt% Zr. Apatite has 44.59 wt% Ca, 0.06 wt% H, 37.24 wt% O, and 18.11 wt% P.

3.3.2 Quantification of heavy minerals

The representative MLA results are shown in *Table 3.4*. The table contains quantification of each heavy mineral based on wt% of total heavy minerals identified in each sample and fraction. A table containing all values including non-heavy minerals (minerals with density less than 2.9 g/cm^3, e.g. quartz, feldspar) and minerals with ~0 wt% can be seen in *Appendix H*. The magnetic fractions have a very high amount of almandine-Ca (10.82-48.74 wt%) and titanite (18.92-43.00 wt%). In total all almandine and titanite cover over 55 wt% of the heavy minerals in the magnetic fractions. Magnetic fractions of sample 387, 391 and 393 have high amounts of rutile (5.67-8.30 wt%). Magnetic fraction of sample BS has a high amount of grossular (15.22 wt%). Magnetic fractions of sample 391 and 393 have high amounts of magnetite with Ti (9.76-17.64 wt%). All magnetic fractions have less than 4.00 wt% of chamosite, amphibole, tourmaline, ilmenite and zircon. The apatite fractions contain mostly apatite (93.13-97.13 wt%). They also have small amounts of almandine-Ca (0.91-4.11 wt%) and titanite (1.05-1.67 wt%). The zircon fractions contain mostly zircon (25.65-81.79 wt%), rutile (6.10-37.46 wt%) and titanite (4.68-46.77 wt%).

Table 3.4: Minerals identified and quantified with MLA. The values are wt% of HM, meaning that minerals with density less than 2.9 g/cm^3 are not included in this table, and yoderite, spessartine, chromite, barite and monazite has not been included in this table because they are ~ 0 wt%. The complete table can be seen in Appendix H.

			Magnetic fractions					**Apatite fractions**			**Zircon fractions**		
#	**Color code**	**Mineral**	**387**	**389**	**391**	**393**	**BS**	**387**	**391**	**BS**	**387**	**391**	**BS**
5		Chamosite	1,78	3,86	1,88	1,61	1,82	0,14	0,18	0,14	0,15	0,17	0,07
7		Amphibole	1,81	3,44	1,81	2,22	1,71	0,04	0,18	0,03	0,01	0,01	0,02
9		Tourmaline	0,20	0,29	0,04	0,11	2,10	0,02	0,05	0,35	0,02	0,01	0,22
10		Almandine-Mn	1,98	4,76	3,18	4,44	1,25	0,02	0,24	0,03	0,02	0,02	0,04
11-14		Almandine-Ca (total)	24,99	48,74	22,20	29,36	10,82	1,21	4,11	0,91	0,91	0,73	0,56
15-16		Grossular (total)	5,32	5,12	1,97	2,75	15,22	0,03	0,02	0,06	0,01	0,03	0,06
20		Magnetite	2,38	1,36	7,37	8,16	3,52		0,01				0,01
21		Magnetite-Ti	3,03	3,18	17,64	9,76	2,88		0,01			0,02	
22		Ilmenite	0,52	0,89	2,18	2,25	0,78				0,24	0,06	
23		Rutile	8,30	3,30	7,32	5,67	1,23	0,24	0,44		37,46	11,14	6,10
26		Titanite	43,00	18,92	27,04	28,52	40,59	1,05	1,55	1,67	23,04	4,68	46,77
27		Titanite-Fe	2,15	2,06	4,43	4,24	2,84	0,02	0,04	0,02	0,10	0,04	0,24
28		Zircon	1,73	3,53	2,57	0,73	1,78	0,10	0,04	0,02	34,80	81,79	25,65
29		Apatite	2,81	0,55	0,37	0,18	13,46	97,13	93,13	96,77	3,24	1,31	20,26
		Total	100,00	100,00	100,00	100,00	100,00	100,00	100,00	100,00	100,00	100,00	100,00

All the grains placed in the mounds have been identified and classified with colors representing the different types of minerals. BSE-images of each fraction have been taken and colors have been applied to illustrate the mineral distribution. An example can be seen in *Figure 3.5* and images for other fractions can be seen in *Appendix I*. The color representing each mineral can be seen in *Table 3.3*.

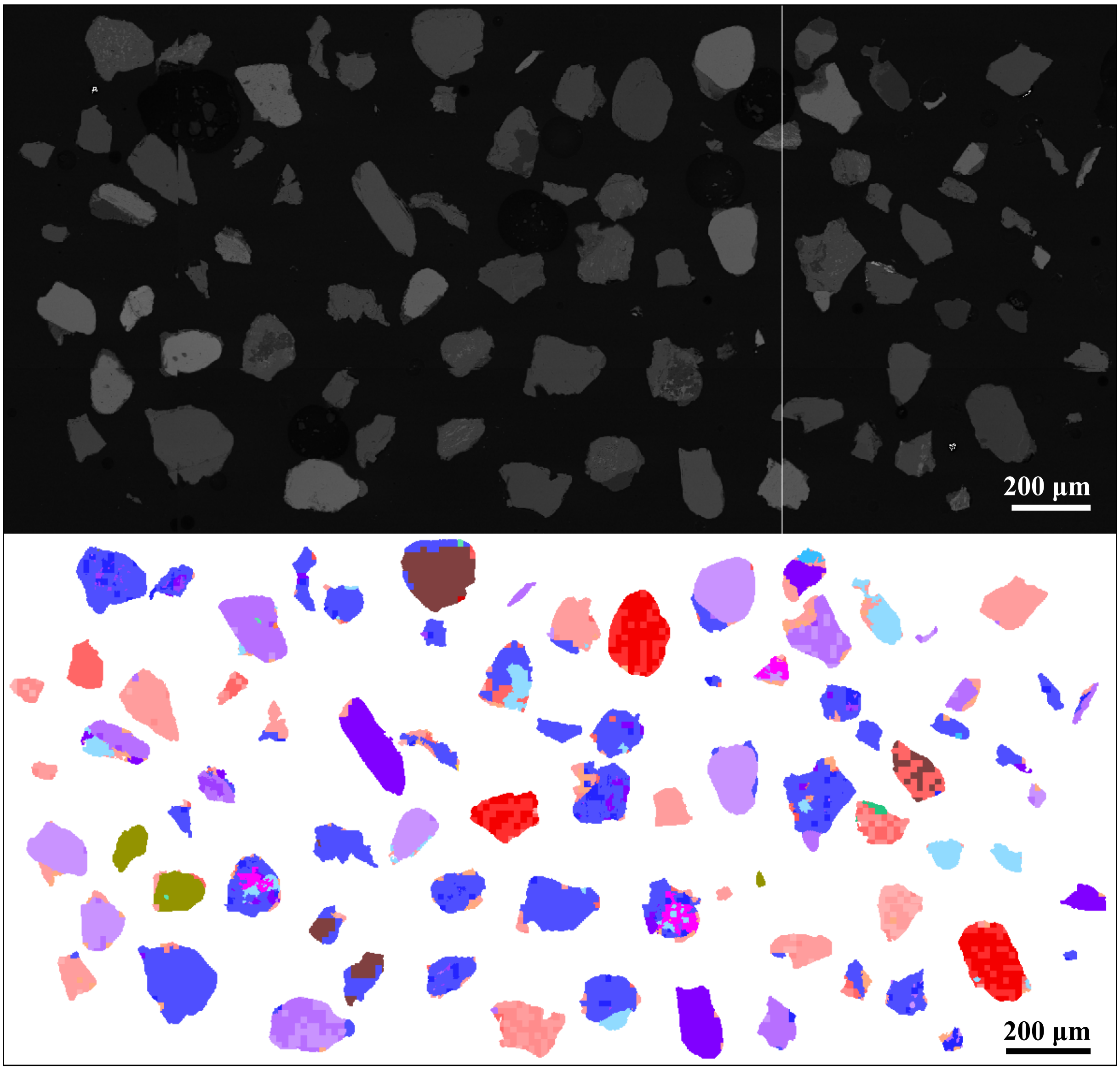

Figure 3.5: BSE-image and processed image from MLA. Image shows processed/identified grains from magnetic fraction of sample 391 where each color represents one type of mineral (legend in Table 3.3). BSE-images and processed images of grains from all fractions can be seen in Appendix I.

3.3.3 Grain shape

The BSE-images and processed images of grains analysed with MLA are used to identify the shape of the grains. Classification scheme by Powers (1953) was used to describe the roundness and sphericity. The magnetic fractions consist of heavy mineral grains that are mostly sub-rounded to angular. The larger grains in the magnetic fractions have usually high sphericity and the smaller grains have low sphericity. Some grains in the magnetic fractions were not polished good enough, and therefore the MLA were not always able to "see" the entire grain. Some grains therefore have very strange shapes in the processed images because the epoxy resin (background color) is lying above parts of the grain. This was considered when evaluating the grain shapes. The almandine grains are mostly sub-angular, some are sub-rounded and fewer are angular (*Figure 3.6*). The grossular grains are mostly sub-rounded to sub-angular, but some are also rounded and angular (*Figure 3.7*).

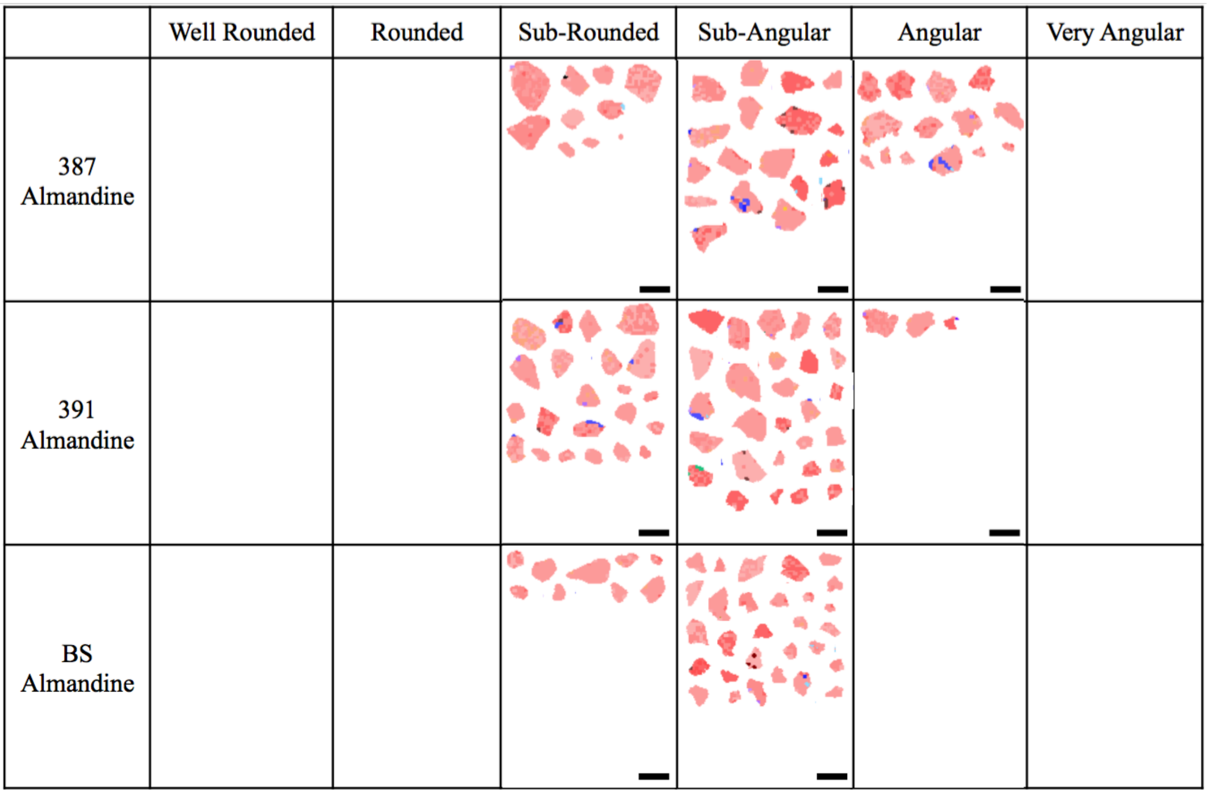

Figure 3.6: A representative selection of almandine grains from magnetic fractions of sample 387, 391 and BS. Scales are 150 µm. All grains can be seen in Appendix I and J.

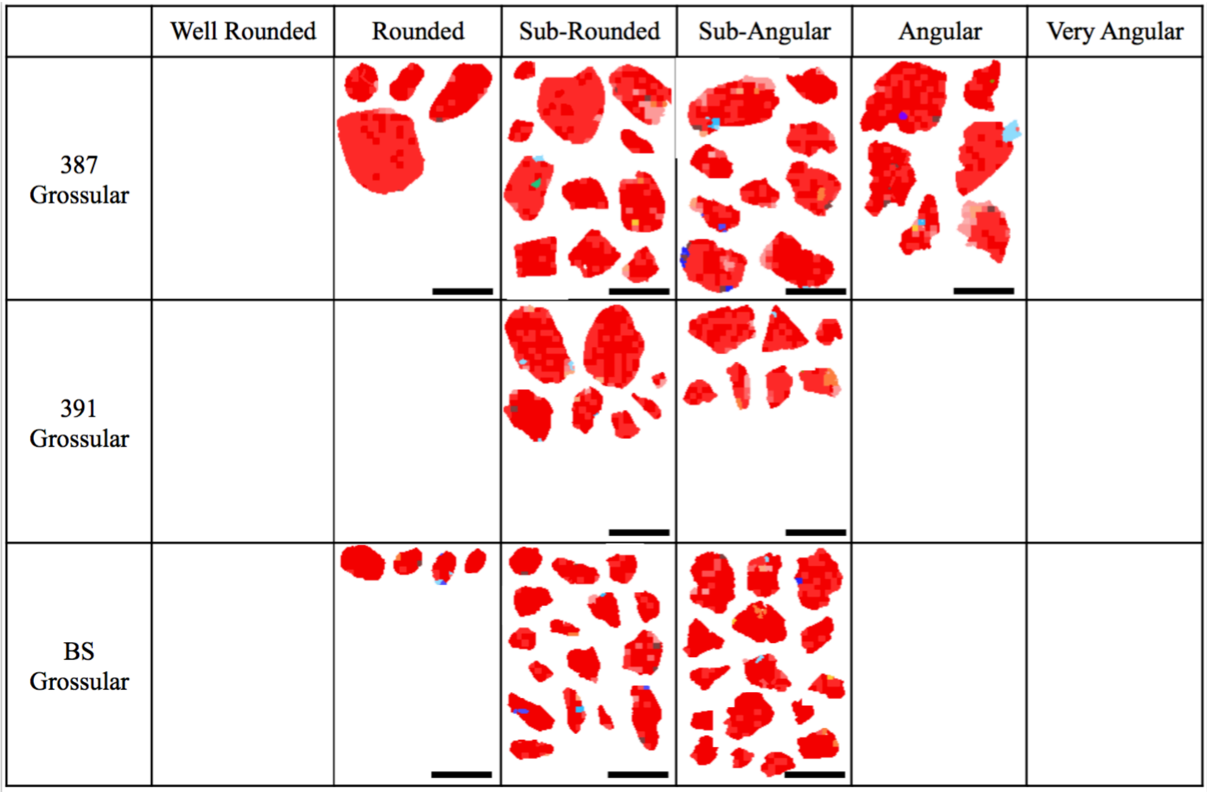

Figure 3.7: A representative selection of grossular grains from magnetic fractions of sample 387, 391 and BS. Scales are 150 µm. All grains can be seen in Appendix I and J.

The apatite fractions consist of heavy mineral grains that are mostly rounded to subrounded. The apatite fractions contain grains that have both high and low sphericity, but most have high sphericity. The apatite grains are mostly rounded to sub-rounded, but some are also well rounded (*Figure 3.8*).

The zircon fractions consist of heavy mineral grains that are mostly rounded to subangular. The zircon fractions also have both high and low sphericity grains, but it is mostly the zircons that have low sphericity and the other minerals have high sphericity. The zircon grains are mostly subrounded, but some are also rounded (*Figure 3.9*). The rutile grains are mostly sub-rounded, some are rounded and some are sub-angular (*Figure 3.10*).

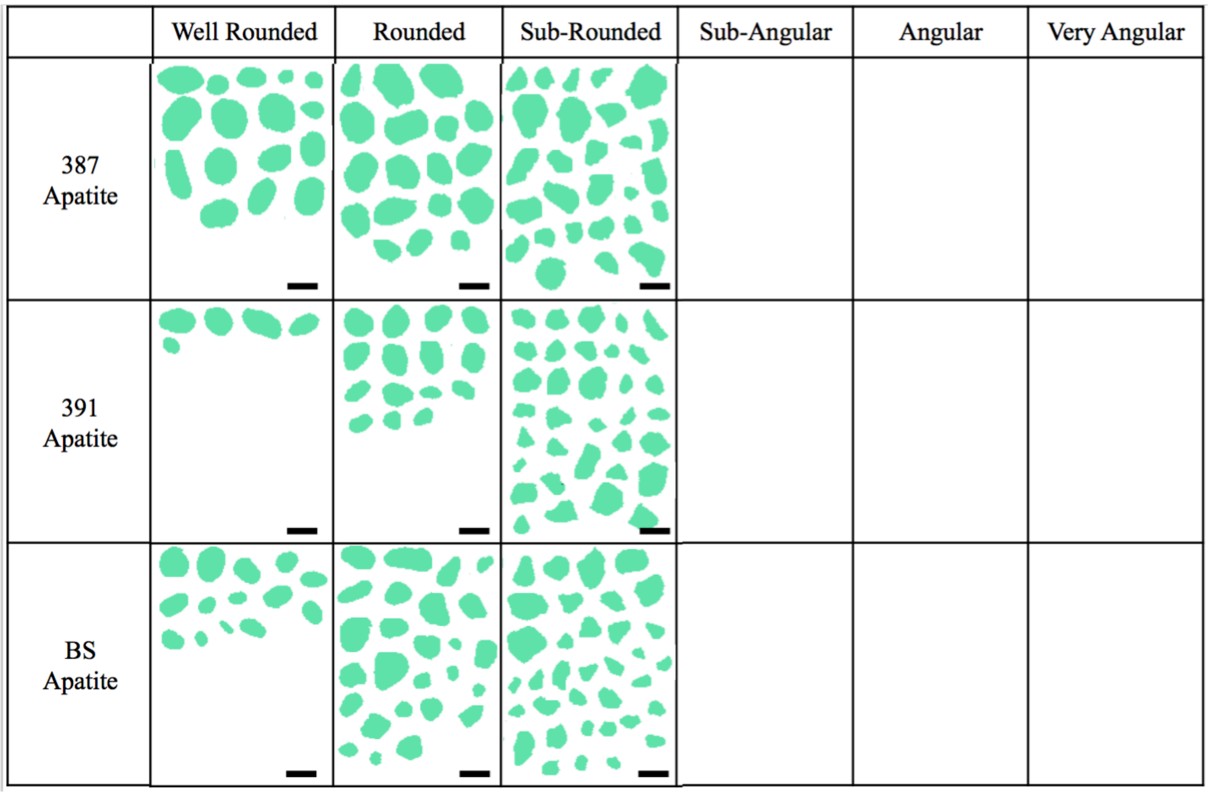

Figure 3.8: A representative selection of apatite grains from apatite fractions of sample 387, 391 and BS. Scales are 150 µm. All grains can be seen in Appendix I and J.

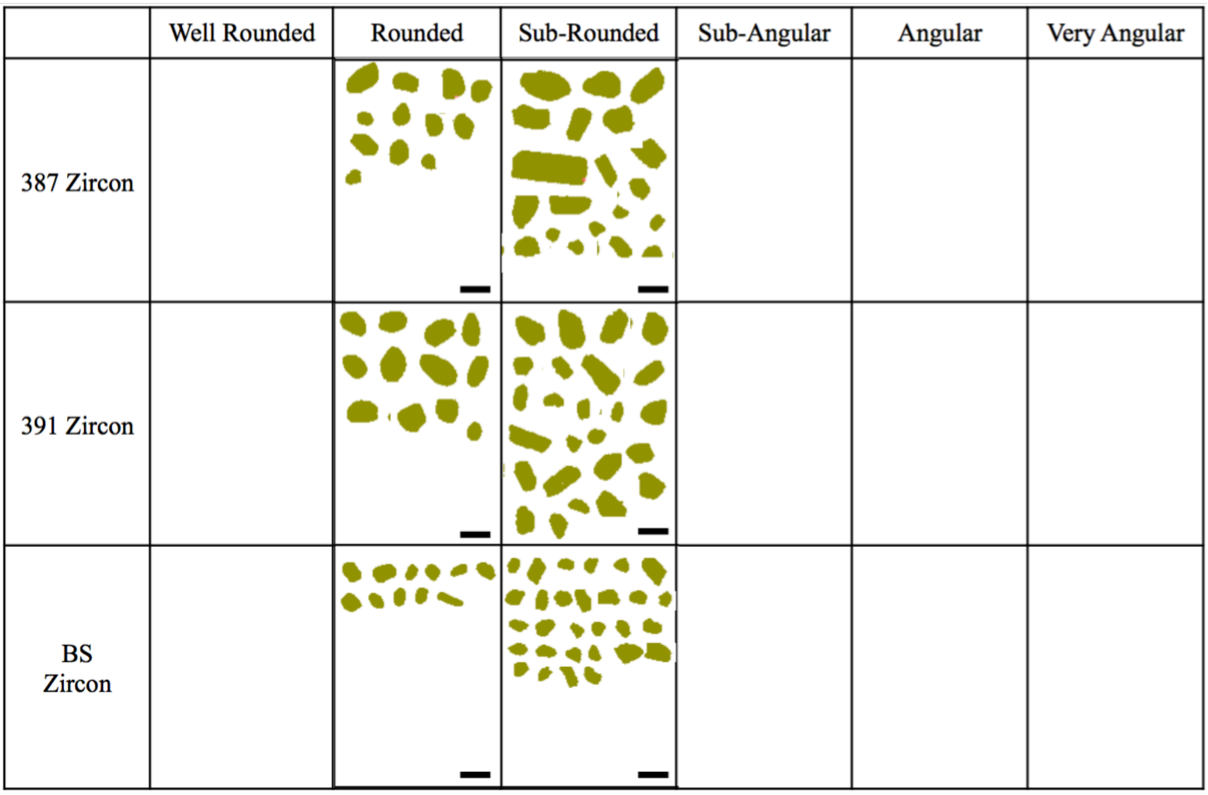

Figure 3.9: A representative selection of zircon grains from zircon fractions of sample 387, 391 and BS. Scales are 150 µm. All grains can be seen in Appendix I and J.

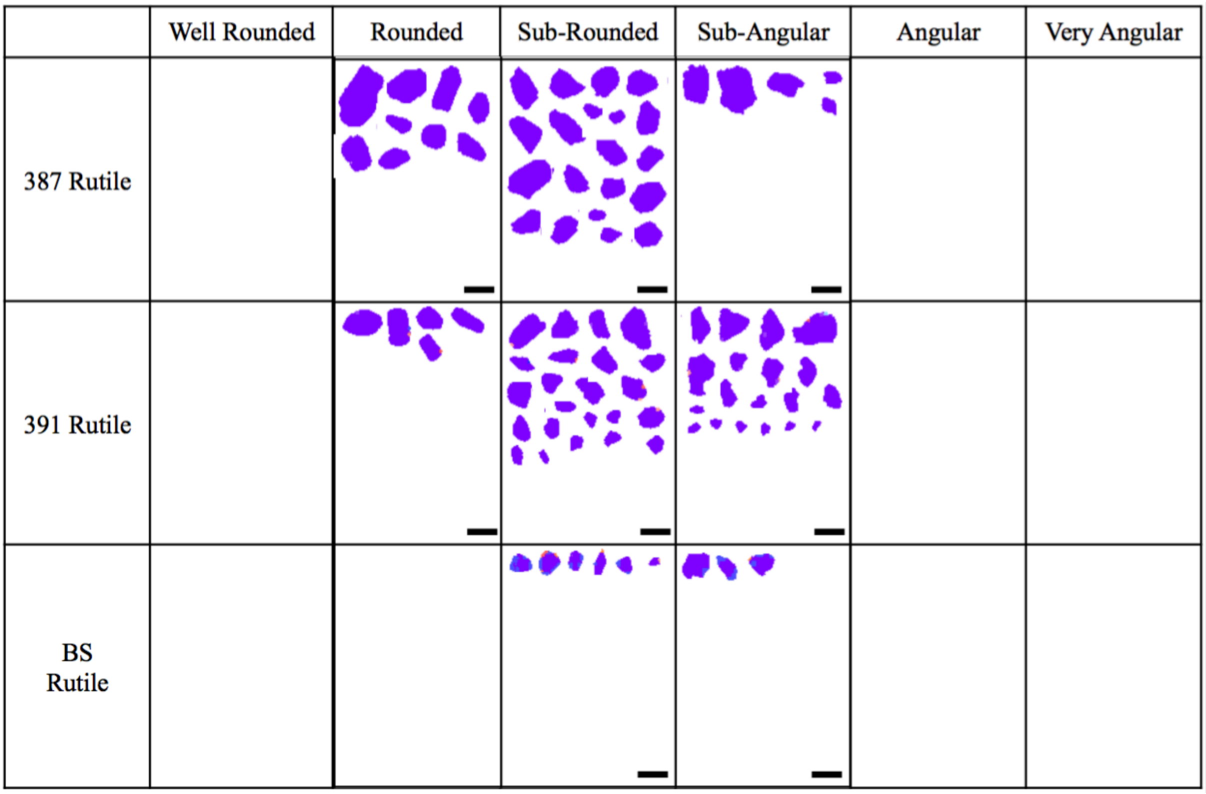

Figure 3.10: A representative selection of rutile grains from zircon fractions of sample 387, 391 and BS. Scales are 150 µm. All grains can be seen in Appendix I and J.

3.3.4 Particle size and particle density distribution

Particle sizes were calculated with the MLA and are displayed in *Table 3.5*. Particle sizes are not divided into the different types of minerals, but represent all particles/grains for each fraction. Wenworth size class was added to the table. *Table 3.5* include the cumulative passing wt%, but tables in *Appendix K* also includes cumulative retained wt% and retained wt%. The magnetic fractions have particles sizes from medium silt to medium sand (sieve size 16-300 µm). The apatite fractions have particle sizes from medium silt to medium sand (sieve size 22-300 µm). The zircon fractions have particles sizes from fine silt to medium sand (8.1-300 µm). The particle size distribution for the magnetic fractions are similar, but with small differences. The general particle size for each fraction increases in the following order: 389, BS, 391, 393, 387 (*Figure 3.11*). For both the apatite fraction and zircon fraction the general particle size for each fraction increases in the same order: BS, 391, 387 (*Figure 3.12* and *3.13*).

Table 3.5: Particle size distribution for all fractions with cumulative passing wt%, sieve size (um) and Wenworth size class.

	Cumulative passing wt%											
Sieve Size (um)	Magnetic fractions					Apatite fractions			Zircon fractions			
	387	389	391	393	BS	387	391	BS	387	391	BS	Wenworth size class
300	100,00			100,00					100,00			Medium sand
250	99,44		100,00	98,18	100,00	100,00	100,00		98,79			Medium sand
212	96,17		97,76	96,14	98,21	97,73	96,72	100,00	97,03	100,00		Fine sand
180	85,81	100,00	94,72	86,78	97,04	80,83	91,27	97,36	85,37	98,12	100,00	Fine sand
150	62,23	99,09	76,89	70,10	89,08	48,00	73,62	80,53	70,22	88,60	98,29	Fine sand
125	38,72	90,13	57,07	49,01	77,41	20,95	42,39	59,79	45,19	65,88	92,78	Fine sand
106	22,94	68,57	41,96	31,90	59,87	8,54	26,52	36,65	29,56	41,41	77,68	Very fine sand
90	11,56	42,82	30,57	20,10	41,03	3,43	13,59	17,76	17,06	25,00	51,97	Very fine sand
75	5,62	20,33	20,06	10,97	23,76	1,27	5,09	6,85	7,94	12,55	27,88	Very fine sand
63	2,94	8,39	12,69	6,11	12,32	0,34	2,42	1,59	3,62	6,49	12,01	Very fine sand
53	1,39	4,08	6,68	3,21	6,22	0,08	0,81	0,43	1,58	3,22	5,82	Coarse silt
45	0,68	2,04	3,44	1,69	3,33	0,03	0,24	0,09	0,73	1,45	2,77	Coarse silt
38	0,41	1,23	1,96	0,72	1,43	0,00	0,12	0,04	0,26	0,62	1,12	Coarse silt
32	0,24	0,72	0,96	0,32	0,77		0,05	0,04	0,12	0,30	0,27	Coarse silt
27	0,15	0,37	0,46	0,15	0,39		0,01	0,00	0,10	0,14	0,15	Medium silt
22	0,06	0,15	0,11	0,07	0,12		0,00		0,06	0,02	0,10	Medium silt
19	0,02	0,05	0,05	0,03	0,04				0,05	0,00	0,06	Medium silt
16	0,00	0,00	0,00	0,00	0,00				0,02		0,04	Medium silt
13,5									0,01		0,00	Fine silt
11,4									0,01			Fine silt
9,6									0,00			Fine silt
8,1												Fine silt

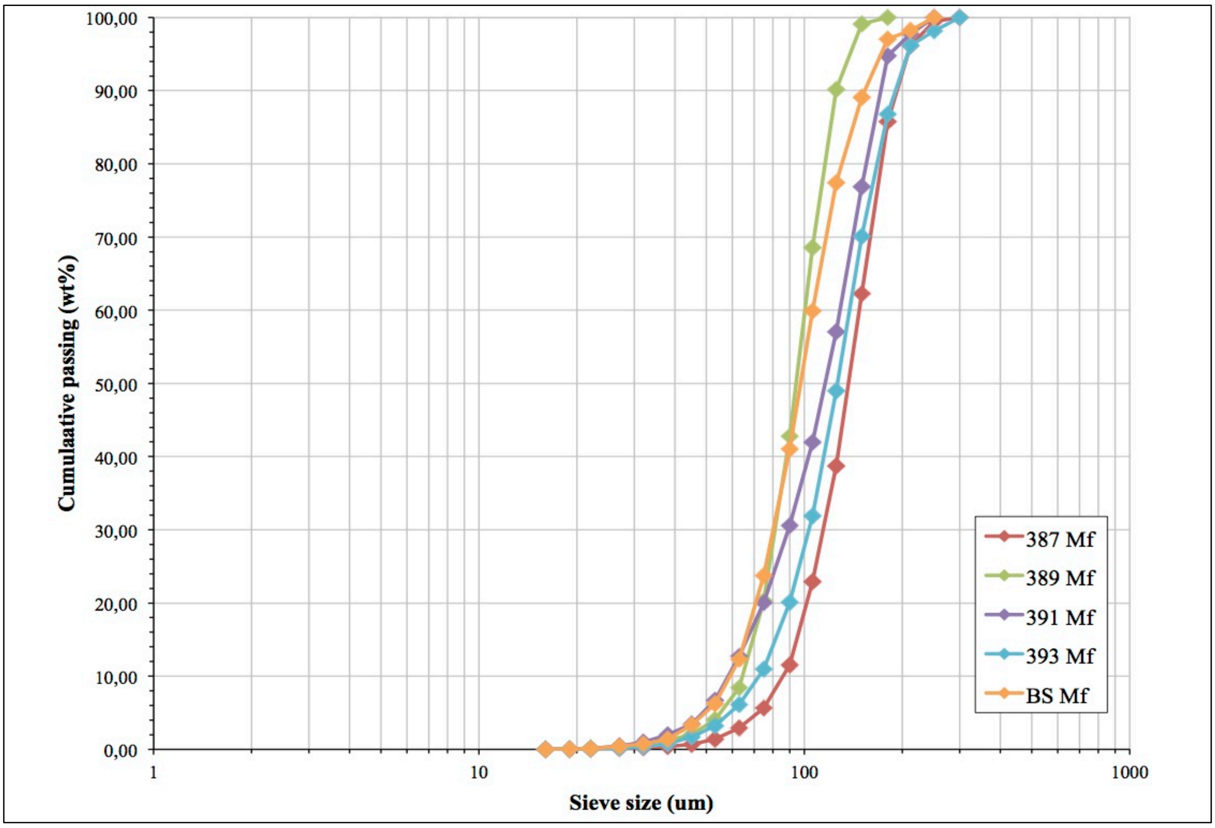

Figure 3.11: Particle size distribution of magnetic fractions. Values used for the plot are in Appendix K.

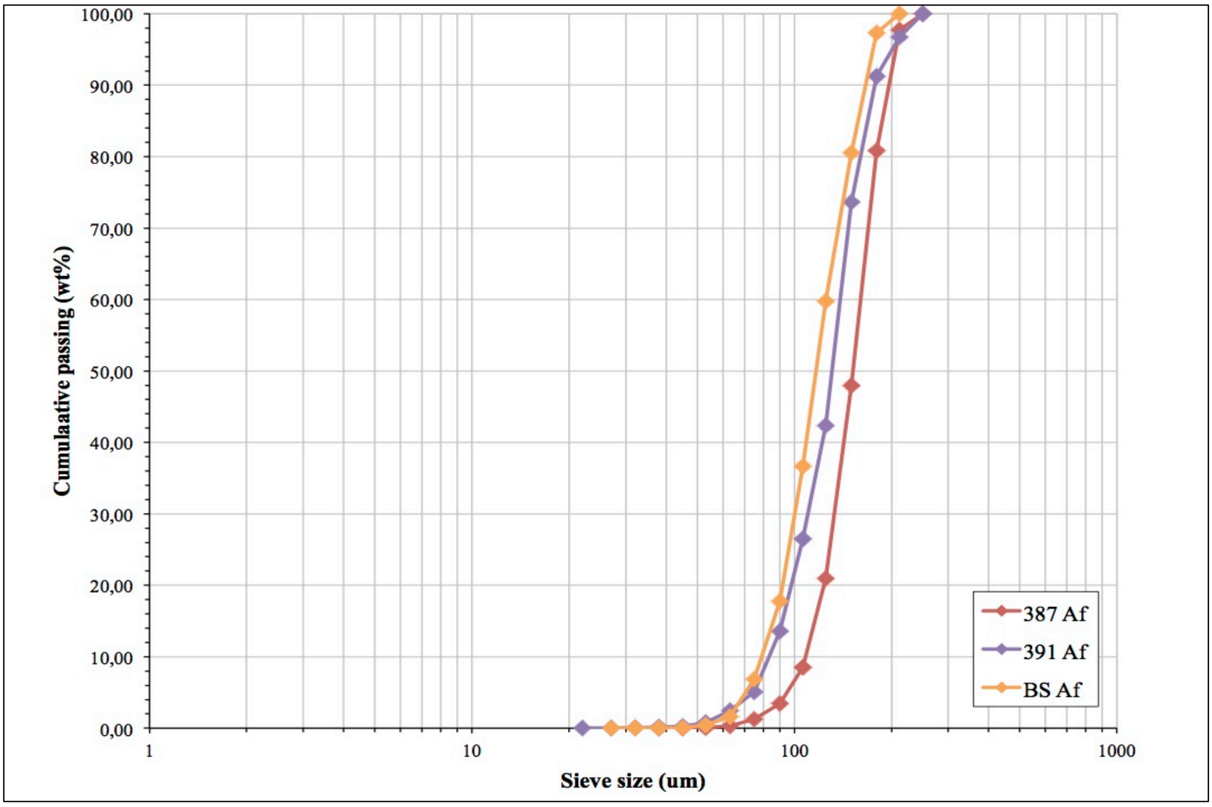

Figure 3.12: Particle size distribution of apatite fractions. Values used for the plot are in Appendix K.

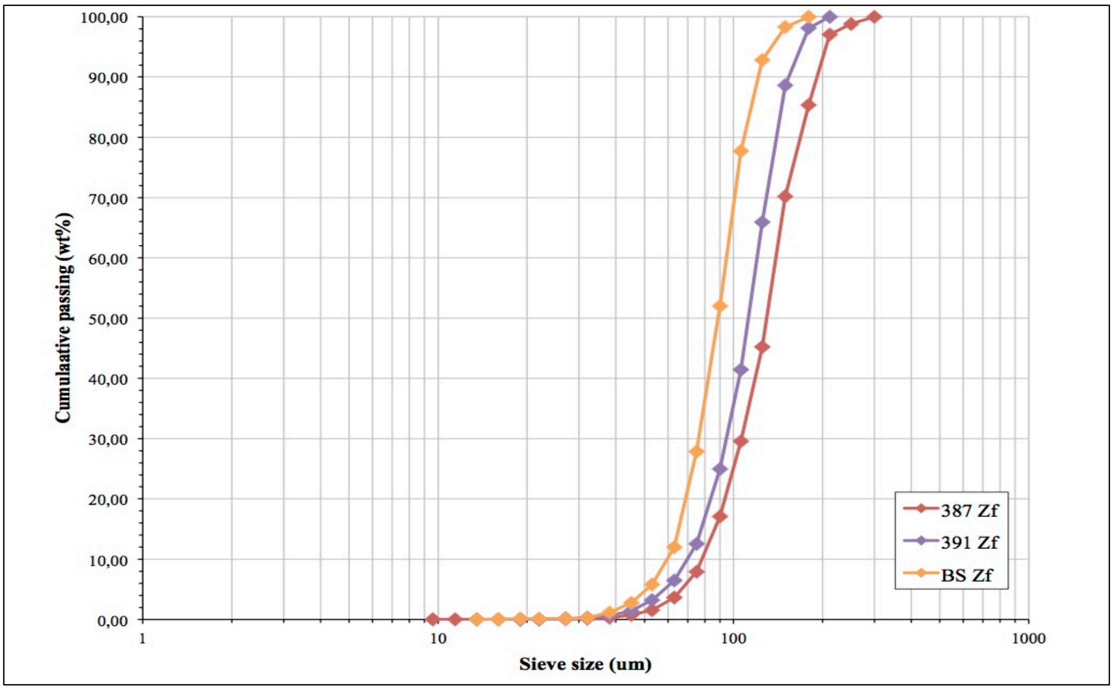

Figure 3.13: Particle size distribution of zircon fractions. Values used for the plot are in Appendix K.

MLA provides particle density distributions for all fractions. *Table 3.6* shows the densities that are most representative for the different fractions (complete list can be seen in *Appendix K*). Most particles in the magnetic fraction have a density of 3.3-3.7 g/cm^3 or 4.1-4.3 g/cm^3. Most particles in the apatite fractions have a density of 3.1-3.3 g/cm^3. Most particles in the zircon fractions have a density of 3.4-3.5 g/cm^3, 4.2-4.3 g/cm^3 or 4.6-4.7 g/cm^3.

Table 3.6: Representative list of particle density distribution for all fractions with weight of particles (%) and density of the particles (g/cm^3). Complete list can be seen in Appendix K.

	Weight of particles (%)										
	Magnetic fractions					Apatite fractions			Zircon fractions		
Density Distribution	**387**	**389**	**391**	**393**	**BS**	**387**	**391**	**BS**	**387**	**391**	**BS**
3.1 < D <= 3.2	1,46	1,51	0,75	0,54	13,28	80,13	30,57	81,26	2,19	1,08	15,53
3.2 < D <= 3.3	2,82	0,78	1,03	0,39	8,58	14,90	18,86	16,67	1,24	0,08	5,81
3.3 < D <= 3.4	4,04	2,80	1,33	2,87	9,63	2,07	0,52	0,34	0,47	0,11	3,54
3.4 < D <= 3.5	20,34	5,90	9,23	8,94	22,64	0,77	0,23	0,34	19,91	4,03	37,31
3.5 < D <= 3.6	21,66	11,29	13,80	12,61	17,23	0,08	0,00	0,00	2,43	0,16	2,11
3.6 < D <= 3.7	6,24	8,43	6,97	8,61	4,74	0,00	0,00		0,31	0,05	0,94
3.7 < D <= 3.8	4,07	5,66	3,61	4,52	2,00	0,00	0,00		0,00	0,20	2,45
3.8 < D <= 3.9	3,15	5,23	3,50	4,64	1,67	0,00	0,00		0,00	0,16	1,63
3.9 < D <= 4.0	4,36	5,12	3,02	3,89	1,00	0,00	0,00		0,27	0,00	1,01
4.0 < D <= 4.1	2,40	4,06	2,44	6,40	0,89	0,00	0,00		0,18	0,08	1,13
4.1 < D <= 4.2	12,52	28,38	14,96	19,28	5,11	0,00	0,00		2,13	0,15	1,40
4.2 < D <= 4.3	8,48	2,20	7,11	6,41	1,03	0,25	0,09		35,54	11,04	2,21
4.3 < D <= 4.4	0,53	0,02	0,87	0,96	0,52	0,00	0,00		0,34	0,39	0,75
4.4 < D <= 4.5	1,43	0,90	2,14	0,55	0,12				1,17	1,44	2,29
4.5 < D <= 4.6	0,81	0,52	2,61	2,01	0,46				5,07	8,03	4,14
4.6 < D <= 4.7	1,48	3,54	4,20	2,71	1,18				28,63	72,72	16,83

3.3.5 Grain size distribution

Grain sizes for each mineral type in each fraction were calculated with the MLA and one example can be seen in *Figure 3.14*. The figure compares the cumulative passing wt% and the sieve size (µm) for all mineral types in magnetic fraction of sample BS. *Appendix L* includes tables with mineral grain size distributions for all samples and fractions. Zircon grains have very different sizes in the zircon fractions for the different samples (*Figure 3.15*). The zircon grains increases in size in the following order: BS, 391, 387.

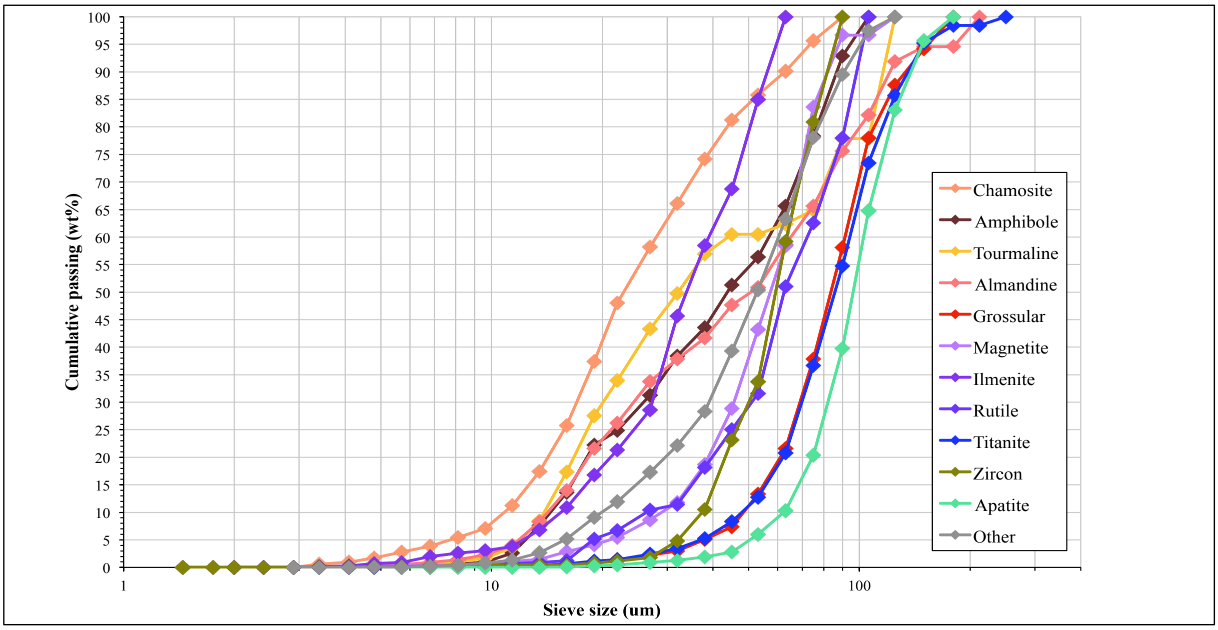

Figure 3.14: Example of a mineral grain size distribution (magnetic fraction of sample BS). Values used for the plot are in Appendix L.

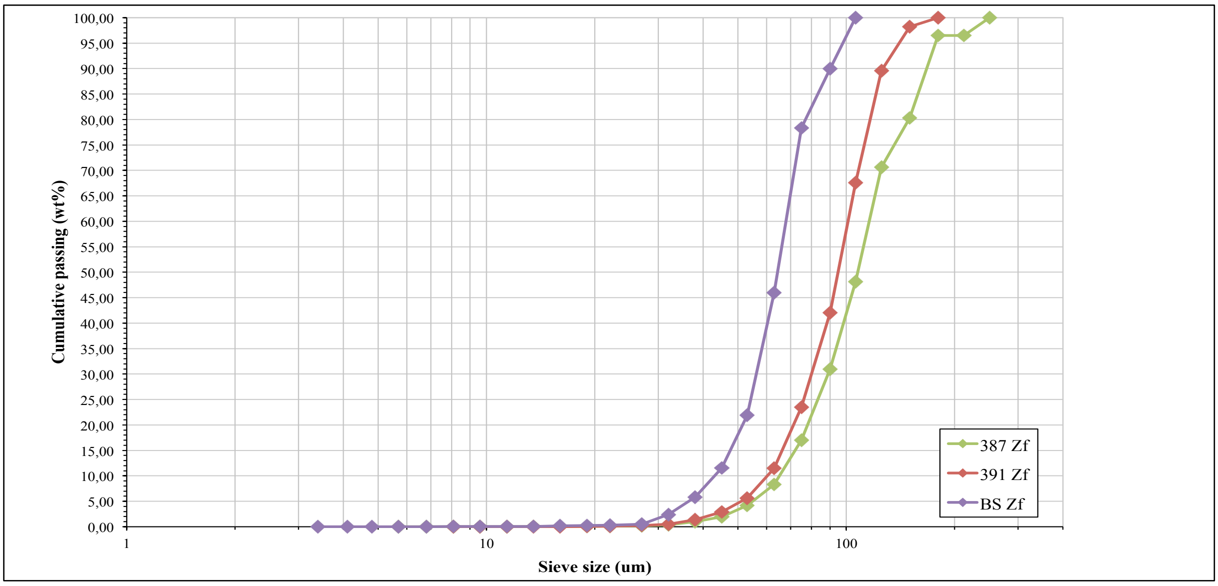

Figure 3.15: Grain size distributions of zircons from zircon fractions of sample 387, 391 and BS. Values used for the plot are in Appendix L.

3.3.6 Sorting

The BSE-images and processed images of grains analysed with MLA are used to distinguish the sorting. Sorting is described according to classification scheme by Longiaru (1987). All magnetic fractions are moderately to poorly sorted. The apatite fractions are well to moderately well sorted and the zircon fractions are moderately well to moderately sorted. An example of sorting of each of the fractions can be seen in *Figure 3.16*. BSE-images can be seen in *Appendix I* and processed images for all samples and fractions were grains are sorted according to particle size can be seen in *Appendix J*.

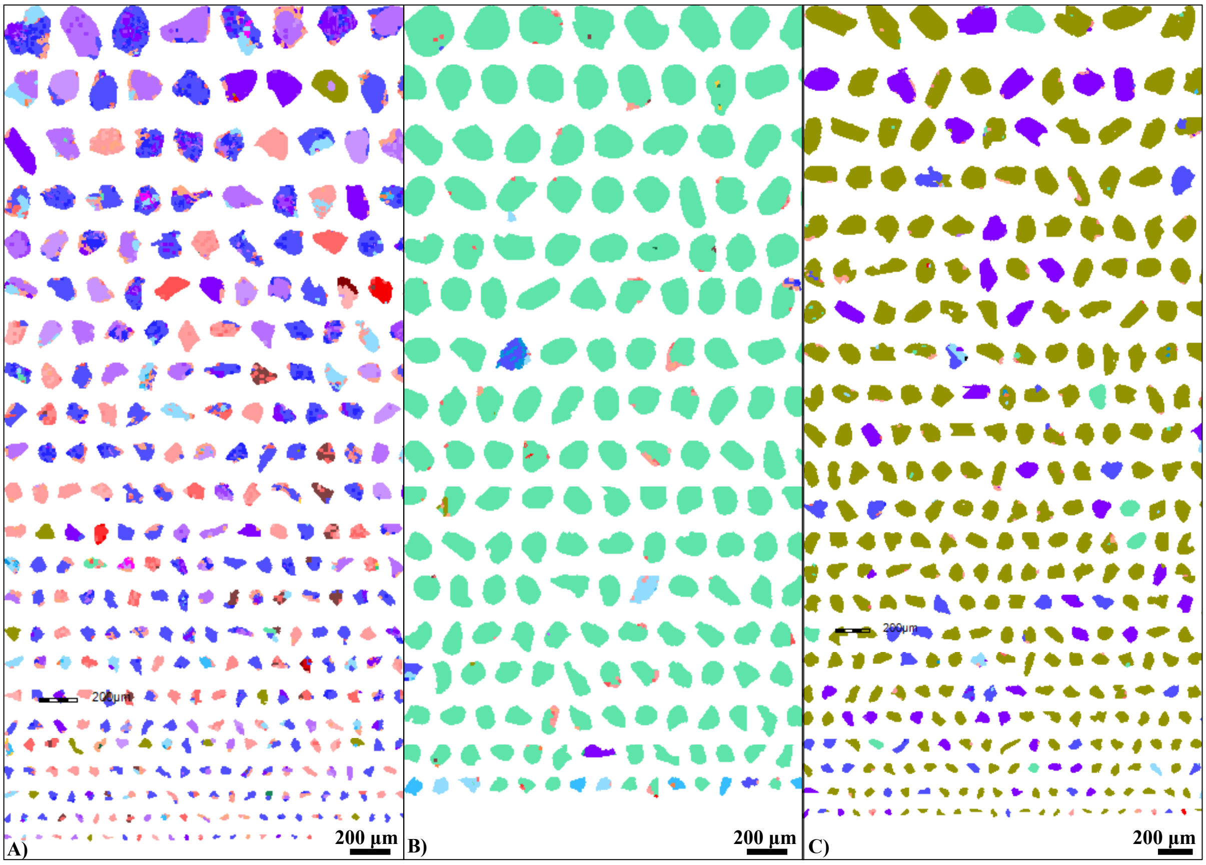

Figure 3.16: Examples of sorting. A) Some grains from the magnetic fraction of sample 391. B) Some grains from the apatite fraction of sample 387. C) Some grains from the zircon fraction of sample 391. All grains are sorted by particle size. Legend for the colors can be seen in Table 3.3. All images of the grains can be seen in Appendix J.

3.4 Results from EMPA

Minerals identified with EMPA are amphibole, rutile, ilmenite, magnetite, garnet, tourmaline and titanite. They were identified based on their chemical composition. In total 65 grains were analysed from the magnetic and zircon fractions of sample 387, 391 and BS. The chemical composition for each grain was measured usually 3-5 times to get more accurate results. The representative EMPA results are shown in *Table 3.7*. The table shows the identified grains with only one measurement per grain (all measurements are shown in *Appendix M*).

The amphibole has the following composition according to EMPA results: 0.01 wt % Na_2O, 6.09 wt % MnO, 0.58 wt% MgO, 9.77 wt% CaO, 24.81 wt% FeO, 19.81 wt% Al_2O_3, and 36.99 wt% SiO_2. Rutile consists of ~100 wt% TiO_2, ilmenite consists of 12.76 wt% TiO_2 and 77.67 wt% FeO, and magnetite consists of 5.49-46.00 wt% TiO_2 and 44.89-84.60 wt% FeO according to EMPA results.

Garnets have the following compositions according to EMPA results: 0.04-3.64 wt % MnO, 0.00-9.15 wt% MgO, 0.72-23.30 wt% CaO, 8.38-34.90 wt% FeO, 20.02-24.86 wt% Al_2O_3, and 36.83-39.49 wt% SiO_2. Two main types of garnets have been identified: almandine and grossular. Tourmalines have a composition of: 1.86-2.18 wt % Na_2O, 3.03-7.77 wt% MnO, 5.09-12.49 wt% FeO, 29.29-30.94 wt% Al_2O_3, 35.37-36.24 wt% SiO_2, and 10.5 wt% B_2O_3. The composition of titanites are: 31.59-44.12 wt % TiO_2, 24.55-28.95 wt% CaO, 0.13-2.60 wt% FeO, 0.73-3.08 wt% Al_2O_3, and 25.25-30.78 wt% SiO_2.

Ternary plots are created for garnet, titanite and tourmaline grains to better illustrate their chemical composition (*Figure 3.17*). Values for the ternary plots can be seen in *Appendix N*. The ternary plot for garnets is based on their composition of Mg, Ca, Fe and Mn. The ternary plot for titanites is based on their composition of Ti, Al and Fe. The two ternary plots for tourmalines are based on their composition of Al, Ca, Mg and Fe.

*Table 3.7: EMPA results with identified grains and one measurement per grain (all measurements are shown in Appendix M). * Tourmaline: Add 10.5 wt% B_2O_3 to the sum. ** Magnetite: Something is wrong with the wt%-values, since the sum is below 90.0 wt%. According to the scientists performing the analyses with EMPA it might be water and Fe^{2+}, as Fe^{3+} is not considered. The FeO (Fe^{2+}) could be Fe_3O_4 (Fe^{3+}).*

Sample/ fraction	Grain name/ measurement number	No.	wt%											Mineral type
			Na2O	K2O	MnO	TiO2	MgO	CaO	FeO	Cr2O3	Al2O3	V2O3	SiO2	Total	
387 Mf	AMf387-Il1-1	173	0,00	0,01	0,09	12,76	0,00	0,02	77,67	0,06	0,06	0,52	0,00	91,19	Ilmenite
387 Mf	AMf387-T1-1	177	0,00	0,00	0,12	38,57	0,00	27,92	0,91	0,05	0,93	0,83	30,24	99,57	Titanite
387 Mf	AMf387-T2-1	181	0,03	0,02	0,21	35,35	0,01	25,87	1,40	0,00	1,12	0,68	29,94	94,64	Titanite
387 Mf	AMf387-G2-1	189	0,00	0,00	0,21	0,01	8,86	0,96	29,75	0,04	21,00	0,02	38,73	99,59	Garnet
387 Mf	AMf387-G3-1	193	0,00	0,00	1,13	0,11	7,06	5,80	26,37	0,03	20,02	0,04	38,65	99,21	Garnet
387 Mf	AMf387-Rt1-1	197	0,00	0,00	0,01	100,77	0,00	0,02	0,28	0,10	0,01	2,51	0,00	101,19	Rutile
387 Mf	AMf387-G4-1	201	0,03	0,00	0,68	0,04	7,03	2,46	29,25	0,00	20,48	0,01	38,68	98,66	Garnet
387 Mf	AMf387-Rt2-1	205	0,04	0,00	0,00	101,45	0,00	0,04	0,13	0,06	0,04	2,42	0,00	101,76	Rutile
387 Mf	AMf387-Rt3-1	209	0,00	0,00	0,05	99,22	0,00	0,03	0,34	0,02	0,08	2,49	0,00	99,76	Rutile
387 Mf	AMf387-G4-1	213	0,00	0,01	0,27	0,13	0,00	22,84	11,38	0,00	21,67	0,07	38,07	94,44	Garnet
387 Mf	AMf387-T3-1	217	0,00	0,01	0,00	36,62	0,00	26,55	1,24	0,00	1,30	0,71	29,39	95,82	Titanite
387 Mf	AMf387-T4-1	221	0,00	0,02	0,04	42,59	0,00	25,98	1,45	0,05	0,92	0,92	27,58	99,56	Titanite
BS Mf	AMf-BS-T1-1	233	0,03	0,00	0,10	38,66	0,00	27,93	0,60	0,03	1,17	0,84	30,34	99,70	Titanite
BS Mf	AMf-BS-T2-1	235	0,01	0,00	0,09	38,69	0,00	28,43	0,76	0,00	1,15	0,86	30,72	100,72	Titanite
BS Mf	AMf-BS-G2-1	238	0,02	0,00	0,23	0,07	0,08	23,20	10,65	0,00	23,04	0,09	38,01	95,39	Garnet
BS Mf	AMf-BS-G3-1	241	0,00	0,00	0,09	0,07	0,05	23,28	11,08	0,00	22,32	0,00	38,11	94,99	Garnet
BS Mf	AMf-BS-G4-1	245	0,02	0,01	0,25	0,08	8,04	1,09	30,88	0,02	20,49	0,03	38,82	99,72	Garnet
BS Mf	AMf-BS-Tu1-1	249	2,18	0,03	0,01	0,52	7,77	0,98	6,85	0,00	29,29	0,03	36,24	83,93	Tourmaline*
BS Mf	AMf-BS-G5-1	253	0,00	0,00	0,13	0,08	9,15	1,06	29,16	0,01	20,90	0,05	39,49	100,02	Garnet
BS Mf	AMf-BS-Tu2-1	256	1,86	0,03	0,00	0,87	7,05	0,78	5,09	0,12	30,94	0,13	36,23	83,10	Tourmaline*
BS Mf	AMf-BS-G6-1	260	0,00	0,02	0,32	0,08	0,03	22,67	10,04	0,05	22,99	0,06	38,14	94,38	Garnet
BS Mf	AMf-BS-Tu3-1	262	1,94	0,04	0,10	0,39	3,03	0,34	12,49	0,02	30,53	0,00	35,37	84,26	Tourmaline*
BS Mf	AMf-BS-G7-1	265	0,00	0,01	0,04	0,17	0,07	23,30	8,38	0,00	24,86	0,00	38,49	95,34	Garnet
BS Mf	AMf-BS-T3-1	268	0,00	0,00	0,08	38,66	0,00	28,67	0,51	0,00	1,24	0,82	30,52	100,51	Titanite
391 Mf	EMf391-T1-4	209	0,00	0,00	0,02	43,17	0,00	25,53	2,60	0,05	0,73	1,00	27,84	100,95	Titanite
391 Mf	EMf391-A1-2	211	0,12	0,00	3,64	0,08	2,64	8,44	25,53	0,00	20,51	0,05	38,01	99,01	Garnet
391 Mf	EMf391-M1-3	216	0,00	0,00	0,10	5,49	0,00	0,01	84,60	0,06	0,06	0,24	0,12	90,68	Magnetite**
391 Mf	EMf391-G2-2	219	0,02	0,01	0,42	0,02	7,81	1,60	29,68	0,00	21,37	0,00	38,58	99,51	Garnet
391 Mf	EMf391-R1-1	221	0,00	0,00	0,06	100,19	0,00	0,05	0,20	0,15	0,07	2,47	0,00	100,72	Rutile
391 Mf	EMf391-M2-1	224	0,00	0,00	0,31	46,00	0,05	0,06	44,89	0,08	0,06	1,06	0,95	93,44	Magnetite**
391 Mf	EMf391-G3-2	229	0,01	0,00	1,60	0,00	5,26	3,14	29,81	0,09	20,83	0,02	38,14	98,92	Garnet
391 Mf	EMf391-M3-1	233	0,00	2,14	0,03	15,78	0,31	0,03	64,89	0,02	2,93	0,34	5,45	91,92	Magnetite**
391 Mf	EMf391-M4-1	237	0,00	0,03	0,09	14,98	0,00	0,00	75,91	0,00	0,01	0,53	0,00	91,55	Magnetite**
391 Mf	EMf391-R2-1	242	0,02	0,02	0,00	103,05	0,00	0,02	0,63	0,04	0,02	2,03	0,00	103,80	Rutile
391 Mf	EMf391-G4-1	245	0,00	0,00	0,14	0,00	8,69	0,72	30,17	0,00	21,37	0,03	38,82	99,95	Garnet
391 Mf	EMf391-T2-1	250	0,02	0,00	0,05	42,00	0,00	26,81	1,41	0,05	0,84	0,90	28,42	100,49	Titanite
391 Mf	EMf391-T3-1	254	0,01	0,02	0,06	35,78	0,00	28,79	0,75	0,08	3,08	0,77	30,78	100,10	Titanite
391 Mf	EMf391-G5-1	258	0,00	0,01	0,07	0,13	0,03	23,00	9,29	0,00	24,43	0,01	38,05	95,02	Garnet
391 Mf	EMf391-R3-1	262	0,00	0,01	0,02	102,50	0,00	0,01	0,19	0,16	0,01	2,21	0,00	102,90	Rutile
391 Mf	EMf391-A2-1	265	0,01	0,00	6,09	0,05	0,58	9,77	24,81	0,02	19,81	0,06	36,99	98,20	Amphibole
391 Mf	EMf391-R4-1	271	0,00	0,01	0,00	101,73	0,00	0,03	0,33	0,06	0,01	2,12	0,00	102,17	Rutile
391 Mf	EMf391-T4-1	274	0,00	0,01	0,07	36,71	0,00	28,04	1,15	0,02	1,60	0,76	30,03	98,39	Titanite
391 Mf	EMf391-G6-1	278	0,05	0,00	0,35	0,00	6,90	1,35	31,02	0,02	21,36	0,03	38,05	99,14	Garnet
391 Mf	EMf391-R5-1	283	0,04	0,00	0,04	101,33	0,00	0,02	0,20	0,11	0,07	2,35	0,04	101,86	Rutile
391 Mf	EMf391-M5-1	287	0,03	0,01	0,06	11,70	0,00	0,01	79,34	0,08	0,02	0,56	0,00	91,81	Magnetite**
391 Mf	EMf391-G7-1	291	0,01	0,00	0,55	0,07	8,44	6,94	22,91	0,10	21,25	0,02	39,05	99,34	Garnet
391 Mf	EMf391-T5-1	295	0,03	0,00	0,00	44,12	0,00	24,55	1,81	0,00	1,20	0,93	26,85	99,48	Titanite
391 Mf	EMf391-R6-1	300	0,00	0,00	0,03	101,17	0,00	0,01	0,48	0,06	0,03	2,20	0,03	101,81	Rutile
391 Mf	EMf391-G8-1	304	0,01	0,01	0,65	0,05	4,43	1,06	34,73	0,04	20,88	0,04	37,59	99,48	Garnet
391 Mf	EMf391-G9-1	308	0,01	0,00	0,56	0,08	8,09	2,62	27,78	0,04	21,45	0,05	38,81	99,48	Garnet
391 Mf	EMf391-G10-1	312	0,01	0,01	3,20	0,01	1,68	2,10	34,90	0,07	20,37	0,05	36,83	99,22	Garnet
387 Zf	CZf387-R1-1	389	0,00	0,00	0,00	100,59	0,00	0,01	0,08	0,15	0,02	2,15	0,00	102,99	Rutile
387 Zf	CZf387-T1-1	392	0,00	0,00	0,03	39,99	0,00	28,73	0,32	0,00	0,91	0,87	30,36	101,21	Titanite
387 Zf	CZf387-R2-1	395	0,03	0,01	0,03	100,00	0,00	0,02	0,25	0,06	0,00	2,22	0,00	102,62	Rutile
387 Zf	CZf387-T2-1	398	0,00	0,00	0,06	38,49	0,00	28,66	0,36	0,06	1,34	0,67	30,54	100,18	Titanite
387 Zf	CZf387-R3-1	401	0,00	0,02	0,00	101,62	0,00	0,02	0,22	0,00	0,06	1,88	0,00	103,82	Rutile
387 Zf	CZf387-T3-1	404	0,01	0,00	0,05	38,72	0,00	28,40	0,25	0,05	1,30	0,69	30,07	99,56	Titanite
BS Zf	CZfBS-T1-1	407	0,05	0,01	0,02	31,59	0,00	24,92	0,13	0,00	1,72	0,55	25,25	84,24	Titanite
BS Zf	CZfBS-T2-1	410	0,00	0,00	0,03	38,43	0,00	28,95	0,40	0,00	1,45	0,73	30,55	100,55	Titanite
BS Zf	CZfBS-R1-1	413	0,00	0,00	0,01	99,85	0,00	0,03	0,14	0,13	0,05	2,36	0,01	102,60	Rutile
391 Zf	CZf391-R1-1	416	0,00	0,01	0,01	102,27	0,00	0,01	0,10	0,03	0,03	2,06	0,07	104,60	Rutile
391 Zf	CZf391-T1-1	419	0,02	0,00	0,07	37,90	0,00	28,87	0,49	0,00	1,67	0,67	30,46	100,15	Titanite
391 Zf	CZf391-R2-1	422	0,00	0,00	0,02	100,38	0,00	0,01	0,01	0,17	0,02	2,35	0,12	103,09	Rutile
391 Zf	CZf391-R3-1	425	0,00	0,00	0,00	98,86	0,00	0,00	0,07	0,40	0,05	2,13	0,40	101,92	Rutile
391 Zf	CZf391-R4-1	428	0,00	0,00	0,02	100,88	0,00	0,03	0,14	0,07	0,00	2,12	0,01	103,27	Rutile

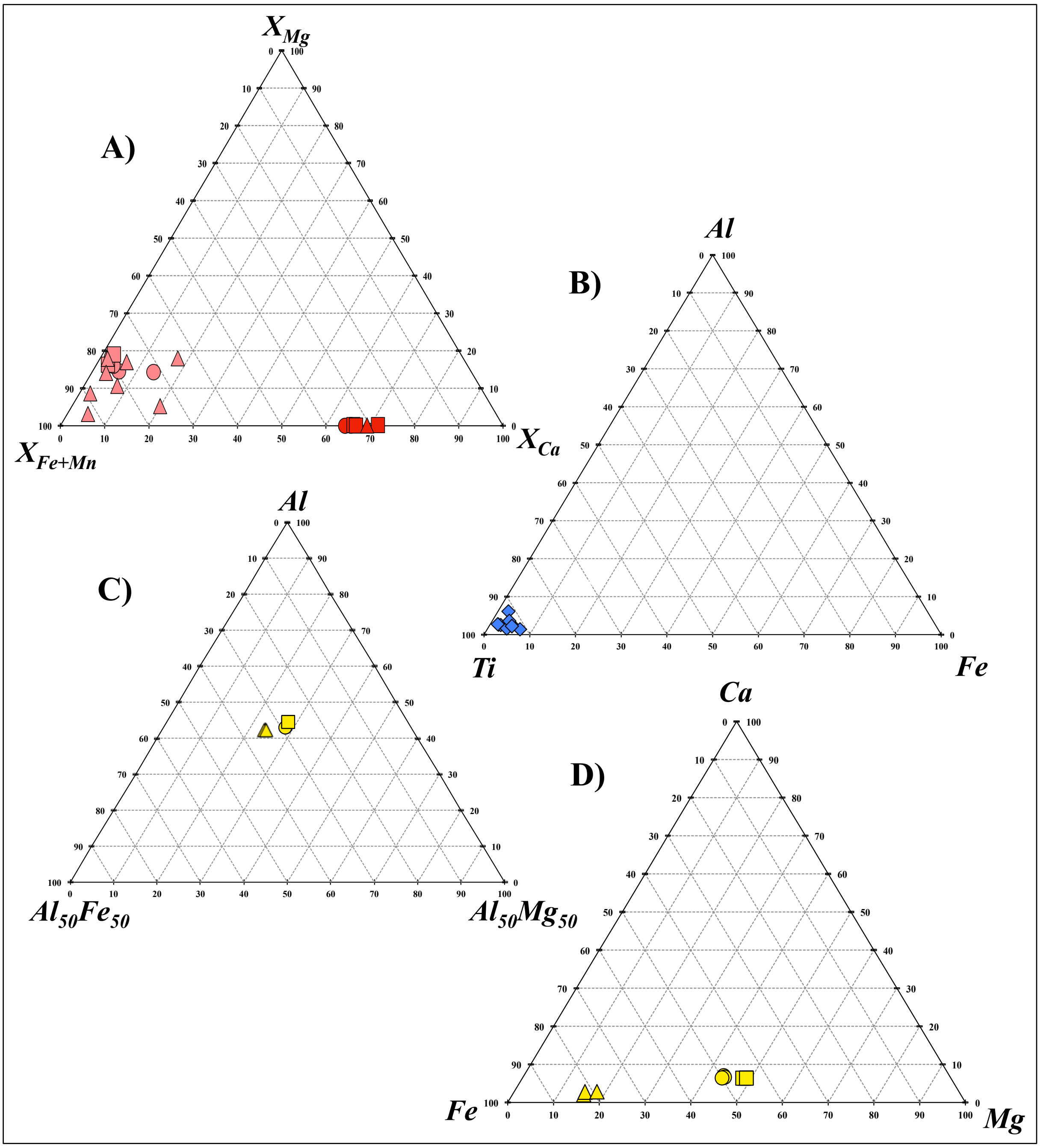

Figure 3.17: Ternary plots of four heavy minerals identified with EMPA. A) Garnets from sample 387, 391 and BS. Almandines are marked with pink points and grossular with red points. XMg, XCa, XFe+Mn = molecular values of Mg, Ca and Fe+Mn respectively. B) Titanite grains from sample 387, 391 and BS marked with blue points. Ti, Al, Fe = molecular values of Ti, Al, and Fe respectively. C) Three tourmaline grains from sample BS marked with yellow points. Al, Al50Mg50, Al50Fe50 = molecular values of Al, Al+Mg, and Al+Fe respectively. D) The same three tourmaline grains from sample BS marked with yellow points. Ca, Mg, Fe = molecular values of Ca, Mg, and Fe respectively. Molecular values for all four ternary plots are calculated on the basis of wt% values from EMPA results. Values can be seen in Appendix N.

4 DISCUSSION AND IMPLICATIONS OF THE RESULTS

Results from the analytical methods have been compared, combined and interpreted. Heavy mineral composition and grain shape have been compared between samples and fractions. Particle size distribution, grain shape and sorting have been considered for evaluation of transporting medium and calculation of potential settling velocities. The relationship between garnet, titanite and tourmaline and possible source rocks has also been evaluated.

4.1 Comparison of heavy mineral compositions

Results from all analytical methods indicate the same type of heavy minerals in each sample. Heavy minerals identified are chamosite, amphibole, tourmaline, garnet (almandine and grossular), magnetite, ilmenite, rutile, titanite, zircon and apatite. The magnetic fractions of the four samples from the Rosenhof Member (sample 387, 389, 391 and 393) are very similar in their heavy mineral composition (*Figure 4.1*). They contain the same heavy minerals and the amount of each of them varies only a little. This is as expected because they are all part of the same member and therefore they are likely to be similar. The magnetic fraction of the one sample from the Haribes Member (sample BS) has a heavy mineral composition that is somewhat different to the Rosenhof samples. Compared to the samples from the Rosenhof Member it has larger amounts of grossular, less amounts of almandine, and larger amounts of tourmaline (*Figure 4.1*).

The heavy mineral compositions of the apatite and zircon fractions are very similar for all samples from both the Rosenhof Member (sample 387 and 391) and Haribes Member (sample BS) (*Figure 4.2*). All apatite fractions contain mostly apatite, and some almandine and titanite. All zircon fractions contain zircon, titanite, rutile, apatite and almandine.

The heavy minerals identified in the magnetic, apatite and zircon fraction for sample 387 are the same, as expected. The same apply to the fractions of sample 391 and BS. However, the heavy mineral grains are not always located in the expected fraction. Apatite grains (with density less than 3.3 g/cm^3) were for example not expected to be found in the zircon fractions. The reason for some of the apatites being in the zircon fraction is that these apatite grains consist of several phases with other minerals, and therefore the grain has a higher average density than for a grain only composed of apatite.

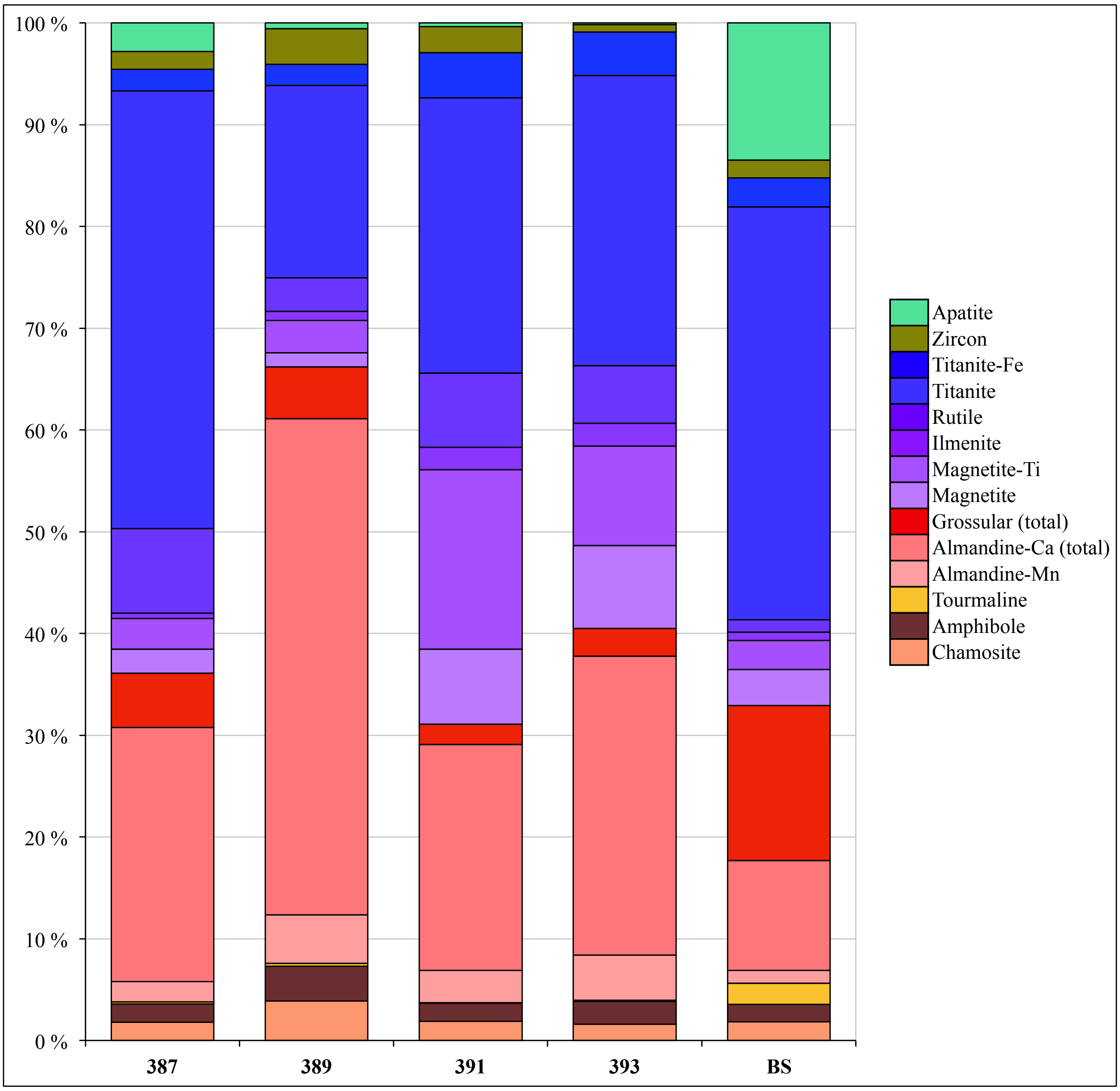

Figure 4.1: Comparison of the heavy mineral compositions for the magnetic fractions of sample 387, 389, 391, 393 and BS. Values are wt% of heavy minerals in the fraction. Histograms are based on values from MLA analyses found in Appendix H.

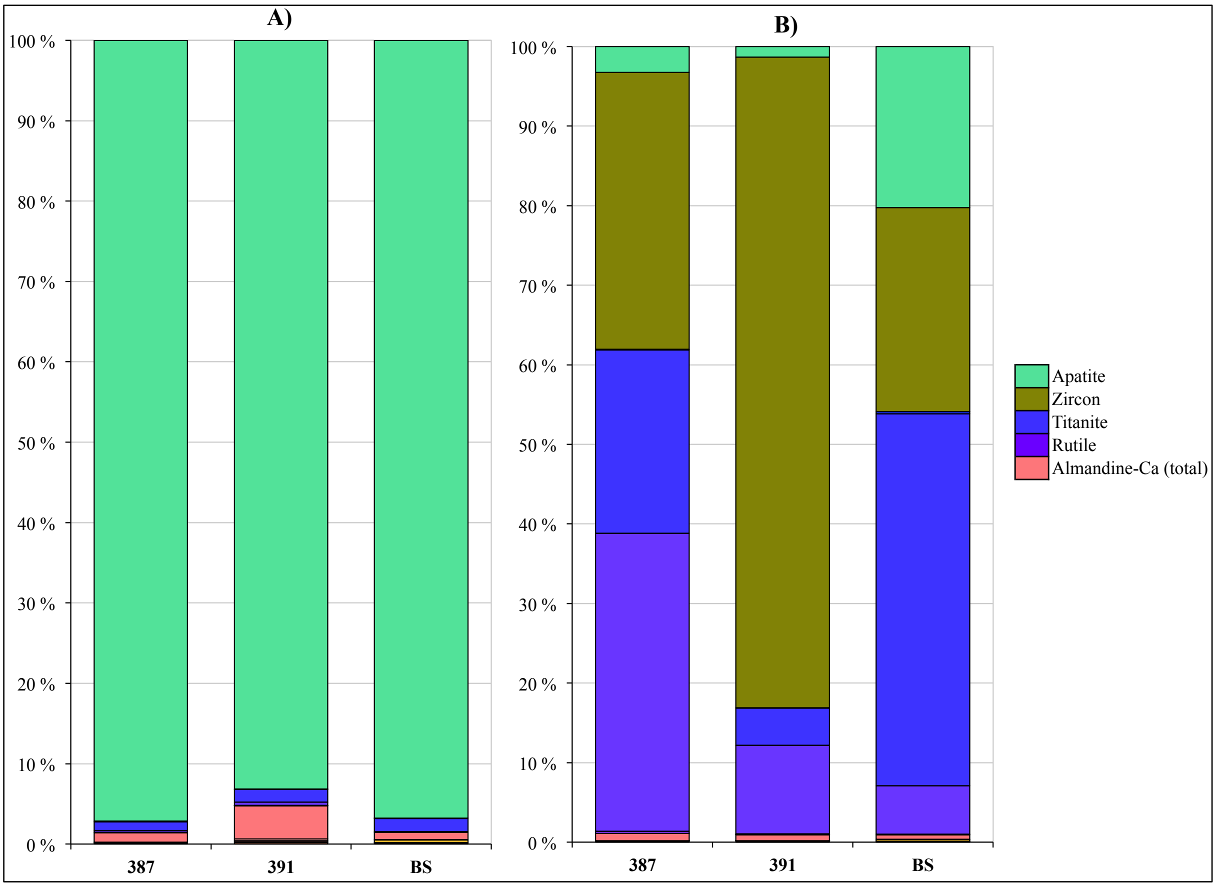

Figure 4.2: Comparison of the heavy mineral compositions for the apatite fractions (A) and zircon fractions (B) of sample 387, 391 and BS. Values are wt% of heavy minerals in the fraction. Histograms are based on values from MLA analyses found in Appendix H.

4.2 Comparison of heavy mineral grain sizes

Grain sizes for one type of mineral are often different in the several fractions. The fractions have been separated based on density and their magnetic potential. Grains in the magnetic fractions should have densities higher than 2.95 g/cm^3 and be magnetic. Grains in the apatite fractions should have densities between 2.95 g/cm^3 and 3.3 g/cm^3, and zircon fractions should have densities higher than 3.3 g/cm^3. *Figure 4.3* show that rutile grains in the apatite fraction have a much smaller grain size than those in the zircon fraction. *Figure 4.4* show that zircon grains in the apatite fraction are much smaller than those in the magnetic fraction and zircon fraction. This is as expected because zircon and rutile, which have densities higher than 4 g/cm^3 and should therefore be in the zircon fractions, should have a much smaller grain size if found in the apatite fractions.

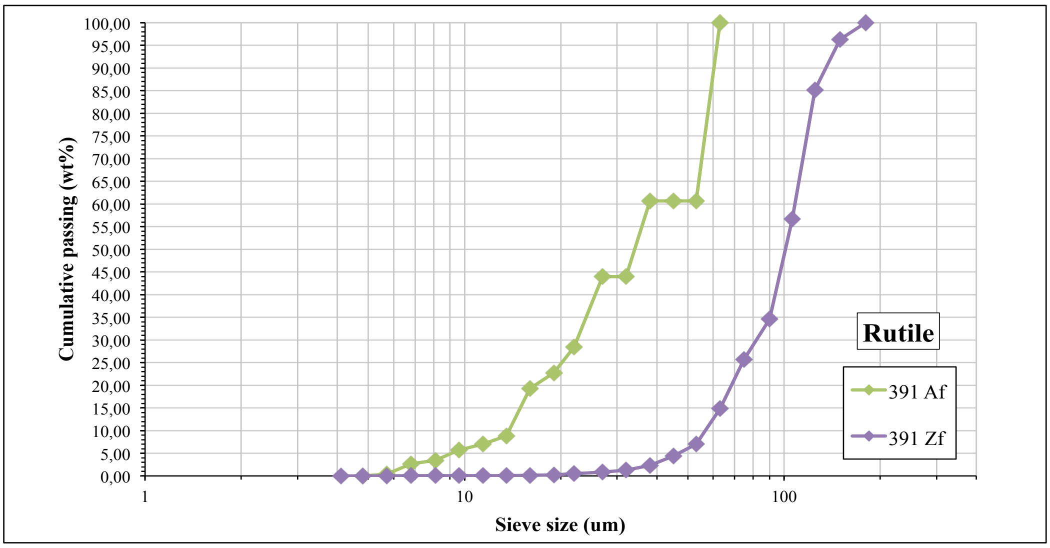

Figure 4.3: Comparison of grain sizes of rutile from apatite and zircon fraction of sample 391.

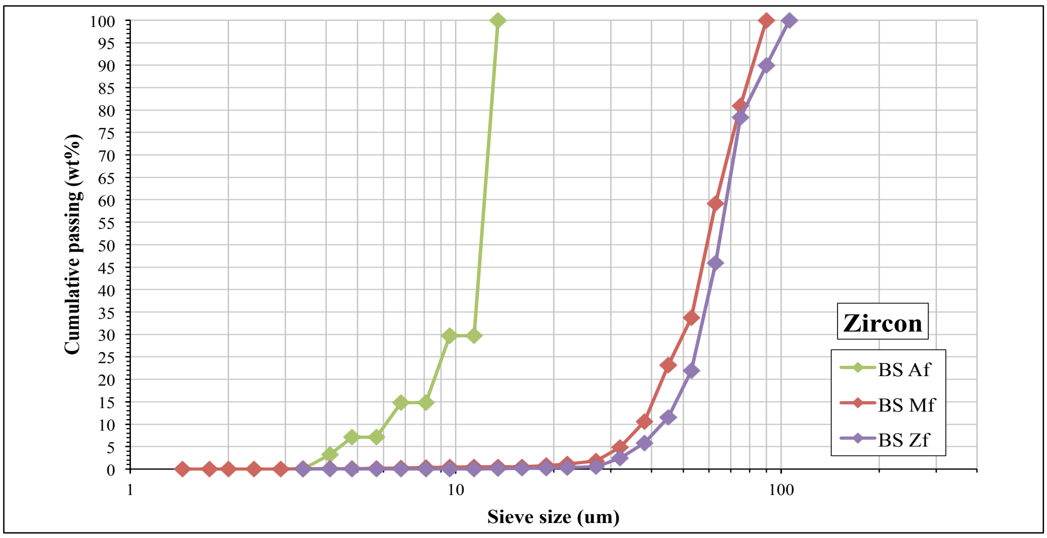

Figure 4.4: Comparison of grain sizes of zircon from all fractions of sample BS.

4.3 Particle size distributions and transporting medium

The particle/grain size distribution, or sorting, is affected by the mode of transportation and the energy of the transporting medium. Sorting is the degree of uniformity of grain size. Particles are sorted based on gravity because of the energy of the transporting medium. Currents with high energy can transport larger particles, but as the energy decreases the heavier particles are deposited and lighter particles continues to be transported. The result is sorting due to density. Fluvial deposits are usually more poorly sorted because the energy, or the velocity, in the river varies with the position of the river and time. Beach deposits and wind deposits often have good sorting because the energy of the transporting medium is more constant (Reading and Levell, 1996). The magnetic fractions are moderately to poorly sorted, indicating that they are fluvial deposits and not beach deposits. The apatite fractions are well to moderately well sorted and the zircon fractions are moderately well to moderately sorted. This can be because these two fractions mostly contain apatite and zircon. The magnetic fractions contain some amount of all types of heavy minerals and are therefore quite representative for the entire sample.

Wind and river transportation are unidirectional flows and can be responsible for a generally positive skewness of dune and river sands. Positive skewed distributions have a fine-particle tail and indicate that the coarser grains have a better sorting than fine grains (*Figure 4.5*). At the coarse end of the frequency distribution curve the tail of the curve is almost chopped off in comparison to a normal distribution curve. Negative skewed distributions have a coarse-particle tail and lack the tail at the fine-grained end (*Figure 4.5*). On a marine beach where sand is exposed to two forces of unequal strength acting in opposite directions, the fine-grained particles are removed, and the frequency distribution curve is negatively skewed (Friedman, 1961).

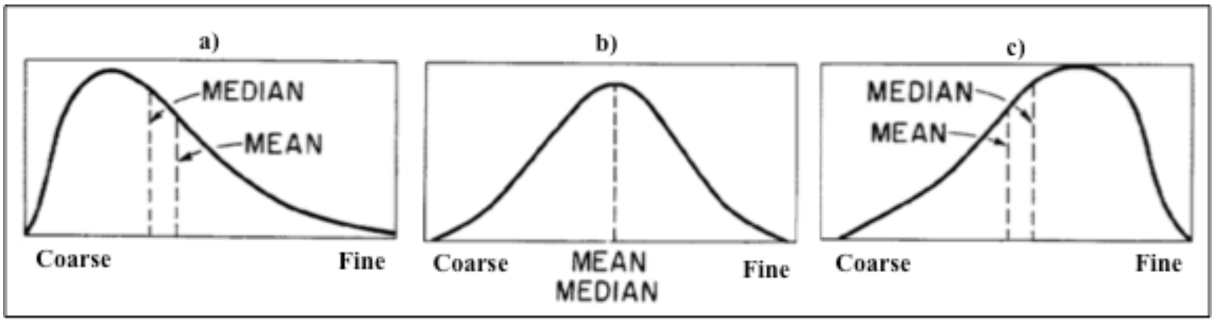

Figure 4.5: Different grain size distribution curves: a) Positively skewed distribution, b) symmetrical distribution, and c) negatively skewed distribution (modified after Friedman (1961)).

The four magnetic fractions from the Rosenhof Member (sample 387, 389, 391 and 393) have a positive skewed particle size distribution, indicating that they all come from dune or river sands (*Figure 4.6*). Since they are placer deposits, deposited by a flow of water, they probably came from river sands. This corresponds to the already suggested theory that the depositional environment for the Rosenhof Member is mostly fluvial. The magnetic fraction from the Haribes Member (sample BS) has a more symmetric particle size distribution (*Figure 4.6*).

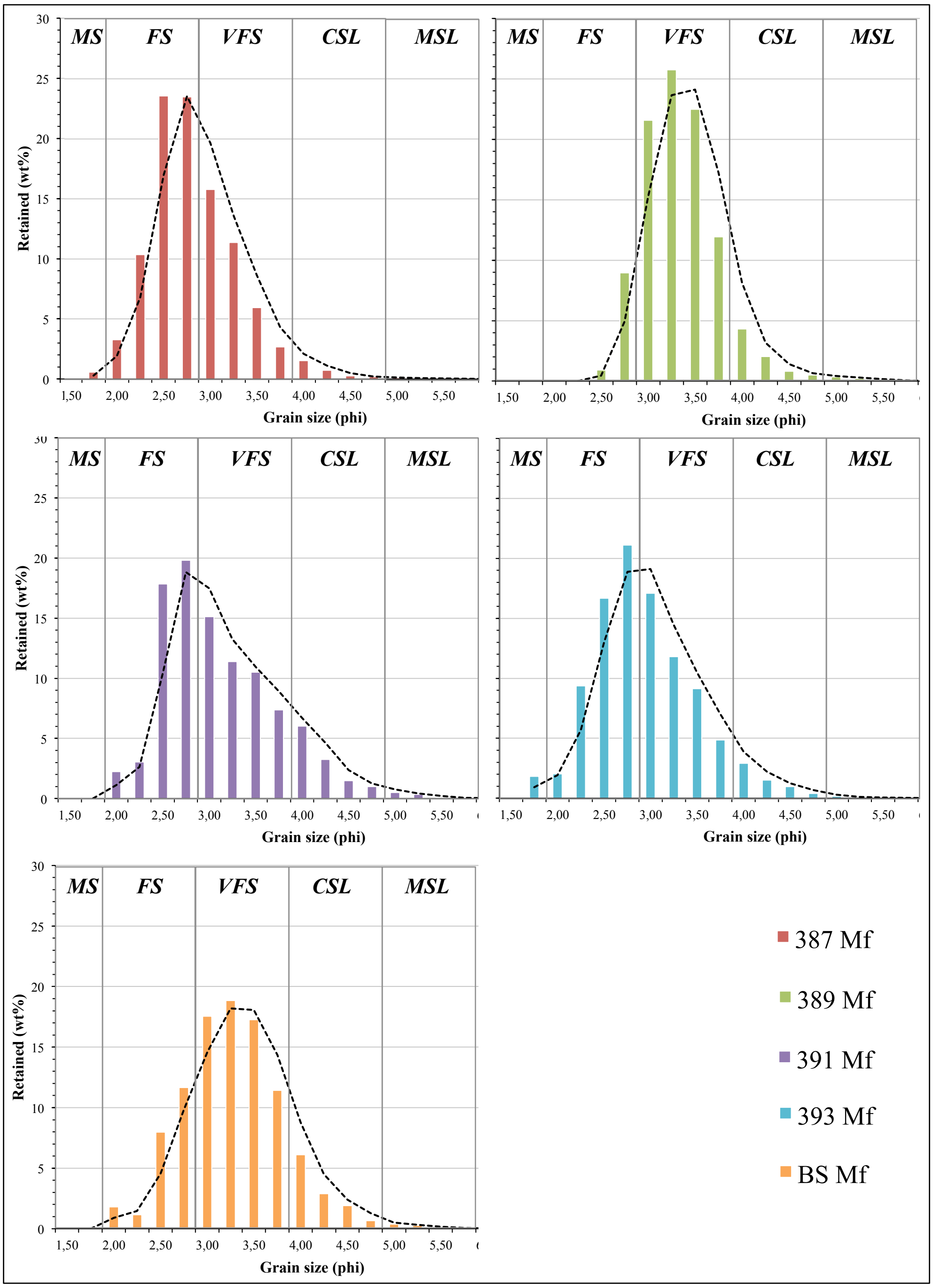

Figure 4.6: Grain/particle size (phi) of grains in the magnetic fractions. Grain size (phi) 1.50-1.75 is medium sand (MS), 2.00-2.75 is fine sand (FS), 3.00-3.75 is very fine sand (VFS), 4.00-4.75 is coarse silt (CSL), and 5.00-5.75 is medium silt (MSL). Values used for the histograms can be seen in Appendix K.

4.4 Grain shape and amount of transport

The degree of roundness and sphericity of detrital particles depend on their grain size, physical properties and characteristics. It also depends on the amount of transport. Grain rounding can be a very slow process, and it becomes slower as the grain size decreases. Larger grains will be more rounded after a given distance of transport than smaller ones. Well-rounded grains can be a result of many cycles of transport or one long transport (Pettijohn et al., 1987). The heavy minerals in the magnetic fractions in the samples in this project are mostly sub-rounded to angular, indicating some degree of transport. The larger grains in all fractions are the mostly rounded and the smaller grains are more angular. Both the larger and smaller grains can therefore have been transported for approximately the same distance.

Some heavy minerals are more resistant than others. The more resistant minerals/grains will preserve their grain size and grain shape inherited from their source rock (Komar, 2007). Ultrastable heavy minerals, meaning minerals that are particularly resistant to chemical and mechanical weathering, are rutile, tourmaline and zircon. They can survive multiple recycling events (Mange and Morton, 2007; Pettijohn et al., 1987). The rutile and zircon grains in the samples in this project are mostly sub-rounded, indicating some amount of transport.

Stable heavy minerals are not as resistant to weathering as ultrastable heavy minerals. Stable heavy minerals are typically apatite and garnet. Apatite is stable during deep burial, but not stable when exposed to weathering, therefore its distribution in sandstones is controlled by weathering during the sedimentary cycle (Morton and Hallsworth, 1999). Apatite typically becomes rounded much faster than many other heavy minerals. This is due to its relatively low hardness. The roundness of apatite can therefore be an indicator of prolonged transport (Morton, 2007). The apatite grains in the samples in this project are mostly rounded to sub-rounded, but some are also well rounded. The apatite grains could therefore not have been transported too far, and probably for a shorter distance than the ultrastable heavy minerals.

Garnet is a relatively stable heavy mineral both under weathering and burial diagenesis (Morton and Hallsworth, 1999). Although the garnets are relatively stable during burial, they can undergo dissolution by high-temperature pore-fluids. Some garnets are more stable than others. Ca-rich garnets (e.g. grossular) are less stable than Ca-poor garnets (e.g. almandine)

(Morton, 1987). The almandine grains in the samples in this project are mostly sub-angular, and the grossular grains are mostly sub-rounded to sub-angular. The most stable garnet, the almandine, are generally not as rounded as the less stable garnet, the grossular. This indicates that the almandine and grossular can have been transported for approximately the same distance, and probably for a shorter distance than the ultrastable heavy minerals.

4.5 Grain size, density and settling velocity

Critical velocity is the fluid velocity where a particle becomes entrained in the flow. There is a relationship between the critical velocity and the mass of the particle. The drag force moving the particle in a flow and the lift force necessary to bring the particle up into the flow will both increase with mass. There is a linear relationship between the flow velocity and the forces, which can be applied to gravel and sand. The Hjülstrom diagram illustrates a relationship between water flow velocity and grain size (*Figure 4.7*). The lower line on the graph show the relationship between flow velocity and particles that are already in motion. The upper line show the flow velocity required moving a particle from the others (Nichols, 2009). The heavy minerals in the samples in this project have grain sizes between ~0.3 mm (medium sand) and ~0.016 mm (medium silt). The diagram shows that these grains will come to rest at ~0.12 to ~2.00 cm/s. The grain size of the particles in a water flow can therefore say something about the velocity at the time of deposition (if the particles are deposited as isolated particles).

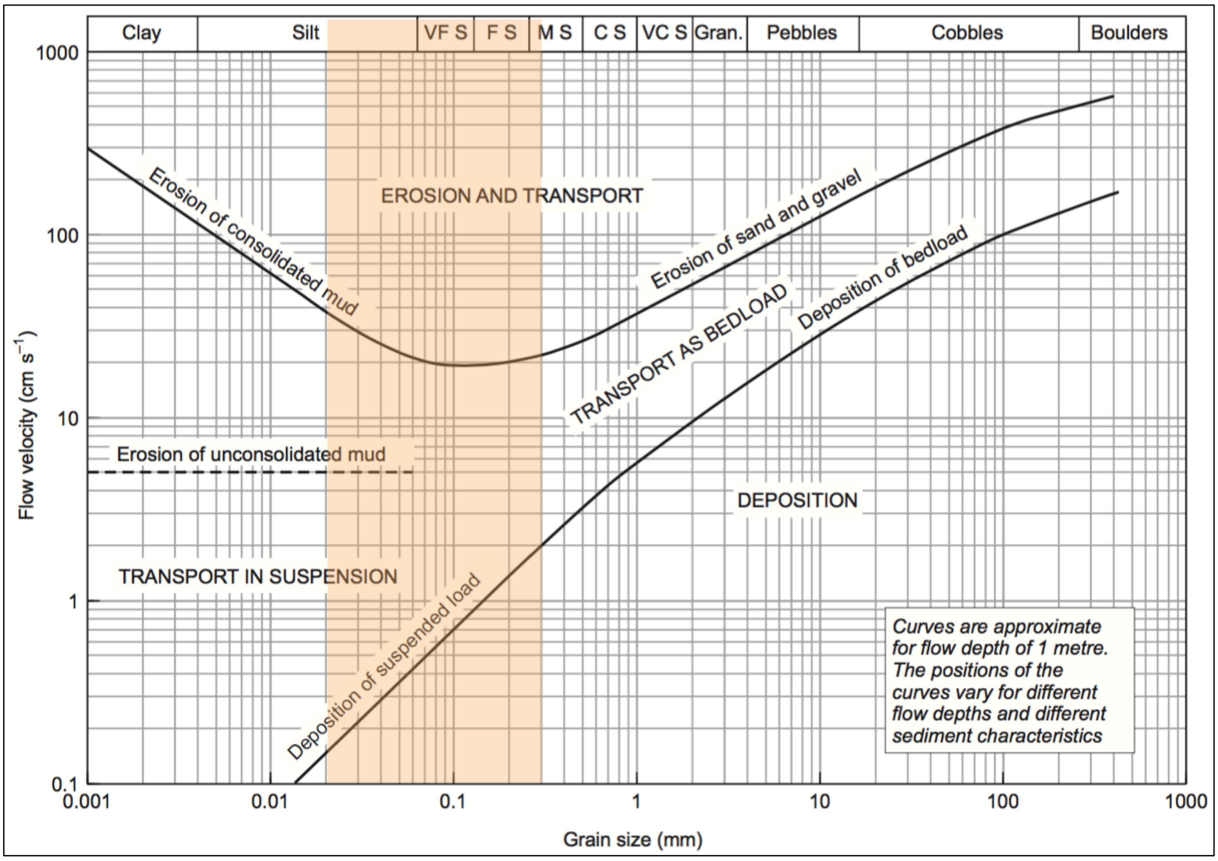

Figure 4.7: The Hjülstrom diagram illustrating the relationship between water flow velocity and grain size (modified after Press and Siever, 1986). The orange area marks the most common grain sizes for the heavy minerals in the samples in this project: ~0.3 mm (medium sand) to ~0.016 mm (medium silt).

The Hjülstrom diagram does not consider the density of the grains, but another method can be used for this. The settling velocity of particles in a fluid can be determined by a relationship between several factors. This relationship is called Stokes Law and is expressed with an equation:

$$V = g \times D^2 \times (\rho_s - \rho_f)/18\mu \tag{4.1}$$

V is the terminal settling velocity, *g* is the acceleration due to gravity, *D* is the grain diameter, ρ_s - ρ_f is the difference between the density of the particle (ρ_s) and the density of the fluid (ρ_f), and μ is the viscosity of the fluid (Nichols, 2009). If assuming that the density of the fluid/water is 1 g/cm^3, the viscosity of the fluid/water is 0.001 kg/ms and the grains are spherical, then the settling velocities for grains in the samples/fractions in this project will be as in *Table 4.1*. Two grain diameters are used representing minimum and maximum grain diameter for the majority of the grains (~99 % of the grains) in the each fraction. Two particle densities have also been used representing minimum and maximum particle density for the majority of the particles (~99 % of the particles) in each fraction.

Table 4.1: Calculated settling velocity of particles by using Strokes Law. The first grey colored column contains minimum settling velocity for grains in the samples/fractions if using minimum particle density and minimum grain diameter. The second grey colored column contains maximum settling velocity for grains in the samples/fractions if using maximum particle density and maximum grain diameter.

	Density (g/cm3)		**Grain diameter (mm)**		**Velocity (cm/s) D_min**		**Velocity (cm/s) D_max**	
	ρs_min	**ρs_max**	**D_min**	**D_max**	**Velocity (cm/s) ρs_min**	**Velocity (cm/s) ρs_max**	**Velocity (cm/s) ρs_min**	**Velocity (cm/s) ρs_max**
387 Mf	2,6	4,3	0,053	0,250	0,24	0,51	5,45	11,24
389 Mf	2,6	4,3	0,045	0,150	0,18	0,36	1,96	4,05
391 Mf	2,6	4,3	0,045	0,212	0,18	0,36	3,92	8,08
393 Mf	2,6	4,3	0,045	0,250	0,18	0,36	5,45	11,24
BS Mf	2,6	4,3	0,038	0,212	0,13	0,26	3,92	8,08
387 Af	2,6	3,3	0,075	0,212	0,49	0,71	3,92	5,63
391 Af	2,6	3,3	0,053	0,212	0,24	0,35	3,92	5,63
BS Af	2,6	3,3	0,053	0,180	0,24	0,35	2,83	4,06
387 Zf	3,1	4,7	0,053	0,250	0,32	0,57	7,15	12,60
391 Zf	3,1	4,7	0,045	0,180	0,23	0,41	3,71	6,53
BS Zf	3,1	4,7	0,038	0,150	0,17	0,29	2,58	4,54

The settling velocities are higher than for the Hjülstrom diagram if taking into account the maximum densities. This can be because the Hjülstrom diagram does not consider difference in the density of grains. The average density for the grains in the samples/fractions in this project are higher than for “normal” sand grains containing for example mostly quartz and feldspar. The minimum density used in the calculations is 2.6 g/cm^3, which is approximately the density of quartz. The maximum density used is 4.7 g/cm^3 (typical for zircon).

The minimum settling velocities for grains in the magnetic fractions are 0.13-0.24 cm/s, and the maximum settling velocities are 4.05-11.24 cm/s. The minimum settling velocities for grains in the apatite fractions are 0.24-0.49 cm/s, and the maximum settling velocities are 4.06-5.63 cm/s. The minimum settling velocities for grains in the zircon fractions are 0.17-0.32 cm/s, and the maximum settling velocities are 4.54-12.60 cm/s. The minimum and maximum grain settling velocities for each fraction are plotted in a diagram (*Figure 4.8*). They align along the dashed curves representing the minimum and maximum grain densities used for the velocity calculations. In general the grains in the fractions from sample BS (from the Haribes Member) have a smaller grain diameter than the other fractions (from the Rosenhof Member), which means that they have lower grain settling velocities. The diagram show that settling velocity is a function of grain size and grain density, so the smaller and denser minerals have the same settling velocity as the larger and less dense minerals.

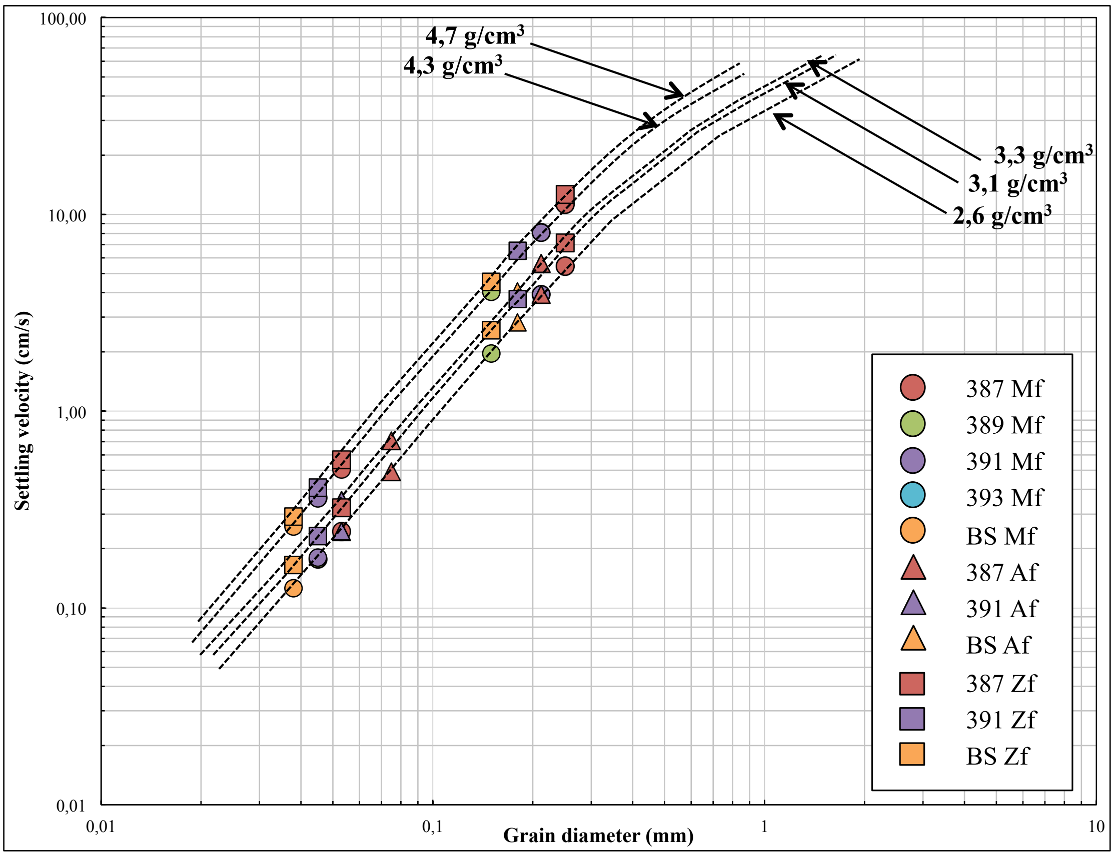

Figure 4.8: Curves for grain settling velocities of the heavy minerals in each fraction. The dashed curves represent the minimum and maximum densities used for calculation of the velocities. The dashed curves are inspired by a diagram with grain settling values after Komar (2007). Both axes are logarithmic.

4.6 Relationship between garnet and source rock

Garnet geochemistry is dependent on and limited by the burial depth of the samples being studied. The burial depth should be relatively shallow because garnets are less stable during burial diagenesis than other ultrastable minerals. Detrital apatite and titanite are typically less stable than garnets in surface conditions, and since they are present it indicates that the garnet assemblage is probably not affected by weathering (Morton, 2012). Ca-rich garnets (e.g. grossular) are less stable than Ca-poor garnets (e.g. almandine) (Morton, 1987). If garnet dissolution has taken place then it can affect the relative abundances of the different garnet types (Morton et al., 2005). Field A, B, C and D on the ternary diagrams in *Figure 4.9*, *4.10* and *4.11* representing type A, B, C and D garnets, are inspired by Morton et al. (2005) and Mange and Morton (2007). The fields indicate the amount of some the elements found in garnets: calcium (Ca), magnesium (Mg), iron (Fe) and manganese (Mn).

Type A garnets have low Ca content, low Mn content and relatively high Mg content (Morton et al., 2005). They are classified as almandine. Sample 389, 391 and 393 have 1-3 of the measured garnets within the area of type A according to FE-SEM-EDS analyses with standard (*Figure 4.9*). According to MLA and EMPA there are no garnets from the samples fitting within this area (*Figure 4.10* and *4.11*). Type A garnets are interpreted to derive from high-grade (granulite facies) metasediments or charnockites (Sabeen et al., 2002).

Type B garnets have low Mg content and variable Ca and Mn content (Morton et al., 2005). They are also classified as almandine, but they contain more Fe and Mn compared to type A garnets. Most of the garnets identified have a composition of type B garnets, according to FE-SEM-EDS analyses, MLA and EMPA (*Figure 4.9, 4.10* and *4.11*). Type B garnets are interpreted to derive from metasediments, including amphibolite facies. They can also derive from higher-grade metamorphic rocks and acidic to intermediate gneisses and granites. Granitic garnets typically have a very high content of Fe and Mn, often above 90 %. Large assemblages of type B garnets most commonly derive from low to moderate grade metasediments (Morton et al., 2005).

Type C garnets have high Ca content and high Mg content (Morton et al., 2005). They are classified as almandine. All samples from the Rosenhof Member (387, 389, 391 and 393) have a few type C garnets, according to FE-SEM-EDS analyses with standard (*Figure 4.9*).

Type C garnets are interpreted to derive from high-grade mafic and ultramafic gneisses, including eclogites (Morton et al., 2005).

Type D garnets have low Mg content and very high Ca content (Mange and Morton, 2007). They are classified as grossular. Type D garnets are identified in all samples, according to FE-SEM-EDS, MLA and EMPA (*Figure 4.9, 4.10* and *4.11*). Most of them are from sample BS from the Haribes Member. Type D garnets are interpreted to typically derive from contact or thermally metamorphosed calcareous sediments and can be associated with metasomatic skarns (Deer et al., 1992).

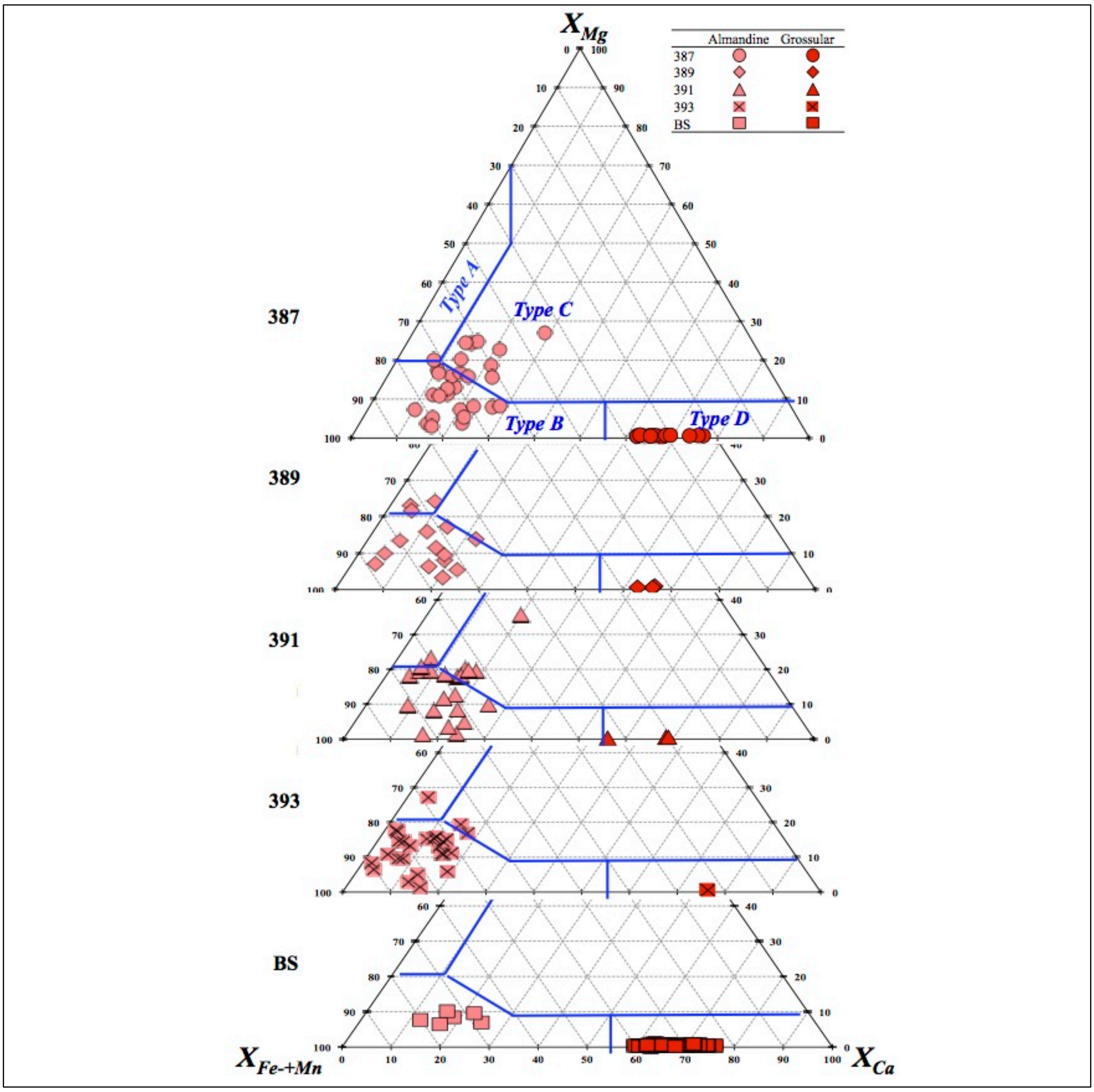

Figure 4.9: Ternary plots with garnet measurements from FE-SEM-EDS analyses with standard. Values for the plot are in Appendix C. Marked areas illustrating type A, B, C and D garnets are inspired by Morton et al. (2005) and Mange and Morton (2007).

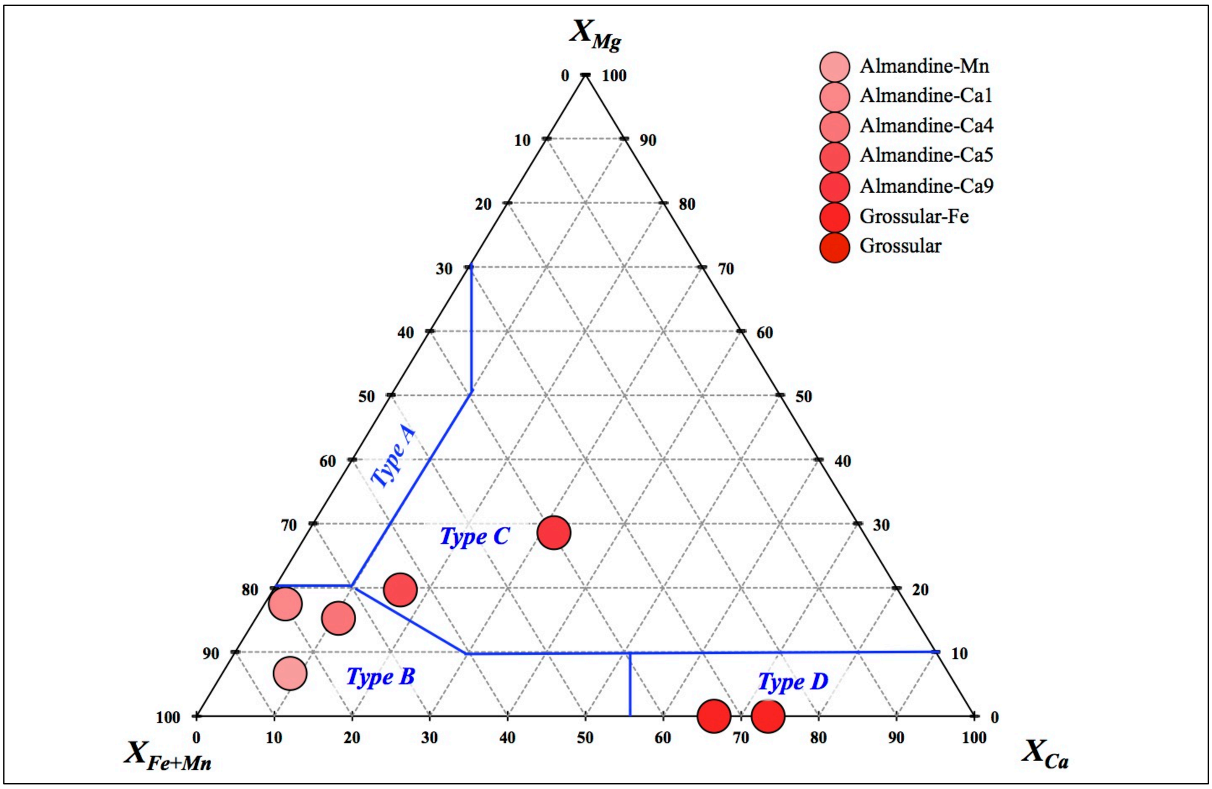

Figure 4.10: Ternary plot with garnets from reference list used for MLA. Values for the plot are in Appendix G. Marked areas illustrating type A, B, C and D garnets are inspired by Morton et al. (2005) and Mange and Morton (2007).

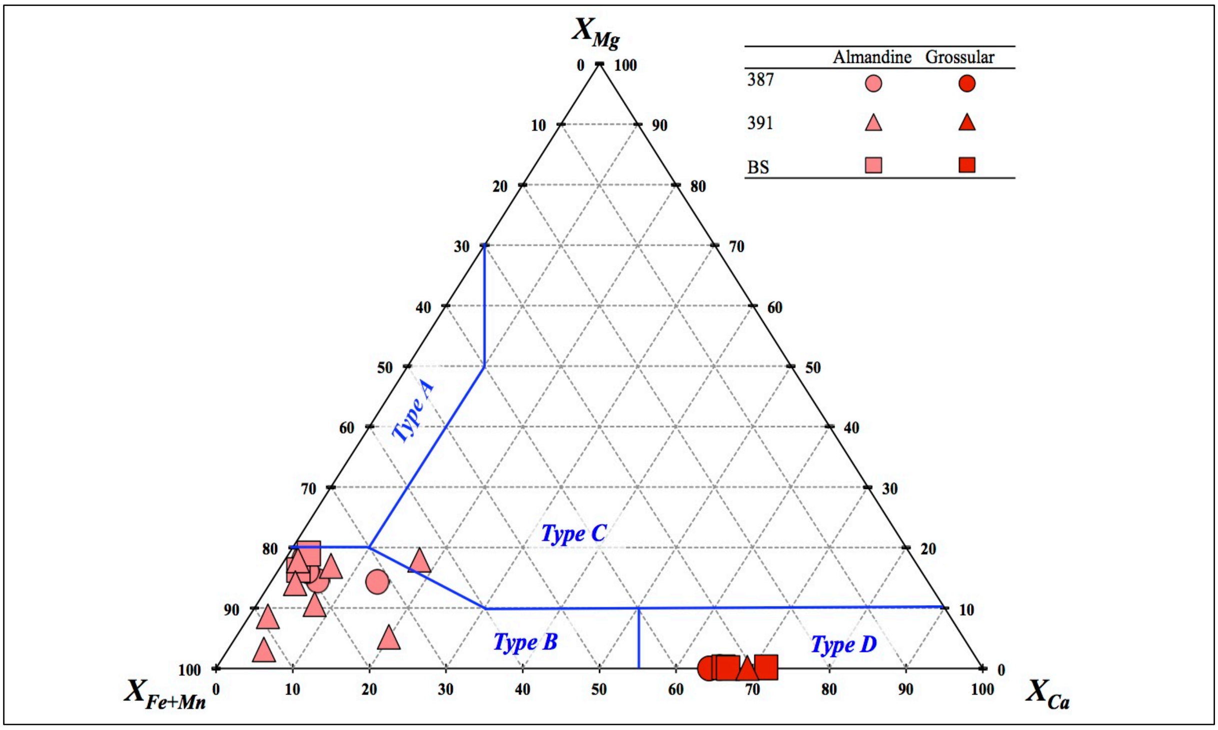

Figure 4.11: Ternary plot with garnet measurements from analyses with EMPA. Values for the plot are in Appendix N. Marked areas illustrating type A, B, C and D garnets are inspired by Morton et al. (2005) and Mange and Morton (2007).

4.7 Relationship between titanite and source rock

Titanite (also called sphene) is a chemically unstable mineral, which often dissolves in the early stages of diagenesis (Mange and Maurer, 1992). For that reason it is rarely found as detrital grains in sandstones. The unstableness of the titanite can however be an advantage because its occurrence in sediments can indicate that the source is monocyclic in origin (Asiedu et al., 2000). Titanite is a common accessory mineral in igneous rocks and there exist a relationship between the composition of the titanite and the type of igneous rocks where they occur, according to Deer et al. (1982). Titanites from mafic and ultramafic rocks are close to the theoretical composition $CaTiSiO_5$. Titanites from acidic and intermediate igneous rocks contain significant amounts of iron, aluminum and rare earth elements (REE). Titanites in metamorphic rocks occur primarily in gneiss and schists that are rich in ferromagnesian minerals. Titanites in metamorphic rocks and skarns typically have higher aluminum contents compared to titanites in igneous rocks (Asiedu et al., 2000).

On the ternary plot with Ti, Al and Fe the titanite grains measured with EMPA lies within the igneous source field (*Figure 4.12*). The type of igneous source rock can be interpreted based on the total REE content (Asiedu et al., 2000). The chemical composition of the titanites from the EMPA does not say anything about the amount of REE, but the totals are very high (mostly 95-100 %). This suggests that the REE contents are quite low, and this can indicate that the titanite derived from mafic igneous rocks (Asiedu et al., 2000).

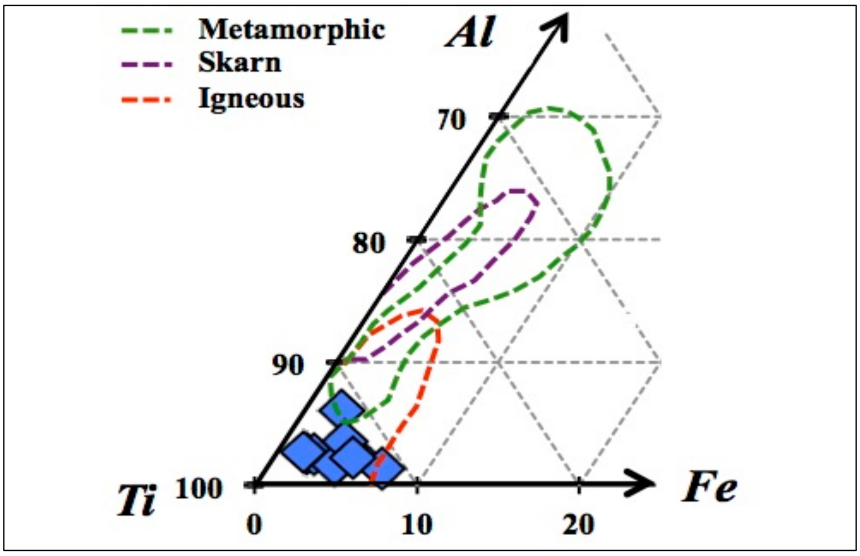

Figure 4.12: Part of ternary plot for titanite, with blue points representing the titanite grains. Ti, Al, Fe = molecular values of Ti, Al, and Fe respectively, calculated on the basis of wt% values from analyses with EMPA. Values used for this plot are in Appendix N. Regions marked with dotted lines represents different types of sources for the titanites and are after Asiedu et al. (2000).

4.8 Relationship between tourmaline and source rock

Tourmalines can be a useful petrogenetic indicator mineral. Tourmalines can have a large number of substitutions making the classification of the tourmalines more difficult. The composition of tourmalines can be plotted in ternary diagrams, and distinct regions for the tourmalines and their potential source rock can be identified (Henry and Guidotti, 1985). *Figure 4.13* shows one ternary diagram for tourmalines based on the composition of aluminum (Al), iron (Fe) and magnesium (Mg). Regions marked with type 1-8 on the diagram and the green dots representing different types of tourmalines are after Henry and Guidotti (1985). The regions are distinctive for different source rocks for tourmalines. The rock types representing the regions marked with type 1-8 are: 1) Li-rich granitoids, pegmatites and aplites, 2) Li-poor granitoids and their associated pegmatites and aplites, 3) Fe^{3+}-rich quartz-tourmaline rocks (hydrothermally altered granites), 4) metapelites and metapsammites coexisting with an Al-saturating phase, 5) metapelites and metapsammites not coexisting with an Al-saturating phase, 6) Fe^{3+}-rich quartz-tourmaline rocks, calc-silicate rocks and metapelites, 7) low-Ca metaultramafics and Cr,V-rich metasediments, and 8) metacarbonates and meta-pyroxenites (Henry and Guidotti, 1985).

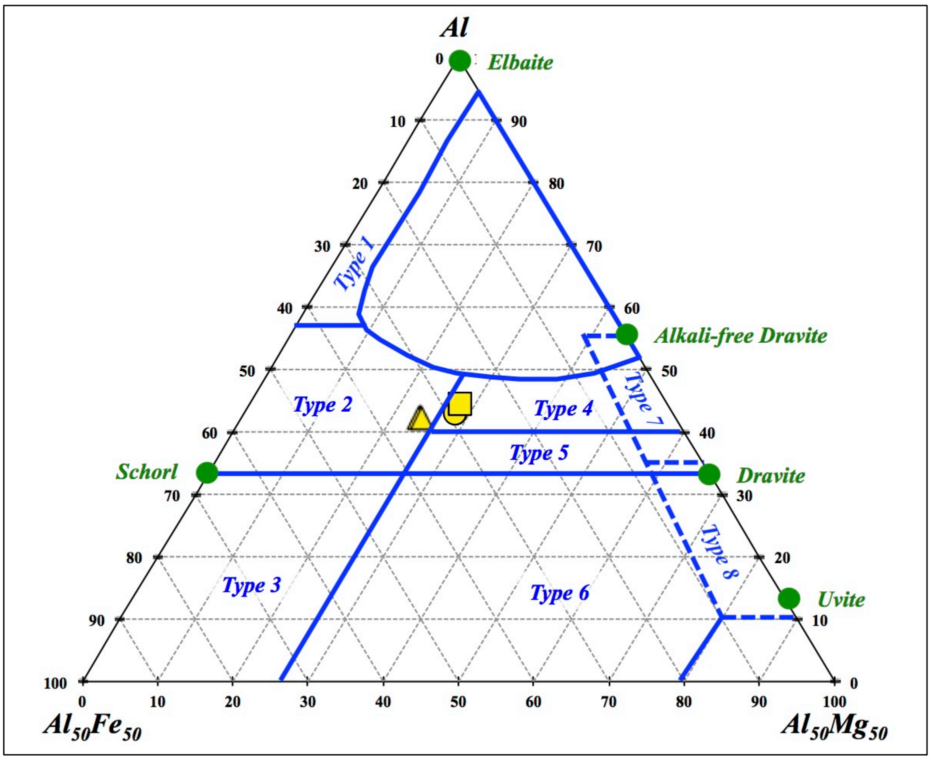

Figure 4.13: Ternary plot for tourmaline with yellow points representing tourmaline grains from sample BS. Al, Al50Mg50, Al50Fe50 = molecular values of Al, Al+Mg, and Al+Fe respectively, calculated on the basis of wt% values from the EMPA. Values used for this plot are in Appendix N. Regions marked with type 1-8 on the diagram and the green dots representing different types of tourmalines are after Henry and Guidotti (1985).

Figure 4.14 shows another ternary diagram for tourmalines based on the composition of calcium (Ca), iron (Fe) and magnesium (Mg). Regions marked with type 1-6 on the diagram and the green dots representing different types of tourmalines are after Henry and Guidotti (1985). The rock types representing the regions marked with type 1-6 are: 1) Li-rich granitoids, pegmatites and aplites, 2) Li-poor granitoids, pegmatites and aplites, 3) Ca-rich metapelites, metapsammites and calc-silicates, 4) Ca-poor metapelites, metapsammites and quartz-tourmaline rocks, 5) metacarbonates, and 6) Metaultramafics (Henry and Guidotti, 1985).

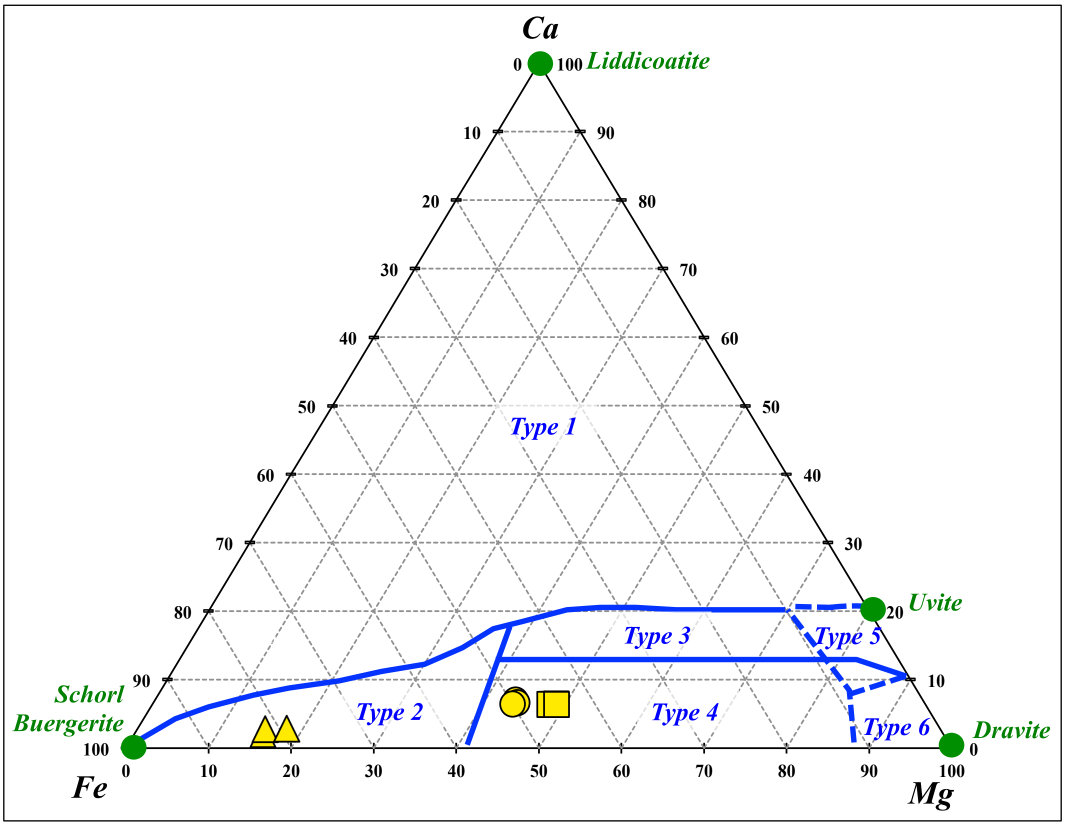

Figure 4.14: Ternary plot for tourmaline with yellow points representing tourmaline grains from sample BS. Ca, Mg, Fe = molecular values of Ca, Mg, and Fe respectively, calculated on the basis of wt% values from the EMPA. Values used for this plot are in Appendix N. Regions marked with type 1-6 on the diagram and the green dots representing different types of tourmalines are after Henry and Guidotti (1985).

The three tourmaline grains identified with the EMPA are located in two regions in both ternary plots (*Figure 4.13* and *4.14*). One tourmaline grain is located in the region of type 2 in both plots, meaning that it probably came from a Li-poor granitoid, pegmatite or aplite. The other two tourmaline grains are located in the region of type 4 in both ternary plots, meaning that they probably came from an aluminous, Ca-poor metapelite or metapsammite.

4.9 Possible provenance areas

The variety of the source rocks is not easily explained. The Nama Basin is the foreland basin to the Damara and Gariep Belts, formed as a result of collision of Congo, Kalahari and Rio de la Plata Cratons (Miller, 1983; Gresse, 1986; Gray et al., 2006). The Damara Belt has been divided into several zones. The Northern and Central Zones consists mostly of a granite-dominated belt, where the granitoids are composite bodies with intrusive phases ranging from syenite to biotite-granite and late-stage aplite dykes. The Southern Zone is composed of metasediments and a long linear zone of amphibolite (Gray et al., 2008). Paleocurrents from previous studies show that most of the detrital sediments of the Nama Group were transported approximately from north to south (Germs, 1983). The Damara Belt is located north of the deposits of the Rosenhof and Haribes Members.

The Namaqua Belt/Namaqua-Natal Metamorphic Province (NNMP) is one of the most high-grade metamorphic belts of Mesoproterozoic age in sub-Saharan Africa. It is divided into several terranes or subprovinces based on distinct plate tectonic and paleogeographic environments (Evans et al., 2007). The NNMP has been divided into two zones. The Northern Volcanic Zone consists mostly of mafic, intermediate and felsic volcanic and intrusive rocks metamorphosed to greenschist or amphibolite facies. The Southern Sedimentary Zone consists mostly of pelitic rocks, metamorphosed at amphibolite to granulite facies and intrusions of syntectonic granites (Evans et al., 2007). The Namaqua Belt is located to the south of the deposits of the Rosenhof and Haribes Members.

It is quite a distance (hundreds of kilometers) from the sampling locality to the Damara Belt. The distance is shorter from the sampling area to the Namaqua Belt (*Figure 1.11* and *1.12*). The rounded grains that have been transported for a longer distance may come from the north from the Damara Belt, and the angular grains that have been transported for a shorter distance may come from the south from the Namaqua Belt. However, the heavy mineral grains are probably river deposits, and therefore it is more reliable that the source rocks are close. It should also not have been such a selection among the heavy mineral grains if they were transported hundreds of kilometers.

4.10 Comparison of analytical methods

FE-SEM combined with EDS can identify heavy minerals and it provides semi-quantitative heavy mineral data, so it is a useful tool when wanting to get some idea of the heavy mineral content in a rock. The measurements with the FE-SEM combined with EDS are however not as accurate as those taken with the MLA and EMPA. The XRD is a useful tool when wanting to check if the measurements with the FE-SEM, MLA and EMPA have been interpreted correctly. It is especially helpful if you have minerals in a rock that are polymorphic and you want to know which of the polymorphs that are present. However, the XRD usually does not provide exact quantitative data like the MLA.

The MLA is a very useful analytical method for exact quantification of heavy minerals in a rock. It is also useful for identification of heavy minerals, but it does not provide detailed element compositions, meaning that some of the lighter elements or elements that have very low wt% in a mineral are often not detected. The EMPA is a very good analytical method for detecting accurate element compositions in heavy minerals. The EMPA detects light elements and elements that have very low wt% in a mineral.

The combination of FE-SEM-EDS and XRD can identify different heavy minerals, and do semi-quantification of minerals in a rock. The XRD is the only method that can distinguish between polymorphic minerals. The MLA is the best analytical method for quantitative analyses, and the EMPA is the most exact method for identification of minerals based on chemical composition. However, combining all analytical methods, FE-SEM-EDS, XRD, MLA and EMPA, they will complement each other and provide the most accurate results.

4.11 Reliability of the data

Reliability of the data is always important to consider when working with all analytical methods. Several circumstances can affect the results. Human error is one factor. When handpicking the heavy mineral grains with a needle it should be a random selection of grains, but with a human making the choice it is not completely random. Pollution of the samples could have occurred, but are unlikely.

All the analytical methods used in this project have a certain source of error in their measurements. For example when using the EDS there are possible errors with the resolution and with the x-rays and how they interact with the sample. Some of the mounds were not polished well enough (until the middle of the grain) and therefore not all grains are representative for particle size distributions, grain size distributions or grain shape analyses. The MLA estimating particle/grain sizes does not take this into account, but it was taken into account when analysing the results, and grains with unrealistic shapes were not considered.

There is a possibility that some of the minerals have been identified as the wrong mineral. It can be that some of the amphibole is tourmaline or pyroxene. There are not many of them and therefore they do not create a large peak in the XRD analyses, and all other analytical methods (FE-SEM, MLA and EMPA) only show the chemical composition, which can be similar for those minerals. This can also be the case for some of the garnet, which can be amphibole or epidote if you only look at the chemical composition. However, it is unlikely because several BSE-images of amphiboles were studied and does not look like tourmaline or pyroxene, and the garnet does not look like amphibole or epidote. If grains have been classified wrong, then it probably does not apply to many of the grains and the results would be very similar to those interpreted.

5 APPLICATION FOR THE HYDROCARBON INDUSTRY

Sediment provenance studies include the origin, composition, transportation and deposition of sediments. It is an important part of understanding the links between basin sedimentation, hinterland tectonics and source rocks (Smyth et al., 2014). Provenance studies and heavy mineral analysis are useful for both hydrocarbon exploration and production. Heavy mineral analysis can for example be used as a geosteering tool for drilling high-angle wells (Morton, 2007).

5.1 Correlation and linking sediment to source

Provenance studies of sandstones can be a very valuable tool when wanting to understand the main characteristics of source areas, adjacent basins and the tectonic setting of which the sedimentary succession was deposited (McLennan et al., 1990). Heavy minerals analyses are very useful for sandstone correlation because heavy minerals are highly sensitive indicators of provenance and transport history of sediments (Mange and Maurer, 1992; Morton and Hallsworth, 1999). Changes in provenance and processes in the sedimentary cycle, e.g. weathering during transport and diagenesis, may affect the heavy minerals. It is important to distinguish between processes affecting the heavy minerals prior, during or after deposition, especially for correlation purposes. Even though heavy minerals might be altered during the sedimentary cycle, they still have a potential for sediment correlation (Morton and Berge, 1995). The use of heavy mineral, mineral chemical and zircon age data to discriminate sandstones and their origin can be crucial to hydrocarbon exploration of an area. These high-resolution heavy mineral studies are useful for both correlation and to pinpoint the type of source rocks (e.g. Fleming et al., 2016).

5.2 Provenance, diagenesis and reservoir quality

Provenance studies are used for learning more about diagenesis, estimating reservoir quality, and linking sediment to a source. Provenance studies can be valuable for many stages in hydrocarbon exploration and production. It is useful for identifying regional scale crustal affinities and for understanding sediment-dispersal patterns. Provenance studies can be used for detailed correlation in producing reservoirs. Provenance studies can help to enhance the understanding of reservoir presence, reservoir distribution and reservoir quality. The source areas control the composition of the clastic rock, grain form, mineral types, which in turn control grain form and size. This information is very important for reservoir characterization in terms of porosity development, and further estimation of the reservoir quality. Quantification of composition can make diagenetic processes more understandable (Smyth et al., 2014). Reservoir presence can be a major area of uncertainty (e.g. in the deep water Norwegian Sea) and provenance studies can help to reduce this uncertainty (Morton et al., 2005). Provenance studies on shales can be used for evaluating sealing capacities and will influence the risk estimations at both play and prospect levels (Smyth et al., 2014).

5.3 Geosteering tool for drilling of high-angle wells

Heavy mineral analysis has been used to monitor the stratigraphy while drilling high-angle wells. It has been used as a tool for drilling horizontal wells in at least three fields (Clair, Ross and Hannay) on the UK continental shelf. Heavy mineral data are used for deciding where the well bore trajectories should be so that they stay within the hydrocarbon-bearing zones, and this process is often referred to as geosteering. Heavy mineral data can be used for drilling in several depositional environments, and it is a very good alternative geosteering tool if biostratigraphic methods are insufficient. For the Clair, Ross and Hannay Fields the heavy mineral analysis has had positive results for geosteering horizontal wells in fluvial, shallow marine and deep marine deposits (Morton, 2007). The heavy mineral analysis is used real-time at the well site to monitor the stratigraphy during drilling. The heavy mineral data can be used for several decisions while drilling. It can help to decide if it is best to maintain the drilling angle, if it is necessary to steer up or down, if a sidetrack is the best option or of the drilling should be terminated. The geosteering of the wells is also important in an economic view, as a large number of high-angle wells can be drilled from the same production facility (Morton, 2007).

6 FURTHER WORK

The results from the ICP-MS analyses were delayed and are therefore not included in this thesis. The ICP-MS analyses would have given estimated ages for the detrital zircons from the zircon concentrates of the samples. Geochronological constraints would have been provided by zircon age dating, and will be considered for further work. The zircon ages can help to determine the provenance of the sediments, e.g. if the sediments come from the Damara Belt (related to the formation of the supercontinent Gondwana) or the Namaqua Belt (related to the formation of the supercontinent Rodinia).

Some of the analyses with EMPA were also delayed. Ages for the few monazite grains can be estimated based on values provided by the EMPA. The age of the monazite grains can further be compared to the age of the zircon grains. The EMPA can identify the chemical composition of a monazite grain and determine the age of the grain by analysing the radioactive elements thorium (Th), uranium (U) and lead (Pb).

The EMPA can also be used to distinguish between different types of apatite, which might say something about the provenance depending on their composition. The FE-SEM-EDS and XRD indicate that most of the apatites are fluorapatite, but the EMPA can provide more accurate chemical compositions for the apatite.

7 CONCLUSION

This study has illustrated the effectiveness of an integrated methodology to provenance evaluation using heavy mineral data from several analytical methods. The heavy mineral data provide the knowledge for identifying different types of sandstones and placer deposits with different provenance. It allows for their source regions to be characterized by analysing lithology and mineralogy. This high-resolution heavy mineral study takes advantage of the single-grain analyses and gives a more complete picture of sediment provenance by using several analytical techniques instead of one technique in isolation. Comparing and combining the results from several analytical techniques gives a more conclusive result.

The value of this approach is illustrated with the case study of placer deposits ("black sands") from the Nama Group (Fish River Subgroup) in Namibia. Heavy minerals in the samples/fractions are identified and quantified. All analytical methods, FE-SEM-EDS, XRD, MLA and EMPA, identifies the same heavy minerals in the samples: chamosite, amphibole, tourmaline, garnet (almandine and grossular), magnetite, ilmenite, rutile, titanite, zircon and apatite. The main difference between the samples is that the sample from the Haribes Member contains larger amounts of grossular, less amounts of almandine and larger amounts of tourmaline, compared to the samples from the Rosenhof Member.

Grain shapes, particle size distributions and sorting indicate that the transporting medium was a river. A fluvial depositional system for the Rosenhof and Haribes Members were assumed before starting the analyses of the samples, because of previous studies on samples from the same area. The results from this project agree with these conclusions. The sediments were generally accumulated in a river and the energy of the water flow caused a selective settling of the heavy minerals. The settling velocity is a function of grain size and grain density, therfore the smaller and denser minerals have the same settling velocity as the larger and less dense minerals. In general the grains in the samples from the Haribes Member have a smaller grain size than the samples from the Rosenhof Member, which means that the grains from the Haribes Member have lower grain settling velocities.

The ultrastable heavy minerals rutile and zircon are in this project mostly sub-rounded, indicating some amount of transport. The stable apatite grains are mostly rounded to sub-rounded, but some are also well rounded. The apatite grains could therefore not have been transported too far, and probably for a shorter distance than the ultrastable heavy minerals. The almandine grains are mostly sub-angular, and the grossular grains are mostly sub-rounded to sub-angular. The most stable garnet, the almandine, are generally not as rounded as the less stable garnet, the grossular. This indicates that the almandine and grossular can have been transported for approximately the same distance, and probably for a shorter distance than the ultrastable heavy minerals.

The chemical composition of the heavy minerals indicates that the sediments derived from several provenances. Garnets are interpreted to derive from three types of source rocks. Most almandines are interpreted to derive from metasediments (including amphibolite facies), from high-grade metamorphic rocks or acidic to intermediate gneisses and granites. Some almandines might derive from high-grade mafic and ultramafic gneisses including eclogites, and the grossulars are interpreted to derive from contact or thermally metamorphosed calcareous sediments or associated with metasomatic skarns. The titanites are interpreted to derive from a mafic igneous rock. Tourmalines are interpreted to derive from two source rocks: Li-poor granitoid, pegmatite or aplite, and aluminous, Ca-poor metapelite or metapsammite.

The detrital heavy mineral record of the deposits of the Fish River Subgroup indicate a complex source region composed of high-grade metamorphic rocks (metasomatic skarns, metapelites, metapsammites and/or gneisses), felsic rocks (granitic, pegmatite and/or aplite) and mafic rocks. The variety of the source rocks is not easily explained. Sources for the detrital heavy minerals in the samples in this project can be the Damara Belt located to the north of the deposits or the Namaqua Belt located to the south of the deposits. However, more results indicate that the source is the Namaqua Belt.

The heavy mineral grains are generally not well rounded, they are probably river deposits, and therefore they are not likely to have been transported hundreds of kilometers. The source for most of the grains seems therefore to be close, indicating that it could be the Namaqua Belt located next to and south of the sampling area. The Northern Volcanic Zone of the Namaqua Belt consists of mafic, intermediate and felsic volcanic and intrusive rocks metamorphosed to greenschist or amphibolite facies, and can therefore be the source for the almandine grains, some of the tourmaline grains and the titanite grains. The Southern Sedimentary Zone contains of pelitic rocks, and can therefore be the source for some of the tourmaline grains.

REFERENCES

Asiedu, D. K., Suzuki, S. and Shibata, T. (2000). Provenance of sandstones from the Lower Cretaceous Sasayama Group, Inner Zone of Southwest Japan. *Sedimentary Geology, 131*, 9-24.

Becker, J. S. (2007). *Inorganic Mass Spectrometry: Principles and Applications.* John Wiley & Sons Ltd, Chichester, England, 514 pp.

Bekkum, J. and Egeland, D. (2016). *Testing the validity of EDS analysis at a FE-SEM for quantification of major elements in rock samples related to EOR experiments.* Bachelor Thesis, University of Stavanger, Stavanger, 62 pp.

Blanco, G. (2008). *Provenance analysis of the Neoproterozoic-Cambrian Nama Group (Namibia) and the Arroyo del Soldado Group (Uruguay): Implications for the palaeogeographic reconstruction of SW Gondwana*. Unpublished PhD thesis, University of Johannesburg, 299 pp.

Blanco, G., Germs, G. J. B., Rajesh, H. M., Chemale Jr., F., Dussin, I. A. and Justino, D. (2011). Provenance and paleogeography of the Nama Group (Ediacaran to early Palaeozoic, Namibia): Petrography, geochemistry and U-Pb detrital zircon geochronology. *Precambrian Research*, *187*, 15-32.

Blanco, G., Rajesh, H. M., Germs, G. J. B. and Zimmermann, U. (2009). Chemical Composition and Tectonic Setting of Chromian Spinels from the Ediacaran-Early Paleozoic Nama Group, Namibia. *The Journal of Geology*, *117*, 325-341.

Blanco, G., Zimmermann, U., Germs, G. J. B. and Gaucher, C. (2006). Provenance study on “black sands”: A case study from the Lower Cambrian Fish River Sub-Group (Nama Group, Namibia). *V South American Symposium on Isotope Geology*, short paper, Punta del Este.

Boggs Jr., S. and Krinsley, D. (2006). *Application of Cathodoluminescence Imaging to the Study of Sedimentary Rocks*. Cambridge University Press, New York, US, pp. 165.

Clemens, K. E. and Komar, P. D. (1988). Oregon beach sand compositions produced by the mixing of sediments under a transgressing sea. *Journal of Sedimentary Petrology, 58*, 519-529.

Conway Morris, S. (1990). Late Precambrian and Cambrian soft-bodied faunas. *Annu. Rev. Earth Planetary Science Letters*, *18*, 101-122.

Deer, W. A., Howie, R. A. and Zussman, J. (1982). *Rock-Forming Minerals, Orthosilicates Volume 1A (2nd ed.)*. Longman, London, 919 pp.

Deer, W. A., Howie, R. A. and Zussman, J. (1992). *An Introduction to the Rock-Forming Minerals (2nd ed.)*. Pearson, London, England, 696 pp.

Evans, A. D. E. (2009). The palaeomagnetically viable, long-lived and all-inclusive Rodinia supercontinent reconstruction. In: Murphy, J. B., Keppie, J. D., Jynes, A. J. (eds.), *Ancient orogens and modern analogues*. Geological Society, London, Special Publications, 327, 371-404.

Evans, D. M., Windrim, D. P. and Armstrong, R. A. (2007). Age of Metamorphic rocks at the northern margin of the Namaqua-Natal Metamorphic Province in the Karas Mountains, Namibia, defined by SHRIMP U-Pb dating of zircons. *South African Journal of Geology, 110*, 47-54.

Fandrich, R., Gu, Y., Burrows, D. and Moeller, K. (2007). Modern SEM-based mineral liberation analysis. *International Journal of Mineral Processing*, *84*, 310-320.

Fleming, E. J., Flowerdew, M. J., Smyth, H. R., Scott, R. A., Morton, A. C., Omma, J. E., Frei, D. and Whitehouse, M. J. (2016). Provenance of Triassic sandstones on the southwest Barents Shelf and the implication for sediment dispersal patterns in northwest Pangaea. *Marine and Petroleum Geology*, *78*, 516- 535.

Foster, D. A. and Goscombe, B. D. (2013). Continental Growth and Recycling in Convergent Orogens with Large Turbidite Fans on Oceanic Crust. *Geosciences, 3,* 354-388.

Friedman, G. M. (1961). Distinction between dune, beach, and river sands from their textural characteristics. *Journal of Sedimentary Petrology, 31(4),* 514-529.

Frimmel, H. E., Basei, M. S. and Gaucher, C. (2011). Neoproterozoic geodynamic evolution of SW-Gondwana: a southern African perspective. *International Journal of Earth Sciences (Geologische Rundschau), 100*, 323-354.

Garzanti, E., Andò, S. and Scutellà, M. (2000). Actualistic ophiolite provenance: the Cyprus case. *The Journal of Geology*, *108*, 199-218.

Garzanti, E., Vezzoli, G., Andò, S., Lavé, J., Attal, M., France-Lanord, C. and DeCelles, P. (2007). Quantifying sand provenance and erosion (Marsyandi River, Nepal Himalaya). *Earth and Planetary Science Letters*, *258*, 500-515.

Gaucher, C., Frimmel, H. E. and Germs, G. J. B. (2010). Tectonic events and Paleogeographic evolution of Southwestern Gondwana in the Neoproterozoic and Cambrian. In: Gaucher, C., Sial, A. N., Halverson, C. P., Frimmel, H. E. (eds.), *Neoproterozoic-Cambrian Tectonics, global change and evolution: A focus on southwestern Gondwana*. Developments in Precambrian Geology, 16, 295-316.

Germs, G. J. B. (1974). The Nama Group in South West Africa and its relationship to the Pan-African geosyncline. *The Journal of Geology*, *82*, 301-317.

Germs, G. J. B. (1983). Implications of sedimentary facies and depositional environmental analysis of the Nama Group in South West Africa/Namibia. In: Miller, R. M. (eds.), *Evolution of the Damara Orogen of South West Africa/Namibia*. *Geological Society of South Africa Special Publication*, *11*, 89-114.

Germs, G. J. B. (1995). The Neoproterozoic of southwestern Africa, with emphasis on platform stratigraphy and paleontology. *Precambrian Research*, *73*, 137-151.

Germs, G. J. B. and Gresse, P. G. (1991). The foreland basin of the Damara and Gariep orogens in Namaqualand and southern Namibia: stratigraphic correlations and basin dynamics. *South African Journal of Geology*, *94*, 159-169.

Geyer, G. (2005). The Fish River Subgroup in Namibia: stratigraphy, depositional environments and the Proterozoic-Cambrian boundary problem revisited. *Geological Magazine*, *142*, 465-498.

Google earth V 7.1.5.1557 (May 20, 2015). Namibia, southern Africa. 26°38′43.87′′S, 19°08′08.01′′E, Eye alt 3238.17 km, and 26°37′30.74′′S, 19°13′28.61′′E, Eye alt 783.37 km. SIO, NOAA, U.S. Navy, NGA, GEBCO. AfriGIS (Pty) Ltd., 2016. http://www.earth.google.com [downloaded May 15, 2017].

Götze, J., Schertl, H.-P., Neuser, R. D., Kempe, U. and Hanchar, J. M. (2013). Optical microscope-cathodoluminescence (OM-CL) imaging as a powerful tool to reveal internal textures of minerals. *Mineralogy and Petrology*, *107*, 373-392.

Gray, D. R., Foster, D. A., Goscombe, B. D., Passchier, C. W. and Trouw, R. A. J. (2006). 40Ar/39Ar thermochronology of the Pan-African Damara Orogen, Namibia, with implications for tectonothermal and geodynamic evolution. *Precambrian Research*, *150*, 49-72.

Gray, D. R., Foster, D. A., Meert, J. G., Goscombe, B. D., Armstrong, R., Trouw, R. A. J. and Passchier, C. W. (2008). A Damara orogen perspective on the assembly of southwestern Gondwana. In: Pankhurst, R. J., Trouw, R. A. J., Neves, B. B. B. and De Wit, M. J. (eds.), *West Gondwana: Pre-Cenozoic Correlations Across the South Atlantic Region*. Geological Society, London, Special Publications, 294, 257-278.

Gresse, P. G. (1986). The Tectono-Sedimentary History of the Vanrhynsdorp Group. Unpublished PhD thesis, University of Cape Town, 155 pp.

Gresse, P. G. and Germs, G. J. B. (1993). The Nama foreland basin: sedimentation, major unconformity bounded sequences and multisided margin advance. *Precambrian Research, 63*, 247-272.

Grotzinger, J. P., Bowring, S. A., Saylor, B. Z. and Kaufman, A. J. (1995). Biostratigraphic and geochronologic constraints on early animal evolution. *Science*, *270*, 598-604.

Harland, W. B., Armstrong, R. L., Cox, A. V., Craig, L. E., Smith, A. G. and Smith, D. G. (eds.) (1990). *A Geological Time Scale 1989*, Cambridge University Press, Cambridge, 263 pp.

Henry, D. J. and Guidotti, C. V. (1985). Tourmaline as a petrogenetic indicator mineral: an example from the staurolite-grade metapelites of NW Maine. *American Mineralogist, 70*, 1-15.

Hessenbruch, A. (2002). A brief history of x-rays. *Endeavour*, *26(4)*, 137-141.

Hjelen, J. (1986). *Scanning elektron-mikroskopi*. SINTEF, Avdeling for metallurgi, NTH, Trondheim, 106 pp.

Hofmann, M., Linnemann, U., Hoffmann, K.-H., Gerdes, A., Eckelmann, K. and Gärtner, A. (2013). The Namuskluft and Dreigratberg sections in southern Namibia (Kalahari Craton, Gariep Belt): a geological history of Neoproterozoic rifting and recycling of cratonic crust during the dispersal of Rodinia until the amalgamation of Gondwana. *International Journal of Earth Sciences (Geologische Rundschau), 103*, 1187-1202.

Irvine, T. N. (1967). Chromian spinel as a petrogenetic indicator. Part 2: petrologic applications. *Canadian Journal of Earth Sciences*, *4*, 71-103.

Jacobs, J., Pisarevsky, S., Thomas, R. J. and Becker, T. (2008). The Kalahari Craton during the assembly and dispersal of Rodinia. *Precambrian Research, 160*, 142-168.

Jenkins, R. J. F. (1984). Ediacaran events: boundary relationships and correlation of key sections, especially in Armorica. *Geological Magazine*, *121*, 635-643.

Kamenetsky, V. S., Crawford, A. J. and Meffre, S. (2001). Factors controlling chemistry of magmatic spinel: an empirical study of associated olivine, Cr-spinel and melt inclusions from primitive rocks. *Journal of Petrology*, *42*, 655-671.

Komar, P. D. (2007). Chapter 1 The Entrainment, Transport and Sorting of Heavy Minerals by Waves and Currents. In: Mange, M. A. and Wright, D. T., *Heavy Minerals in Use*. Elsevier, Amsterdam, Developments in Sedimentology, 58, 3-48.

Landmann, M., Rauls, E. and Schmidt, W. G. (2012). The electronic structure and optical response of rutile, anatase and brookite TiO_2. *Journal of Physics: Condensed Matter*, *24*, 1-6.

Leeder, M. (2011). Clastic sediment as a chemical and physical breakdown product. In: *Sedimentology and Sedimentary Basins: From Turbulence to Tectonics*, 3-26.

Leng, Y. (2013). *Materials Characterization: Introduction to Microscopic and Spectroscopic Methods (2nd ed.)*. Wiley-VCH, Weinheim, Germany, 392 pp.

Li, Z. X., Bogdanova, S. V., Collins, A. S., Davidson, A., De Waele, B., Ernst, R. E., Fitzsimons, I. C. W., Fuck, R. A., Gladkochub, D. P., Jacobs, J., Karlstrom, K. E., Lu, S., Natapov, L. M., Pease, V., Pisarevsky, S. A., Thrane, K. and Vernikovsky, V. (2008). Assembly, configuration, and break-up history of Rodinia: A synthesis. *Precambrian Research, 160*, 179-210.

Longiaru, S. (1987). Visual comparators for estimating the degree of sorting from plane and thin section. *Journal of Sedimentary Petrology, 57(4)*, 791-794.

Mange, M. A. and Maurer, H. F. W. (1992). *Heavy Minerals in Colour*. Chapman & Hall, London, 147 pp.

Mange, M. A. and Morton, A. C. (2007). Chapter 13 Geochemistry of Heavy Minerals. In: Mange, M. A. and Wright, D. T. (eds.), *Heavy Minerals in Use*. Elsevier, Amsterdam, Developments in Sedimentology, 58, 345-391.

McLennan, S. M., Taylor, S. R., McCulloch, M. T. and Maynard, J. B. (1990). Geochemical and Nd-Sr isotopic composition of deep-sea turbidites: Crustal evolution and plate tectonic associations. *Geochimica et Cosmochimica Acta*, *54*, 2015-2050.

Miller, R. McG. (1983). The Pan-African Damara Orogen of South West Africa/Namibia. *Geological Society of South Africa Special Publication*, *11*, 431-515.

Morton, A. C. (1987). Influences of provenance and diagenesis on detrital garnet suites in the Forties sandstone, Paleocene, central North Sea. *Journal of Sedimentary Petrology, 57*, 1027-1032.

Morton, A. C. (2007). Chapter 44 The Role of Heavy Mineral Analysis as a Geosteering Tool During Drilling of High-Angle Wells. In: Mange, A. M. and Wright, D. T. (eds.), *Heavy Minerals in Use.* Elsevier, Amsterdam, Developments in Sedimentology, 58, 1123-1142.

Morton, A. C. (2012). Value of heavy minerals in sediments and sedimentary rocks for provenance, transport history and stratigraphic correlation. In: Sylvester, P. (ed.), *Quantitative Mineralogy and Microanalysis of Sediments and Sedimentary Rocks.* Mineralogical Association of Canada Short Course Series, 42, 133-165.

Morton, A. C. and Berge, C. (1995). Heavy mineral suites in the Statfjord and Nansen Formations of the Brent Field, North Sea: a new tool for reservoir subdivision and correlation. *Petroleum Geoscience, 1*, 355-364.

Morton, A. C. and Hallsworth, C. R. (1999). Processes controlling the composition of heavy mineral assemblages in sandstones. *Sedimentary Geology, 124*, 3-29.

Morton, A. C., Whitham, A. G. and Fanning, C. M. (2005). Provenance of Late Cretaceous to Paleocene submarine fan sandstones in the Norwegian Sea: Integration of heavy mineral, mineral chemical and zircon age data. *Sedimentary Geology, 182*, 3-28.

Nichols, G. (2009). *Sedimentology and Stratigraphy (2nd ed.)*. Blackwell Publishing, West Sussex, UK, 419 pp.

Osterkamp, W. R. and Morton R. A. (2005). Mining of Coastal Materials. In: Schwartz, M. L. (ed.), *Encyclopedia of Coastal Science*. Springer, Dordrecht, The Netherlands, pp. 1213.

Pettijohn, F. J., Potter, P. E. and Siever, R. (1987). *Sand and Sandstone (2nd ed.)*. Springer-Verlag, New York, 553 pp.

Pisarevsky, S. A., Wingate, M. T. D., Powell, C. McA., Johnson, S. and Evans, D. A. D. (2003). Models of Rodinia assembly and fragmentation. In: Yoshida, M., Windley, B. F., Dasgupta, S. (eds.), *Proterozoic East Gondwana: Supercontinent Assembly and Breakup*. Geological Society, London, Special Publications, 206, 35-55.

Powers, M. C. (1953). A new roundness scale for sedimentary particles. *Journal of Sedimentary Petrology, 23*, 117-119.

Press, F. and Siever, R. (1986). *Earth (2nd ed.)*. W. H. Freeman, New York, pp. 649.

Reading, H. G. and Levell, B. K. (1996). Controls on the sedimentary rock record. In: Reading, H. G. (ed.), *Sedimentary Environments: Processes, Facies and Stratigraphy (3rd ed.)*. Blackwell Publishing, Malden, USA, 5-36.

Reed, S. J. B. (2005). *Electron microprobe analysis and scanning electron microscopy in geology (2nd ed.)*. Cambridge University Press, Cambridge, UK, 192 pp.

Rollinson, H. R. (1993). *Using Geochemical Data: Evaluation, Presentation, Interpretation*. Longman Group UK Limited, Harlow, Essex, England, 352 pp.

SACS (South African Committee for Stratigraphy) (1980). The Nama Group. In: Kent, L. E. (eds.), *Lithostratigraphy of the Republic of South Africa, SW Africa/Namibia, and the Republics of Bophuthatswana, Transkei and Venda*. Handbook Geological Survey of South Africa, 8, 690 pp.

Sabeen, H. M., Ramanujam, N. and Morton, A. C. (2002). The provenance of garnet: constraints provided by studies of coastal sediments from southern India. *Sedimentary Geology, 152*, 279-287.

Saylor, B. Z., Grotzinger, J. P. and Germs, G. J. B. (1995). Sequence stratigraphy and sedimentology of the Neoproterozoic Kuibis and Schwarzrand Subgroup (Nama Group, southwestern Namibia). *Precambrian Research*, *73*, 153-171.

Severin, K. P. (2004). *Energy Dispersive Spectrometry of Common Rock Forming Minerals*. Kluwer Academic Publishers, Dordrecht, The Netherlands, 225 pp.

Smyth, H. R., Morton, A., Richardson, N. and Scott, R. A. (2014). Sediment provenance studies in hydrocarbon exploration and production: an introduction. In: Scott. R. A., Smyth, H. R., Morton, A. C. and Richardson, N. (eds.), *Sediment Provenance Studies in Hydrocarbon Exploration and Production*. Geological Society, London, UK, Special Publications, 386, 1-6.

Sylvester, P. J. (2012). Use of the Mineral Liberation Analyser (MLA) for mineralogical studies of sediments and sedimentary rocks. *Mineral Association of Canada Short Course 42*, 1-16.

Trompette, R. (1994). *Geology of Western Gondwana (2000-500 Ma)*. Taylor & Francis, New York, 350 pp.

Westman-Brinkmalm, A. and Brinkmalm, G. (2008). A mass spectrometer´s building blocks. In: Ekman, R., Silberring, J. and Brinkmalm, A. M. (eds.), *Wiley Series on Mass Spectrometry Ser.: Mass Spectrometry: Instrumentation, Interpretation, and Applications.* John Wiley & Sons, Hoboken, USA, 405 pp.

APPENDICES

Appendix A: Spectrums from FE-SEM-EDS analyses

Spectrums for minerals identified with FE-SEM and EDS are listed as mineral 1-23. EDS measurements on grains/phases similar to spectrums 1-23 are classified as the corresponding mineral type.

#	Mineral
1	Quartz
2	Albite
3	Orthoclase
4	Calcite
5	Chamosite
6	Muscovite
7	Amphibole
8	Tourmaline
9	Almandine-Mn
10	Almandine
11	Grossular
12	Magnetite
13	Magnetite-Ti
14	Ilmenite
15	Rutile
16	Titanite
17	Titanite-Fe
18	Zircon
19	Apatite-Cl
20	Apatite-F
21	Apatite-OH
22	Barite
23	Monazite-Ce

1) Quartz

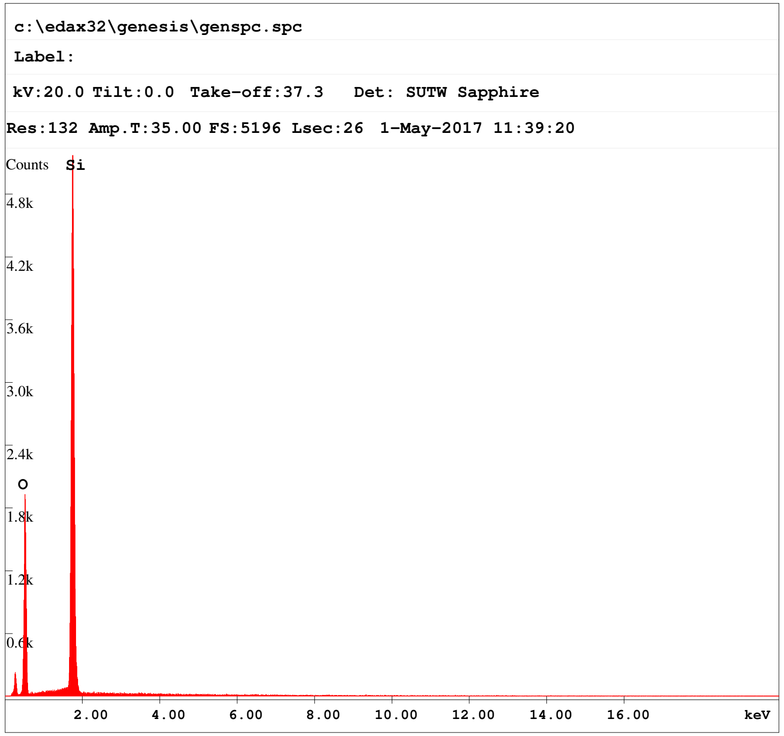

EDAX ZAF Quantification (Standardless)
Element Normalized
SEC Table : User c:\edax32\eds\genuser.sec

Element	Wt %	At %	K-Ratio	Z	A	F
O K	56.24	69.29	0.2173	1.0183	0.3794	1.0005
SiK	43.76	30.71	0.3544	0.9761	0.8297	1.0000
Total	100.00	100.00				

Element	Net Inte.	Bkgd Inte.	Inte. Error	P/B
O K	387.46	3.61	0.99	107.43
SiK	1403.00	12.27	0.52	114.35

2) Albite

c:\edax32\genesis\genspc.spc
Label:
kV:20.0 Tilt:0.0 Take-off:35.1 Det: SUTW Sapphire
Res:132 Amp.T:35.00 FS:3394 Lsec:23 28-Feb-2017 12:38:08

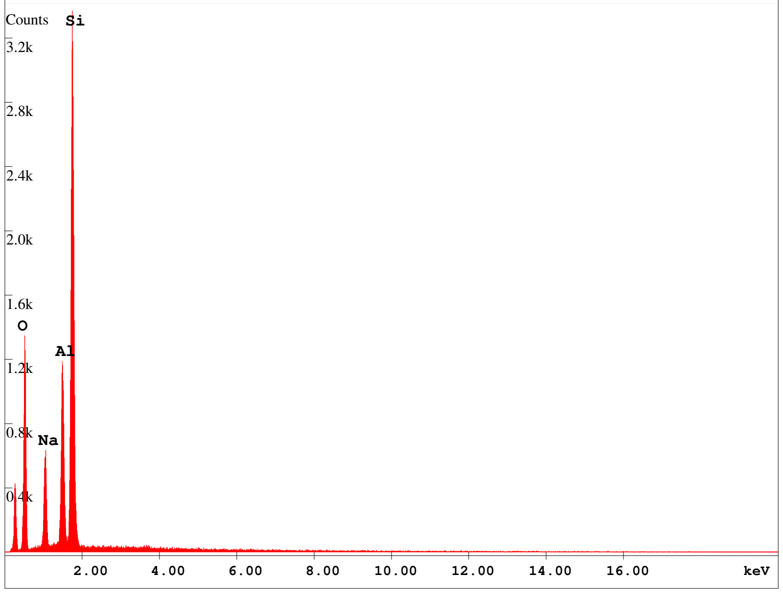

EDAX ZAF Quantification (Standardless)
Element Normalized
SEC Table : User c:\edax32\eds\genuser.sec

Element	Wt %	At %	K-Ratio	Z	A	F
O K	46.07	59.07	0.1741	1.0307	0.3664	1.0006
NaK	5.05	4.51	0.0219	0.9647	0.4466	1.0055
AlK	24.04	18.28	0.1631	0.9599	0.7011	1.0077
SiK	24.84	18.14	0.1445	0.9879	0.5888	1.0000
Total	100.00	100.00				

Element	Net Inte.	Bkgd Inte.	Inte. Error	P/B
O K	307.12	4.52	1.20	67.89
NaK	160.93	11.72	1.75	13.73
AlK	327.59	13.10	1.19	25.01
SiK	1002.54	13.96	0.66	71.81

3) Orthoclase

c:\edax32\genesis\genspc.spc
Label:
kV:25.0 Tilt:0.0 Take-off:37.2 Det: SUTW Sapphire
Res:131 Amp.T:50.00 FS:1181 Lsec:12 18-Feb-2017 15:09:54

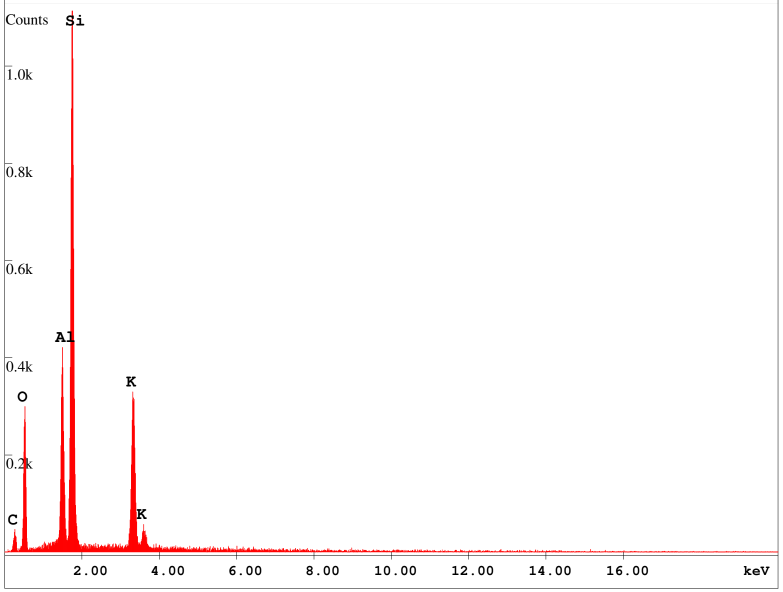

EDAX ZAF Quantification (Standardless)
Element Normalized
SEC Table : Default

Element	Wt %	At %	K-Ratio	Z	A	F
O K	37.82	53.15	0.0783	1.0333	0.2004	1.0005
AlK	11.05	9.21	0.0710	0.9653	0.6541	1.0171
SiK	36.49	29.21	0.2322	0.9940	0.6388	1.0024
K K	14.65	8.42	0.1139	0.9429	0.8247	1.0000
Total	100.00	100.00				

Element	Net Inte.	Bkgd Inte.	Inte. Error	P/B
O K	138.58	1.68	2.43	82.71
AlK	215.09	8.94	2.00	24.07
SiK	671.53	8.62	1.10	77.94
K K	249.40	5.74	1.83	43.42

4) Calcite

c:\edax32\genesis\genspc.spc
Label:
kV:20.0 Tilt:0.0 Take-off:35.1 Det: SUTW Sapphire
Res:131 Amp.T:50.00 FS:2366 Lsec:22 28-Feb-2017 13:36:45

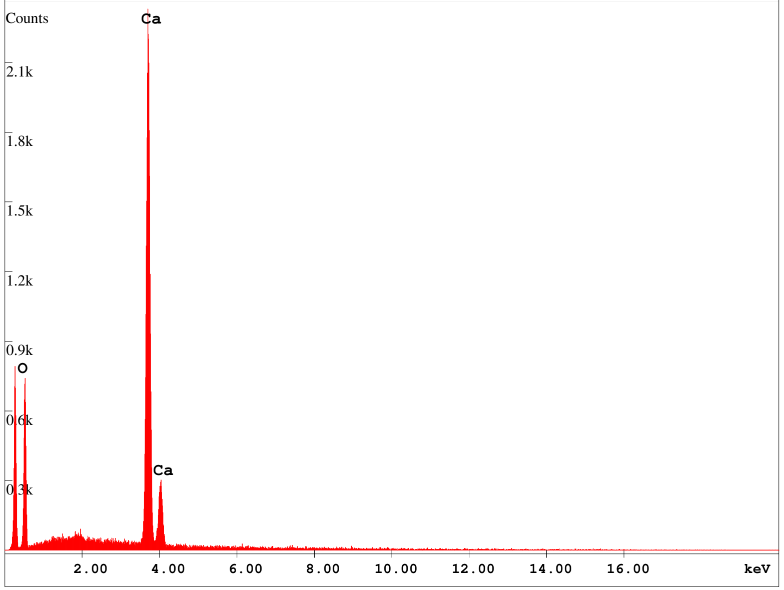

EDAX ZAF Quantification (Standardless)
Element Normalized
SEC Table : User c:\edax32\eds\genuser.sec

Element	Wt %	At %	K-Ratio	Z	A	F
O K	69.06	84.83	0.1434	1.0194	0.2037	1.0000
CaK	30.94	15.17	0.2959	0.9485	1.0085	1.0000
Total	100.00	100.00				

Element	Net Inte.	Bkgd Inte.	Inte. Error	P/B
O K	176.04	3.31	1.61	53.15
CaK	892.01	8.79	0.71	101.49

5) Chamosite

c:\edax32\genesis\genspc.spc
Label:
kV:20.0 Tilt:0.0 Take-off:37.3 Det: SUTW Sapphire
Res:131 Amp.T:50.00 FS:526 Lsec:13 1-May-2017 10:43:58

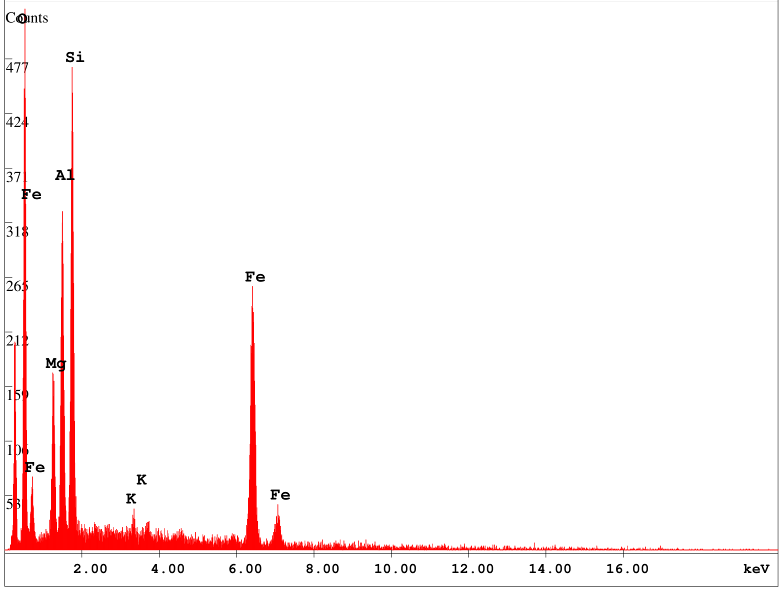

EDAX ZAF Quantification (Standardless)
Element Normalized
SEC Table : User c:\edax32\eds\genuser.sec

Element	Wt %	At %	K-Ratio	Z	A	F
O K	38.44	58.29	0.1616	1.0585	0.3967	1.0011
MgK	6.17	6.15	0.0256	1.0153	0.4075	1.0040
AlK	10.95	9.84	0.0545	0.9853	0.5031	1.0040
SiK	14.13	12.21	0.0800	1.0140	0.5580	1.0007
K K	1.87	1.16	0.0163	0.9640	0.8958	1.0091
FeK	28.45	12.36	0.2558	0.8976	1.0017	1.0000
Total	100.00	100.00				

Element	Net Inte.	Bkgd Inte.	Inte. Error	P/B
O K	200.76	2.04	1.92	98.52
MgK	70.52	10.48	3.66	6.73
AlK	148.39	10.48	2.37	14.16
SiK	220.80	11.13	1.90	19.83
K K	11.72	9.61	12.80	1.22
FeK	199.33	4.37	1.95	45.65

6) Muscovite

c:\edax32\genesis\genspc.spc
Label:
kV:20.0 Tilt:0.0 Take-off:36.8 Det: SUTW Sapphire
Res:132 Amp.T:35.00 FS:566 Lsec:6 9-Mar-2017 16:58:04

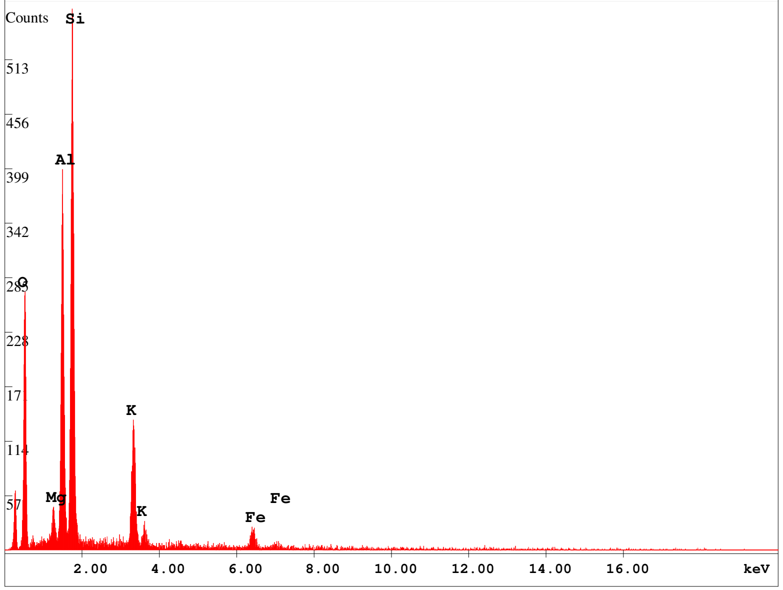

EDAX ZAF Quantification (Standardless)
Element Normalized
SEC Table : User c:\edax32\eds\genuser.sec

Element	Wt %	At %	K-Ratio	Z	A	F
O K	44.06	58.69	0.1481	1.0372	0.3239	1.0006
MgK	0.85	0.74	0.0049	0.9951	0.5773	1.0116
AlK	30.01	23.71	0.2074	0.9658	0.7116	1.0054
SiK	17.11	12.98	0.0951	0.9940	0.5591	1.0007
K K	5.07	2.76	0.0424	0.9428	0.8856	1.0009
FeK	2.91	1.11	0.0254	0.8767	0.9972	1.0000
Total	100.00	100.00				

Element	Net Inte.	Bkgd Inte.	Inte. Error	P/B
O K	235.06	1.08	2.57	218.57
MgK	32.88	11.83	8.96	2.78
AlK	369.49	12.29	2.11	30.06
SiK	584.73	12.44	1.66	46.99
K K	178.68	7.37	3.05	24.23
FeK	37.33	2.30	6.80	16.20

7) Amphibole

c:\edax32\genesis\genspc.spc
Label:
kV:20.0 Tilt:0.0 Take-off:37.3 Det: SUTW Sapphire
Res:131 Amp.T:50.00 FS:608 Lsec:12 1-May-2017 10:22:29

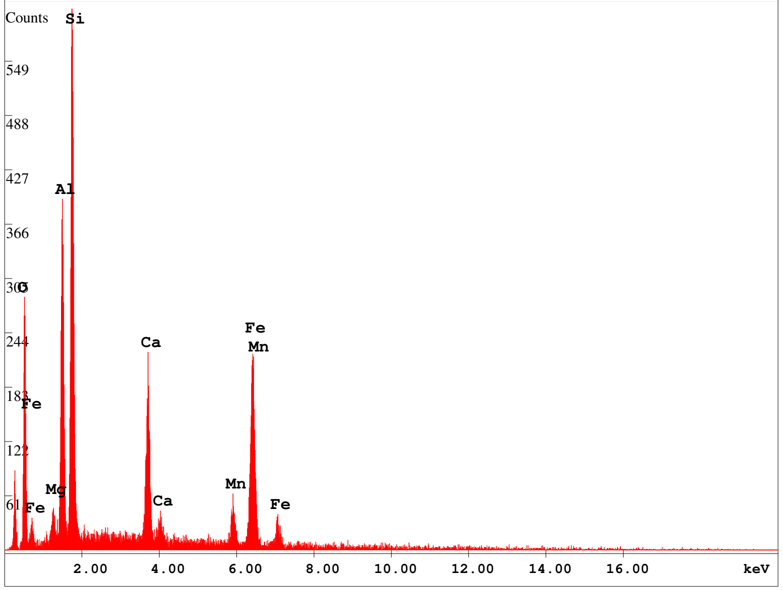

EDAX ZAF Quantification (Standardless)
Element Normalized
SEC Table : User c:\edax32\eds\genuser.sec

Element	Wt %	At %	K-Ratio	Z	A	F
O K	29.89	49.00	0.0908	1.0648	0.2850	1.0010
MgK	1.41	1.53	0.0060	1.0211	0.4146	1.0056
AlK	12.84	12.48	0.0697	0.9910	0.5448	1.0061
SiK	19.93	18.62	0.1177	1.0198	0.5781	1.0013
CaK	8.00	5.24	0.0743	0.9928	0.9229	1.0135
MnK	3.02	1.44	0.0264	0.8871	0.9854	1.0000
FeK	24.90	11.70	0.2232	0.9036	0.9920	1.0000
Total	100.00	100.00				

c:\edax32\genesis\genspc.spc

Element	Net Inte.	Bkgd Inte.	Inte. Error	P/B
O K	121.53	1.46	2.62	83.16
MgK	17.86	7.79	9.23	2.29
AlK	204.68	7.79	2.07	26.26
SiK	349.76	8.20	1.56	42.65
CaK	126.17	9.66	2.72	13.06
MnK	37.35	6.82	5.45	5.48
FeK	187.46	6.09	2.15	30.79

8) Tourmaline

c:\edax32\genesis\genspc.spc

Label:

kV:20.0 Tilt:0.0 Take-off:36.5 Det: SUTW Sapphire

Res:130 Amp.T:100.00 FS:639 Lsec:29 22-Feb-2017 10:07:02

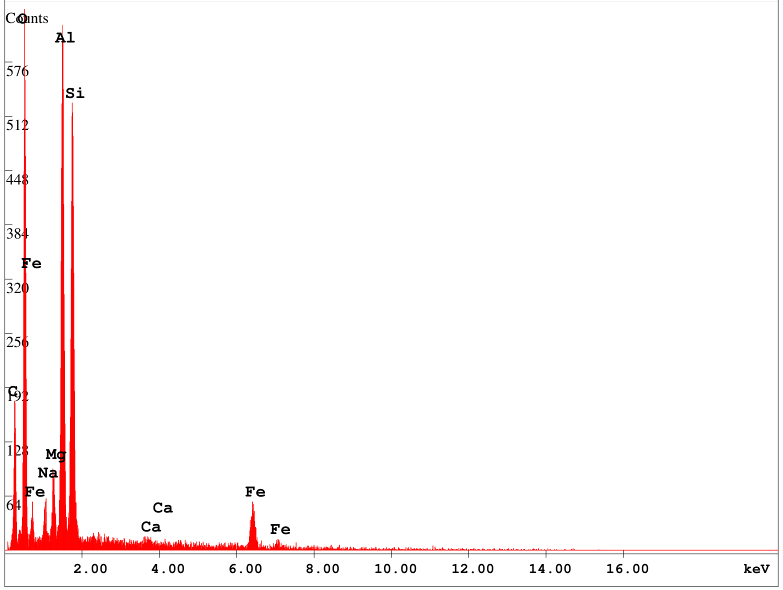

EDAX ZAF Quantification (Standardless)
Element Normalized
SEC Table : User c:\edax32\eds\genuser.sec

Element	Wt %	At %	K-Ratio	Z	A	F
O K	48.69	62.70	0.2034	1.0353	0.4033	1.0007
NaK	0.90	0.81	0.0035	0.9689	0.4032	1.0056
MgK	1.19	1.01	0.0066	0.9933	0.5521	1.0108
AlK	33.31	25.43	0.2205	0.9641	0.6845	1.0031
SiK	11.38	8.35	0.0592	0.9922	0.5241	1.0001
CaK	0.26	0.13	0.0023	0.9631	0.9271	1.0023
FeK	4.27	1.57	0.0374	0.8747	1.0033	1.0000
Total	100.00	100.00				

c:\edax32\genesis\genspc.spc

Element	Net Inte.	Bkgd Inte.	Inte. Error	P/B
O K	110.20	1.23	1.78	89.44
NaK	7.91	3.29	8.90	2.41
MgK	15.13	4.96	6.12	3.05
AlK	134.43	4.89	1.65	27.47
SiK	124.54	4.52	1.72	27.57
CaK	3.01	1.51	15.08	2.00
FeK	18.86	1.03	4.49	18.37

9) Almandine-Mn

c:\edax32\genesis\genspc.spc

Label:

kV:25.0 Tilt:0.0 Take-off:37.2 Det: SUTW Sapphire

Res:131 Amp.T:50.00 FS:1828 Lsec:38 18-Feb-2017 15:07:16

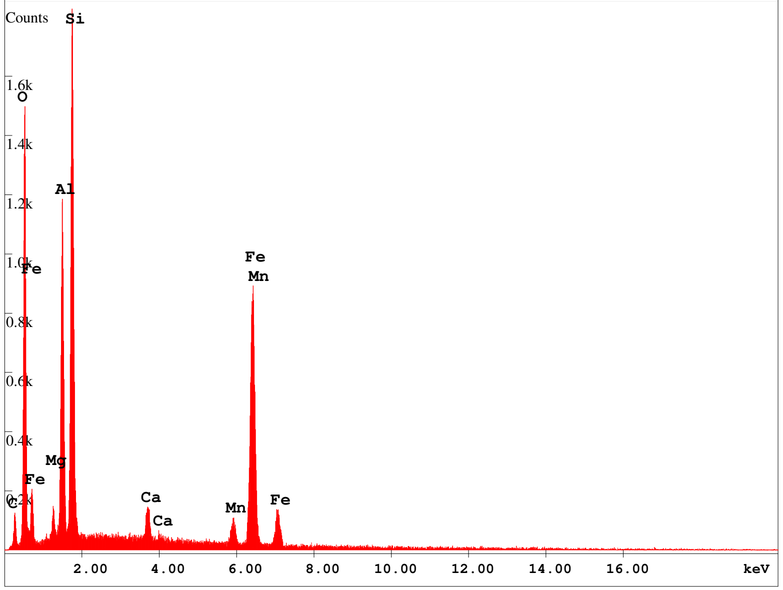

EDAX ZAF Quantification (Standardless)
Element Normalized
SEC Table : Default

Element	Wt %	At %	K-Ratio	Z	A	F
O K	34.36	53.53	0.1131	1.0560	0.3113	1.0012
MgK	1.55	1.59	0.0052	1.0157	0.3301	1.0064
AlK	13.17	12.17	0.0586	0.9863	0.4478	1.0069
SiK	21.99	19.52	0.1059	1.0156	0.4737	1.0008
CaK	1.48	0.92	0.0131	0.9898	0.8800	1.0167
MnK	2.14	0.97	0.0189	0.8902	0.9904	1.0000
FeK	25.30	11.30	0.2292	0.9075	0.9980	1.0000
Total	100.00	100.00				

c:\edax32\genesis\genspc.spc

Element	Net Inte.	Bkgd Inte.	Inte. Error	P/B
O K	215.33	2.15	1.11	100.29
MgK	16.84	7.44	5.41	2.26
AlK	191.17	8.43	1.22	22.67
SiK	329.57	10.47	0.92	31.47
CaK	28.59	8.80	3.85	3.25
MnK	24.43	6.10	4.01	4.00
FeK	261.13	5.47	1.02	47.72

10) Almandine

c:\edax32\genesis\genspc.spc
Label:
kV:25.0 Tilt:0.0 Take-off:37.2 Det: SUTW Sapphire
Res:131 Amp.T:50.00 FS:1214 Lsec:24 18-Feb-2017 15:03:20

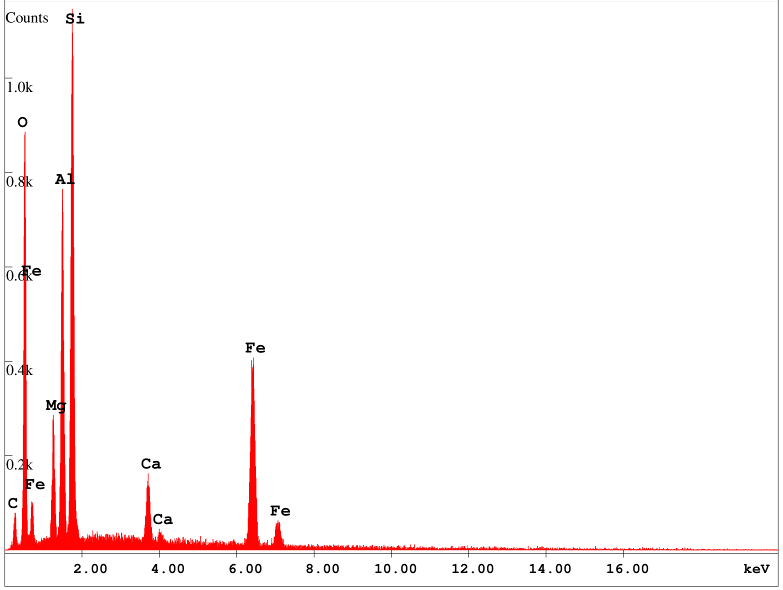

EDAX ZAF Quantification (Standardless)
Element Normalized
SEC Table : Default

Element	Wt %	At %	K-Ratio	Z	A	F
O K	36.18	53.73	0.1109	1.0473	0.2925	1.0010
MgK	5.28	5.16	0.0198	1.0074	0.3698	1.0069
AlK	13.53	11.92	0.0614	0.9783	0.4605	1.0073
SiK	22.80	19.29	0.1104	1.0073	0.4804	1.0008
CaK	2.73	1.62	0.0238	0.9808	0.8796	1.0114
FeK	19.48	8.29	0.1744	0.8994	0.9958	1.0000
Total	100.00	100.00				

Element	Net Inte.	Bkgd Inte.	Inte. Error	P/B
O K	211.02	2.03	1.40	103.73
MgK	63.55	11.96	2.97	5.31
AlK	200.10	10.86	1.50	18.42
SiK	343.32	10.29	1.12	33.35
CaK	51.75	7.00	3.16	7.40
FeK	198.51	4.27	1.46	46.47

11) Grossular

c:\edax32\genesis\genspc.spc
Label:
kV:20.0 Tilt:0.0 Take-off:36.8 Det: SUTW Sapphire
Res:132 Amp.T:35.00 FS:561 Lsec:11 9-Mar-2017 19:16:12

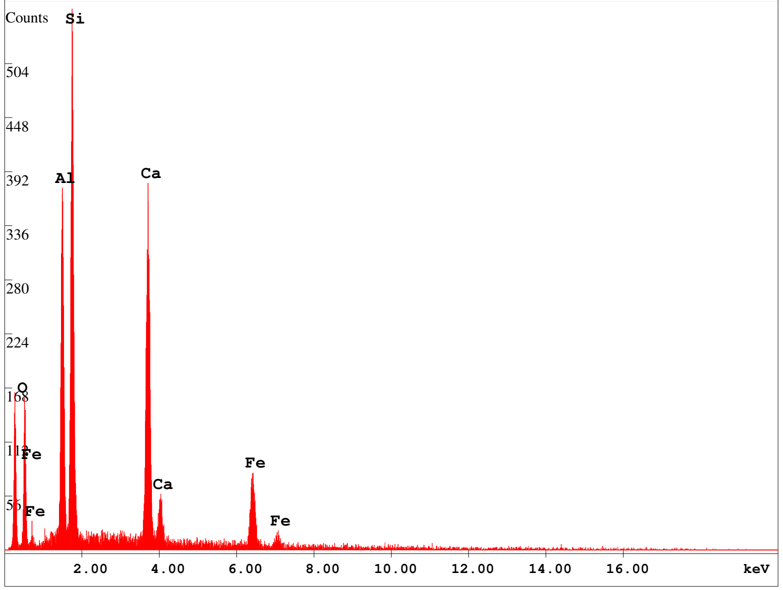

EDAX ZAF Quantification (Standardless)
Element Normalized
SEC Table : User c:\edax32\eds\genuser.sec

Element	Wt %	At %	K-Ratio	Z	A	F
O K	30.46	46.31	0.0743	1.0513	0.2319	1.0007
AlK	30.20	27.22	0.1991	0.9787	0.6701	1.0054
SiK	16.40	14.20	0.0892	1.0072	0.5394	1.0015
CaK	13.24	8.04	0.1197	0.9793	0.9189	1.0042
FeK	9.69	4.22	0.0850	0.8905	0.9852	1.0000
Total	100.00	100.00				

Element	Net Inte.	Bkgd Inte.	Inte. Error	P/B
O K	67.74	0.59	3.57	114.13
AlK	203.66	9.50	2.13	21.45
SiK	314.91	9.92	1.69	31.74
CaK	262.51	6.53	1.84	40.21
FeK	71.73	3.82	3.62	18.80

12) Magnetite

c:\edax32\genesis\genspc.spc

Label:

kV:20.0 Tilt:0.0 Take-off:37.3 Det: SUTW Sapphire

Res:131 Amp.T:50.00 FS:1516 Lsec:30 1-May-2017 10:02:17

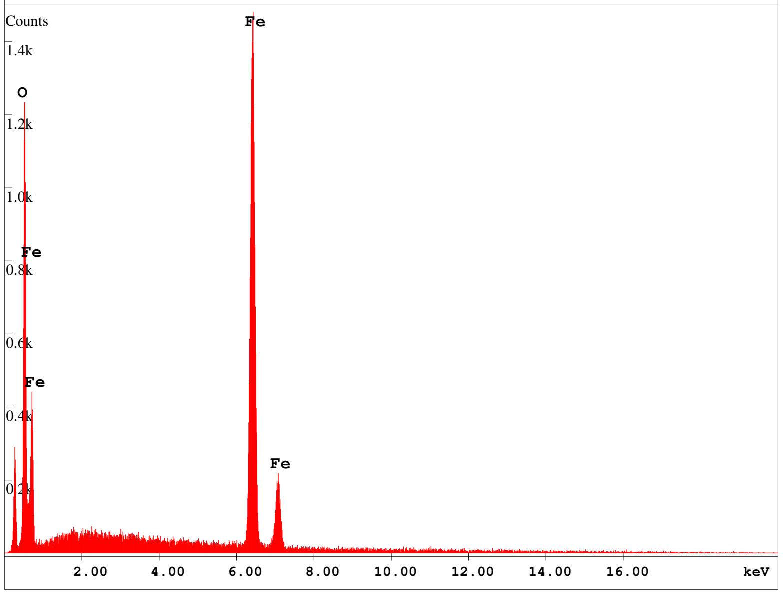

EDAX ZAF Quantification (Standardless)
Element Normalized
SEC Table : User c:\edax32\eds\genuser.sec

Element	Wt %	At %	K-Ratio	Z	A	F
O K	29.97	59.90	0.1710	1.1064	0.5144	1.0026
FeK	70.03	40.10	0.6647	0.9433	1.0062	1.0000
Total	100.00	100.00				

Element	Net Inte.	Bkgd Inte.	Inte. Error	P/B
O K	227.07	2.02	1.21	112.20
FeK	553.64	9.04	0.78	61.23

13) Magnetite-Ti

c:\edax32\genesis\genspc.spc

Label:

kV:25.0 Tilt:0.0 Take-off:37.2 Det: SUTW Sapphire

Res:131 Amp.T:50.00 FS:1762 Lsec:32 18-Feb-2017 15:13:26

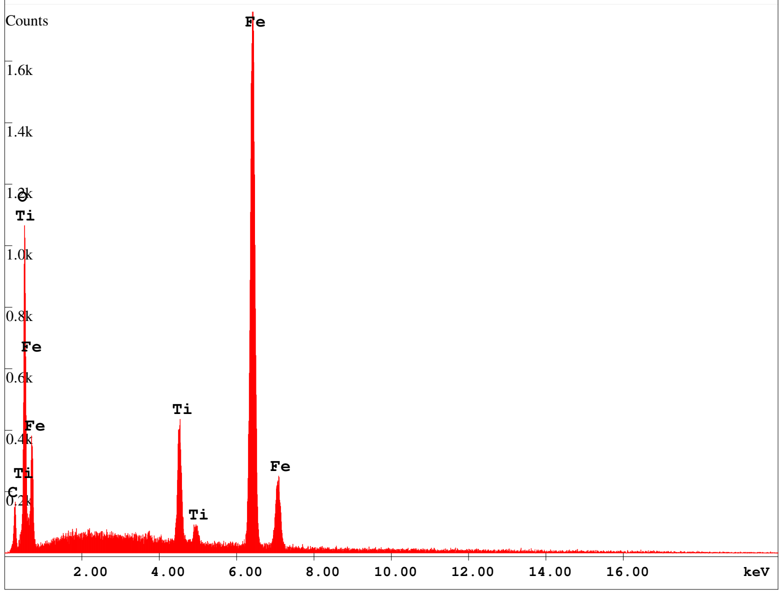

EDAX ZAF Quantification (Standardless)
Element Normalized
SEC Table : Default

Element	Wt %	At %	K-Ratio	Z	A	F
O K	28.48	57.76	0.0997	1.1019	0.3169	1.0021
TiK	7.15	4.84	0.0731	0.9488	0.9763	1.1037
FeK	64.37	37.40	0.6089	0.9507	0.9949	1.0000
Total	100.00	100.00				

Element	Net Inte.	Bkgd Inte.	Inte. Error	P/B
O K	175.51	2.24	1.35	78.40
TiK	122.37	12.50	1.75	9.79
FeK	641.46	7.99	0.70	80.28

14) Ilmenite

c:\edax32\genesis\genspc.spc

Label:

kV:20.0 Tilt:0.0 Take-off:36.7 Det: SUTW Sapphire

Res:130 Amp.T:100.00 FS:585 Lsec:34 22-Feb-2017 09:31:31

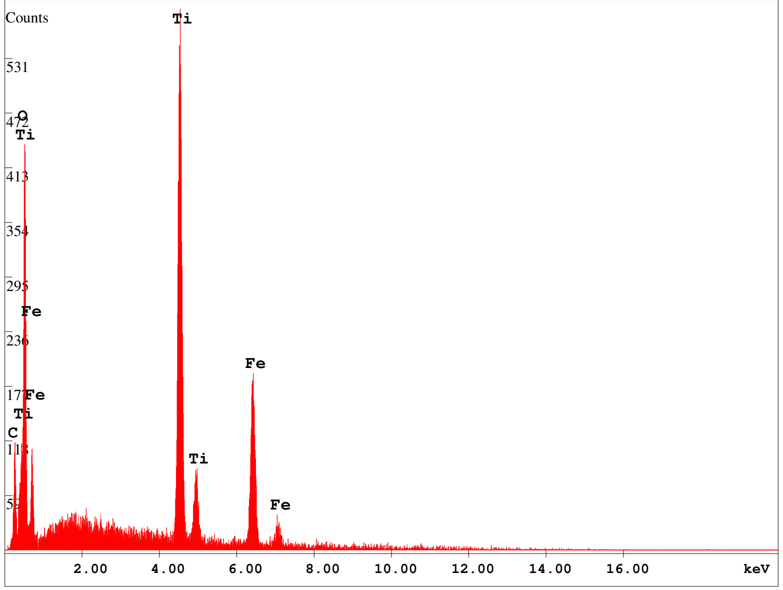

EDAX ZAF Quantification (Standardless)
Element Normalized
SEC Table : User c:\edax32\eds\genuser.sec

Element	Wt %	At %	K-Ratio	Z	A	F
O K	58.27	81.45	0.1316	1.0599	0.2130	1.0003
TiK	27.76	12.96	0.2568	0.9019	1.0080	1.0176
FeK	13.97	5.59	0.1226	0.8983	0.9769	1.0000
Total	100.00	100.00				

Element	Net Inte.	Bkgd Inte.	Inte. Error	P/B
O K	68.76	0.70	2.09	97.54
TiK	157.88	3.44	1.39	45.94
FeK	59.39	2.09	2.30	28.48

15) Rutile

c:\edax32\genesis\genspc.spc

Label:

kV:20.0 Tilt:0.0 Take-off:38.0 Det: SUTW Sapphire

Res:131 Amp.T:50.00 FS:983 Lsec:16 23-Apr-2017 12:04:21

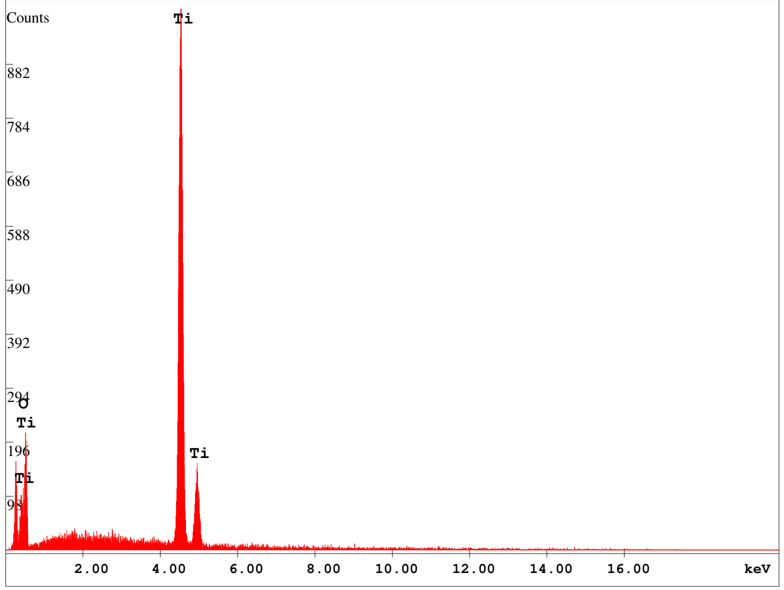

EDAX ZAF Quantification (Standardless)
Element Normalized
SEC Table : Default

Element	Wt %	At %	K-Ratio	Z	A	F
O K	35.97	62.71	0.0428	1.0985	0.1084	1.0000
TiK	64.03	37.29	0.6042	0.9362	1.0080	1.0000
Total	100.00	100.00				

Element	Net Inte.	Bkgd Inte.	Inte. Error	P/B
O K	63.27	1.72	3.14	36.86
TiK	576.88	5.39	1.02	107.11

16) Titanite

c:\edax32\genesis\genspc.spc
Label:
kV:20.0 Tilt:0.0 Take-off:39.0 Det: SUTW Sapphire
Res:131 Amp.T:50.00 FS:501 Lsec:16 8-Mar-2017 09:18:22

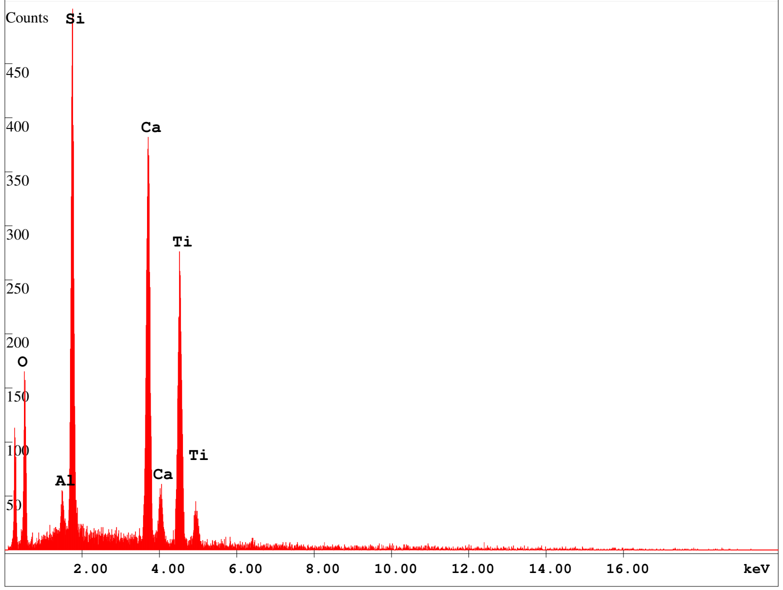

EDAX ZAF Quantification (Standardless)
Element Normalized
SEC Table : User c:\edax32\eds\genuser.sec

Element	Wt %	At %	K-Ratio	Z	A	F
O K	47.25	68.09	0.0800	1.0513	0.1610	1.0001
AlK	3.42	2.93	0.0203	0.9787	0.6018	1.0057
SiK	11.67	9.58	0.0825	1.0072	0.6994	1.0033
CaK	13.52	7.78	0.1333	0.9793	0.9725	1.0353
TiK	24.14	11.62	0.2065	0.8944	0.9566	1.0000
Total	100.00	100.00				

Element	Net Inte.	Bkgd Inte.	Inte. Error	P/B
O K	52.43	1.42	3.53	36.83
AlK	14.67	6.93	9.06	2.12
SiK	205.65	8.54	1.81	24.07
CaK	205.46	3.65	1.77	56.25
TiK	155.26	3.22	2.04	48.23

17) Titanite-Fe

c:\edax32\genesis\genspc.spc
Label:
kV:20.0 Tilt:0.0 Take-off:36.9 Det: SUTW Sapphire
Res:130 Amp.T:100.00 FS:508 Lsec:13 26-Apr-2017 09:07:15

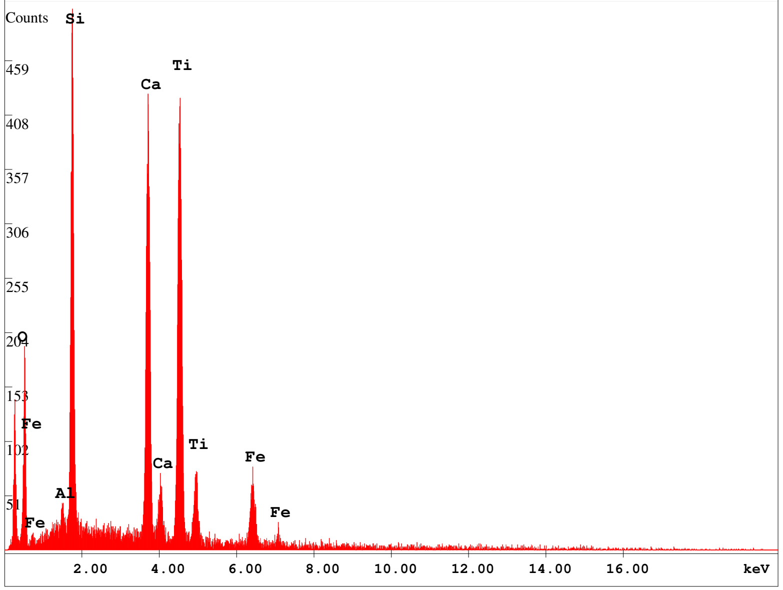

EDAX ZAF Quantification (Standardless)
Element Normalized
SEC Table : User c:\edax32\eds\genuser.sec

Element	Wt %	At %	K-Ratio	Z	A	F
O K	39.95	61.36	0.0709	1.0518	0.1686	1.0003
AlK	1.04	0.95	0.0059	0.9790	0.5688	1.0073
SiK	16.30	14.26	0.1138	1.0075	0.6907	1.0036
CaK	22.39	13.73	0.2141	0.9802	0.9601	1.0164
TiK	10.48	5.38	0.0873	0.8953	0.9222	1.0081
FeK	9.84	4.33	0.0850	0.8918	0.9687	1.0000
Total	100.00	100.00				

Element	Net Inte.	Bkgd Inte.	Inte. Error	P/B
O K	71.93	2.12	3.34	33.96
AlK	13.09	10.36	12.22	1.26
SiK	257.39	12.93	1.80	19.90
CaK	276.91	5.82	1.69	47.55
TiK	314.35	4.92	1.58	63.94
FeK	54.38	3.40	3.96	15.98

18) Zircon

c:\edax32\genesis\genspc.spc

Label:

kV:20.0 Tilt:0.0 Take-off:36.4 Det: SUTW Sapphire

Res:132 Amp.T:35.00 FS:2803 Lsec:38 4-Mar-2017 09:11:29

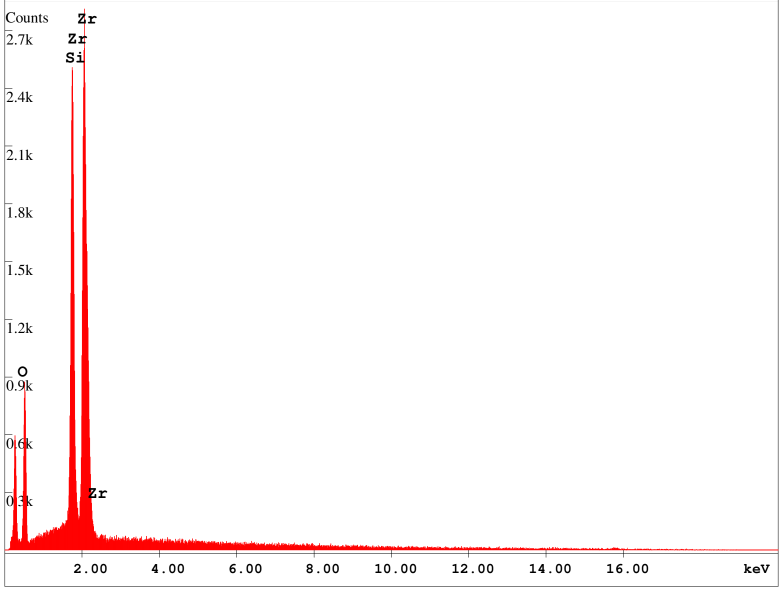

EDAX ZAF Quantification (Standardless)
Element Normalized
SEC Table : User c:\edax32\eds\genuser.sec

Element	Wt %	At %	K-Ratio	Z	A	F
O K	47.91	76.87	0.1128	1.0834	0.2172	1.0003
SiK	13.40	12.25	0.1061	1.0373	0.7526	1.0144
ZrL	38.68	10.88	0.2929	0.8377	0.9037	1.0000
Total	100.00	100.00				

Element	Net Inte.	Bkgd Inte.	Inte. Error	P/B
O K	121.73	5.33	1.52	22.84
SiK	445.24	26.41	0.81	16.86
ZrL	504.74	20.75	0.75	24.33

19) Apatite-Cl

c:\edax32\genesis\genspc.spc

Label:

kV:20.0 Tilt:0.0 Take-off:36.5 Det: SUTW Sapphire

Res:130 Amp.T:100.00 FS:612 Lsec:25 22-Feb-2017 09:34:01

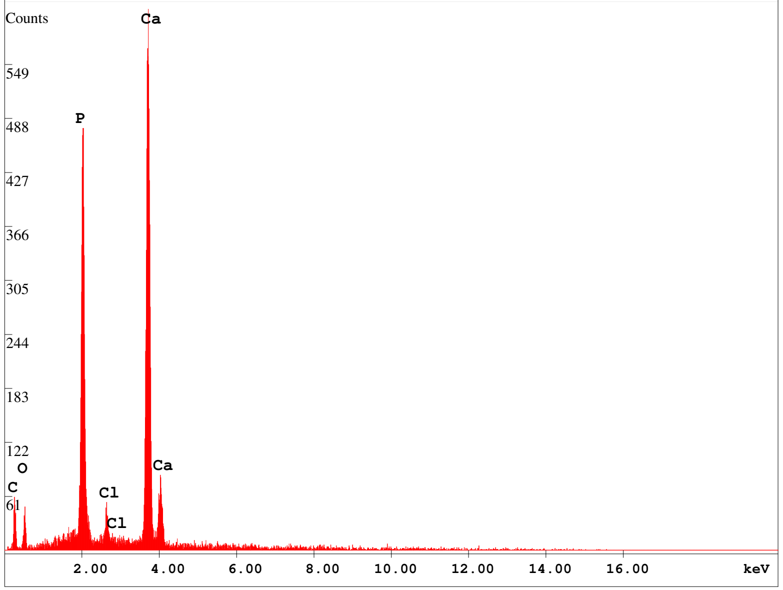

EDAX ZAF Quantification (Standardless)
Element Normalized
SEC Table : User c:\edax32\eds\genuser.sec

Element	Wt %	At %	K-Ratio	Z	A	F
O K	31.14	50.75	0.0414	1.0488	0.1267	1.0002
P K	22.23	18.72	0.1855	0.9710	0.8491	1.0117
ClK	2.14	1.57	0.0172	0.9503	0.8214	1.0269
CaK	44.49	28.95	0.4100	0.9776	0.9426	1.0000
Total	100.00	100.00				

Element	Net Inte.	Bkgd Inte.	Inte. Error	P/B
O K	8.52	0.28	7.06	30.57
P K	134.36	3.30	1.76	40.66
ClK	11.11	2.79	7.34	3.99
CaK	203.87	1.99	1.41	102.42

20) Apatite-F

c:\edax32\genesis\genspc.spc

Label:

kV:20.0 Tilt:0.0 Take-off:36.6 Det: SUTW Sapphire

Res:132 Amp.T:35.00 FS:638 Lsec:6 27-Feb-2017 09:30:03

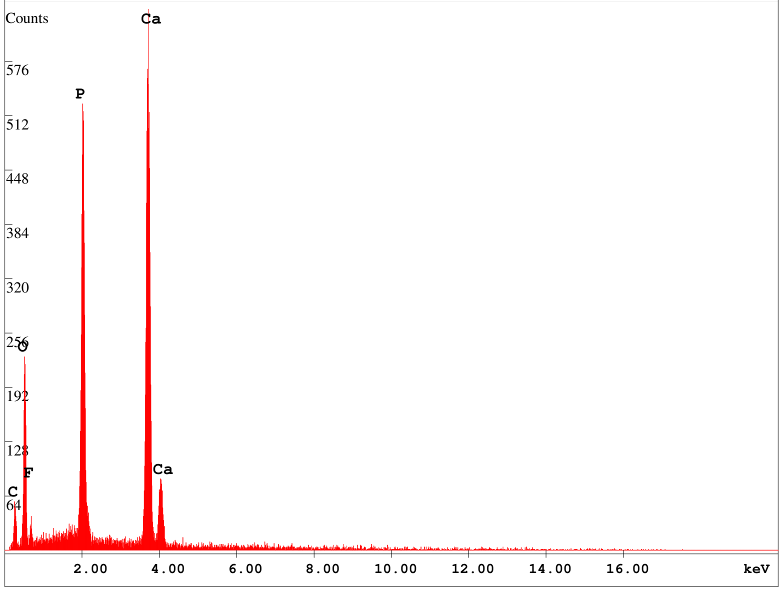

EDAX ZAF Quantification (Standardless)
Element Normalized
SEC Table : User c:\edax32\eds\genuser.sec

Element	Wt %	At %	K-Ratio	Z	A	F
O K	57.50	73.73	0.1254	1.0285	0.2120	1.0002
F K	4.16	4.49	0.0054	0.9667	0.1337	1.0003
P K	14.34	9.50	0.1146	0.9498	0.8360	1.0064
CaK	24.01	12.29	0.2230	0.9571	0.9706	1.0000
Total	100.00	100.00				

Element	Net Inte.	Bkgd Inte.	Inte. Error	P/B
O K	184.36	5.29	2.95	34.83
F K	19.21	7.71	11.92	2.49
P K	592.71	17.85	1.64	33.21
CaK	791.44	8.47	1.40	93.45

21) Apatite-OH

c:\edax32\genesis\genspc.spc

Label:

kV:20.0 Tilt:0.0 Take-off:36.6 Det: SUTW Sapphire

Res:156 Amp.T:4.00 FS:1310 Lsec:17 27-Feb-2017 14:35:34

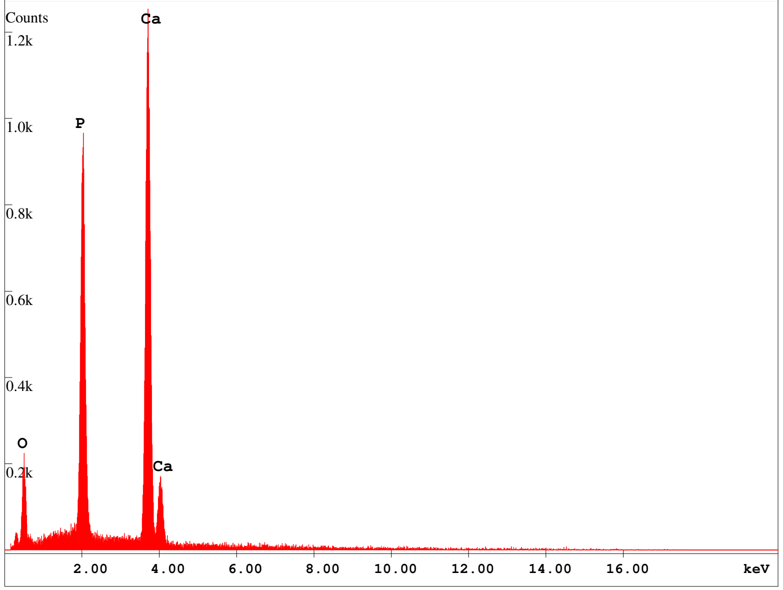

EDAX ZAF Quantification (Standardless)
Element Normalized
SEC Table : User c:\edax32\eds\genuser.sec

Element	Wt %	At %	K-Ratio	Z	A	F
O K	50.01	69.46	0.0868	1.0341	0.1678	1.0001
P K	17.31	12.42	0.1407	0.9559	0.8429	1.0085
CaK	32.68	18.12	0.3031	0.9629	0.9634	1.0000
Total	100.00	100.00				

Element	Net Inte.	Bkgd Inte.	Inte. Error	P/B
O K	98.19	5.92	2.52	16.59
P K	559.14	23.16	1.04	24.14
CaK	826.79	14.79	0.84	55.89

22) Barite

c:\edax32\genesis\genspc.spc

Label:

kV:20.0 Tilt:0.0 Take-off:36.8 Det: SUTW Sapphire

Res:132 Amp.T:35.00 FS:2785 Lsec:58 9-Mar-2017 17:53:56

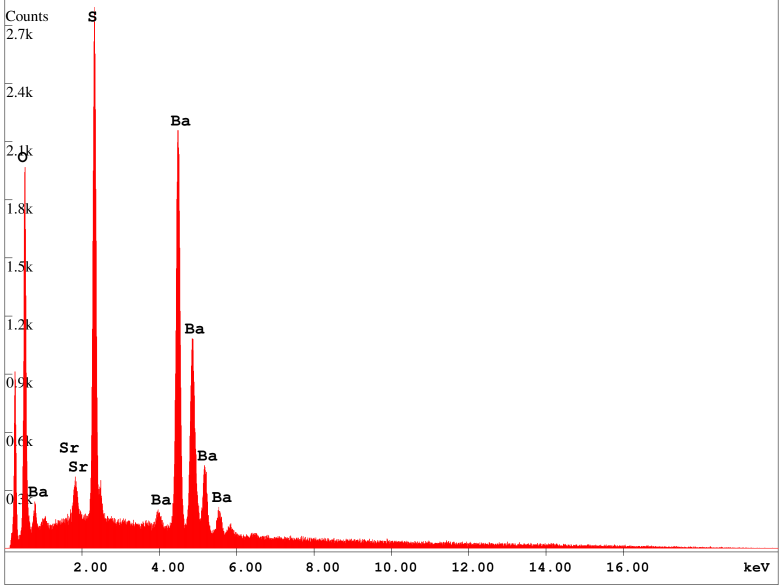

EDAX ZAF Quantification (Standardless)
Element Normalized
SEC Table : User c:\edax32\eds\genuser.sec

Element	Wt %	At %	K-Ratio	Z	A	F
O K	37.05	75.51	0.1591	1.1419	0.3760	1.0001
SrL	2.31	0.86	0.0137	0.8961	0.6574	1.0054
S K	11.85	12.05	0.0904	1.1041	0.6865	1.0060
BaL	48.79	11.58	0.4156	0.8229	1.0352	1.0000
Total	100.00	100.00				

Element	Net Inte.	Bkgd Inte.	Inte. Error	P/B
O K	182.42	6.02	1.00	30.29
SrL	28.00	25.81	4.18	1.08
S K	347.25	25.73	0.75	13.50
BaL	361.14	19.27	0.73	18.74

Element	Net Inte.	Bkgd Inte.	Inte. Error	P/B
O K	129.04	3.90	0.77	33.07
AlK	8.03	13.44	6.27	0.60
SiK	15.41	17.24	3.91	0.89
S K	267.00	19.55	0.56	13.66
CaK	4.80	16.61	10.96	0.29
BaL	306.33	16.48	0.51	18.59
FeK	9.96	12.22	5.02	0.82

23) Monazite

c:\edax32\genesis\genspc.spc

Label:

kV:20.0 Tilt:0.0 Take-off:37.3 Det: SUTW Sapphire

Res:131 Amp.T:50.00 FS:4288 Lsec:176 1-May-2017 11:47:47

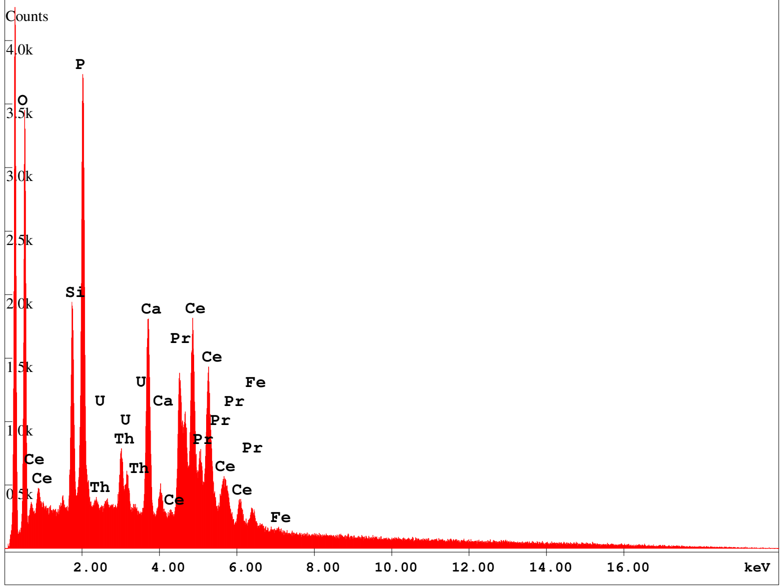

EDAX ZAF Quantification (Standardless)
Element Normalized
SEC Table : User c:\edax32\eds\genuser.sec

Element	Wt %	At %	K-Ratio	Z	A	F
O K	16.28	47.15	0.0490	1.1869	0.2537	1.0001
SiK	2.93	4.83	0.0147	1.1338	0.4395	1.0055
P K	16.60	24.84	0.0991	1.1200	0.5318	1.0025
ThM	7.72	1.54	0.0613	0.8074	0.9823	1.0006
U M	1.88	0.37	0.0153	0.8104	1.0033	1.0007
CaK	3.40	3.93	0.0318	1.1170	0.8186	1.0249
CeL	35.26	11.66	0.3015	0.8696	0.9827	1.0006
PrL	15.07	4.96	0.1313	0.8782	0.9917	1.0005
FeK	0.87	0.72	0.0079	1.0316	0.8898	1.0000
Total	100.00	100.00				

Element	Net Inte.	Bkgd Inte.	Inte. Error	P/B
O K	98.73	7.25	0.81	13.61
SiK	65.58	15.58	1.13	4.21
P K	153.03	17.12	0.67	8.94
ThM	25.59	16.46	2.25	1.55
U M	6.15	17.40	7.84	0.35
CaK	81.29	14.45	0.97	5.62
CeL	91.11	13.65	0.90	6.68
PrL	37.74	14.13	1.62	2.67
FeK	10.03	11.61	4.33	0.86

Appendix B: Results from FE-SEM-EDS analyses

Results from the FE-SEM and EDS analyses. Table includes number of analysed grains/phases in each sample and fraction, and percentage values based on these analyses. Table includes both heavy minerals and non-heavy minerals identified.

			Magnetic fractions										Apatite fractions						Zircon fractions					
			387		389		391		393		BS		387		391		BS		387		391		BS	
#	Color code	Mineral	Analysed grains	%	Analysed grains	%	Analysed grains	%	Analysed grains	%	Analysed grains	%	Analysed grains	%	Analysed grains	%	Analysed grains	%	Analysed grains	%	Analysed grains	%	Analysed grains	%
1		Quartz	26	8,25	18	10,78	20	11,83	21	12,73	21	8,05	6	3,92	48	42,86			4	1,83	3	1,41	7	3,21
2		Albite	3	0,95	2	1,20	1	0,59	2	1,21	9	3,45	4	2,61	12	10,71	3	1,99					1	0,46
3		Orthoclase	2	0,63							2	0,77											1	0,46
4		Calcite									3	1,15											2	0,92
5		Chamosite	15	4,76	30	17,96	17	10,06	14	8,48	6	2,30							5	2,28	1	0,47		
6		Muscovite	5	1,59			2	1,18	2	1,21	22	8,43					2	1,32					2	0,92
7		Amphibole	2	0,63	2	1,20	4	2,37			2	0,77												
8		Tourmaline									2	0,77												
9		Almandine-Mn	10	3,17	1	0,60	1	0,59	6	3,64	1	0,38							1	0,46				
10		Almandine	56	17,78	43	25,75	35	20,71	37	22,42	13	4,98			1	0,89			5	2,28				
11		Grossular	15	4,76	3	1,80	3	1,78	2	1,21	27	10,34												
12		Magnetite	1	0,32			3	1,78	1	0,61	4	1,53												
13		Magnetite-Ti	16	5,08	10	5,99	26	15,38	19	11,52	16	6,13												
14		Ilmenite	1	0,32	5	2,99	2	1,18	5	3,03	5	1,92												
15		Rutile	12	3,81	13	7,78	7	4,14	6	3,64	3	1,15	1	0,65					51	23,29	24	11,27	9	4,13
16		Titanite	130	41,27	31	18,56	41	24,26	42	25,45	83	31,80	3	1,96	4	3,57	3	1,99	72	32,88	23	10,80	109	50,00
17		Titanite-Fe	2	0,63	3	1,80	1	0,59	5	3,03	5	1,92												
18		Zircon	7	2,22	1	0,60	2	1,18			10	3,83	1	0,65					69	31,51	155	72,77	45	20,64
19		Apatite-Cl	3	0,95			1	0,59			6	2,30	42	27,45	13	11,61	41	27,15	2	0,91	4	1,88	9	4,13
20		Apatite-F	5	1,59	1	0,60					7	2,68	85	55,56	33	29,46	84	55,63	6	2,74	3	1,41	21	9,63
21		Apatite-OH							1	0,61	5	1,92	10	6,54	1	0,89	18	11,92	3	1,37			12	5,50
22		Barite	2	0,63			2	1,18					1	0,65					1	0,46				
23		Monazite-Ce					1	0,59																
24		Unknown	2	0,63	4	2,40			2	1,21	9	3,45												
		Total:	315	100,00	167	100,00	169	100,00	165	100,00	261	100,00	153	100,00	112	100,00	151	100,00	219	100,00	213	100,00	218	100,00

Appendix C: Garnet values from FE-SEM-EDS analyses

Chemical compositions of garnets from FE-SEM and EDS analyses using a standard. Garnets are classified to be either almandine or grossular. The values are used for ternary plots in the thesis.

Garnet values measured with EDS and standard															Numbers for the ternary plot		
Sample name	Fraction	Grain name	Garnet type	Color code	Wt%										XMg	XCa	XFe + XMn
					O	Mg	Al	Si	Ca	Ti	Mn	Fe	Total				
387	Magnetic	A_Line1_010	Grossular		34,64	0,16	15,76	23,21	17,09	0,02	0,18	8,93	100,0		0,61	64,83	34,56
387	Magnetic	A_Line1_015	Almandine		38,58	5,05	12,78	19,60	2,97	0,06	0,31	20,65	100,0		17,43	10,25	72,33
387	Magnetic	A_Line1_021	Almandine		41,37	3,59	12,25	18,69	4,50	0,03	0,50	19,07	100,0		12,98	16,27	70,75
387	Magnetic	A_Line1_025	Almandine		40,36	2,09	12,17	18,62	5,82	0,08	1,72	19,14	100,0		7,26	20,23	72,51
387	Magnetic	A_Line1_033	Almandine		41,26	4,42	12,05	18,81	3,89	0,05	0,55	18,97	100,0		15,88	13,98	70,14
387	Magnetic	A_Line1_039	Almandine		42,30	4,93	12,44	18,76	5,64	0,03	0,23	15,67	100,0		18,62	21,31	60,07
387	Magnetic	A_Line1_040	Almandine		38,99	5,01	12,03	18,96	4,64	0,03	0,55	19,78	100,0		16,71	15,48	67,81
387	Magnetic	A_Line1_052	Grossular		43,48	0,13	16,08	18,98	16,43	0,00	0,11	4,79	100,0		0,61	76,56	22,83
387	Magnetic	A_Line1_057	Grossular		42,06	0,08	14,62	19,11	16,38	0,04	0,29	7,42	100,0		0,33	67,77	31,90
387	Magnetic	A_Line1_060	Almandine		37,78	2,50	11,86	18,90	8,41	0,17	0,56	19,82	100,0		7,99	26,88	65,13
387	Magnetic	A_Line1_062	Almandine		37,63	3,35	12,90	19,65	4,59	0,02	0,50	21,35	100,0		11,25	15,41	73,35
387	Magnetic	A_Line1_069	Almandine		27,13	7,17	15,79	25,42	6,69	0,05	0,55	17,21	100,0		22,68	21,16	56,17
387	Magnetic	A_Line1_072	Grossular		41,71	0,16	14,37	18,86	16,51	0,01	0,26	8,13	100,0		0,64	65,88	33,48
387	Magnetic	A_Line1_075	Grossular		41,24	0,12	13,48	19,15	16,24	0,02	0,15	9,60	100,0		0,46	62,20	37,34
387	Magnetic	A_Line1_077	Grossular		40,32	0,12	14,81	19,61	16,84	0,04	0,11	8,15	100,0		0,48	66,77	32,75
387	Magnetic	A_Line1_092	Almandine		30,78	4,90	14,71	22,97	7,24	0,06	0,29	19,05	100,0		15,57	23,00	61,44
387	Magnetic	A_Line1_094	Grossular		42,71	0,20	13,47	18,81	15,68	0,00	0,10	9,04	100,0		0,80	62,67	36,53
387	Magnetic	A_Line1_098	Almandine		27,06	3,77	15,15	23,73	4,20	0,04	0,33	25,72	100,0		11,08	12,35	76,57
387	Magnetic	A_Line1_100	Almandine		37,85	1,18	12,28	18,67	6,95	0,05	0,66	22,37	100,0		3,79	22,30	73,91
387	Magnetic	A_Line1_109	Grossular		43,68	0,14	16,06	18,99	16,02	0,03	0,12	4,96	100,0		0,66	75,42	23,92
387	Magnetic	A_Line1_122	Almandine		39,73	2,37	12,26	19,19	8,18	0,01	0,78	17,48	100,0		8,23	28,39	63,38
387	Magnetic	A_Line2_010	Grossular		41,75	0,17	15,04	19,47	16,20	0,03	0,16	7,17	100,0		0,72	68,35	30,93
387	Magnetic	A_Line3_006	Almandine		41,30	3,54	12,14	18,80	4,06	0,00	0,19	19,96	100,0		12,76	14,63	72,61
387	Magnetic	A_Line3_007	Grossular		41,58	0,13	13,68	19,47	15,66	0,02	0,13	9,33	100,0		0,51	62,02	37,47
387	Magnetic	A_Line3_010	Almandine		40,70	5,61	12,24	19,25	3,85	0,02	0,36	17,97	100,0		20,19	13,85	65,96
387	Magnetic	A_Line3_017	Almandine		42,03	6,35	12,55	19,27	3,70	0,02	0,19	15,90	100,0		24,29	14,15	61,55
387	Magnetic	A_Line3_024	Almandine		44,30	6,48	12,41	19,29	6,90	0,02	0,16	10,44	100,0		27,02	28,77	44,20
387	Magnetic	A_Line3_030	Almandine		40,22	6,73	12,65	19,96	4,15	0,02	0,27	15,99	100,0		24,80	15,29	59,91
387	Magnetic	A_Line3_036	Almandine		41,32	4,57	12,19	19,02	2,96	0,02	0,18	19,75	100,0		16,64	10,78	72,58
387	Magnetic	A_Line3_042	Almandine		40,77	5,52	12,33	19,34	2,22	0,01	0,42	19,39	100,0		20,04	8,06	71,91
387	Magnetic	A_Line3_049	Almandine		35,36	1,14	13,00	20,23	4,64	0,02	2,25	23,37	100,0		3,63	14,78	81,59
387	Magnetic	A_Line3_052	Almandine		38,33	2,16	12,45	19,48	3,05	0,01	0,59	23,93	100,0		7,27	10,26	82,48
387	Magnetic	A_Line3_055	Grossular		28,46	0,14	17,44	25,45	18,64	0,02	0,10	9,75	100,0		0,49	65,11	34,40
387	Magnetic	A_Line3_057	Almandine		39,51	1,55	12,07	18,81	4,51	0,01	1,03	22,51	100,0		5,24	15,24	79,53
387	Magnetic	A_Line3_065	Almandine		35,71	0,94	12,49	20,09	5,10	0,02	2,76	22,88	100,0		2,97	16,10	80,93

Garnet values measured with EDS and standard														Numbers for the ternary plot		
Sample name	Fraction	Grain name	Garnet type	Color code	Wt%									XMg	XCa	XFe + XMn
					O	Mg	Al	Si	Ca	Ti	Mn	Fe	Total			
387	Magnetic	A_Line3_067	Almandine		27,22	3,98	13,59	22,28	5,13	0,02	0,54	27,24	100,0	10,79	13,91	75,30
387	Magnetic	A_Line3_070	Almandine		40,86	2,14	12,76	19,85	6,03	0,01	0,42	17,93	100,0	8,07	22,74	69,19
387	Magnetic	A_Line3_071	Almandine		41,47	6,45	12,55	19,63	3,36	0,01	0,17	16,36	100,0	24,49	12,76	62,76
387	Magnetic	A_Line3_074	Grossular		41,63	0,11	14,05	19,54	15,80	0,01	0,16	8,71	100,0	0,44	63,76	35,79
387	Magnetic	A_Line3_078	Almandine		38,72	1,56	12,88	19,46	6,36	0,02	1,24	19,77	100,0	5,39	21,98	72,62
387	Magnetic	A_Line3_084	Grossular		40,58	0,13	16,40	20,74	16,37	0,03	0,08	5,67	100,0	0,58	73,57	25,84
387	Magnetic	A_Line3_090	Almandine		42,36	4,26	11,99	18,61	4,79	0,01	0,23	17,75	100,0	15,76	17,72	66,52
387	Magnetic	A_Line3_097	Grossular		39,88	0,17	15,41	20,05	17,08	0,03	0,15	7,23	100,0	0,69	69,35	29,96
BS	Magnetic	A_Line5_010	Almandine		38,85	2,04	12,53	19,38	7,29	0,01	0,46	19,44	100,0	6,98	24,94	68,08
BS	Magnetic	A_Line5_013	Grossular		42,25	0,11	13,12	19,24	15,69	0,01	0,00	9,57	100,0	0,43	61,84	37,72
BS	Magnetic	A_Line5_017	Grossular		42,93	0,17	13,46	19,35	15,12	0,01	0,11	8,84	100,0	0,70	62,38	36,92
BS	Magnetic	A_Line5_021	Grossular		42,38	0,11	14,64	19,40	15,72	0,00	0,02	7,73	100,0	0,47	66,67	32,87
BS	Magnetic	A_Line5_022	Grossular		40,20	0,10	16,31	19,90	17,90	0,02	0,06	5,51	100,0	0,42	75,94	23,63
BS	Magnetic	A_Line5_027	Grossular		45,42	0,25	13,43	18,52	14,31	0,01	0,15	7,90	100,0	1,11	63,29	35,60
BS	Magnetic	A_Line5_028	Grossular		46,83	0,16	15,12	18,50	13,89	0,01	0,16	5,33	100,0	0,82	71,08	28,10
BS	Magnetic	A_Line5_033	Grossular		47,61	0,10	15,09	18,64	13,83	0,02	0,10	4,62	100,0	0,54	74,16	25,31
BS	Magnetic	A_Line5_035	Grossular		40,95	0,08	14,00	19,82	15,97	0,02	0,18	8,98	100,0	0,32	63,35	36,33
BS	Magnetic	A_Line5_042	Grossular		45,60	0,11	12,69	18,42	14,31	0,01	0,12	8,73	100,0	0,47	61,50	38,03
BS	Magnetic	A_Line5_052	Grossular		43,75	0,08	13,43	18,84	14,99	0,00	0,15	8,76	100,0	0,33	62,51	37,16
BS	Magnetic	A_Line5_058	Grossular		44,18	0,19	14,29	19,31	14,80	0,01	0,14	7,08	100,0	0,86	66,64	32,51
BS	Magnetic	A_Line5_065	Grossular		43,35	0,13	15,20	19,86	15,32	0,02	0,14	5,97	100,0	0,60	71,06	28,34
BS	Magnetic	A_Line5_075	Grossular		43,34	0,05	13,48	18,97	15,21	0,02	0,20	8,73	100,0	0,21	62,88	36,92
BS	Magnetic	A_Line5_088	Grossular		37,33	0,15	16,29	20,92	18,44	0,03	0,14	6,70	100,0	0,59	72,51	26,90
BS	Magnetic	A_Line6_016	Grossular		41,79	0,12	12,98	19,34	15,40	0,01	0,13	10,24	100,0	0,46	59,48	40,05
BS	Magnetic	A_Line6_019	Grossular		43,42	0,09	13,10	18,85	15,38	0,01	0,17	8,98	100,0	0,37	62,47	37,16
BS	Magnetic	A_Line6_022	Grossular		41,11	0,11	13,83	19,85	16,20	0,03	0,03	8,84	100,0	0,44	64,34	35,23
BS	Magnetic	A_Line6_023	Grossular		44,75	0,11	14,73	19,22	14,96	0,01	0,10	6,12	100,0	0,52	70,27	29,22
BS	Magnetic	A_Line6_027	Almandine		41,94	2,29	12,16	18,87	4,99	0,01	2,07	17,68	100,0	8,47	18,46	73,07
BS	Magnetic	A_Line6_032	Grossular		42,93	0,11	14,23	19,37	15,37	0,02	0,18	7,80	100,0	0,47	65,52	34,02
BS	Magnetic	A_Line6_035	Grossular		43,59	0,15	13,76	18,94	15,04	0,02	0,16	8,35	100,0	0,63	63,46	35,91
BS	Magnetic	A_Line6_039	Grossular		44,12	0,15	14,08	18,93	15,15	0,01	0,07	7,50	100,0	0,66	66,24	33,10
BS	Magnetic	A_Line6_043	Almandine		42,05	2,77	11,88	18,81	4,45	0,02	0,54	19,49	100,0	10,17	16,33	73,50
BS	Magnetic	A_Line6_049	Almandine		37,73	1,90	12,87	20,06	4,90	0,01	0,54	21,99	100,0	6,48	16,71	76,82
BS	Magnetic	A_Line6_051	Almandine		40,73	2,18	12,15	18,80	3,43	0,01	0,34	22,37	100,0	7,70	12,11	80,19
BS	Magnetic	A_Line6_059	Grossular		42,18	0,15	15,60	19,70	15,73	0,02	0,10	6,51	100,0	0,67	69,94	29,39
BS	Magnetic	A_Line6_064	Grossular		42,90	0,07	12,87	19,08	15,18	0,01	0,10	9,79	100,0	0,28	60,38	39,34
BS	Magnetic	A_Line6_069	Almandine		35,55	2,86	13,42	21,23	6,60	0,03	0,69	19,62	100,0	9,61	22,17	68,22
BS	Magnetic	A_Line6_081	Grossular		43,59	0,18	15,30	19,27	15,53	0,03	0,10	5,99	100,0	0,83	71,24	27,94
BS	Magnetic	A_Line6_085	Grossular		42,35	0,15	14,05	19,48	15,66	0,03	0,25	8,04	100,0	0,62	64,98	34,40
BS	Magnetic	A_Line6_088	Grossular		38,11	0,15	13,61	20,00	17,51	0,02	0,38	10,22	100,0	0,53	61,96	37,51
BS	Magnetic	A_Line6_091	Grossular		43,16	0,06	14,30	19,35	15,72	0,01	0,12	7,27	100,0	0,26	67,85	31,89
389	Magnetic	D_Line1_002	Almandine		38,82	6,80	12,85	20,23	2,44	0,02	0,58	18,25	100,0	24,23	8,69	67,08
389	Magnetic	D_Line1_003	Almandine		38,53	6,61	12,80	19,98	1,21	0,03	0,39	20,45	100,0	23,06	4,22	72,71

Garnet values measured with EDS and standard

Sample name	Fraction	Grain name	Garnet type	Color code	Wt% O	Mg	Al	Si	Ca	Ti	Mn	Fe	Total
389	Magnetic	D_Line1_008	Almandine		38,19	0,99	12,31	19,15	6,30	0,04	3,38	19,64	100,0
389	Magnetic	D_Line1_013	Grossular		41,02	0,23	14,45	19,41	16,57	0,04	0,14	8,15	100,0
389	Magnetic	D_Line1_021	Almandine		38,12	4,03	12,46	19,32	2,03	0,02	0,41	23,59	100,0
389	Magnetic	D_Line1_030	Grossular		40,82	0,13	14,34	19,56	16,60	0,04	0,15	8,35	100,0
389	Magnetic	D_Line1_037	Almandine		37,00	2,24	12,35	18,84	1,54	0,01	0,39	27,63	100,0
389	Magnetic	D_Line1_041	Almandine		37,45	3,04	12,44	19,30	1,67	0,03	1,18	24,88	100,0
389	Magnetic	D_Line1_043	Almandine		38,07	2,44	12,31	19,37	5,66	0,02	0,49	21,64	100,0
389	Magnetic	D_Line1_046	Almandine		38,16	3,43	12,33	19,48	4,58	0,03	0,35	21,63	100,0
389	Magnetic	D_Line1_050	Almandine		38,81	4,95	12,73	19,66	4,24	0,04	0,41	19,16	100,0
389	Magnetic	D_Line1_066	Almandine		39,38	6,10	12,71	19,65	1,46	0,01	0,39	20,3	100,0
389	Magnetic	D_Line1_068	Almandine		38,24	2,84	12,31	19,52	5,39	0,03	0,65	21,01	100,0
389	Magnetic	D_Line1_071	Almandine		38,71	4,66	12,44	19,49	3,28	0,02	0,72	20,68	100,0
389	Magnetic	D_Line1_083	Almandine		37,72	1,68	12,07	19,29	6,99	0,02	0,89	21,34	100,0
389	Magnetic	D_Line1_086	Almandine		37,38	1,97	12,13	19,18	5,11	0,02	0,45	23,76	100,0
389	Magnetic	D_Line1_087	Almandine		38,51	4,07	12,45	19,67	6,56	0,03	0,51	18,19	100,0
389	Magnetic	D_Line1_097	Grossular		40,67	0,16	13,56	19,41	16,49	0,03	0,23	9,44	100,0
391	Magnetic	E_Line1_006	Almandine		39,63	6,59	12,59	19,62	1,93	0,03	0,33	19,27	100,0
391	Magnetic	E_Line1_009	Almandine		38,29	5,88	12,70	20,16	4,53	0,03	0,30	18,11	100,0
391	Magnetic	E_Line1_010	Almandine		38,38	2,96	12,10	18,97	2,71	0,02	0,42	24,43	100,0
391	Magnetic	E_Line1_012	Almandine		37,92	5,41	12,49	20,08	1,45	0,00	0,26	22,4	100,0
391	Magnetic	E_Line1_023	Almandine		37,56	2,99	12,49	19,53	7,89	0,03	0,58	18,93	100,0
391	Magnetic	E_Line1_024	Almandine		36,70	1,57	12,20	19,13	7,42	0,03	1,95	21,00	100,0
391	Magnetic	E_Line1_026	Almandine		40,95	5,40	12,20	19,02	1,81	0,01	0,40	20,21	100,0
391	Magnetic	E_Line1_037	Grossular		42,13	0,07	11,49	18,60	15,56	0,03	0,14	11,99	100,0
391	Magnetic	E_Line1_043	Almandine		43,32	4,68	11,99	18,58	3,99	0,02	0,44	16,99	100,0
391	Magnetic	E_Line1_045	Almandine		38,28	0,47	11,72	18,96	7,23	0,01	3,28	20,04	100,0
391	Magnetic	E_Line1_048	Grossular		41,73	0,12	14,57	19,19	16,73	0,02	0,06	7,58	100,0
391	Magnetic	E_Line1_059	Almandine		33,13	2,94	12,29	19,50	7,04	0,05	0,36	24,7	100,0
391	Magnetic	E_Line1_060	Almandine		38,43	5,70	12,67	19,75	2,57	0,04	0,27	20,57	100,0
391	Magnetic	E_Line1_068	Grossular		39,21	0,14	14,92	19,76	17,93	0,04	0,11	7,89	100,0
391	Magnetic	E_Line1_073	Almandine		45,55	4,89	11,65	17,72	4,61	0,10	0,18	15,29	100,0
391	Magnetic	E_Line1_074	Almandine		39,16	3,72	12,21	19,33	5,11	0,01	0,65	19,81	100,0
391	Magnetic	E_Line1_080	Almandine		34,57	1,19	11,98	19,59	6,96	0,01	4,29	21,41	100,0
391	Magnetic	E_Line1_083	Almandine		39,57	5,20	12,36	19,55	4,50	0,04	0,55	18,23	100,0
391	Magnetic	E_Line1_085	Almandine		38,67	9,46	13,45	21,35	5,28	0,03	0,39	11,37	100,0
391	Magnetic	E_Line1_087	Almandine		38,21	3,52	12,23	19,44	4,67	0,04	0,40	21,49	100,0
391	Magnetic	E_Line1_089	Almandine		37,86	6,07	12,74	20,17	1,78	0,01	0,28	21,08	100,0
391	Magnetic	E_Line1_092	Almandine		37,50	0,43	11,50	18,50	5,27	0,03	1,37	25,40	100,0
391	Magnetic	E_Line1_093	Almandine		38,97	5,37	12,60	19,60	3,55	0,00	0,20	19,71	100,0
391	Magnetic	E_Line1_094	Almandine		40,61	5,44	12,37	19,42	4,61	0,05	0,38	17,14	100,0
391	Magnetic	E_Line1_097	Almandine		39,17	2,52	11,81	18,59	4,59	0,04	0,69	22,61	100,0
393	Magnetic	F_Line1_002	Almandine		39,05	5,12	12,19	19,28	0,81	0,03	0,52	22,99	100,0

Numbers for the ternary plot

XMg	XCa	XFe + XMn
3,27	20,79	75,95
0,92	66,04	33,04
13,41	6,75	79,84
0,52	65,79	33,69
7,04	4,84	88,11
9,88	5,43	84,69
8,07	18,72	73,21
11,44	15,27	73,29
17,21	14,74	68,05
21,59	5,17	73,24
9,50	18,03	72,47
15,88	11,18	72,94
5,44	22,62	71,94
6,30	16,33	77,37
13,88	22,37	63,76
0,61	62,65	36,74
23,44	6,86	69,70
20,40	15,72	63,88
9,70	8,88	81,42
18,33	4,91	76,76
9,84	25,96	64,20
4,92	23,23	71,85
19,41	6,51	74,08
0,25	56,05	43,70
17,93	15,29	66,78
1,52	23,31	75,18
0,49	68,31	31,20
8,39	20,09	71,52
19,58	8,83	71,59
0,54	68,78	30,69
19,58	18,46	61,95
12,70	17,45	69,85
3,52	20,56	75,92
18,26	15,80	65,94
35,70	19,92	44,38
11,70	15,53	72,77
20,78	6,09	73,13
1,32	16,23	82,45
18,63	12,31	69,06
19,73	16,72	63,55
8,29	15,09	76,62
17,39	2,75	79,86

Garnet values measured with EDS and standard

Sample name	Fraction	Grain name	Garnet type	Color code	Wt%								
					O	Mg	Al	Si	Ca	Ti	Mn	Fe	Total
393	Magnetic	F_Line1_005	Almandine		38,37	3,94	12,24	19,18	4,14	0,03	0,48	21,61	100,0
393	Magnetic	F_Line1_006	Almandine		38,78	3,26	12,17	18,89	1,22	0,02	0,13	25,53	100,0
393	Magnetic	F_Line1_007	Almandine		38,33	2,93	12,20	18,90	2,39	0,01	0,78	24,45	100,0
393	Magnetic	F_Line1_011	Almandine		37,12	0,95	11,70	18,43	4,03	0,04	0,62	27,1	100,0
393	Magnetic	F_Line1_012	Almandine		38,80	0,44	11,56	18,23	4,88	0,02	0,99	25,08	100,0
393	Magnetic	F_Line1_013	Almandine		37,36	4,69	12,42	19,75	3,49	0,01	0,60	21,69	100,0
393	Magnetic	F_Line1_015	Almandine		37,80	4,60	12,45	19,45	3,03	0,04	0,55	22,09	100,0
393	Magnetic	F_Line1_018	Almandine		37,19	1,62	11,52	18,45	4,34	0,01	0,69	26,19	100,0
393	Magnetic	F_Line1_021	Almandine		36,01	3,49	12,42	19,43	5,05	0,02	0,39	23,19	100,0
393	Magnetic	F_Line1_025	Almandine		40,10	4,13	12,41	18,92	3,95	0,01	0,30	20,19	100,0
393	Magnetic	F_Line1_027	Almandine		38,36	5,68	12,54	19,83	4,37	0,05	0,64	18,53	100,0
393	Magnetic	F_Line1_034	Almandine		39,20	4,45	12,12	19,34	4,16	0,04	0,62	20,07	100,0
393	Magnetic	F_Line1_037	Almandine		30,24	3,19	12,26	19,41	0,71	0,04	0,46	33,69	100,0
393	Magnetic	F_Line1_038	Almandine		41,32	2,74	11,90	18,25	1,96	0,02	0,72	23,10	100,0
393	Magnetic	F_Line1_039	Almandine		37,86	2,02	11,97	18,67	1,05	0,02	0,65	27,77	100,0
393	Magnetic	F_Line1_045	Almandine		41,00	3,18	11,64	18,45	4,41	0,04	0,84	20,44	100,0
393	Magnetic	F_Line1_046	Almandine		37,84	4,76	12,35	19,68	3,52	0,05	0,49	21,31	100,0
393	Magnetic	F_Line1_050	Grossular		40,30	0,19	16,45	19,92	17,69	0,00	0,03	5,43	100,0
393	Magnetic	F_Line1_054	Almandine		40,19	4,18	12,10	19,15	1,28	0,01	0,20	22,88	100,0
393	Magnetic	F_Line1_068	Almandine		46,39	7,57	11,09	14,65	1,20	0,03	0,49	18,57	100,0
393	Magnetic	F_Line1_070	Almandine		39,28	4,90	12,30	19,47	5,14	0,01	0,39	18,52	100,0
393	Magnetic	F_Line1_079	Almandine		39,70	4,23	12,08	18,95	1,60	0,02	0,46	22,97	100,0
393	Magnetic	F_Line1_080	Almandine		38,28	5,28	12,59	19,39	0,69	0,03	0,13	23,60	100,0
393	Magnetic	F_Line1_096	Almandine		31,41	4,67	12,82	20,54	2,62	0,03	0,54	27,36	100,0
393	Magnetic	F_Line1_097	Grossular		39,51	0,13	16,44	19,96	18,30	0,06	0,14	5,46	100,0
393	Magnetic	F_Line1_099	Almandine		38,72	1,79	12,09	18,95	5,72	0,02	0,95	21,74	100,0
393	Magnetic	F_Line1_100	Almandine		38,64	3,37	12,31	19,19	5,12	0,03	0,38	20,97	100,0

Numbers for the ternary plot

XMg	XCa	XFe + XMn
13,06	13,72	73,22
10,82	4,05	85,14
9,59	7,82	82,59
2,91	12,32	84,77
1,40	15,55	83,05
15,39	11,45	73,15
15,20	10,01	74,79
4,93	13,22	81,85
10,87	15,72	73,41
14,46	13,83	71,72
19,44	14,96	65,61
15,19	14,20	70,61
8,38	1,87	89,75
9,61	6,87	83,52
6,41	3,33	90,25
11,01	15,28	73,71
15,82	11,70	72,47
0,81	75,79	23,39
14,65	4,48	80,87
27,20	4,31	68,49
16,93	17,75	65,32
14,46	5,47	80,08
17,78	2,32	79,90
13,27	7,45	79,28
0,54	76,15	23,30
5,93	18,94	75,13
11,29	17,16	71,55

Appendix D: Spectrums from XRD analyses

XRD spectrums for each fraction analysed.

#	Sample name	Fraction type
1	387	Magnetic fraction
2	387	Apatite fraction
3	387	Zircon fraction
4	387	Zircon concentrate
5	389	Magnetic fraction
6	391	Magnetic fraction
7	391	Apatite fraction
8	391	Zircon fraction
9	391	Zircon concentrate
10	393	Magnetic fraction
11	BS	Magnetic fraction
12	BS	Apatite fraction
13	BS	Zircon fraction
14	BS	Zircon concentrate

1) 387 Magnetic fraction

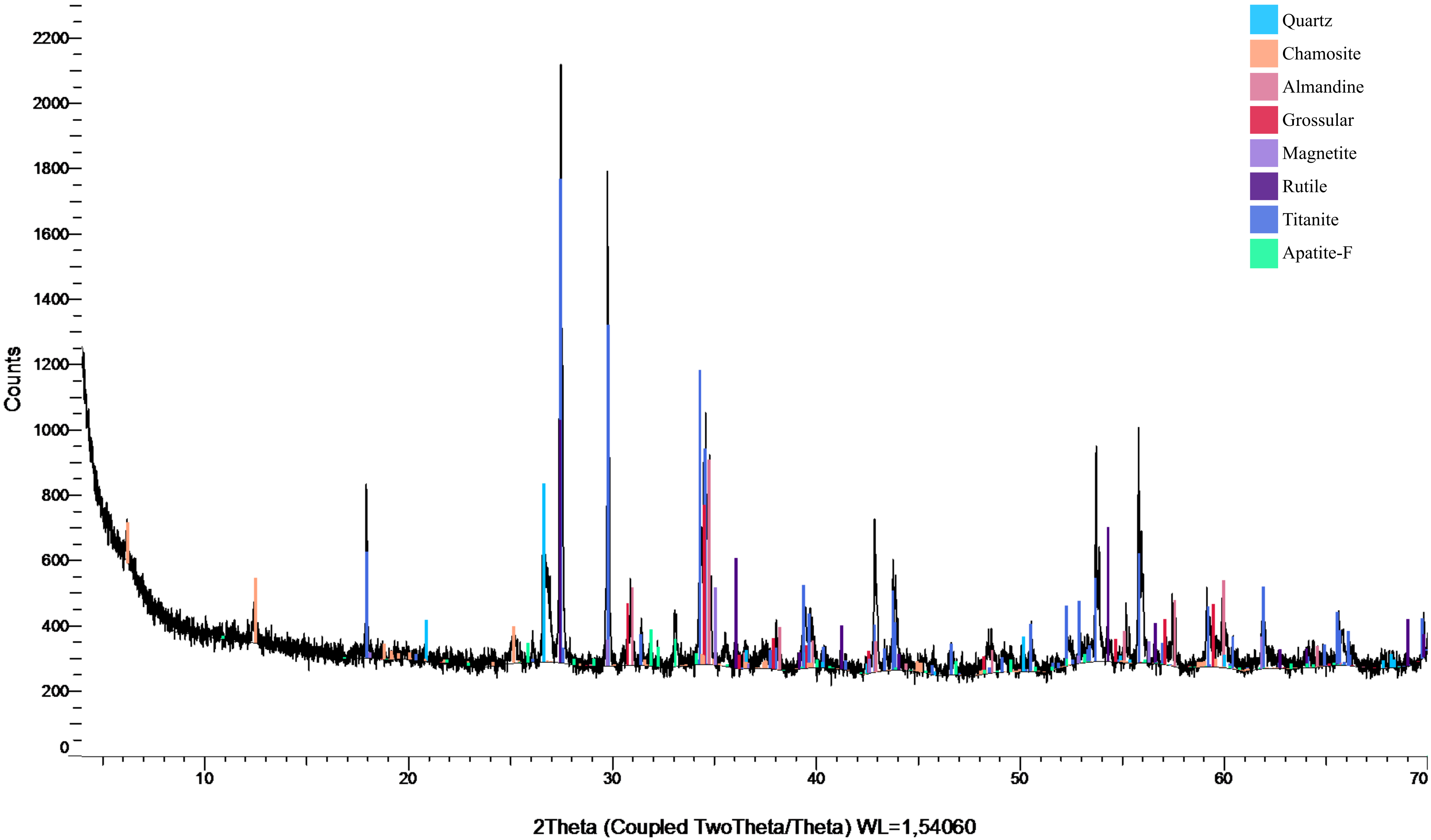

2) 387 Apatite fraction

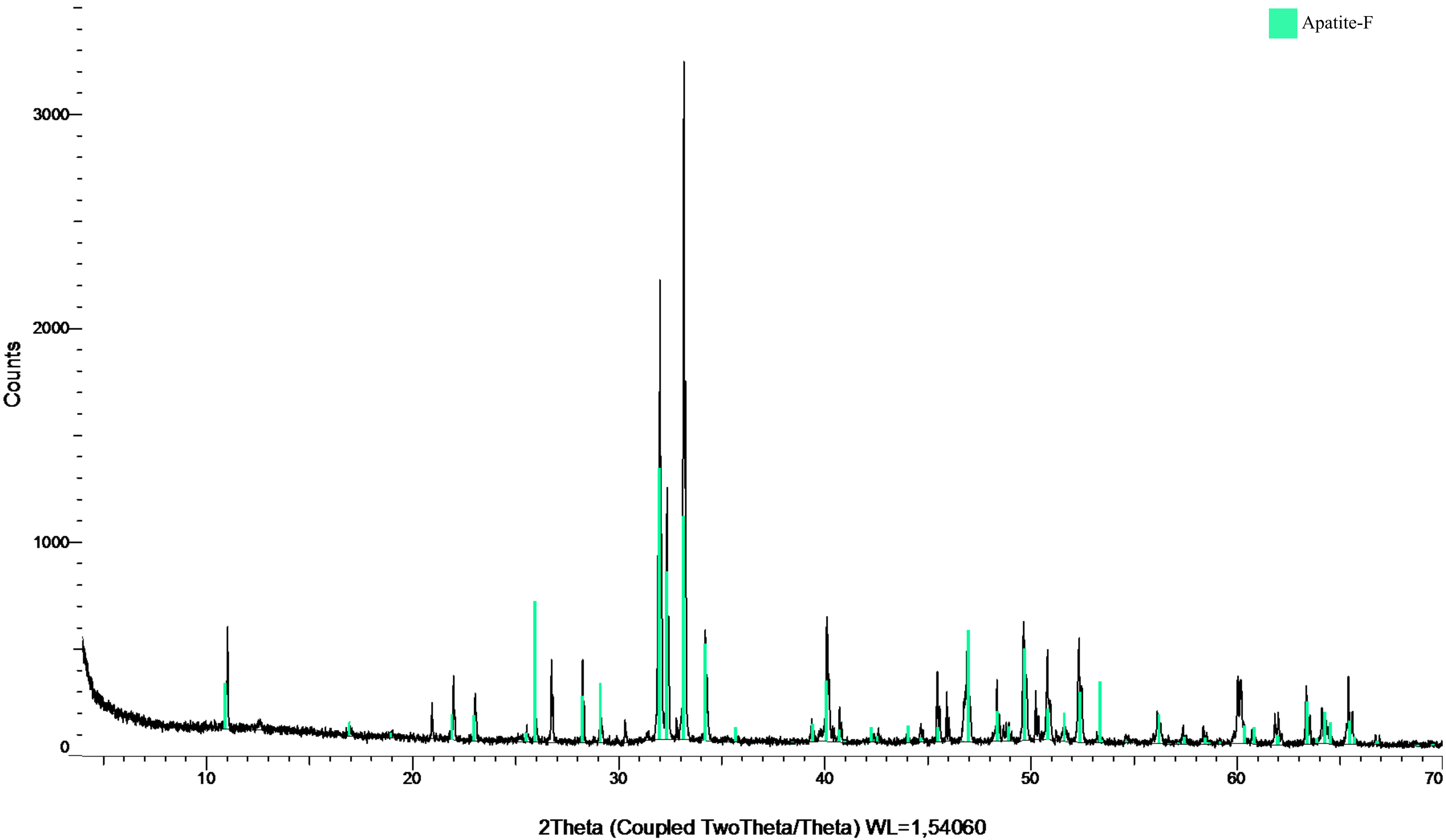

3) 387 Zircon fraction

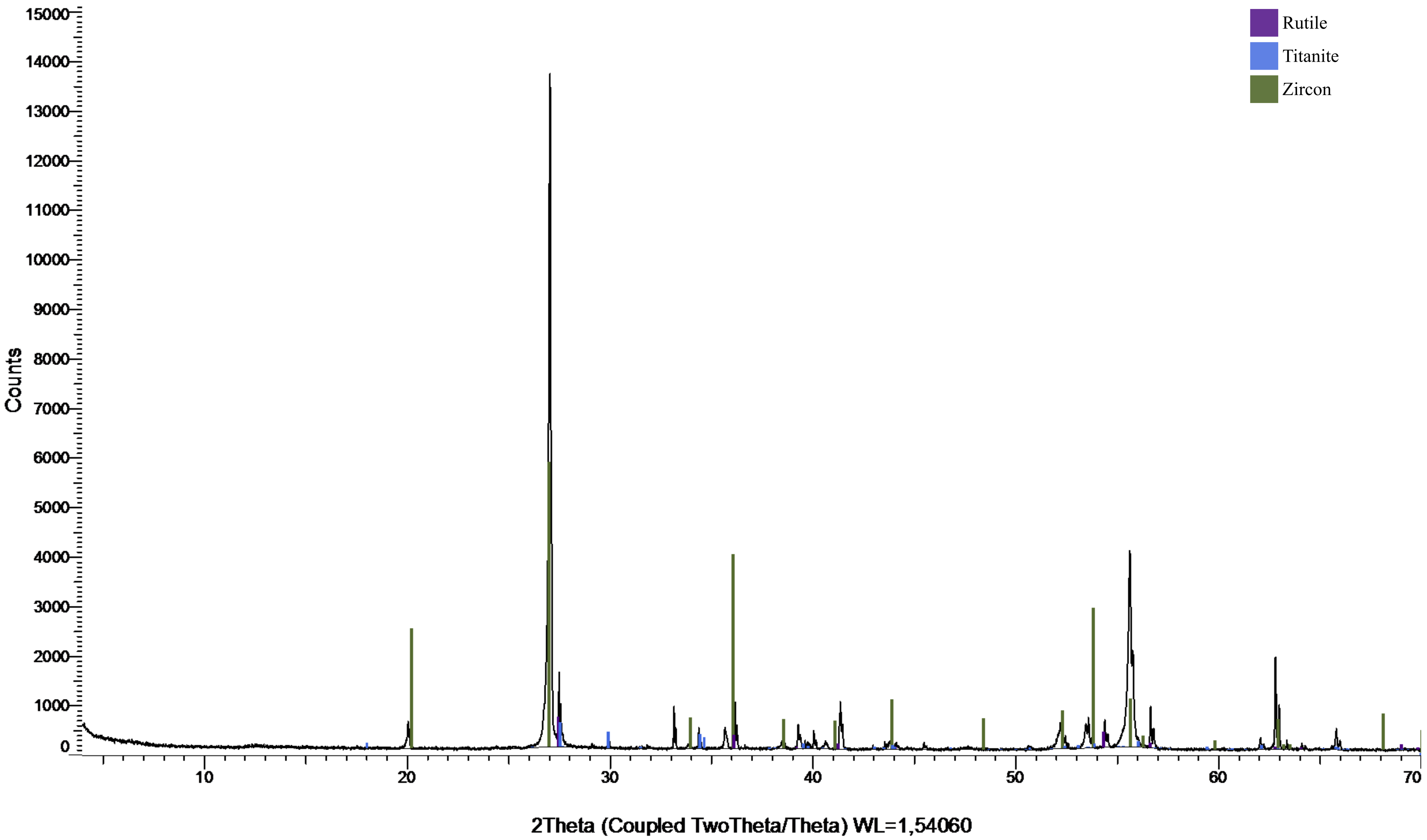

4) 387 Zircon concentrate

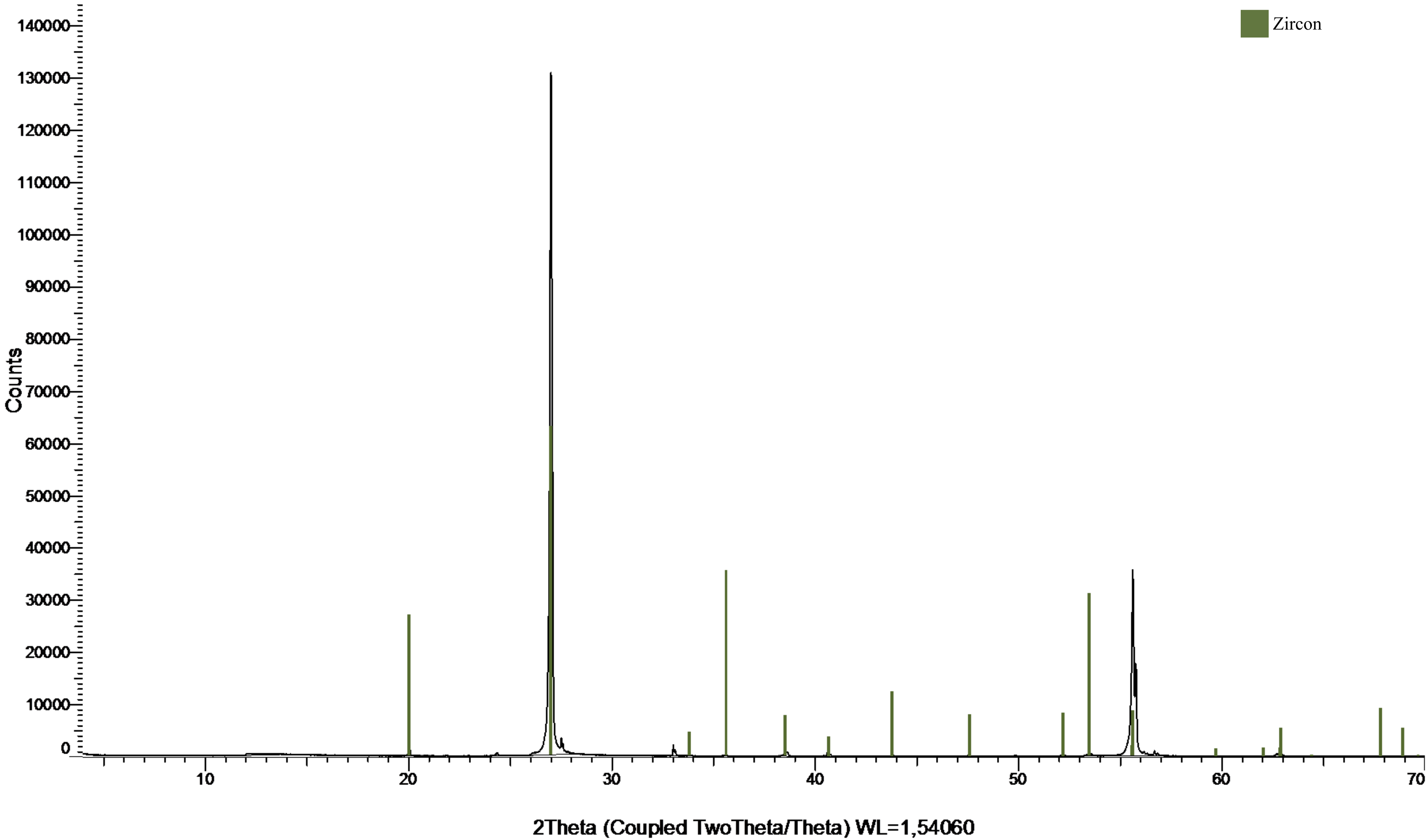

5) 389 Magnetic fraction

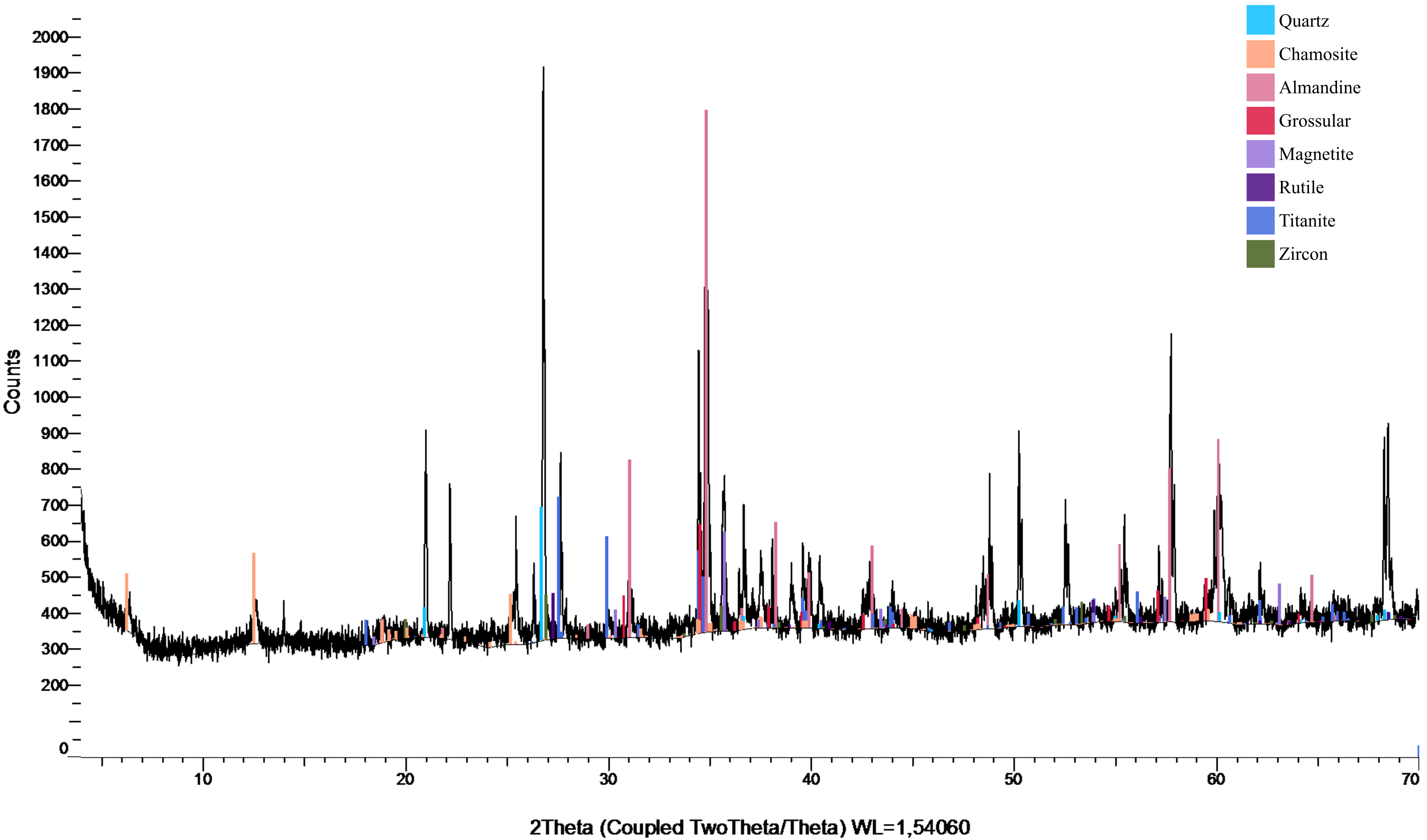

6) 391 Magnetic fraction

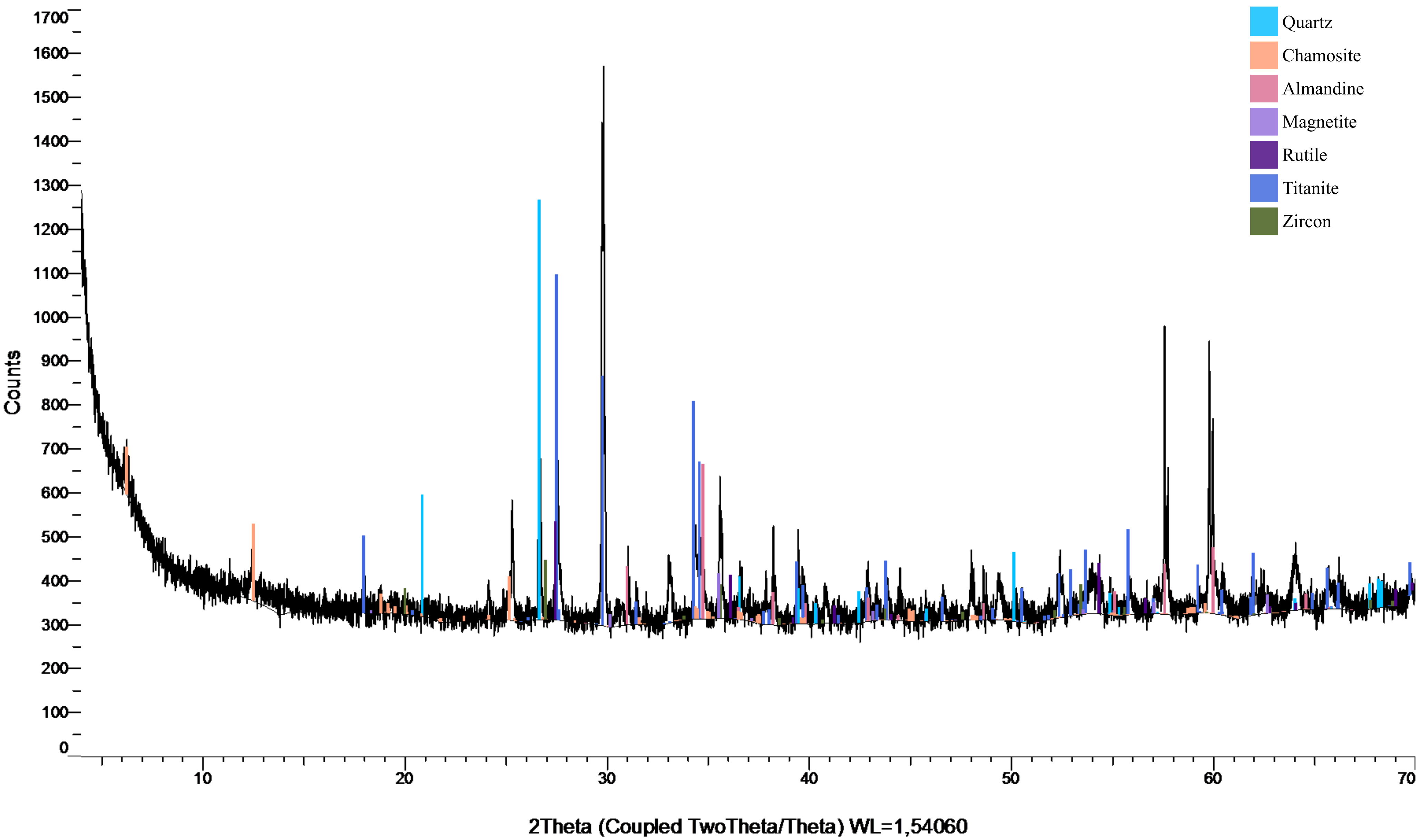

7) 391 Apatite fraction

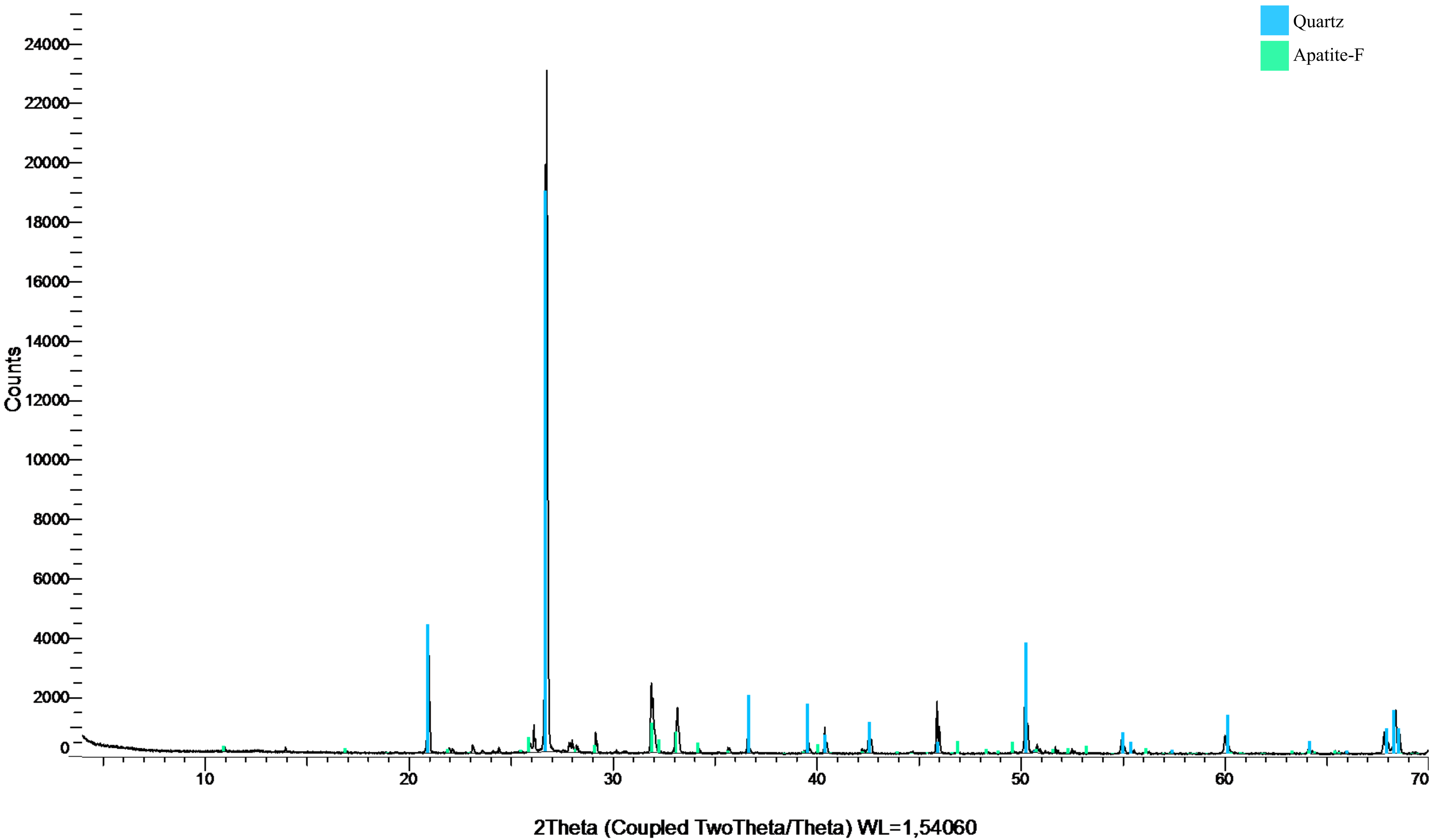

8) 391 Zircon fraction

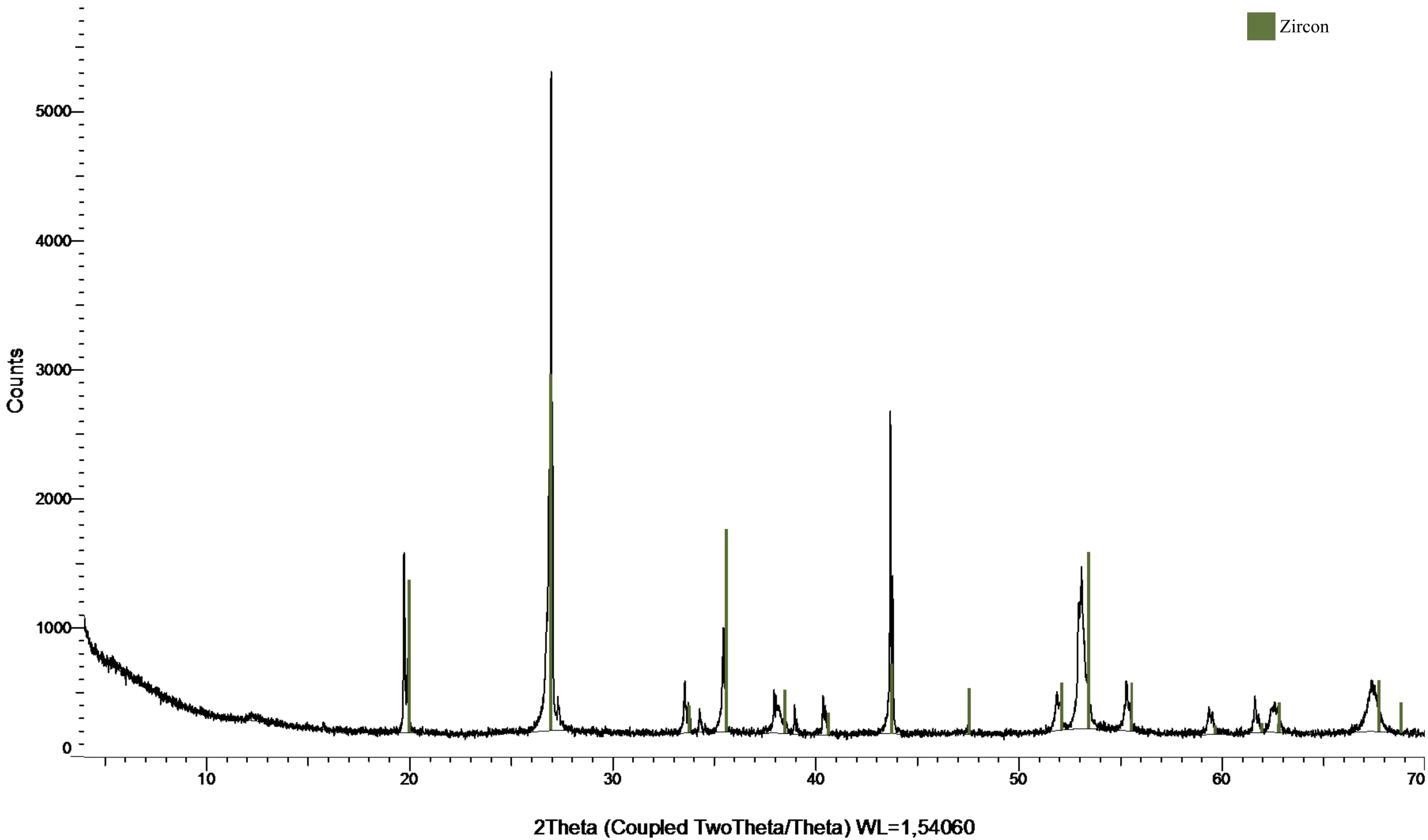

9) 391 Zircon concentrate

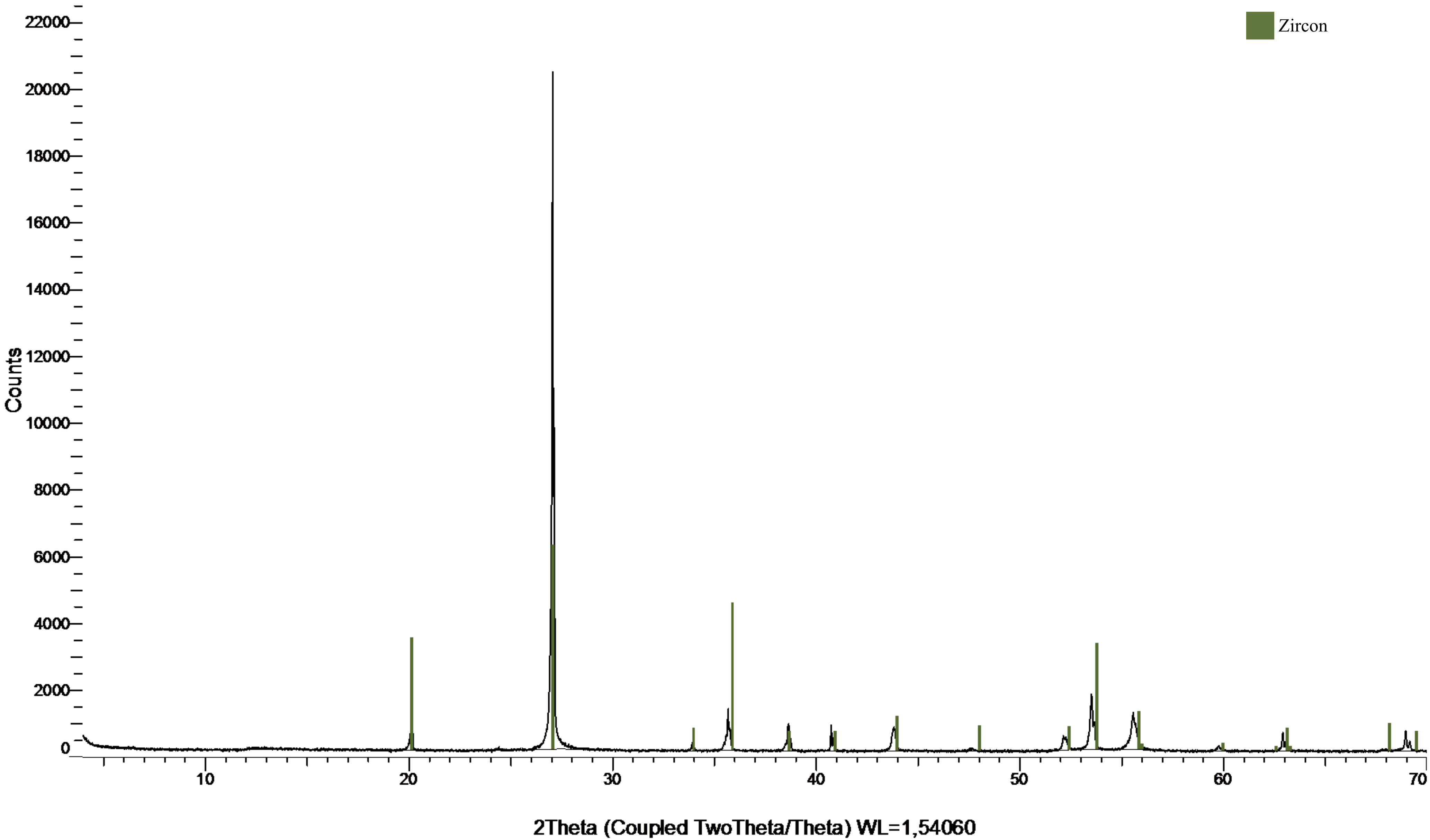

10) 393 Magnetic fraction

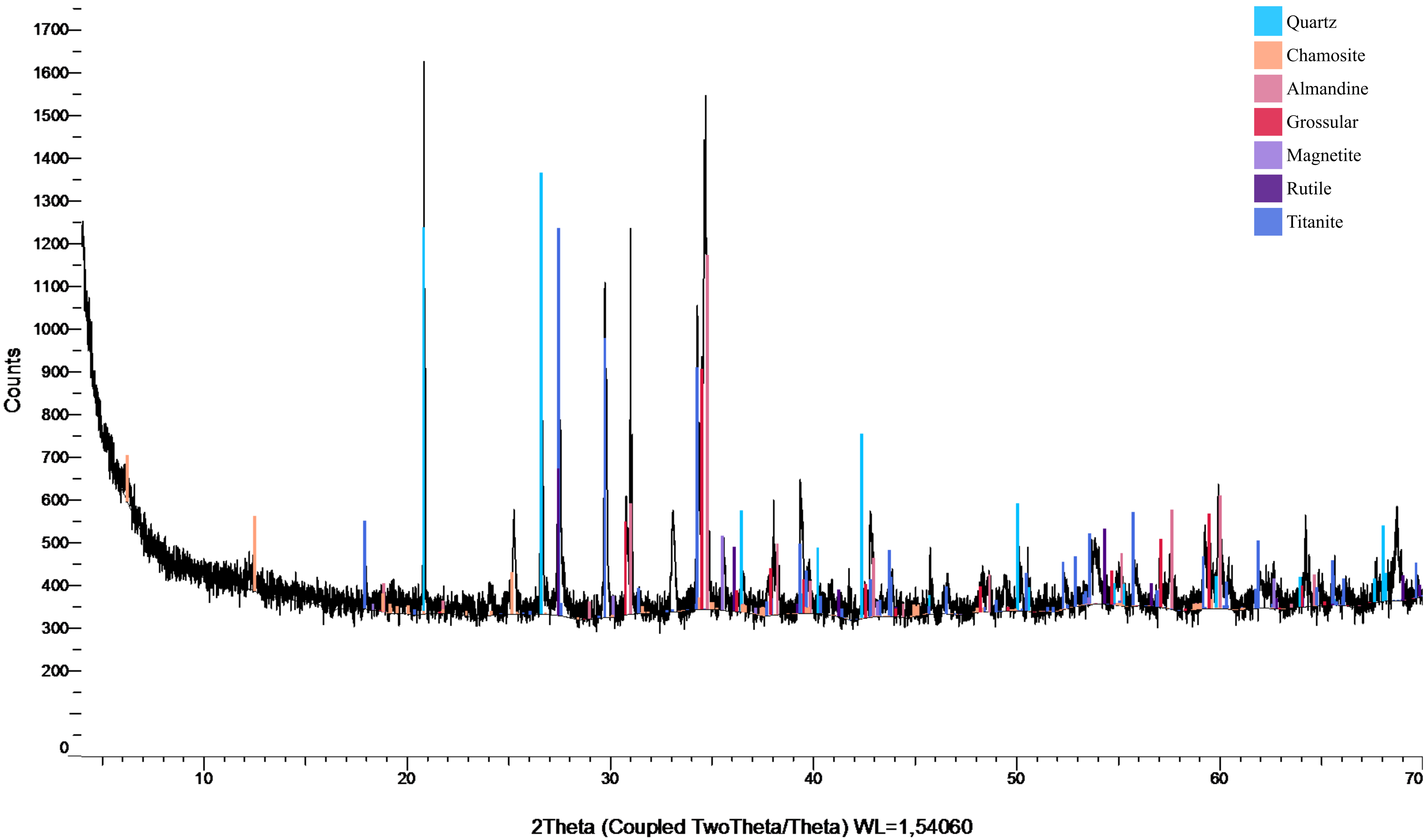

11) BS Magnetic fraction

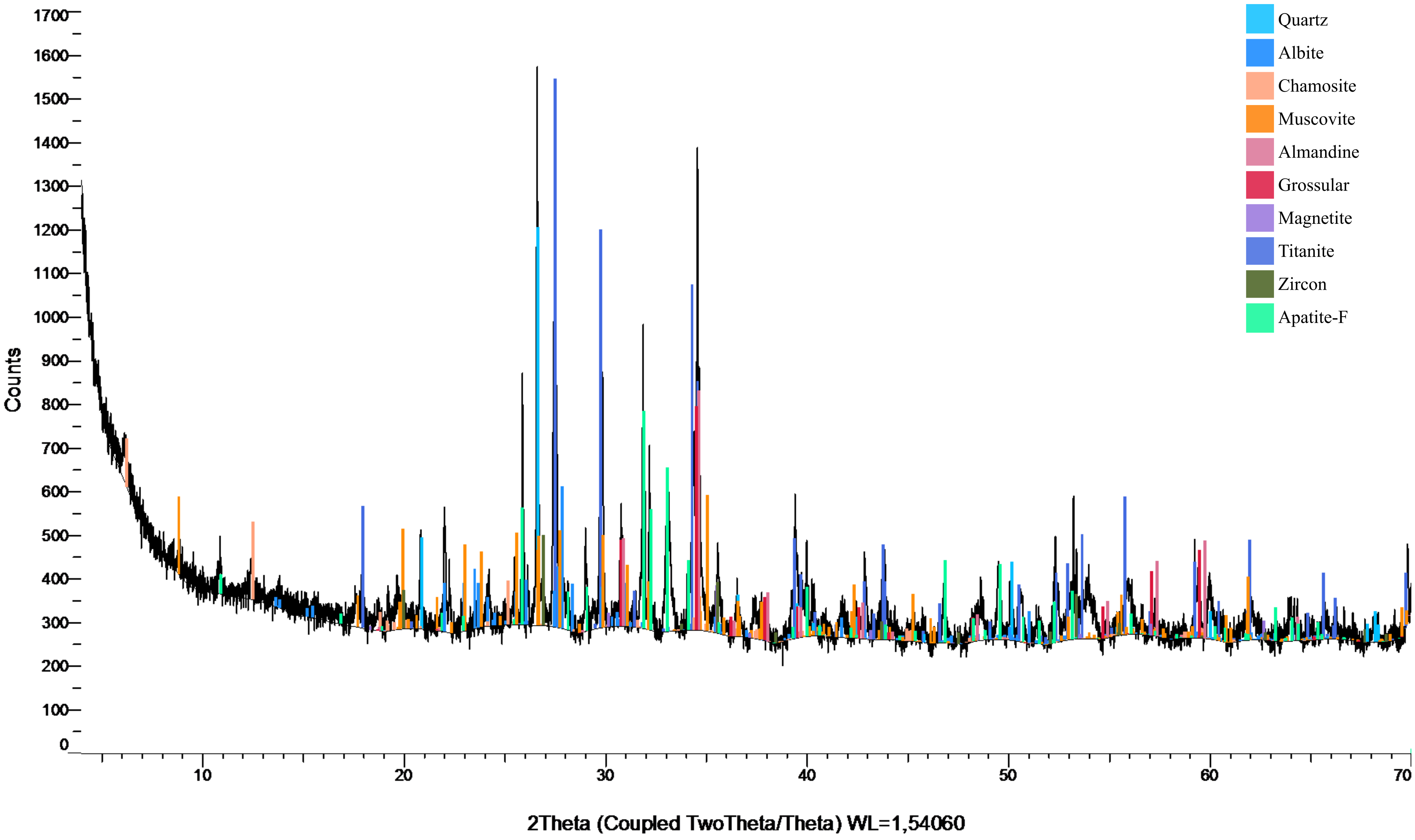

12) BS Apatite fraction

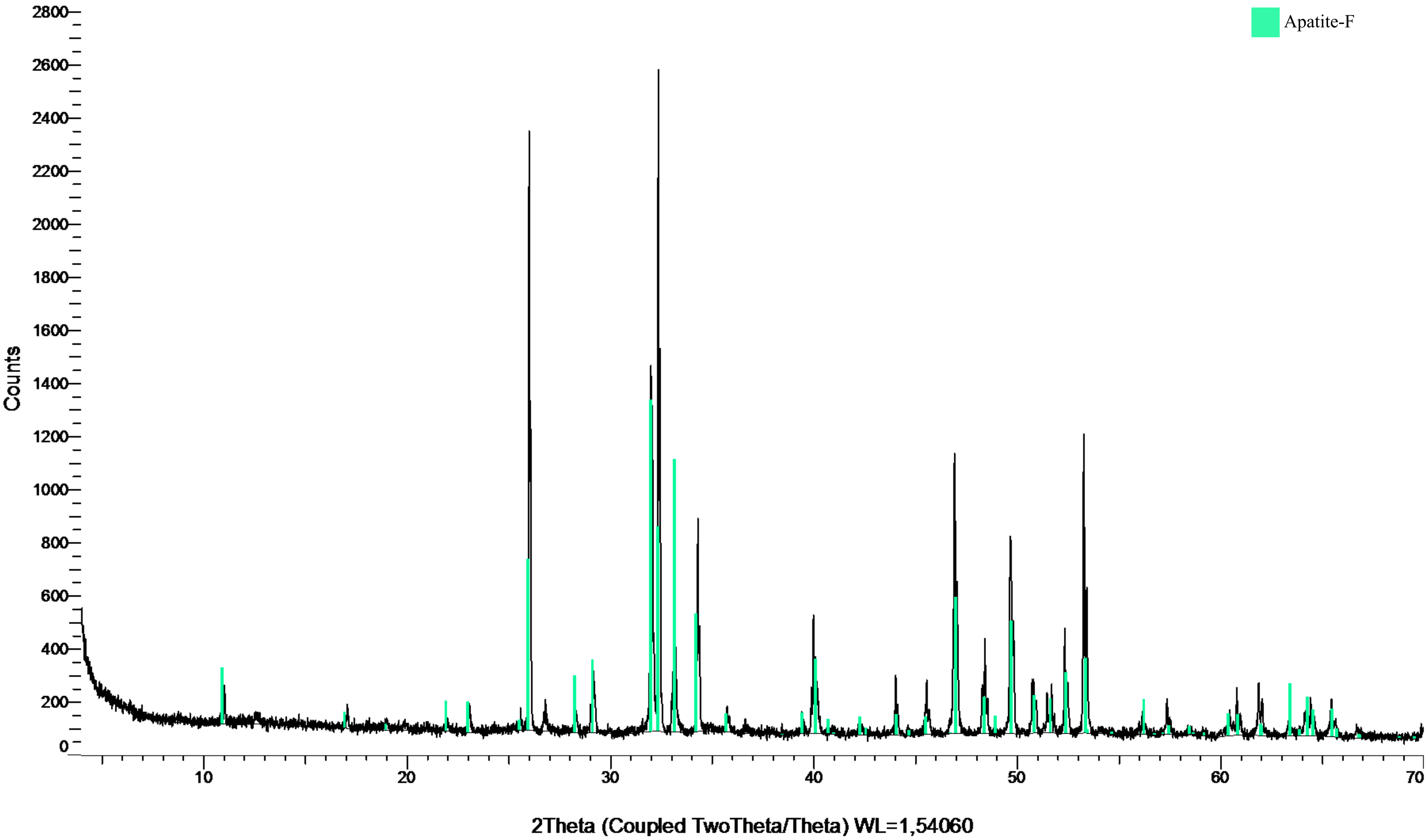

13) BS Zircon fraction

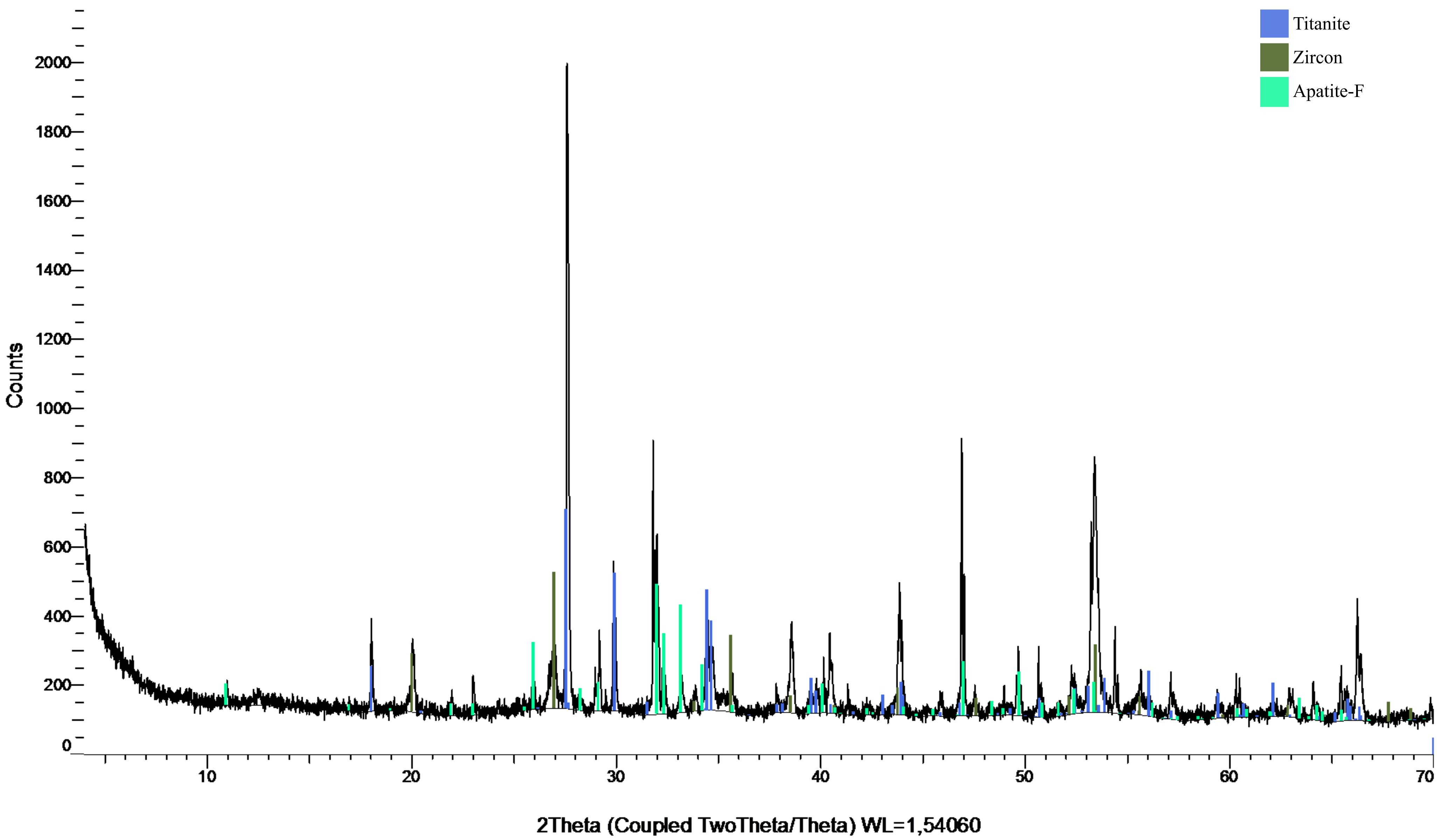

14) BS Zircon concentrate

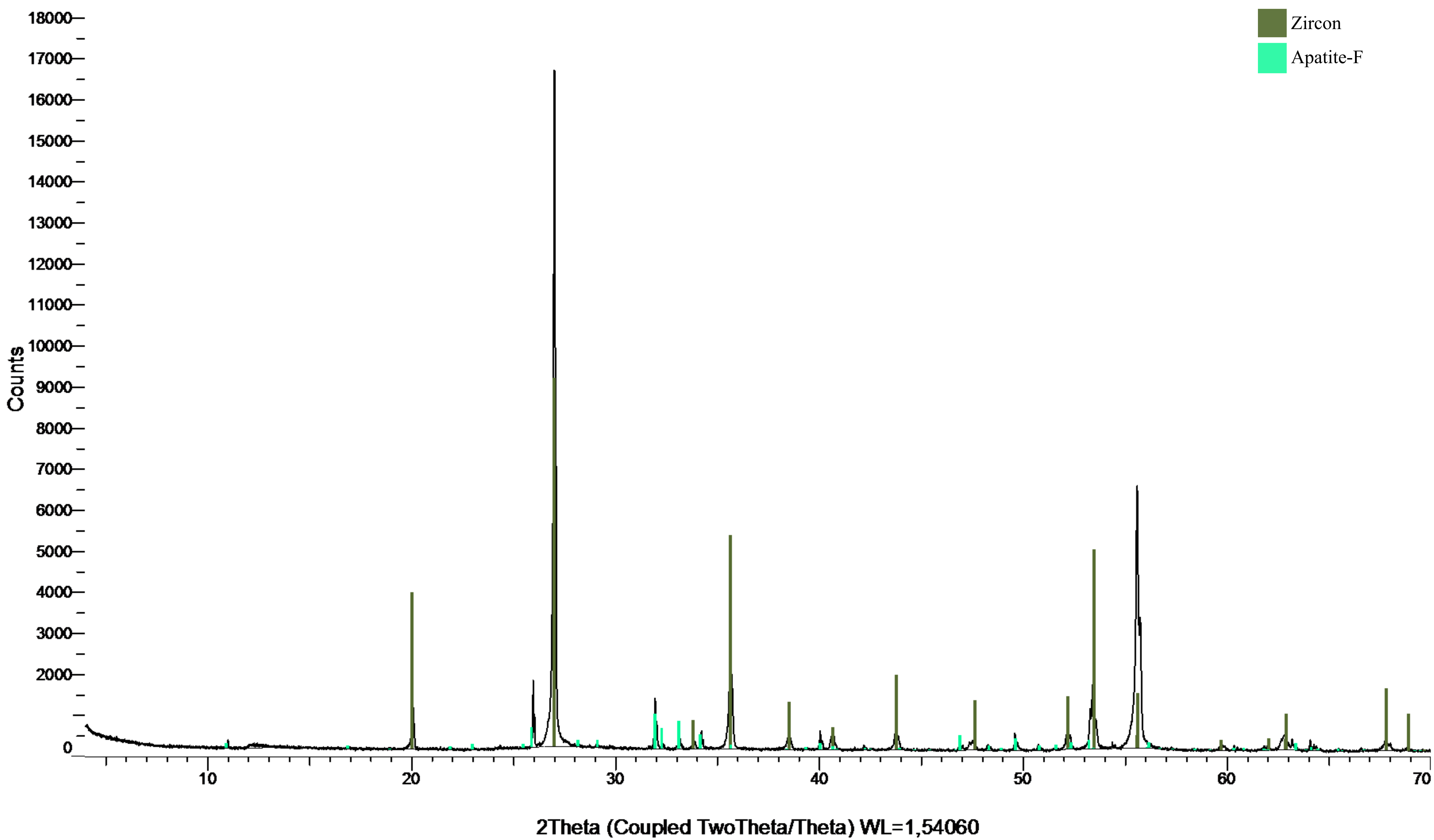

Appendix E: Mineral reference list used for MLA

Mineral list/reference library used for the MLA. Table includes mineral name, mineral group, chemical formula, density, atomic number (Z) and wt% of each element (see next page).

#	Color code	Mineral	Abbreviation	Mineral group	Chemical formula	Density (g/cm3)	Z	Comment
1		Quartz	Qz	Silicate	SiO2	2,63	10,80	Not HM (density < 2,9 g/cm3)
2		Albite	Ab	Feldspar	NaAlSi3O8	2,62	10,79	Not HM (density < 2,9 g/cm3)
3		Orthoclase	Or	Feldspar	KAlSi3O8	2,56	12,04	Not HM (density < 2,9 g/cm3)
4		Calcite	Cal	Cabonate	Ca(CO3)	2,71	12,57	Not HM (density < 2,9 g/cm3)
5		Chamosite	Chm	Mica	(Fe2+,Mg,Fe3+)5Al(AlSi3)O10(OH,O)8	3,20	14,85	
6		Muscovite	Ms	Mica	KAl3Si3O10(OH)1.9F0.1	2,83	11,88	Not HM (density < 2,9 g/cm3)
7		Amphibole	Amp	Amphibole	(Na0.5(Na,K)0.5)(Ca(Ca,Na))((Fe2+,Mg)3.5(Fe2+,Mg, Fe3+)Fe3+0.5)(Si5.5Al1.5(Si,Al))O22(OH,F,Cl)2	3,33	15,39	
8		Yoderite	Yod	Neosilicate	(Mg,Al)8Si4(O,OH)20	3,39	11,62	
9		Tourmaline	Tur	Tourmaline	NaMg3Al6(BO3)3Si6O18(OH)4	3,10	11,66	
10		Almandine-Mn	Alm	Garnet	Fe2+3Al2(SiO4)3	4,20	15,45	Contain ~2 Mass% Mn
11		Almandine-Ca1	Alm	Garnet	Fe2+3Al2(SiO4)3	4,20	14,71	Contain ~1 Mass% Ca
12		Almandine-Ca4	Alm	Garnet	Fe2+3Al2(SiO4)3	4,20	14,75	Contain ~4 Mass% Ca
13		Almandine-Ca5	Alm	Garnet	Fe2+3Al2(SiO4)3	4,20	14,18	Contain ~5 Mass% Ca
14		Almandine-Ca9	Alm	Garnet	Fe2+3Al2(SiO4)3	4,20	13,26	Contain ~9 Mass% Ca
15		Grossular-Fe	Grs	Garnet	Ca3Al2(SiO4)3	3,57	13,80	Contain ~10 Mass% Fe
16		Grossular	Grs	Garnet	Ca3Al2(SiO4)3	3,57	13,39	Contain ~7 Mass% Fe
17		Spessartine-Ca	Sps	Garnet	Mn2+3Al2(SiO4)3	4,18	15,38	
18		Spessartine	Sps	Garnet	Mn2+3Al2(SiO4)3	4,18	16,01	
19		Spessartine-Fe	Sps	Garnet	Mn2+3Al2(SiO4)3	4,18	15,23	
20		Magnetite	Mag	Spinel	FeO	5,00	21,22	Contain no Ti
21		Magnetite-Ti	Mag	Spinel	Fe3+2Fe2+O4	5,15	20,67	Contain ~6 Mass% Ti
22		Ilmenite	Ilm	Oxide	Fe2+TiO3	4,72	17,51	
23		Rutile	Rt	Oxide	TiO2	4,25	16,16	
24		Chromite	Chr	Spinel	Fe2+Cr2O4	4,8	18,78	Contain no Mn
25		Chromite-Mn	Chr	Spinel	Fe2+Cr2O4	4,8	18,43	Contain ~11 Mass% Mn
26		Titanite	Ttn	Neosilicate	CaTiSiO5	3,48	13,81	Contain ~1 Mass% Fe
27		Titanite-Fe	Ttn	Neosilicate	CaTiSiO5	3,48	16,44	Contain ~18 Mass% Fe
28		Zircon	Zrn	Silicate	ZrSiO4	4,65	24,84	
29		Apatite	Ap	Phosphate	Ca5(PO4)(F,Cl,OH)	3,19	14,61	
30		Barite	Brt	Sulphate	Ba(SO4)	4,48	39,46	
31		Monazite-Ce	Mnz	Phosphate	Ce0.5La0.25Nd0.2Th0.05(PO4)	5,15	41,77	

All numbers are wt%.

#	Color code	Mineral	Al	B	Ba	C	Ca	Ce	Cl	Cr	F	Fe	H	K	La	Mg	Mn	Na	Nd	O	P	RE	S	Si	Sm	Sr	Th	Ti	V	Zr
1		Quartz	0	0	0	0	0	0	0	0	0	0	0	0	0	0	0	0	0	53,26	0	0	0	46,74	0	0	0	0	0	0
2		Albite	13,40	0	0	0	0	0	0	0	0	0	0	0	0	0	0	7,58	0	47,47	0	0	0	31,55	0	0	0	0	0	0
3		Orthoclase	12,51	0	0	0	0	0	0	0	0	0	0	15,42	0	0	0	0,45	0	43,20	0	0	0	28,42	0	0	0	0	0	0
4		Calcite	0	0	0	12,00	40,04	0	0	0	0	0	0	0	0	0	0	0	0	47,95	0	0	0	0	0	0	0	0	0	0
5		Chamosite	11,27	0	0	0	0	0	0	0	0	28,84	0,91	1,23	0	5,99	0,55	0	0	39,65	0	0	0	11,56	0	0	0	0	0	0
6		Muscovite	21,58	0	0	0	2,77	0	0	0	0	0,44	0,45	7,81	0	0	0	0	0	44,99	0	0	0	18,90	0	0	0	3,06	0	0
7		Amphibole	11,98	0	0	0	11,32	0	0	0	0	24,51	0	0	0	0	0,82	0	0	36,60	0	0	0	14,77	0	0	0	0	0	0
8		Yoderite	24,14	0	0	0	2,21	0	0	2,01	0	2,39	0	0	0	6,90	0	0	0	44,38	0	0	0	17,39	0	0	0	0,58	0	0
9		Tourmaline	21,28	0	0	0	0,70	0	0	0	0	7,04	0	0	0	5,11	0	2,09	0	48,17	0	0	0	15,10	0	0	0	0,51	0	0
10		Almandine-Mn	13,27	0	0	0	3,11	0	0	0	0	27,68	0	0	0	2,36	2,48	0	0	35,82	0	0	0	15,28	0	0	0	0	0	0
11		Almandine-Ca1	13,71	0	0	0	0,89	0	0	0	0	26,27	0	0	0	5,79	0,19	0	0	37,73	0	0	0	15,42	0	0	0	0	0	0
12		Almandine-Ca4	13,64	0	0	0	3,58	0	0	0	0	24,73	0	0	0	5,12	0,21	0	0	37,01	0	0	0	15,71	0	0	0	0	0	0
13		Almandine-Ca5	14,02	0	0	0	5,18	0	0	0	0	19,91	0	0	0	6,22	0,32	0	0	38,12	0	0	0	16,23	0	0	0	0	0	0
14		Almandine-Ca9	14,31	0	0	0	9,29	0	0	0	0	11,57	0	0	0	8,39	0,10	0	0	39,72	0	0	0	16,62	0	0	0	0	0	0
15		Grossular-Fe	14,24	0	0	0	19,88	0	0	0	0	10,00	0	0	0	0	0	0	0	40,77	0	0	0	15,11	0	0	0	0	0	0
16		Grossular	16,19	0	0	0	19,69	0	0	0	0	7,10	0	0	0	0	0	0	0	41,31	0	0	0	15,71	0	0	0	0	0	0
17		Spessartine-Ca	11,46	0	0	0	11,83	0	0	0	0	12,78	0	0	0	0	12,71	0	0	35,81	0	0	0	15,41	0	0	0	0	0	0
18		Spessartine	12,37	0	0	0	1,19	0	0	0	0	11,75	0	0	0	0,79	24,80	0	0	34,27	0	0	0	14,83	0	0	0	0	0	0
19		Spessartine-Fe	10,90	0	0	0	0	0	0	0	0	0	0	0	0	0	33,29	0	0	38,78	0	0	0	17,02	0	0	0	0	0	0
20		Magnetite	0	0	0	0	0	0	0	0	0	73,21	0	0	0	0	0,26	0	0	26,53	0	0	0	0	0	0	0	0	0	0
21		Magnetite-Ti	0	0	0	0	0	0	0	0	0	65,76	0	0	0	0	0	0	0	28,32	0	0	0	0	0	0	0	5,92	0	0
22		Ilmenite	0	0	0	0	0	0	0	0	0	25,26	0	0	0	0	0	0	0	39,30	0	0	0	0	0	0	0	35,44	0	0
23		Rutile	0	0	0	0	0,95	0	0	0	0	0,22	0	0	0	0	0	0	0	41,57	0	0	0	0,15	0	0	0	57,11	0	0
24		Chromite	8,59	0	0	0	0	0	0	31,17	0	28,26	0	0	0	4,31	0	0	0	26,93	0	0	0	0	0	0	0	0,39	0,35	0
25		Chromite-Mn	5,20	0	0	0	0	0	0	44,64	0	5,87	0	0	0	3,63	10,75	0	0	29,91	0	0	0	0	0	0	0	0	0	0
26		Titanite	2,72	0	0	0	19,26	0	0	0	0,96	1,41	0	0	0	0	0	0	0	39,65	0	3,64	0	14,20	0	0	0	18,16	0	0
27		Titanite-Fe	1,03	0	0	0	16,74	0	0	0	0	18,15	0	0	0	0	0	0	0	37,09	0	0	0	8,34	0	0	0	18,65	0	0
28		Zircon	0	0	0	0	0	0	0	0	0	0	0	0	0	0	0	0	0	34,91	0	0	0	15,32	0	0	0	0	0	49,76
29		Apatite	0	0	0	0	44,59	0	0	0	0	0	0,06	0	0	0	0	0	0	37,24	18,11	0	0	0	0	0	0	0	0	0
30		Barite	0	0	62,06	0	0	0	0	0	0	0	0	0	0	0	0	0	0	21,49	0	0	14,83	0	0	1,62	0	0	0	0
31		Monazite-Ce	0	0	0	0	0,99	28,63	0	0	0	0	0	0	13,68	0	0	0	14,21	24,32	12,88	0	0	0	0	0	5,29	0	0	0

Appendix F: Spectrums from MLA

Spectrums and element compositions for mineral 1-31 used as standards for analyses with MLA. The MLA compares these spectrums with measurements from the samples.

#	Mineral	Color code
1	Quartz	
2	Albite	
3	Orthoclase	
4	Calcite	
5	Chamosite	
6	Muscovite	
7	Amphibole	
8	Yoderite	
9	Tourmaline	
10	Almandine-Mn	
11	Almandine-Ca1	
12	Almandine-Ca4	
13	Almandine-Ca5	
14	Almandine-Ca9	
15	Grossular-Fe	
16	Grossular	
17	Spessartine-Ca	
18	Spessartine	
19	Spessartine-Fe	
20	Magnetite	
21	Magnetite-Ti	
22	Ilmenite	
23	Rutile	
24	Chromite	
25	Chromite-Mn	
26	Titanite	
27	Titanite-Fe	
28	Zircon	
29	Apatite	
30	Barite	
31	Monazite-Ce	

1) Quartz

Mineral characteristics

#	Color code	Mineral	Chemical formula	Density	Z
1		Quartz	SiO_2	2,63	10,80

Spectrum chart

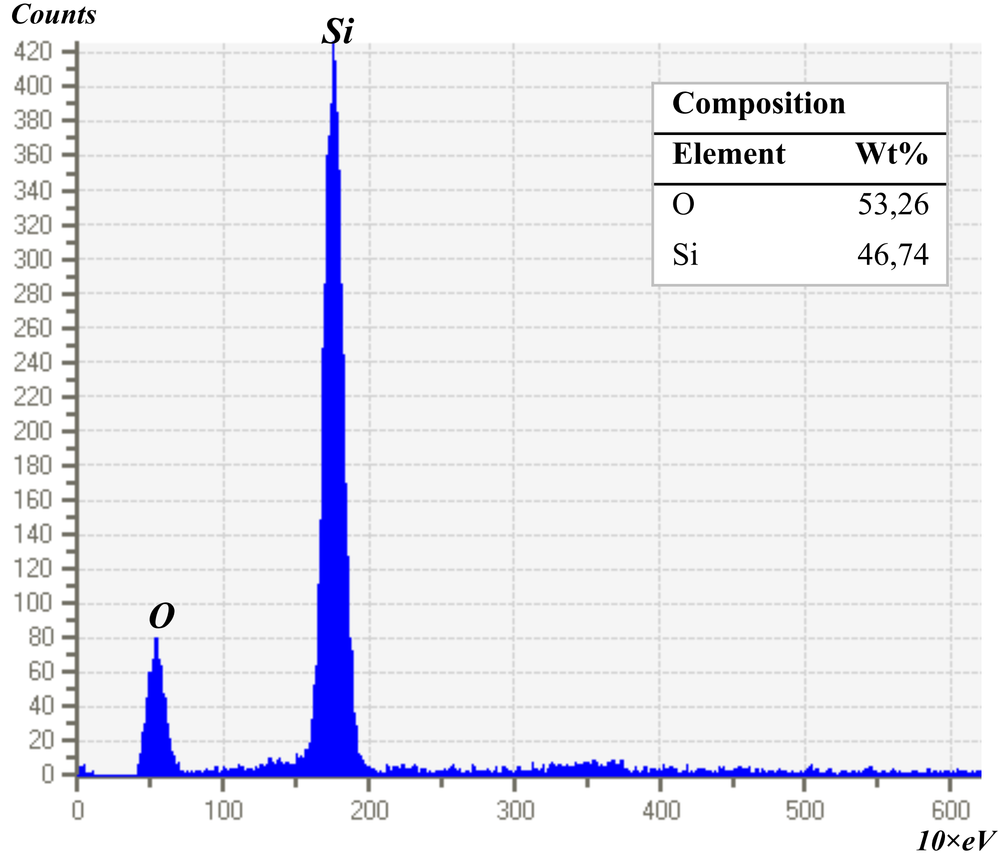

2) Albite

Mineral characteristics

#	Color code	Mineral	Chemical formula	Density	Z
2		Albite	NaAlSi3O8	2,62	10,79

Spectrum chart

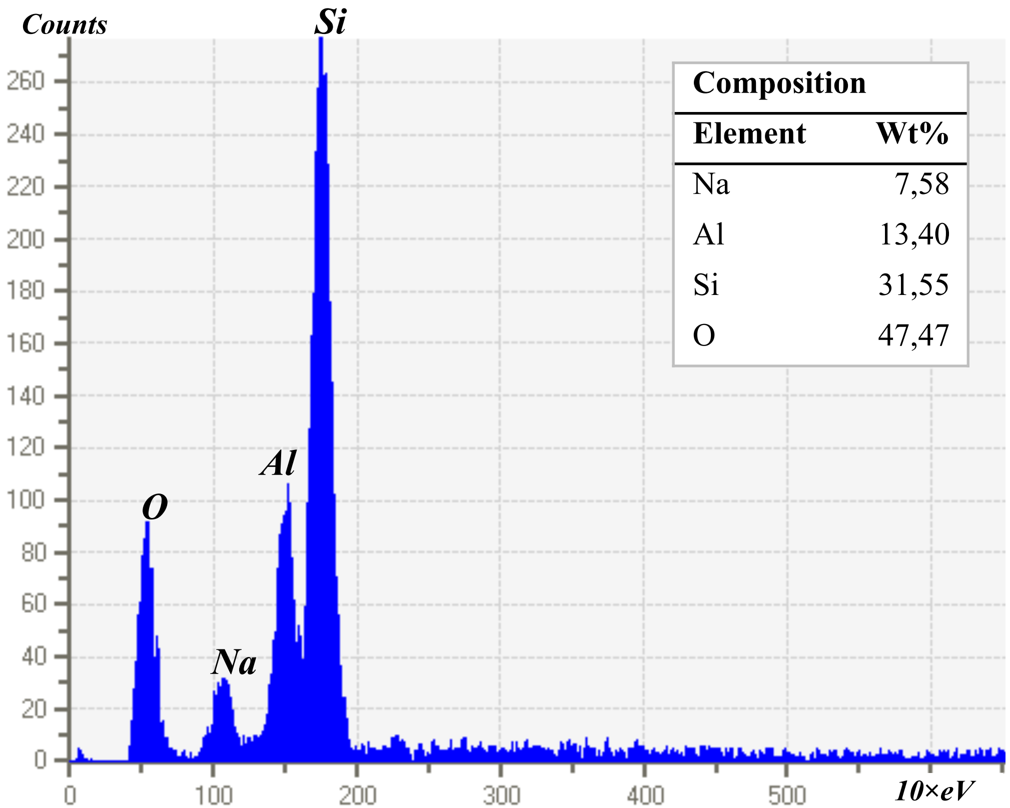

3) Orthoclase

Mineral characteristics

#	Color code	Mineral	Chemical formula	Density	Z
3		Orthoclase	KAlSi3O8	2,56	12,04

Spectrum chart

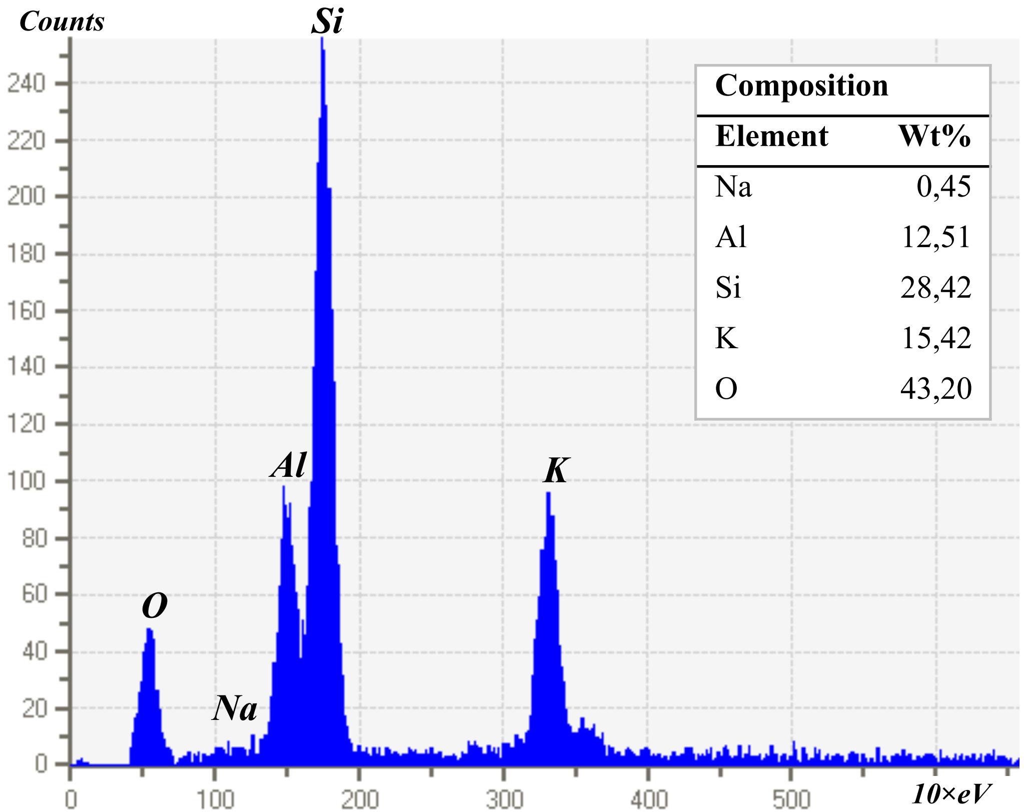

4) Calcite

Mineral characteristics

#	Color code	Mineral	Chemical formula	Density	Z
4		Calcite	Ca(CO3)	2,71	12,57

Spectrum chart

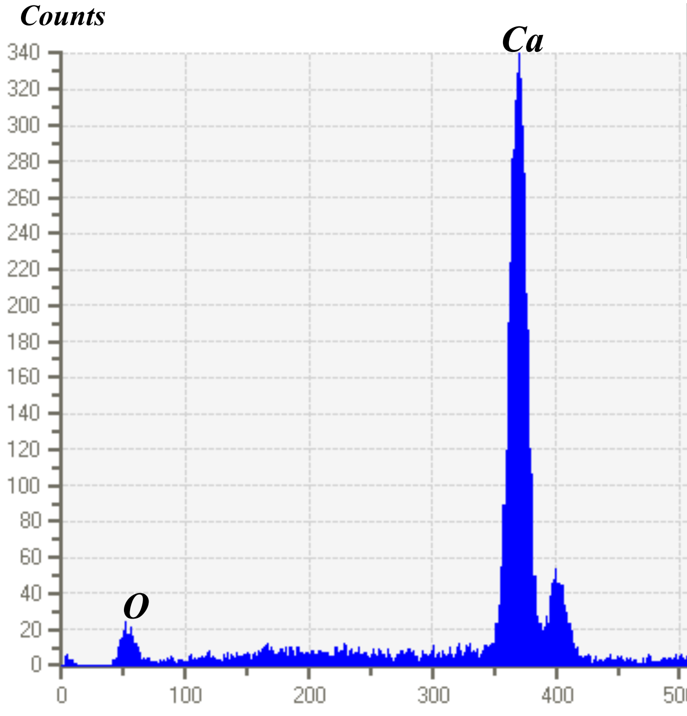

Composition	
Element	**Wt%**
C	12,00
O	47,95
Ca	40,04

5) Chamosite

Mineral characteristics

#	Color code	Mineral	Chemical formula	Density	Z
5		Chamosite	(Fe2+,Mg,Fe3+)5Al(AlSi3)O10(OH,O)8	3,20	14,85

Spectrum chart

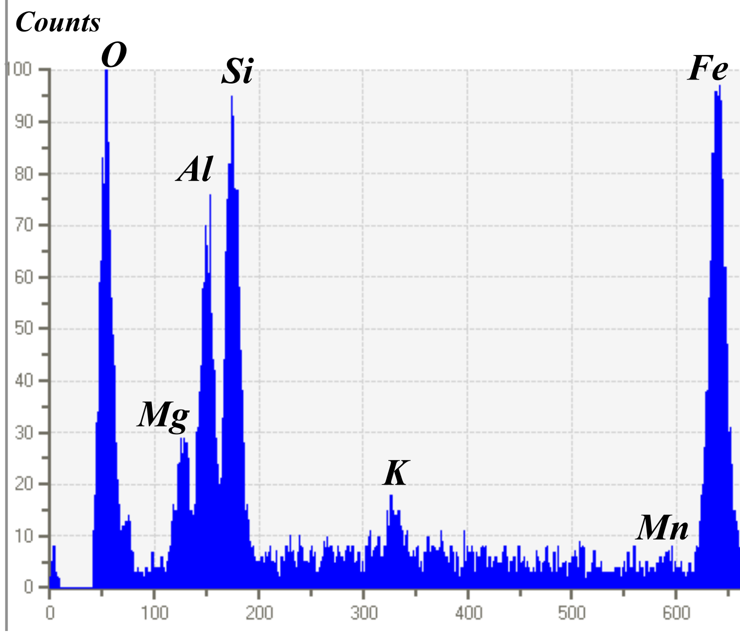

Composition	
Element	**Wt%**
H	0,91
Mg	5,99
Al	11,27
Si	11,56
Fe	28,84
Mn	0,55
K	1,23
O	39,65

6) Muscovite

Mineral characteristics

#	Color code	Mineral	Chemical formula	Density	Z
6		Muscovite	KAl3Si3O10(OH)1.9F0.1	2,83	11,88

Spectrum chart

Composition	
Element	**Wt%**
H	0,45
Fe	0,44
F	0,00
Al	21,58
Si	18,90
K	7,81
Ca	2,77
Ti	3,06
O	44,99

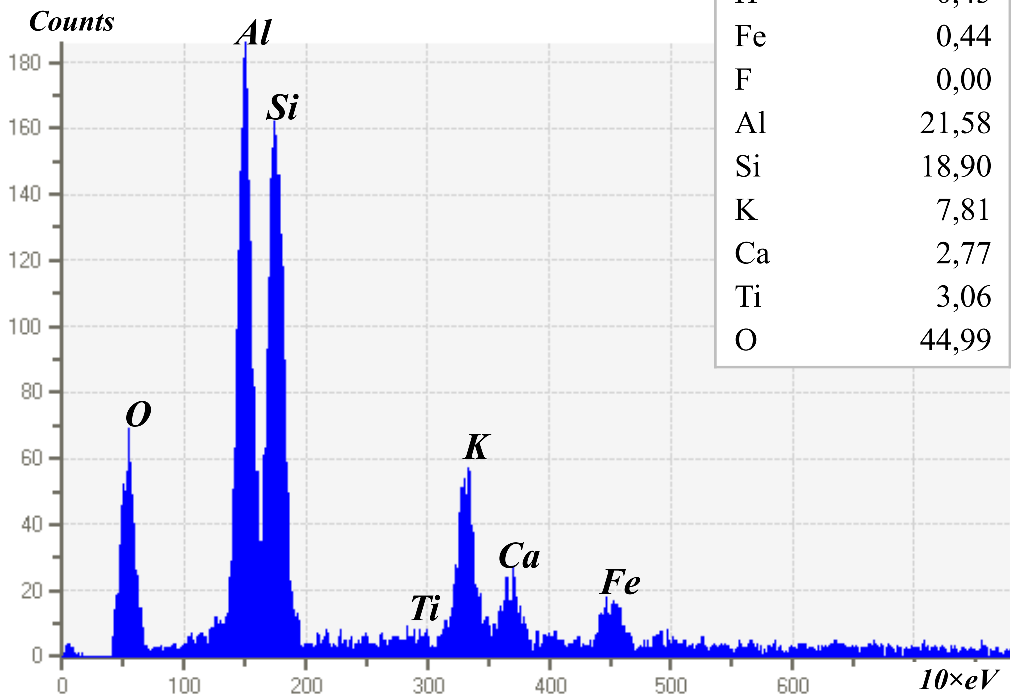

7) Amphibole

Mineral characteristics

#	Color code	Mineral	Chemical formula	Density	Z
7		Amphibole	(Na0.5(Na,K)0.5)(Ca(Ca,Na)) ((Fe2+,Mg)3.5(Fe2+,Mg,Fe3+)Fe3+0.5) (Si5.5Al1.5(Si,Al))O22(OH,F,Cl)2	3,33	15,39

Spectrum chart

Composition	
Element	**Wt%**
Fe	24,51
Si	14,77
Al	11,98
Ca	11,32
Mn	0,82
O	36,60

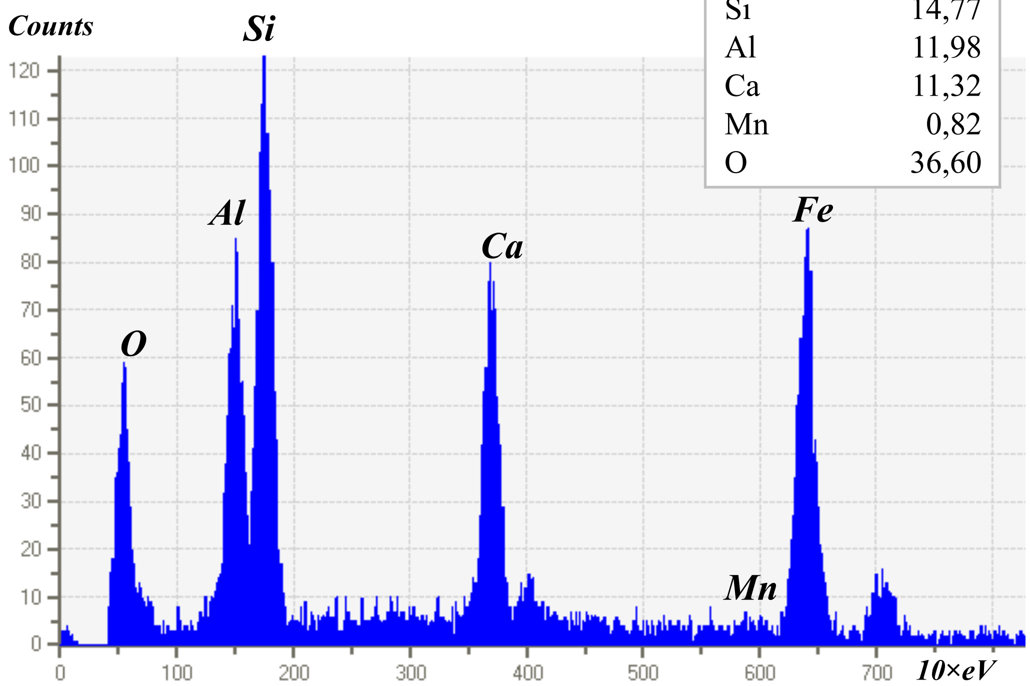

8) Yoderite

Mineral characteristics

#	Color code	Mineral	Chemical formula	Density	Z
8		Yoderite	(Mg,Al)8Si4(O,OH)20	3,39	11,62

Spectrum chart

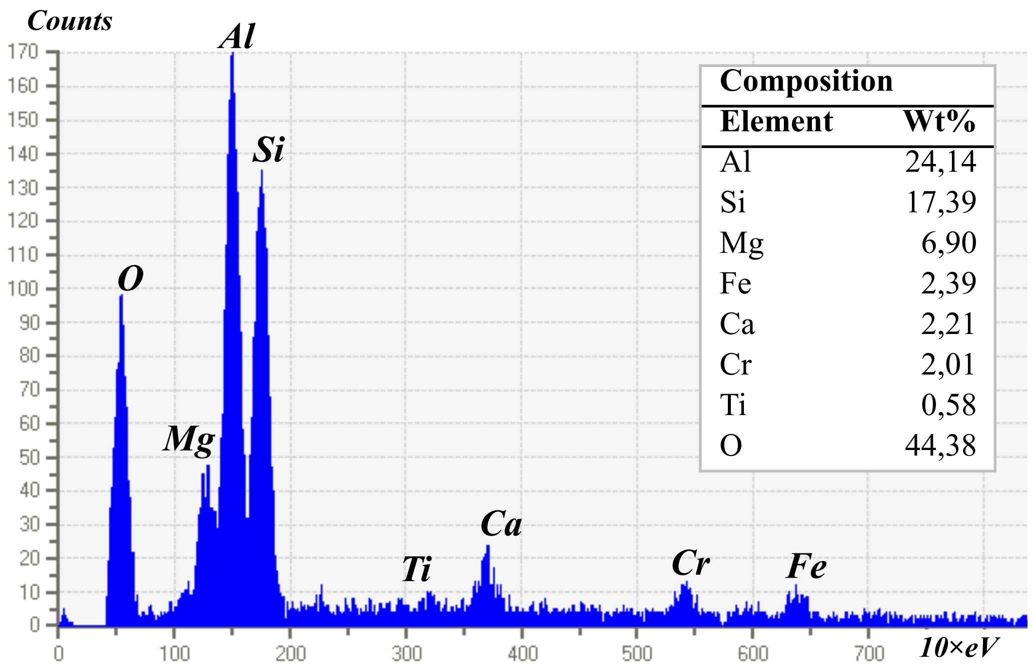

Element	Wt%
Al	24,14
Si	17,39
Mg	6,90
Fe	2,39
Ca	2,21
Cr	2,01
Ti	0,58
O	44,38

Composition

9) Tourmaline

Mineral characteristics

#	Color code	Mineral	Chemical formula	Density	Z
9		Tourmaline	NaMg3Al6(BO3)3Si6O18(OH)4	3,10	11,66

Spectrum chart

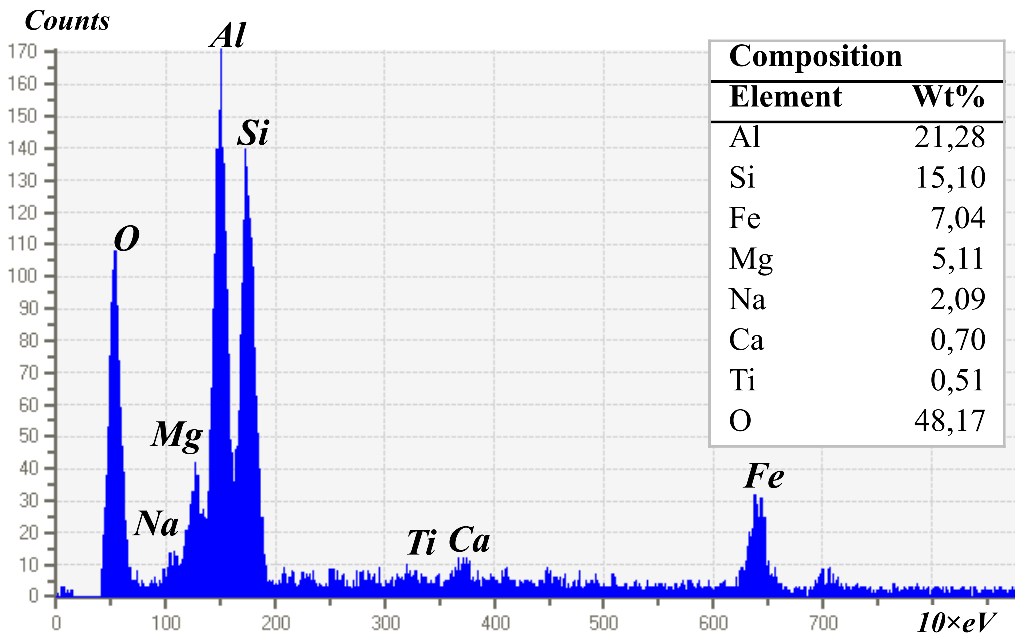

Element	Wt%
Al	21,28
Si	15,10
Fe	7,04
Mg	5,11
Na	2,09
Ca	0,70
Ti	0,51
O	48,17

Composition

10) Almandine-Mn

Mineral characteristics

#	Color code	Mineral	Chemical formula	Density	Z
10		Almandine-Mn	Fe2+3Al2(SiO4)3	4,20	15,45

Spectrum chart

Composition	
Element	**Wt%**
O	35,82
Al	13,27
Si	15,28
Fe	27,68
Ca	3,11
Mn	2,48
Mg	2,36

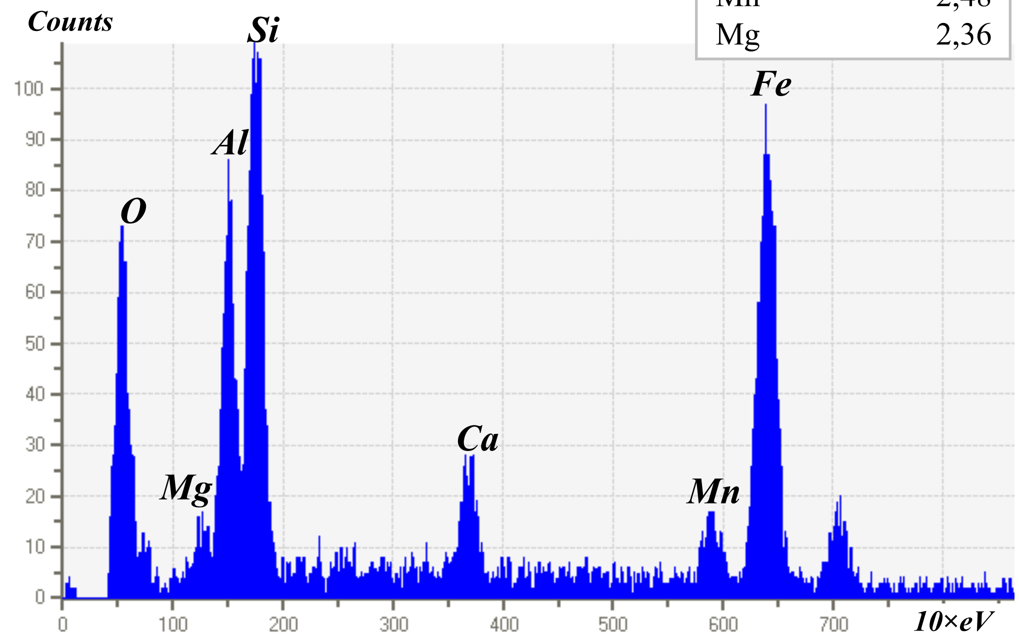

11) Almandine-Ca1

Mineral characteristics

#	Color code	Mineral	Chemical formula	Density	Z
11		Almandine-Ca1	Fe2+3Al2(SiO4)3	4,20	14,71

Spectrum chart

Composition	
Element	**Wt%**
O	37,73
Al	13,71
Si	15,42
Fe	26,27
Ca	0,89
Mn	0,19
Mg	5,79

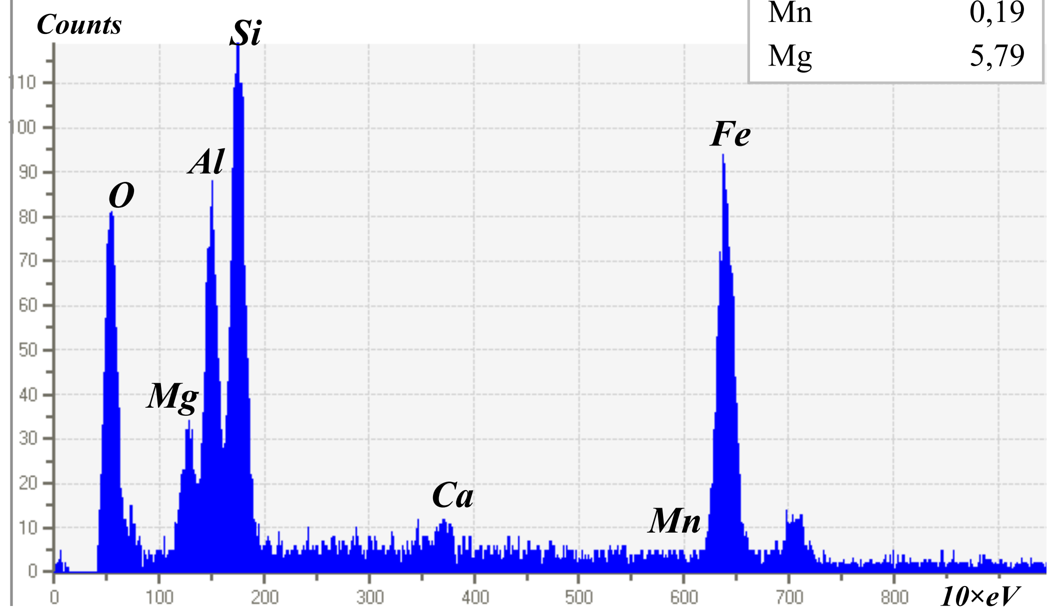

12) Almandine-Ca4

Mineral characteristics

#	Color code	Mineral	Chemical formula	Density	Z
12		Almandine-Ca4	Fe2+3Al2(SiO4)3	4,20	14,75

Spectrum chart

Composition	
Element	**Wt%**
O	37,01
Al	13,64
Si	15,71
Fe	24,73
Mg	5,12
Ca	3,58
Mn	0,21

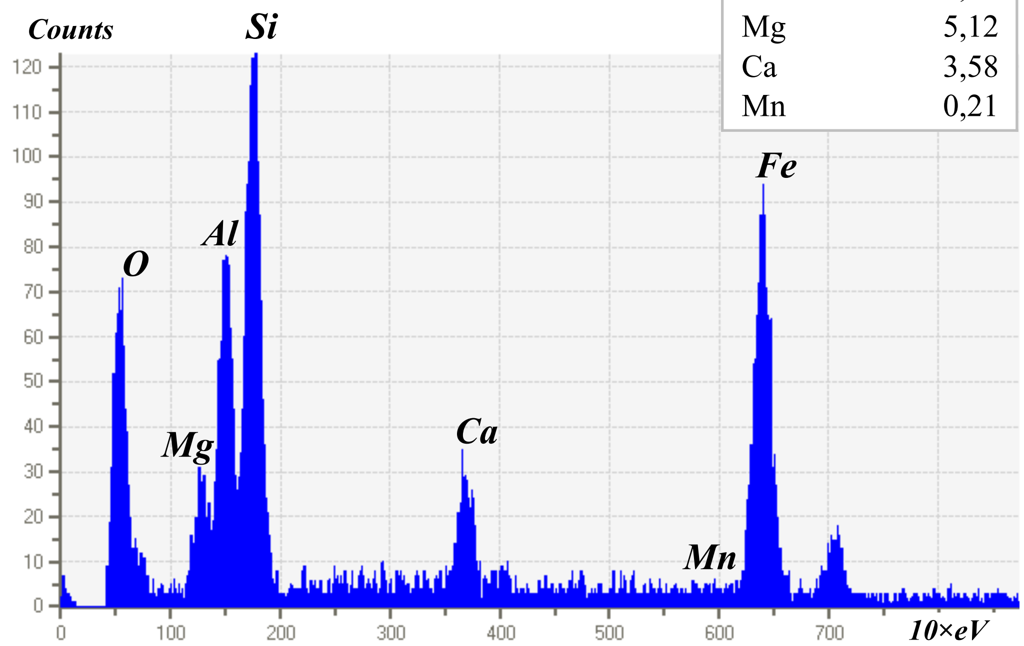

13) Almandine-Ca5

Mineral characteristics

#	Color code	Mineral	Chemical formula	Density	Z
13		Almandine-Ca5	Fe2+3Al2(SiO4)3	4,20	14,18

Spectrum chart

Composition	
Element	**Wt%**
Mn	0,32
Si	16,23
Fe	19,91
Al	14,02
Mg	6,22
Ca	5,18
O	38,12

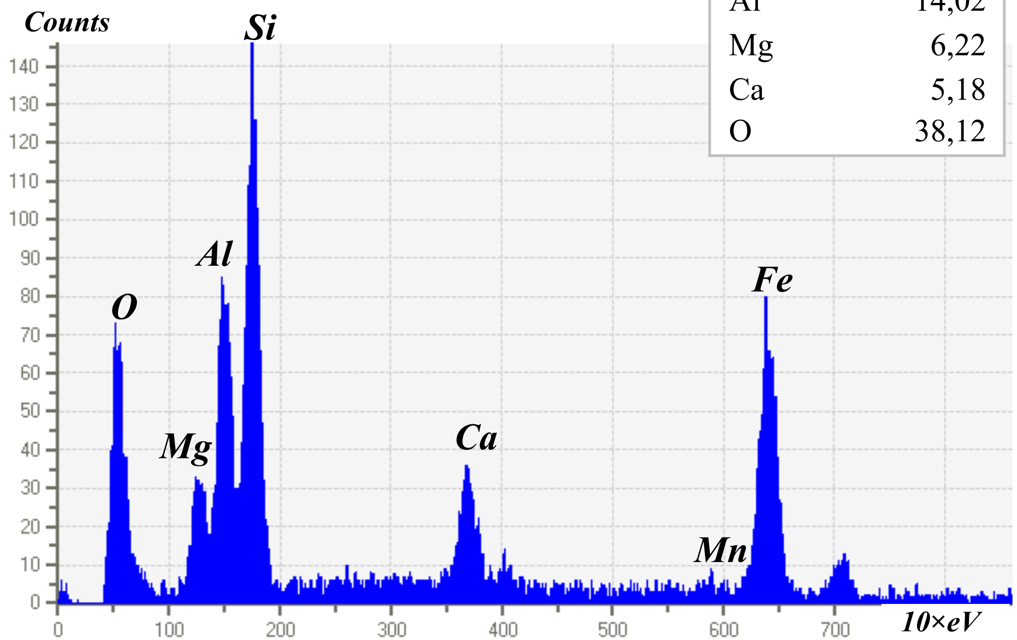

14) Almandine-Ca9

Mineral characteristics

#	Color code	Mineral	Chemical formula	Density	Z
14		Almandine-Ca9	Fe2+3Al2(SiO4)3	4,20	13,26

Spectrum chart

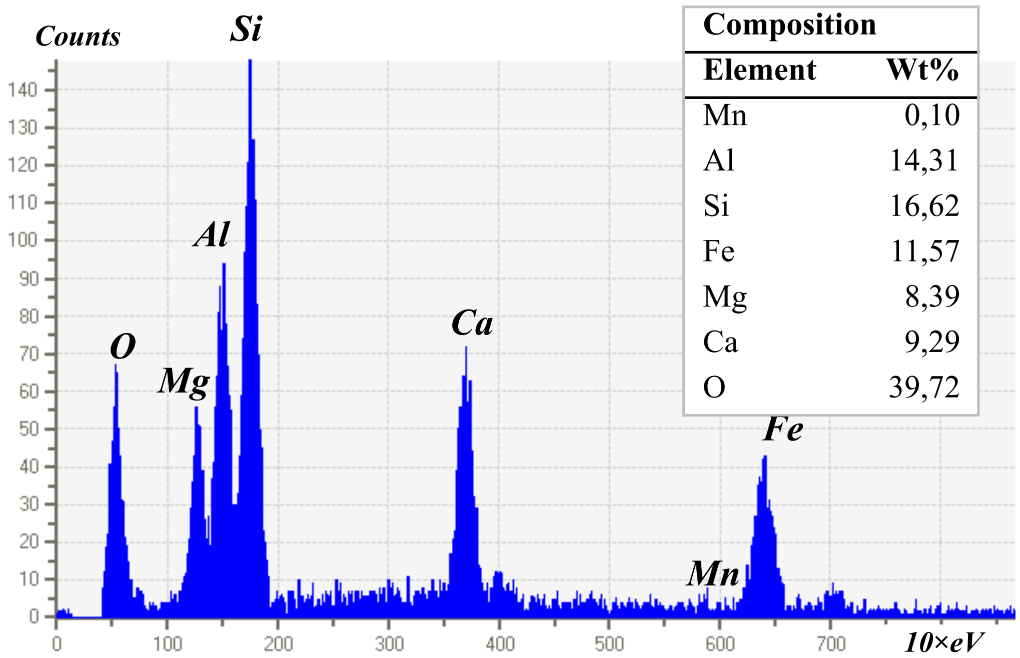

Composition	
Element	**Wt%**
Mn	0,10
Al	14,31
Si	16,62
Fe	11,57
Mg	8,39
Ca	9,29
O	39,72

15) Grossular-Fe

Mineral characteristics

#	Color code	Mineral	Chemical formula	Density	Z
15		Grossular-Fe	Ca3Al2(SiO4)3	3,57	13,80

Spectrum chart

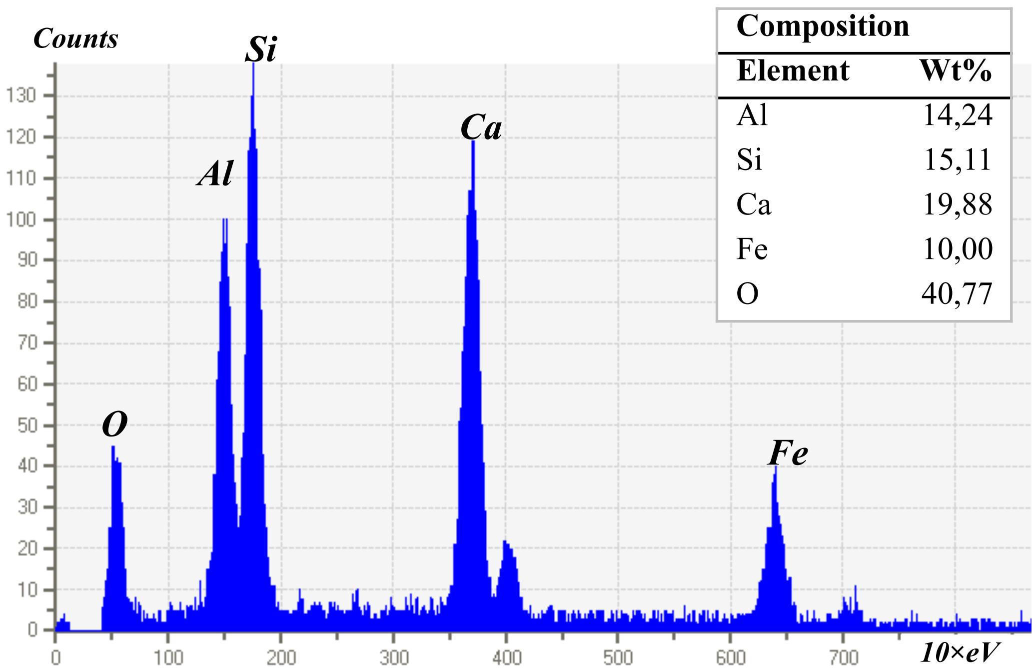

Composition	
Element	**Wt%**
Al	14,24
Si	15,11
Ca	19,88
Fe	10,00
O	40,77

16) Grossular

Mineral characteristics

#	Color code	Mineral	Chemical formula	Density	Z
16		Grossular	Ca3Al2(SiO4)3	3,57	13,39

Spectrum chart

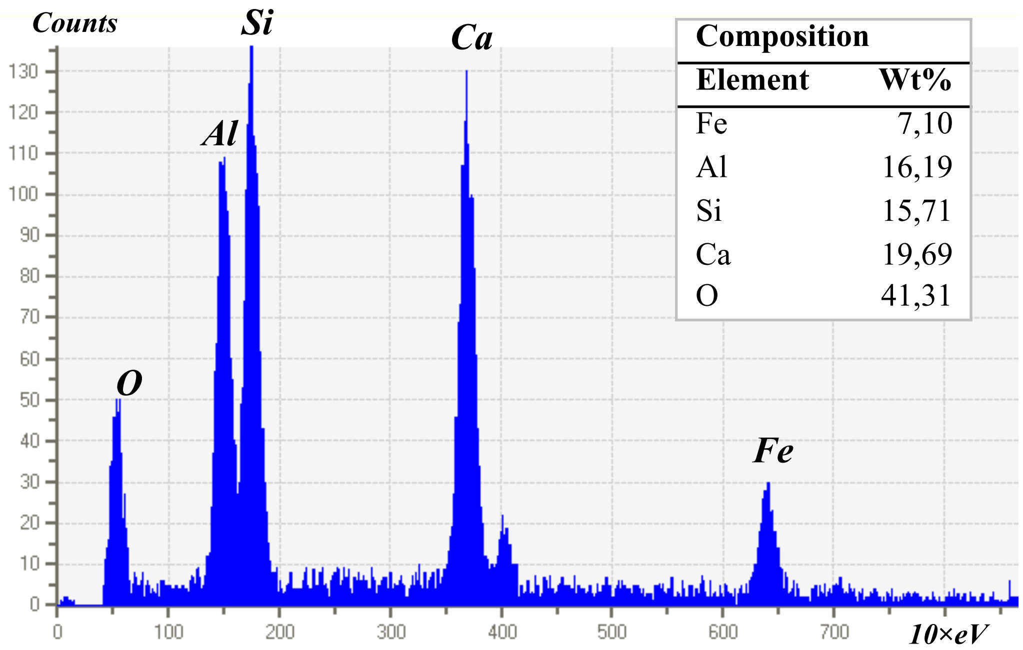

17) Spessartine-Ca

Mineral characteristics

#	Color code	Mineral	Chemical formula	Density	Z
17		Spessartine-Ca	Mn2+3Al2(SiO4)3	4,18	15,38

Spectrum chart

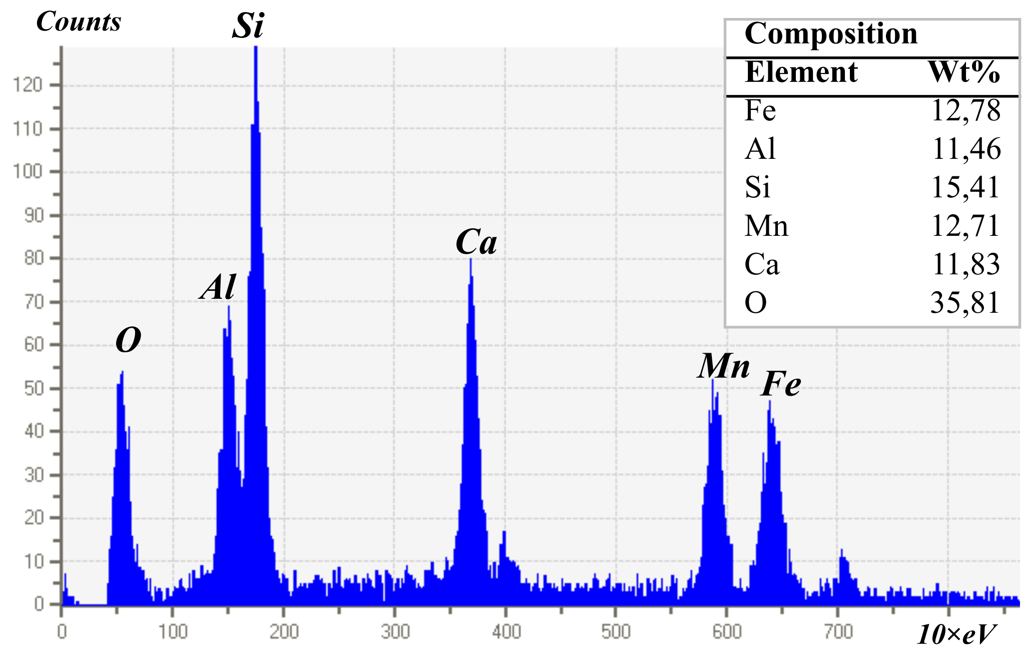

18) Spessartine

Mineral characteristics

#	Color code	Mineral	Chemical formula	Density	Z
18		Spessartine	Mn2+3Al2(SiO4)3	4,18	16,01

Spectrum chart

Composition	
Element	**Wt%**
Fe	11,75
Al	12,37
Si	14,83
Mn	24,80
Mg	0,79
Ca	1,19
O	34,27

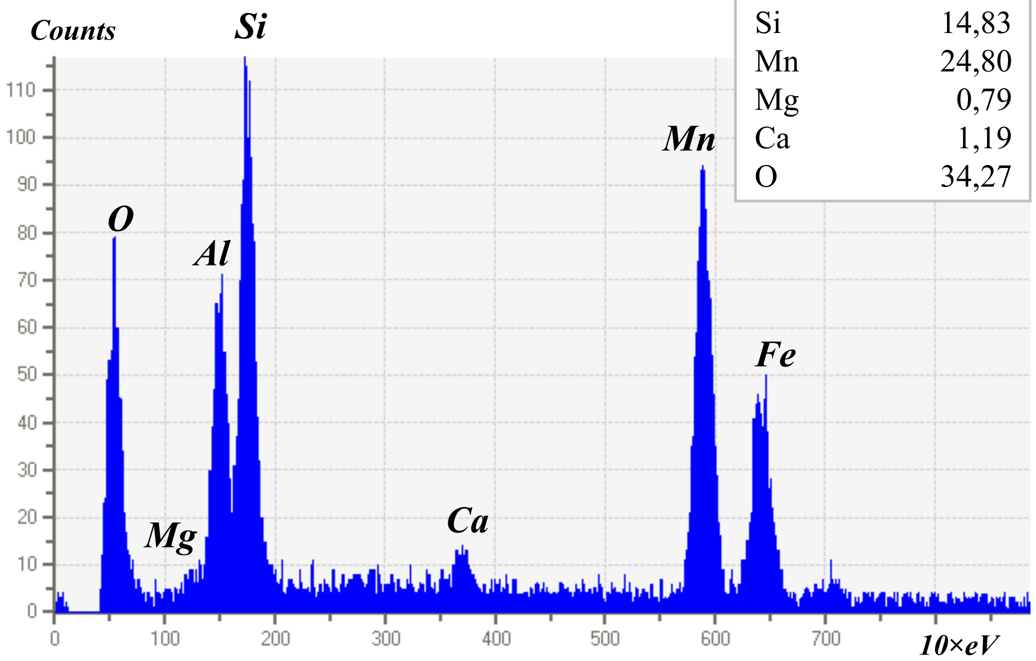

19) Spessartine-Fe

Mineral characteristics

#	Color code	Mineral	Chemical formula	Density	Z
19		Spessartine-Fe	Mn2+3Al2(SiO4)3	4,18	15,23

Spectrum chart

Composition	
Element	**Wt%**
O	38,78
Al	10,90
Si	17,02
Mn	33,29

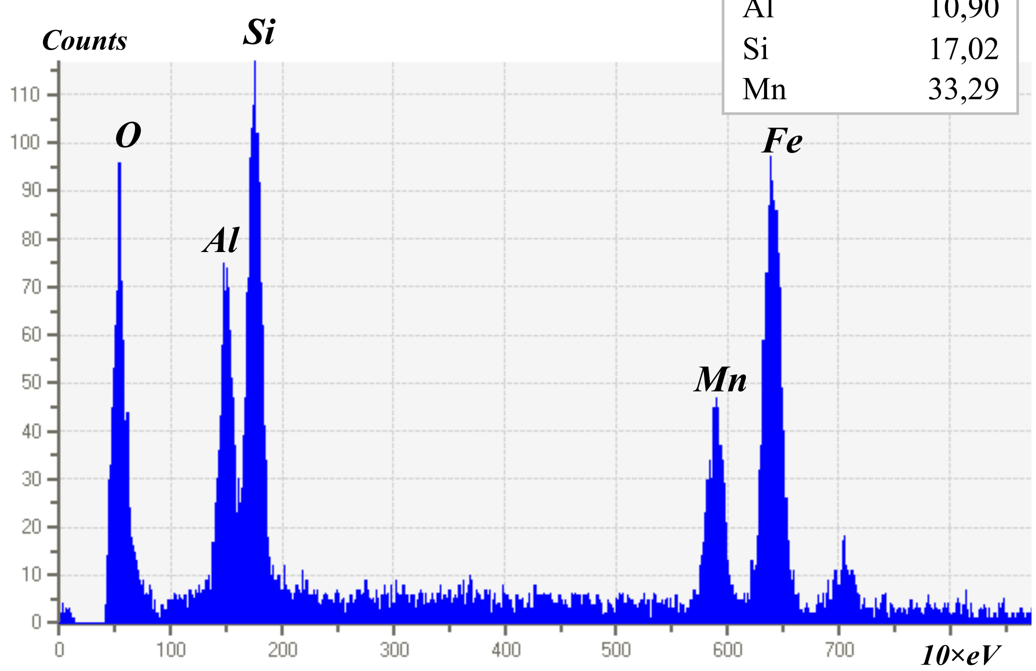

20) Magnetite

Mineral characteristics

#	Color code	Mineral	Chemical formula	Density	Z
20		Magnetite	FeO	5,00	21,22

Spectrum chart

Composition	
Element	**Wt%**
Fe	73,21
Mn	0,26
O	26,53

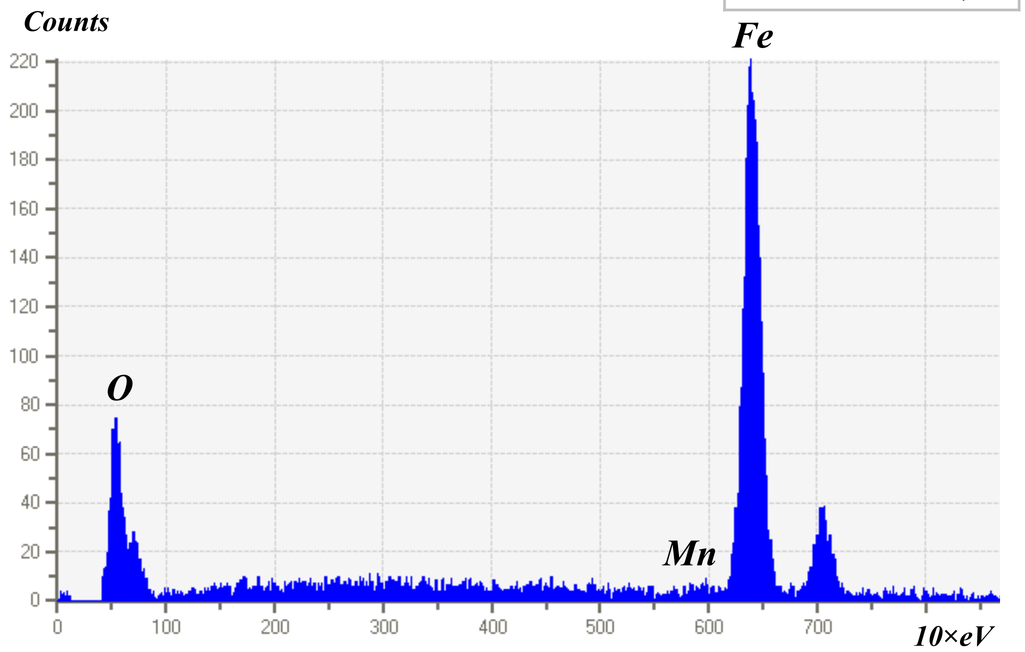

21) Magnetite-Ti

Mineral characteristics

#	Color code	Mineral	Chemical formula	Density	Z
21		Magnetite-Ti	Fe3+2Fe2+O4	5,15	20,67

Spectrum chart

Composition	
Element	**Wt%**
O	28,32
Fe	65,76
Ti	5,92

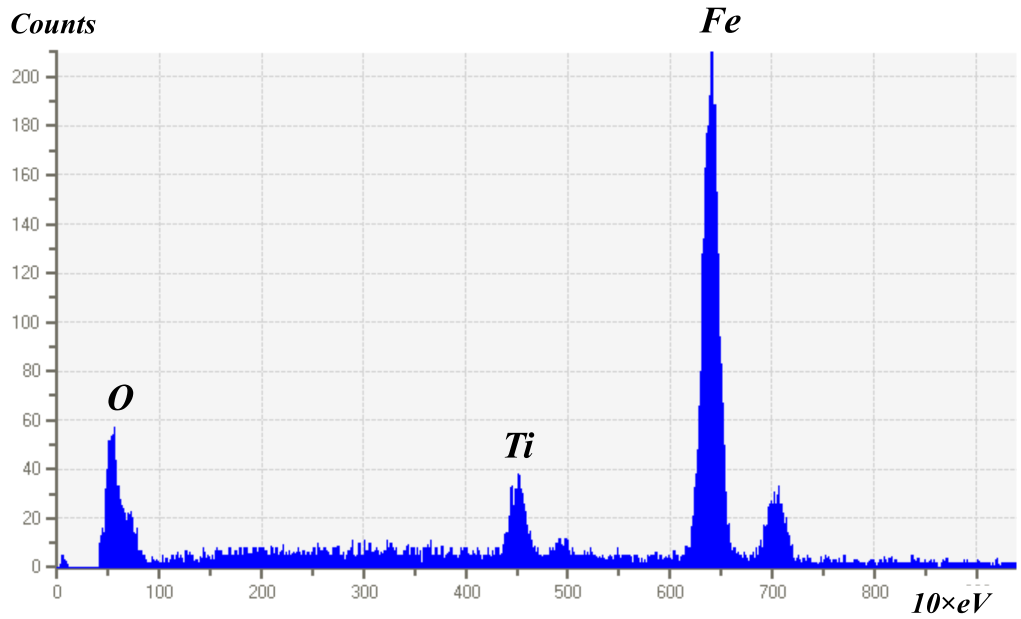

22) Ilmenite

Mineral characteristics

#	Color code	Mineral	Chemical formula	Density	Z
22		Ilmenite	Fe2+TiO3	4,72	17,51

Spectrum chart

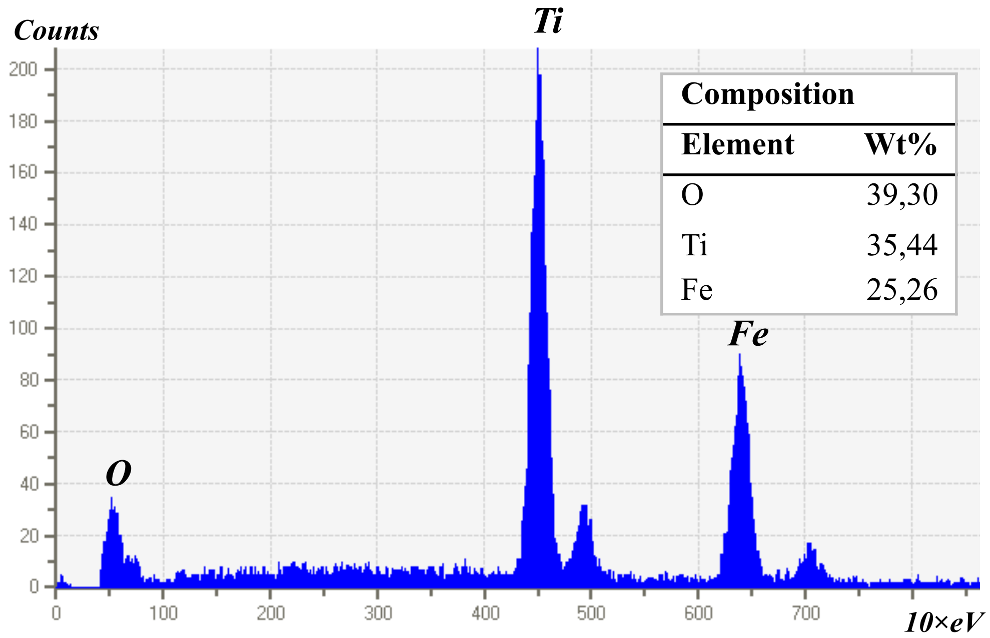

Composition	
Element	Wt%
O	39,30
Ti	35,44
Fe	25,26

23) Rutile

Mineral characteristics

#	Color code	Mineral	Chemical formula	Density	Z
23		Rutile	TiO2	4,25	16,16

Spectrum chart

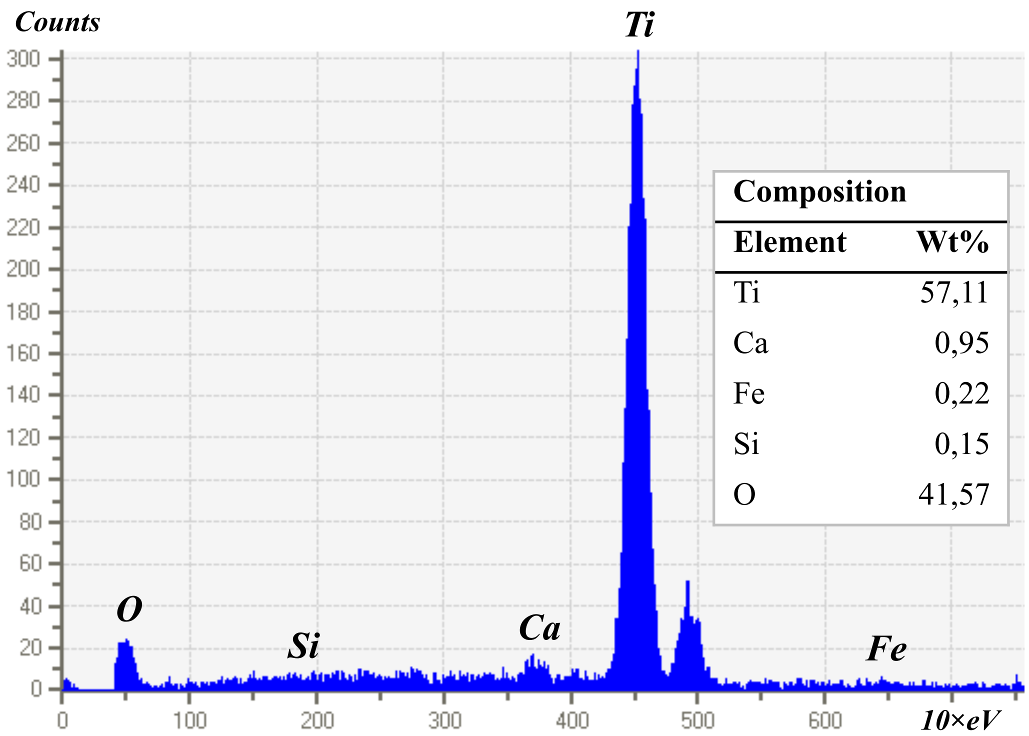

Composition	
Element	Wt%
Ti	57,11
Ca	0,95
Fe	0,22
Si	0,15
O	41,57

24) Chromite

Mineral characteristics

#	Color code	Mineral	Chemical formula	Density	Z
24		Chromite	Fe2+Cr2O4	4,8	18,78

Spectrum chart

Composition	
Element	**Wt%**
O	26,93
Cr	31,17
Fe	28,26
Al	8,59
Mg	4,31
Ti	0,39
V	0,35

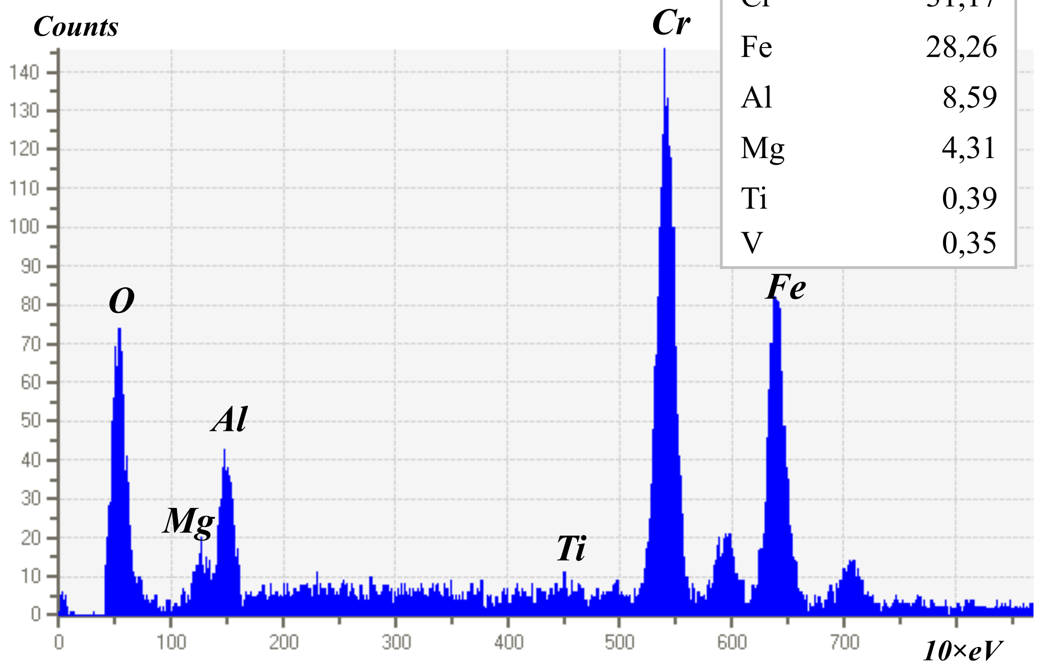

25) Chromite-Mn

Mineral characteristics

#	Color code	Mineral	Chemical formula	Density	Z
25		Chromite-Mn	Fe2+Cr2O4	4,8	18,43

Spectrum chart

Composition	
Element	**Wt%**
O	29,91
Cr	44,64
Fe	5,87
Mn	10,75
Al	5,20
Mg	3,63

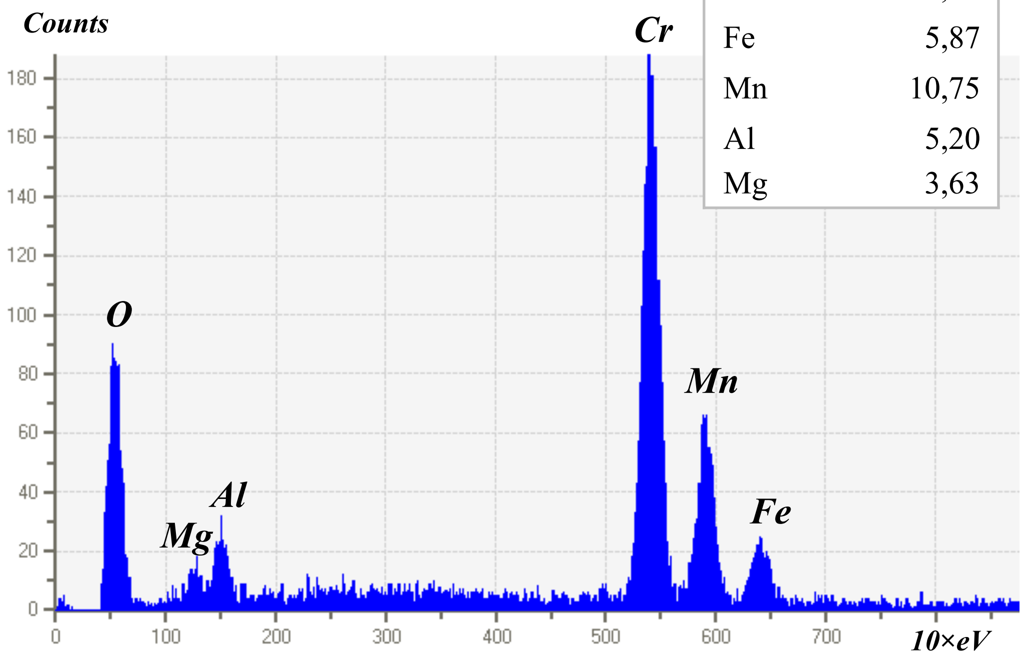

26) Titanite

Mineral characteristics

#	Color code	Mineral	Chemical formula	Density	Z
26		Titanite	CaTiSiO5	3,48	13,81

Spectrum chart

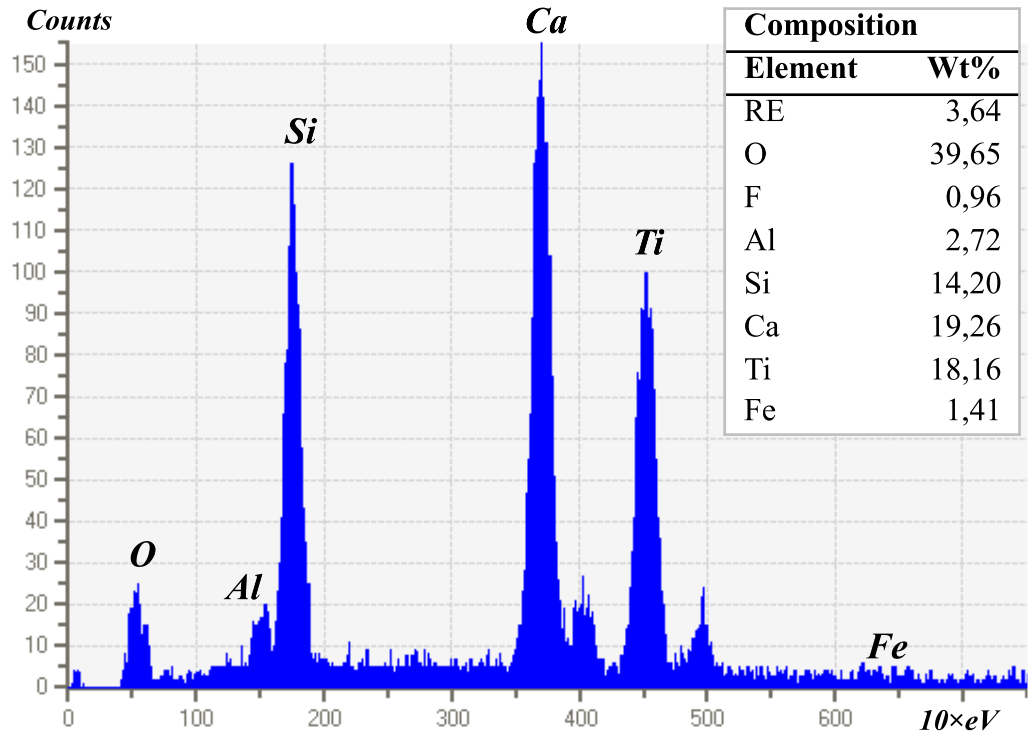

Composition

Element	Wt%
RE	3,64
O	39,65
F	0,96
Al	2,72
Si	14,20
Ca	19,26
Ti	18,16
Fe	1,41

27) Titanite-Fe

Mineral characteristics

#	Color code	Mineral	Chemical formula	Density	Z
27		Titanite-Fe	CaTiSiO5	3,48	16,44

Spectrum chart

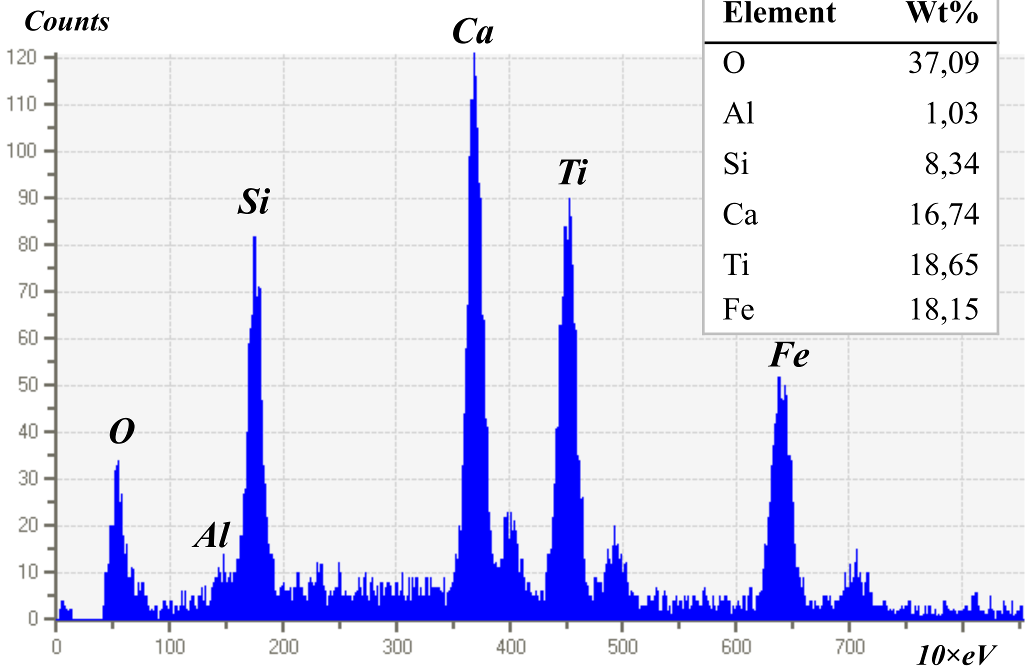

Composition

Element	Wt%
O	37,09
Al	1,03
Si	8,34
Ca	16,74
Ti	18,65
Fe	18,15

28) Zircon

Mineral characteristics

#	Color code	Mineral	Chemical formula	Density	Z
28		Zircon	$ZrSiO_4$	4,65	24,84

Spectrum chart

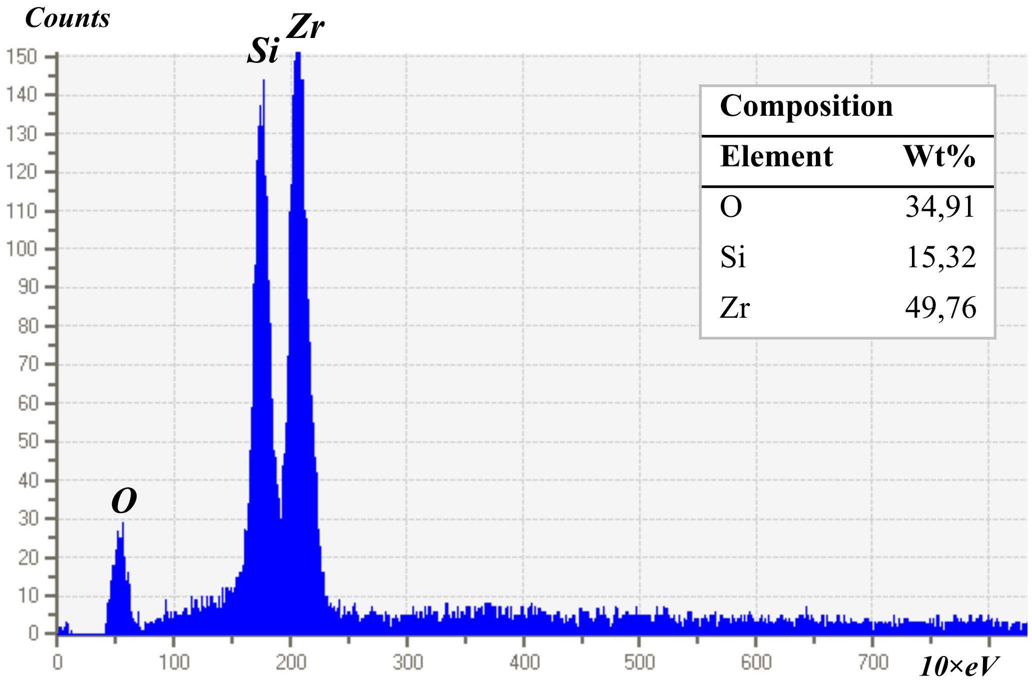

Composition	
Element	**Wt%**
O	34,91
Si	15,32
Zr	49,76

29) Apatite

Mineral characteristics

#	Color code	Mineral	Chemical formula	Density	Z
29		Apatite	$Ca_5(PO_4)(F,Cl,OH)$	3,19	14,61

Spectrum chart

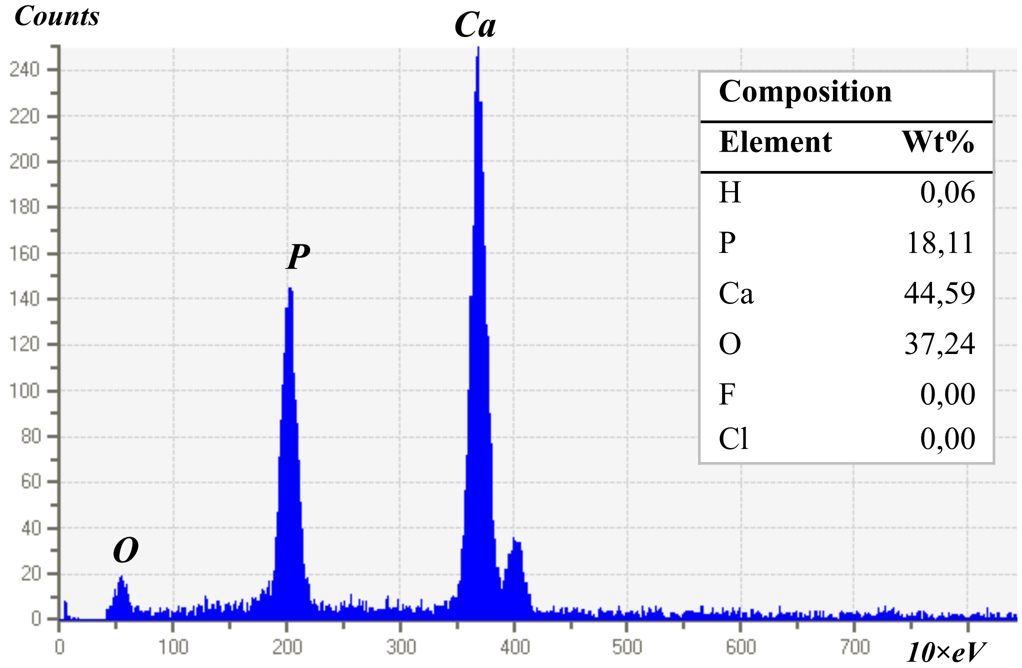

Composition	
Element	**Wt%**
H	0,06
P	18,11
Ca	44,59
O	37,24
F	0,00
Cl	0,00

30) Barite

Mineral characteristics

#	Color code	Mineral	Chemical formula	Density	Z
30		Barite	Ba(SO4)	4,48	39,46

Spectrum chart

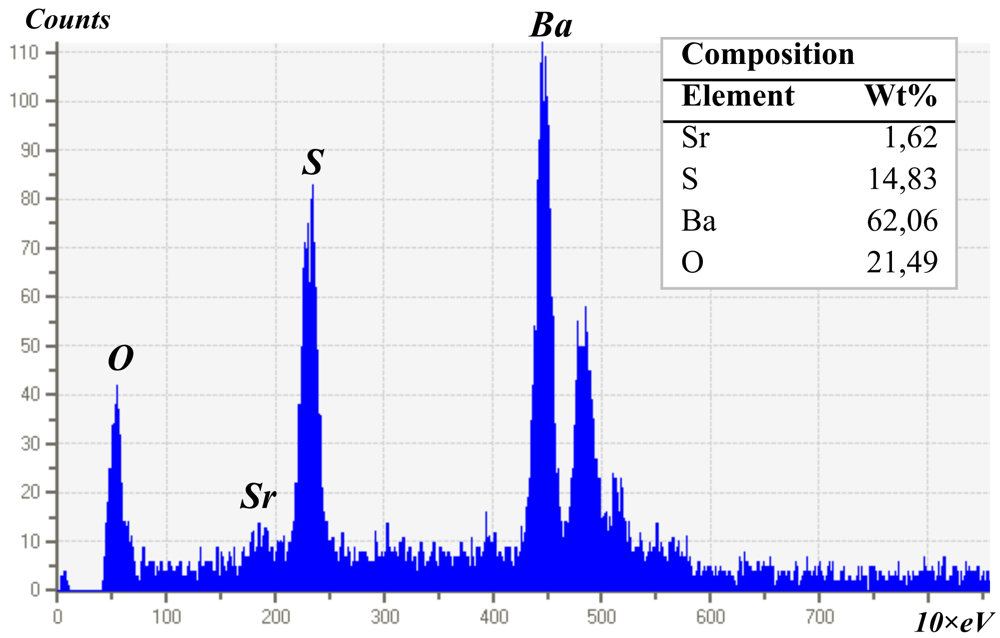

Composition	
Element	**Wt%**
Sr	1,62
S	14,83
Ba	62,06
O	21,49

31) Monazite-Ce

Mineral characteristics

#	Color code	Mineral	Chemical formula	Density	Z
31		Monazite-Ce	Ce0.5La0.25Nd0.2Th0.05(PO4)	5,15	41,77

Spectrum chart

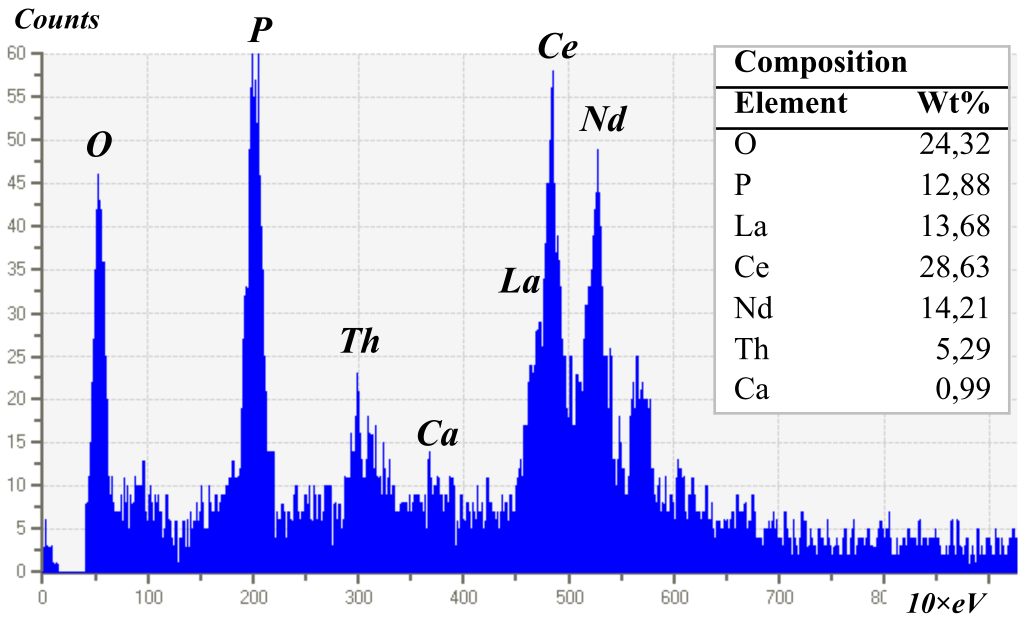

Composition	
Element	**Wt%**
O	24,32
P	12,88
La	13,68
Ce	28,63
Nd	14,21
Th	5,29
Ca	0,99

Appendix G: Garnet values from MLA

Chemical composition of garnets from the MLA mineral reference list. Values have been used in ternary plots in the thesis.

Garnets identified with MLA

#	Garnet type	Color code	Wt%								
			O	Mg	Al	Si	Ca	Ti	Mn	Fe	Total
1	Almandine-Mn		35,82	2,36	13,27	15,28	3,11	0,00	2,48	27,68	100,0
2	Almandine-Ca1		37,73	5,79	13,71	15,42	0,89	0,00	0,19	26,27	100,0
3	Almandine-Ca4		37,01	5,12	13,64	15,71	3,58	0,00	0,21	24,73	100,0
4	Almandine-Ca5		38,12	6,22	14,02	16,23	5,18	0,00	0,32	19,91	100,0
5	Almandine-Ca9		39,72	8,39	14,31	16,62	9,29	0,00	0,10	11,57	100,0
6	Grossular-Fe		40,77	0,00	14,24	15,11	19,88	0,00	0,00	10,00	100,0
7	Grossular		41,31	0,00	16,19	15,71	19,69	0,00	0,00	7,10	100,0

Numbers for the ternary plot

XMg	XCa	XFe + XMn
6,62	8,73	84,65
17,47	2,69	79,84
15,22	10,64	74,14
19,66	16,38	63,96
28,59	31,65	39,76
0,00	66,53	33,47
0,00	73,50	26,50

Appendix H: Results from MLA

Tables with results from MLA. Tables include minerals identified in each fraction, and wt%, area%, area (micron), particle count and grain count.

			Magnetic fractions (Wt%)					Apatite fractions (Wt%)			Zircon fractions (Wt%)		
#	Color code	Mineral	387	389	391	393	BS	387	391	BS	387	391	BS
1		Quartz	3,00	10,51	2,94	3,34	4,34	0,85	40,55	0,64	0,37	0,26	0,73
2		Albite	0,22	0,83	0,25	0,33	2,30	0,41	7,15	0,67	0,06	0,06	0,28
3		Orthoclase	0,29	0,04	0,05	0,01	1,66	0,39	0,08	0,37	0,02	0,02	0,38
4		Calcite	0,01	0,00	0,00	0,00	0,71	0,01	0,00	0,14	0,01	0,00	0,43
5		Chamosite	1,71	3,40	1,80	1,54	1,61	0,14	0,09	0,14	0,15	0,17	0,07
6		Muscovite	0,37	0,20	0,11	0,05	2,72	0,02	0,04	0,53	0,04	0,01	0,68
7		Amphibole	1,74	3,03	1,74	2,12	1,51	0,04	0,10	0,03	0,01	0,01	0,02
8		Yoderite	0,00	0,00	0,00	0,00	0,00	0,00	0,00	0,00	0,00	0,00	0,00
9		Tourmaline	0,19	0,25	0,04	0,11	1,85	0,02	0,03	0,34	0,02	0,01	0,21
10		Almandine-Mn	1,90	4,19	3,05	4,25	1,10	0,02	0,12	0,03	0,02	0,02	0,04
11		Almandine-Ca1	13,83	27,09	12,91	15,83	4,57	0,79	1,43	0,23	0,64	0,55	0,15
12		Almandine-Ca4	3,68	7,64	3,18	4,86	1,27	0,10	0,21	0,05	0,06	0,08	0,06
13		Almandine-Ca5	5,89	7,85	4,79	7,13	2,33	0,24	0,47	0,29	0,17	0,09	0,19
14		Almandine-Ca9	0,61	0,33	0,41	0,24	1,38	0,06	0,04	0,32	0,03	0,01	0,15
15		Grossular-Fe	2,33	2,82	0,81	1,46	5,95	0,02	0,01	0,03	0,00	0,01	0,05
16		Grossular	2,78	1,69	1,08	1,16	7,46	0,01	0,00	0,03	0,01	0,02	0,01
17		Spessartine-Ca	0,02	0,07	0,06	0,04	0,07	0,00	0,00	0,00	0,00	0,00	0,00
18		Spessartine	0,00	0,01	0,00	0,00	0,00	0,00	0,00	0,00	0,00	0,00	0,00
19		Spessartine-Fe	0,00	0,30	0,30	0,00	0,01	0,00	0,00	0,00	0,00	0,00	0,00
20		Magnetite	2,29	1,20	7,07	7,80	3,11	0,00	0,01	0,00	0,00	0,00	0,01
21		Magnetite-Ti	2,91	2,80	16,93	9,33	2,54	0,00	0,01	0,00	0,00	0,02	0,00
22		Ilmenite	0,50	0,79	2,09	2,15	0,69	0,00	0,00	0,00	0,23	0,06	0,00
23		Rutile	7,97	2,90	7,03	5,42	1,08	0,24	0,23	0,00	37,20	11,10	5,94
24		Chromite	0,00	0,00	0,03	0,37	0,00	0,00	0,00	0,00	0,00	0,00	0,00
25		Chromite-Mn	0,00	0,00	0,01	0,04	0,00	0,00	0,00	0,00	0,00	0,00	0,00
26		Titanite	41,31	16,65	25,94	27,26	35,79	1,03	0,81	1,63	22,88	4,66	45,59
27		Titanite-Fe	2,07	1,81	4,25	4,05	2,51	0,02	0,02	0,02	0,10	0,04	0,24
28		Zircon	1,66	3,11	2,47	0,70	1,57	0,09	0,02	0,02	34,56	81,49	25,00
29		Apatite	2,70	0,49	0,36	0,17	11,87	95,47	48,59	94,49	3,22	1,31	19,74
30		Barite	0,01	0,00	0,03	0,05	0,00	0,01	0,00	0,00	0,19	0,01	0,00
31		Monazite-Ce	0,00	0,00	0,29	0,18	0,00	0,01	0,00	0,00	0,00	0,01	0,00
32		Unknown	0,00	0,01	0,02	0,02	0,01	0,00	0,00	0,00	0,00	0,00	0,01
		Total	100,00	100,00	100,00	100,00	100,00	100,00	100,00	100,00	100,00	100,00	100,00

Magnetic fractions (part 1)

			Wt%					Area%					Area (micron)				
#	Color code	Mineral	387	389	391	393	BS	387	389	391	393	BS	387	389	391	393	BS
1		Quartz	3,00	10,51	2,94	3,34	4,34	4,23	14,93	4,47	4,99	5,68	378912,47	664671,62	227766,38	300082,98	412262,03
2		Albite	0,22	0,83	0,25	0,33	2,30	0,31	1,17	0,37	0,50	3,02	27642,06	52280,78	19072,96	30134,73	218823,82
3		Orthoclase	0,29	0,04	0,05	0,01	1,66	0,42	0,05	0,07	0,02	2,23	37349,52	2386,93	3766,00	1160,85	162093,14
4		Calcite	0,01	0,00	0,00	0,00	0,71	0,01	0,00	0,00	0,00	0,90	722,15	0,00	0,00	0,00	65133,31
5		Chamosite	1,71	3,40	1,80	1,54	1,61	1,98	3,96	2,25	1,88	1,73	177346,10	176297,74	114547,98	113263,40	125283,54
6		Muscovite	0,37	0,20	0,11	0,05	2,72	0,48	0,26	0,15	0,06	3,31	43416,96	11662,44	7687,22	3849,24	239833,77
7		Amphibole	1,74	3,03	1,74	2,12	1,51	1,94	3,39	2,09	2,50	1,56	173274,14	151006,61	106154,34	150106,73	113051,92
8		Yoderite	0,00	0,00	0,00	0,00	0,00	0,00	0,00	0,00	0,00	0,00	164,23	182,23	0,00	0,00	0,00
9		Tourmaline	0,19	0,25	0,04	0,11	1,85	0,23	0,31	0,05	0,14	2,05	20825,47	13610,69	2587,16	8247,40	148570,19
10		Almandine-Mn	1,90	4,19	3,05	4,25	1,10	1,68	3,72	2,90	3,96	0,90	150252,96	165505,93	147564,57	238357,97	65320,04
11		Almandine-Ca1	13,83	27,09	12,91	15,83	4,57	12,21	24,05	12,28	14,78	3,74	1093048,25	1070670,48	625340,11	888480,77	271460,05
12		Almandine-Ca4	3,68	7,64	3,18	4,86	1,27	3,25	6,78	3,03	4,54	1,04	290535,26	301849,00	154097,70	272767,13	75076,99
13		Almandine-Ca5	5,89	7,85	4,79	7,13	2,33	5,20	6,97	4,55	6,65	1,91	465564,17	310463,10	231707,85	399902,17	138163,08
14		Almandine-Ca9	0,61	0,33	0,41	0,24	1,38	0,54	0,29	0,39	0,23	1,13	48312,31	12863,78	20017,83	13684,93	81607,87
15		Grossular-Fe	2,33	2,82	0,81	1,46	5,95	2,43	2,95	0,91	1,61	5,73	217109,55	131186,76	46337,07	96626,87	415710,82
16		Grossular	2,78	1,69	1,08	1,16	7,46	2,88	1,76	1,21	1,28	7,18	258132,83	78485,28	61394,31	76750,77	521053,02
17		Spessartine-Ca	0,02	0,07	0,06	0,04	0,07	0,02	0,06	0,06	0,03	0,06	1730,02	2611,90	3113,58	1995,48	4285,68
18		Spessartine	0,00	0,01	0,00	0,00	0,00	0,00	0,01	0,00	0,00	0,00	11,25	377,95	0,00	27,00	0,00
19		Spessartine-Fe	0,00	0,30	0,30	0,00	0,01	0,00	0,27	0,29	0,00	0,01	202,47	12049,39	14573,56	269,96	515,18
20		Magnetite	2,29	1,20	7,07	7,80	3,11	1,70	0,90	5,65	6,12	2,13	151908,74	39871,43	287655,64	367697,72	154819,86
21		Magnetite-Ti	2,91	2,80	16,93	9,33	2,54	2,10	2,03	13,13	7,10	1,69	187867,95	90206,22	668410,62	426853,58	122907,86
22		Ilmenite	0,50	0,79	2,09	2,15	0,69	0,39	0,62	1,77	1,79	0,50	35156,06	27709,56	89956,50	107477,17	36535,13
23		Rutile	7,97	2,90	7,03	5,42	1,08	6,96	2,55	6,60	5,00	0,87	622818,20	113411,88	336159,17	300598,17	63365,05
24		Chromite	0,00	0,00	0,03	0,37	0,00	0,00	0,00	0,02	0,30	0,00	0,00	0,00	1226,09	18103,34	0,00
25		Chromite-Mn	0,00	0,00	0,01	0,04	0,00	0,00	0,00	0,00	0,03	0,00	0,00	0,00	233,97	1734,52	0,00
26		Titanite	41,31	16,65	25,94	27,26	35,79	44,02	17,84	29,77	30,70	35,34	3940642,03	794504,06	1515640,89	1846128,57	2563175,46
27		Titanite-Fe	2,07	1,81	4,25	4,05	2,51	2,20	1,94	4,88	4,57	2,48	197381,93	86505,46	248308,39	274494,90	179573,30
28		Zircon	1,66	3,11	2,47	0,70	1,57	1,32	2,49	2,12	0,59	1,16	118541,19	110862,97	107828,12	35572,26	83936,31
29		Apatite	2,70	0,49	0,36	0,17	11,87	3,14	0,57	0,45	0,21	12,79	281405,98	25241,63	22721,97	12609,57	927576,06
30		Barite	0,01	0,00	0,03	0,05	0,00	0,01	0,00	0,02	0,04	0,00	1041,61	157,48	1151,85	2645,65	0,00
31		Monazite-Ce	0,00	0,00	0,29	0,18	0,00	0,00	0,00	0,22	0,13	0,00	60,74	0,00	11295,74	8098,92	0,00
32		Unknown	0,00	0,01	0,02	0,02	0,01	0,34	0,13	0,29	0,25	0,86	30751,15	5720,99	14609,55	15041,49	62507,91
		Total	100,00	100,00	100,00	100,00	100,00	100,00	100,00	100,00	100,00	100,00	8952127,76	4452354,29	5090927,14	6012764,22	7252641,38

Magnetic fractions (part 2)

			Particle count					Grain count				
#	**Color code**	**Mineral**	**387**	**389**	**391**	**393**	**BS**	**387**	**389**	**391**	**393**	**BS**
1		Quartz	205	236	139	158	332	338	294	193	208	493
2		Albite	51	60	32	31	252	76	80	44	42	379
3		Orthoclase	39	14	10	5	307	76	19	17	9	472
4		Calcite	1	0	0	0	77	1	0	0	0	102
5		Chamosite	273	371	294	271	308	660	745	605	615	730
6		Muscovite	108	31	20	15	486	163	45	28	16	862
7		Amphibole	128	91	68	102	154	270	195	115	231	264
8		Yoderite	1	1	0	0	0	1	1	0	0	0
9		Tourmaline	55	36	15	13	286	63	42	17	14	412
10		Almandine-Mn	130	118	118	227	158	291	216	205	467	249
11		Almandine-Ca1	532	617	455	400	360	1377	1331	939	856	658
12		Almandine-Ca4	279	216	169	227	160	577	493	329	572	246
13		Almandine-Ca5	480	284	261	291	356	1126	555	427	586	549
14		Almandine-Ca9	139	41	41	50	309	195	55	48	71	479
15		Grossular-Fe	64	41	19	29	230	208	79	66	73	509
16		Grossular	65	38	18	20	241	183	100	47	86	472
17		Spessartine-Ca	1	3	5	5	5	1	6	8	5	11
18		Spessartine	1	4	0	1	0	1	4	0	1	0
19		Spessartine-Fe	1	8	4	1	1	1	13	6	1	3
20		Magnetite	57	24	96	87	118	138	34	143	131	149
21		Magnetite-Ti	109	76	239	212	126	266	131	449	440	176
22		Ilmenite	55	58	130	108	55	111	133	345	259	107
23		Rutile	105	116	151	167	34	273	220	285	366	56
24		Chromite	0	0	1	1	0	0	0	2	1	0
25		Chromite-Mn	0	0	1	1	0	0	0	1	1	0
26		Titanite	582	328	500	456	715	1026	523	839	815	1052
27		Titanite-Fe	272	136	257	286	283	664	360	838	1004	496
28		Zircon	31	23	39	18	53	39	24	40	18	59
29		Apatite	47	13	16	17	184	58	13	18	20	198
30		Barite	3	3	2	15	0	3	5	4	31	0
31		Monazite-Ce	1	0	7	8	0	1	0	8	19	0
32		Unknown	17	7	13	9	27	21	11	18	16	27
		Total	894	851	891	764	1377	8208	5727	6084	6974	9210

Apatite fractions

#	Color code	Mineral	Wt% 387	Wt% 391	Wt% BS	Area% 387	Area% 391	Area% BS	Area (micron) 387	Area (micron) 391	Area (micron) BS	Particle count 387	Particle count 391	Particle count BS	Grain count 387	Grain count 391	Grain count BS
1		Quartz	0,85	40,55	0,64	1,04	44,96	0,77	38357,39	1718656,07	24886,18	9	195	21	11	206	23
2		Albite	0,41	7,15	0,67	0,50	7,94	0,82	18573,52	303459,78	26341,74	9	64	17	9	68	24
3		Orthoclase	0,39	0,08	0,37	0,49	0,09	0,46	18121,33	3401,55	14746,78	4	5	36	14	12	52
4		Calcite	0,01	0,00	0,14	0,01	0,00	0,17	398,20	157,48	5487,02	2	1	8	2	1	8
5		Chamosite	0,14	0,09	0,14	0,14	0,08	0,14	5223,80	3187,82	4503,90	16	29	28	27	36	42
6		Muscovite	0,02	0,04	0,53	0,02	0,04	0,60	899,88	1622,03	19414,91	5	5	65	5	10	81
7		Amphibole	0,04	0,10	0,03	0,04	0,08	0,03	1451,06	3185,58	893,13	7	15	5	7	19	5
8		Yoderite	0,00	0,00	0,00	0,00	0,00	0,00	0,00	0,00	0,00	0	0	0	0	0	0
9		Tourmaline	0,02	0,03	0,34	0,02	0,03	0,35	629,92	958,37	11306,99	2	6	51	3	6	60
10		Almandine-Mn	0,02	0,12	0,03	0,02	0,09	0,02	571,42	3300,31	719,90	4	17	4	4	17	4
11		Almandine-Ca1	0,79	1,43	0,23	0,60	0,99	0,17	22314,77	37860,20	5505,02	33	118	27	52	202	33
12		Almandine-Ca4	0,10	0,21	0,05	0,07	0,14	0,04	2699,64	5509,52	1248,58	10	34	9	12	40	9
13		Almandine-Ca5	0,24	0,47	0,29	0,18	0,33	0,22	6677,11	12452,09	7194,54	36	69	43	41	84	57
14		Almandine-Ca9	0,06	0,04	0,32	0,05	0,03	0,24	1775,01	996,62	7790,71	10	9	53	11	9	69
15		Grossular-Fe	0,02	0,01	0,03	0,02	0,01	0,02	659,16	254,22	733,40	4	1	4	6	1	4
16		Grossular	0,01	0,00	0,03	0,01	0,00	0,03	321,71	0,00	983,12	3	0	6	3	0	6
17		Spessartine-Ca	0,00	0,00	0,00	0,00	0,00	0,00	0,00	0,00	0,00	0	0	0	0	0	0
18		Spessartine	0,00	0,00	0,00	0,00	0,00	0,00	0,00	0,00	0,00	0	0	0	0	0	0
19		Spessartine-Fe	0,00	0,00	0,00	0,00	0,00	0,00	0,00	0,00	0,00	0	0	0	0	0	0
20		Magnetite	0,00	0,01	0,00	0,00	0,00	0,00	0,00	132,73	40,49	0	1	1	0	1	1
21		Magnetite-Ti	0,00	0,01	0,00	0,00	0,00	0,00	76,49	164,23	0,00	1	1	0	1	1	0
22		Ilmenite	0,00	0,00	0,00	0,00	0,00	0,00	0,00	0,00	0,00	0	0	0	0	0	0
23		Rutile	0,24	0,23	0,00	0,18	0,16	0,00	6587,12	5970,70	0,00	1	14	0	1	20	0
24		Chromite	0,00	0,00	0,00	0,00	0,00	0,00	0,00	0,00	0,00	0	0	0	0	0	0
25		Chromite-Mn	0,00	0,00	0,00	0,00	0,00	0,00	0,00	0,00	0,00	0	0	0	0	0	0
26		Titanite	1,03	0,81	1,63	0,95	0,68	1,49	35054,83	25851,30	48031,10	7	24	20	8	29	34
27		Titanite-Fe	0,02	0,02	0,02	0,02	0,02	0,02	767,15	618,67	589,42	2	3	2	2	3	2
28		Zircon	0,09	0,02	0,02	0,06	0,01	0,01	2395,93	503,93	348,70	3	2	6	4	2	6
29		Apatite	95,47	48,59	94,49	95,57	44,33	94,39	3539250,55	1694586,53	3039616,93	230	148	342	233	151	346
30		Barite	0,01	0,00	0,00	0,01	0,00	0,00	227,22	89,99	0,00	1	2	0	2	4	0
31		Monazite-Ce	0,01	0,00	0,00	0,01	0,00	0,00	191,22	11,25	0,00	1	1	0	2	1	0
32		Unknown	0,00	0,00	0,00	0,00	0,00	0,00	58,49	11,25	0,00	1	1	0	1	1	0
		Total	100,00	100,00	100,00	100,00	100,00	100,00	3703282,93	3822942,22	3220382,57	247	382	359	461	924	866

Zircon fractions

			Wt%			Area%			Area (micron)			Particle count			Grain count		
#	**Color code**	**Mineral**	**387**	**391**	**BS**	**387**	**391**	**BS**	**387**	**391**	**BS**	**387**	**391**	**BS**	**387**	**391**	**BS**
1		Quartz	0,37	0,26	0,73	0,58	0,44	1,02	27642,06	26233,75	25455,36	34	35	38	37	37	53
2		Albite	0,06	0,06	0,28	0,09	0,10	0,40	4339,67	5716,49	9903,18	8	8	23	10	8	27
3		Orthoclase	0,02	0,02	0,38	0,03	0,04	0,54	1455,56	2110,22	13430,71	3	9	47	6	10	64
4		Calcite	0,01	0,00	0,43	0,01	0,00	0,58	445,44	0,00	14560,06	1	0	15	1	0	19
5		Chamosite	0,15	0,17	0,07	0,19	0,23	0,08	8920,06	13862,65	1905,50	31	63	18	43	76	21
6		Muscovite	0,04	0,01	0,68	0,06	0,01	0,88	3030,35	521,93	22008,82	12	2	89	13	2	113
7		Amphibole	0,01	0,01	0,02	0,02	0,01	0,02	724,40	449,94	506,18	3	2	5	5	2	5
8		Yoderite	0,00	0,00	0,00	0,00	0,00	0,00	0,00	0,00	0,00	0	0	0	0	0	0
9		Tourmaline	0,02	0,01	0,21	0,03	0,01	0,25	1347,57	452,19	6254,17	5	2	35	5	2	36
10		Almandine-Mn	0,02	0,02	0,04	0,02	0,02	0,04	809,89	1050,61	947,12	5	8	6	5	8	6
11		Almandine-Ca1	0,64	0,55	0,15	0,63	0,59	0,13	30121,23	34728,62	3302,56	66	115	19	99	138	20
12		Almandine-Ca4	0,06	0,08	0,06	0,05	0,09	0,05	2582,66	5286,80	1223,84	17	39	9	17	41	9
13		Almandine-Ca5	0,17	0,09	0,19	0,17	0,10	0,16	8031,43	5642,25	4051,71	39	43	23	50	44	29
14		Almandine-Ca9	0,03	0,01	0,15	0,03	0,01	0,13	1478,05	490,43	3320,56	10	3	23	10	3	27
15		Grossular-Fe	0,00	0,01	0,05	0,00	0,01	0,05	200,22	587,17	1264,33	1	3	6	1	3	6
16		Grossular	0,01	0,02	0,01	0,01	0,03	0,01	382,45	1509,55	335,21	2	4	3	3	4	4
17		Spessartine-Ca	0,00	0,00	0,00	0,00	0,00	0,00	0,00	0,00	0,00	0	0	0	0	0	0
18		Spessartine	0,00	0,00	0,00	0,00	0,00	0,00	0,00	0,00	0,00	0	0	0	0	0	0
19		Spessartine-Fe	0,00	0,00	0,00	0,00	0,00	0,00	0,00	0,00	0,00	0	0	0	0	0	0
20		Magnetite	0,00	0,00	0,01	0,00	0,00	0,01	0,00	170,98	164,23	0	1	1	0	1	2
21		Magnetite-Ti	0,00	0,02	0,00	0,00	0,01	0,00	166,48	773,90	0,00	3	6	0	4	7	0
22		Ilmenite	0,23	0,06	0,00	0,20	0,06	0,00	9770,45	3568,02	29,25	39	22	2	65	28	2
23		Rutile	37,20	11,10	5,94	35,93	11,72	5,12	1720948,52	693096,58	127681,72	166	108	41	181	114	66
24		Chromite	0,00	0,00	0,00	0,00	0,00	0,00	0,00	0,00	0,00	0	0	0	0	0	0
25		Chromite-Mn	0,00	0,00	0,00	0,00	0,00	0,00	0,00	0,00	0,00	0	0	0	0	0	0
26		Titanite	22,88	4,66	45,59	26,98	6,01	47,93	1292342,42	355297,37	1195902,28	207	106	287	215	113	347
27		Titanite-Fe	0,10	0,04	0,24	0,11	0,05	0,25	5442,02	3169,83	6204,67	33	18	34	36	20	42
28		Zircon	34,56	81,49	25,00	30,51	78,61	19,67	1461333,14	4649011,82	490733,81	166	648	139	169	655	141
29		Apatite	3,22	1,31	19,74	4,15	1,84	22,64	198533,78	108685,26	565000,91	33	51	126	41	59	130
30		Barite	0,19	0,01	0,00	0,17	0,01	0,00	8319,39	362,20	85,49	2	3	1	2	5	1
31		Monazite-Ce	0,00	0,01	0,00	0,00	0,00	0,00	9,00	292,46	38,24	1	2	1	1	2	1
32		Unknown	0,00	0,00	0,01	0,02	0,01	0,03	902,13	710,91	767,15	7	7	4	8	8	5
		Total	100,00	100,00	100,00	100,00	100,00	100,00	4789278,37	5913781,92	2495077,04	545	855	517	1027	1390	1176

Appendix I: BSE- and processed images from MLA

BSE-images of analysed grains and processed images with colors for each mineral. Legend with wt% include those minerals >1 wt%. The complete legend can be seen in *Appendix E*.

#	Sample name	Fraction type
1	387	Magnetic fraction
2	389	Magnetic fraction
3	391	Magnetic fraction
4	393	Magnetic fraction
5	BS	Magnetic fraction
6	387	Apatite fraction
7	391	Apatite fraction
8	BS	Apatite fraction
9	387	Zircon fraction
10	391	Zircon fraction
11	BS	Zircon fraction

1) 387 Magnetic fraction (BSE-image)

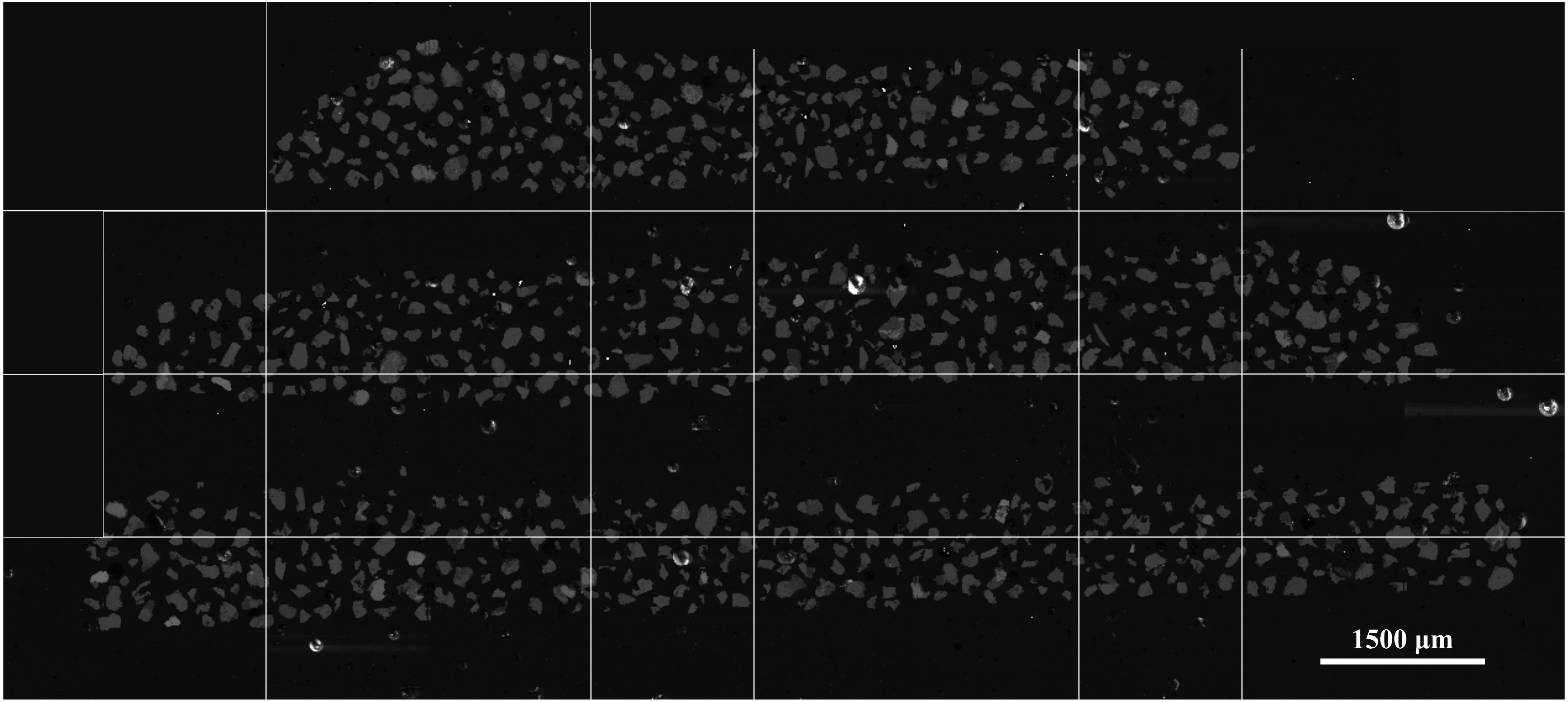

1) 387 Magnetic fraction (processed image)

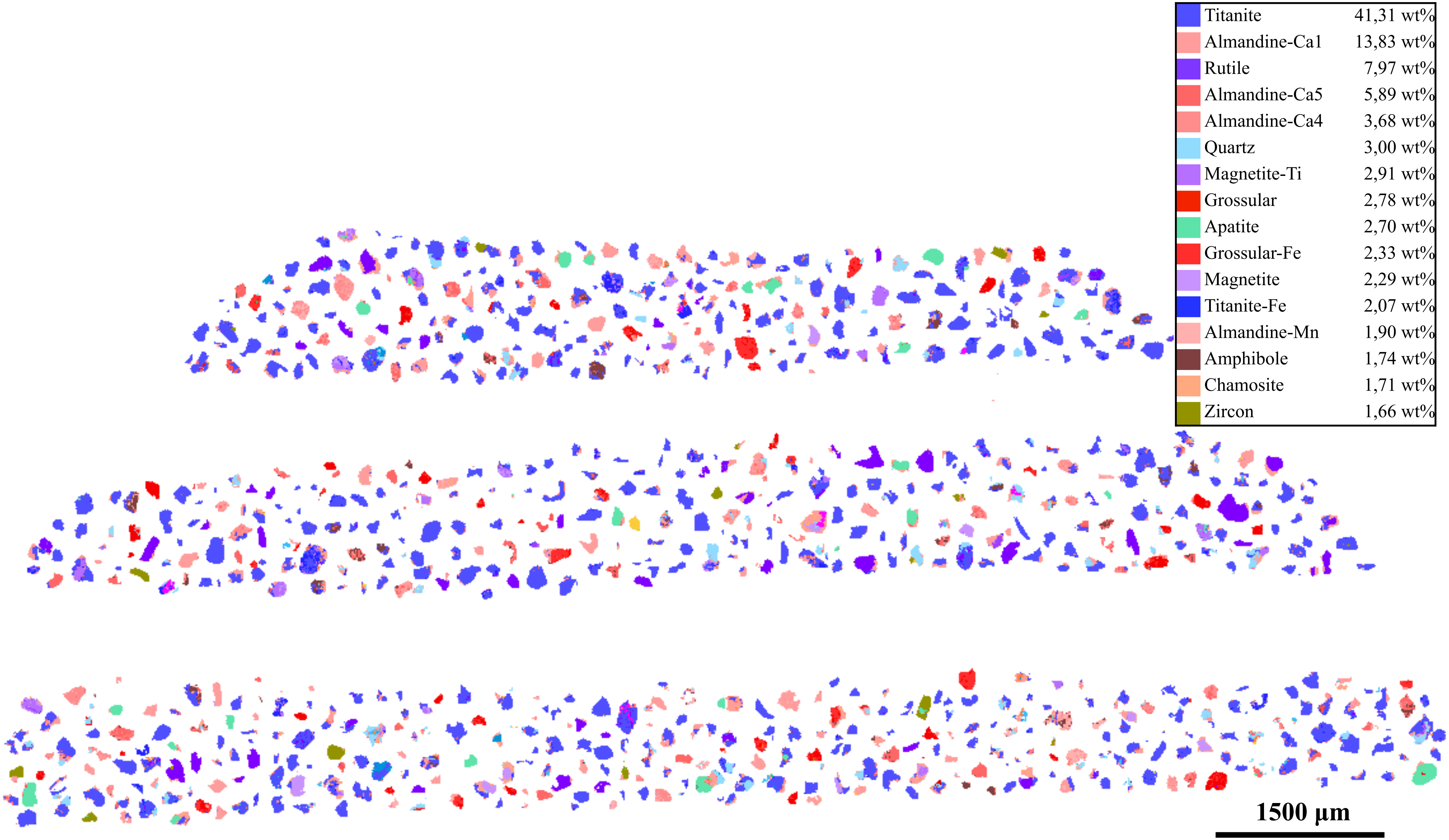

2) 389 Magnetic fraction (BSE-image)

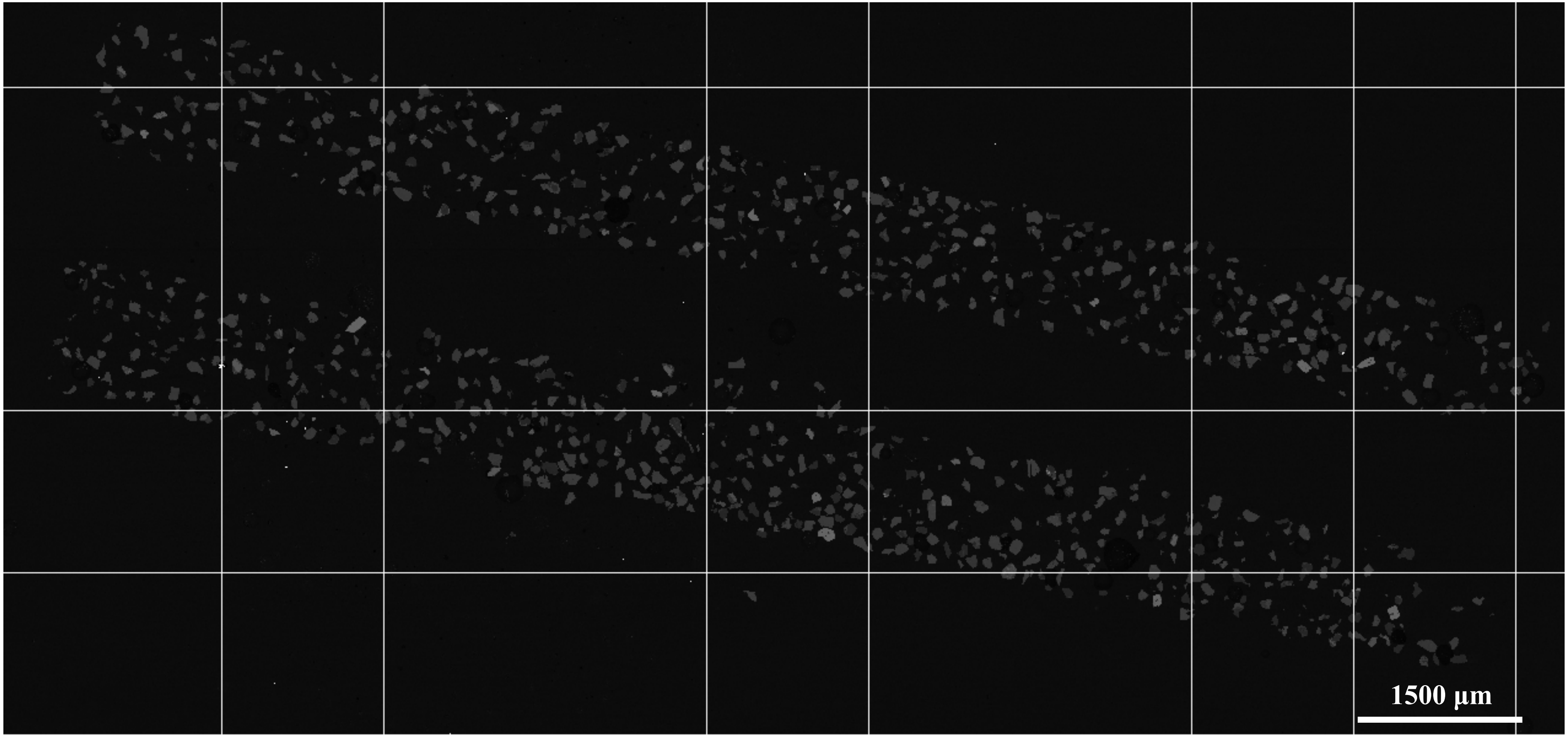

2) 389 Magnetic fraction (processed image)

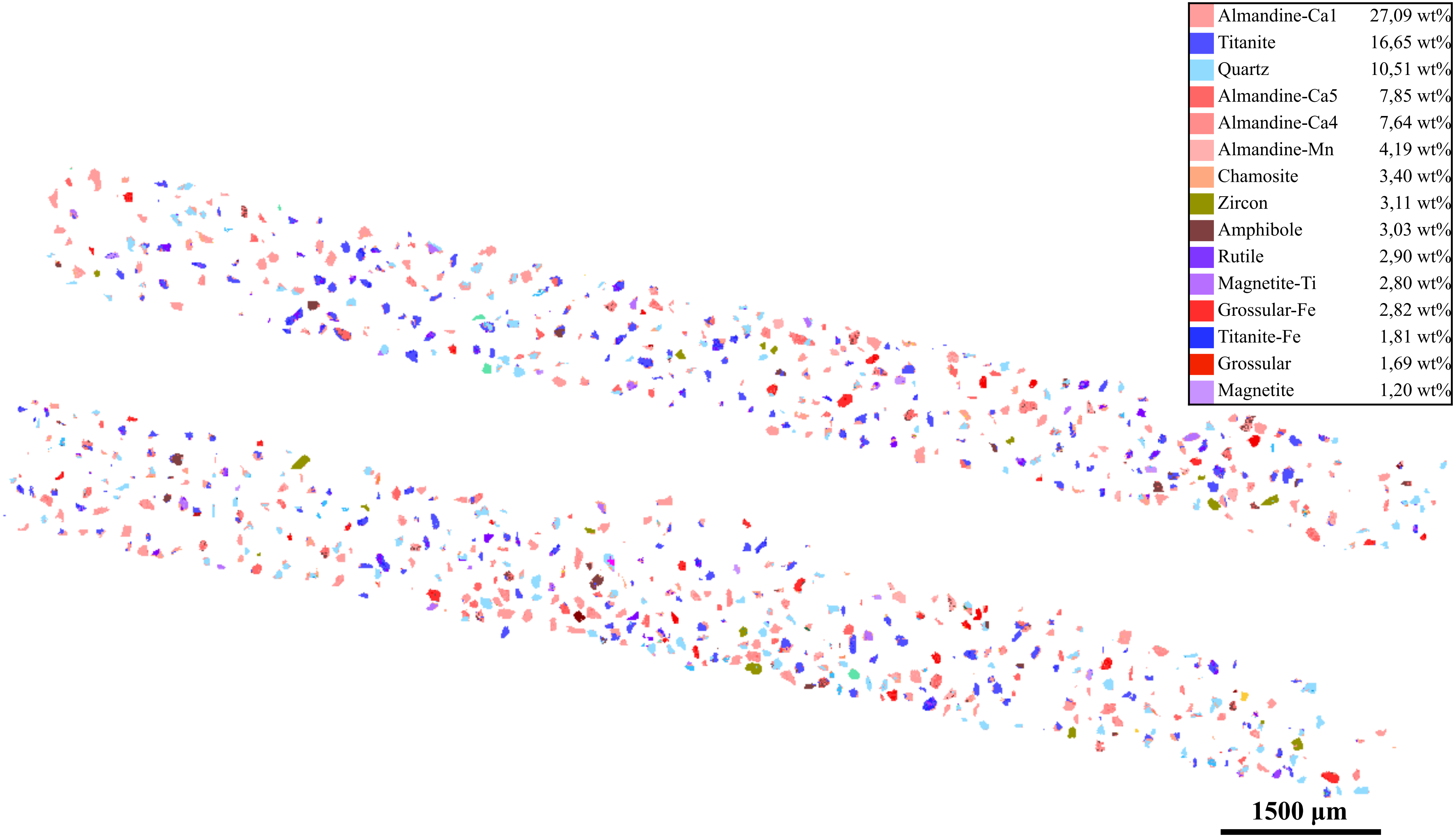

3) 391 Magnetic fraction (BSE-image)

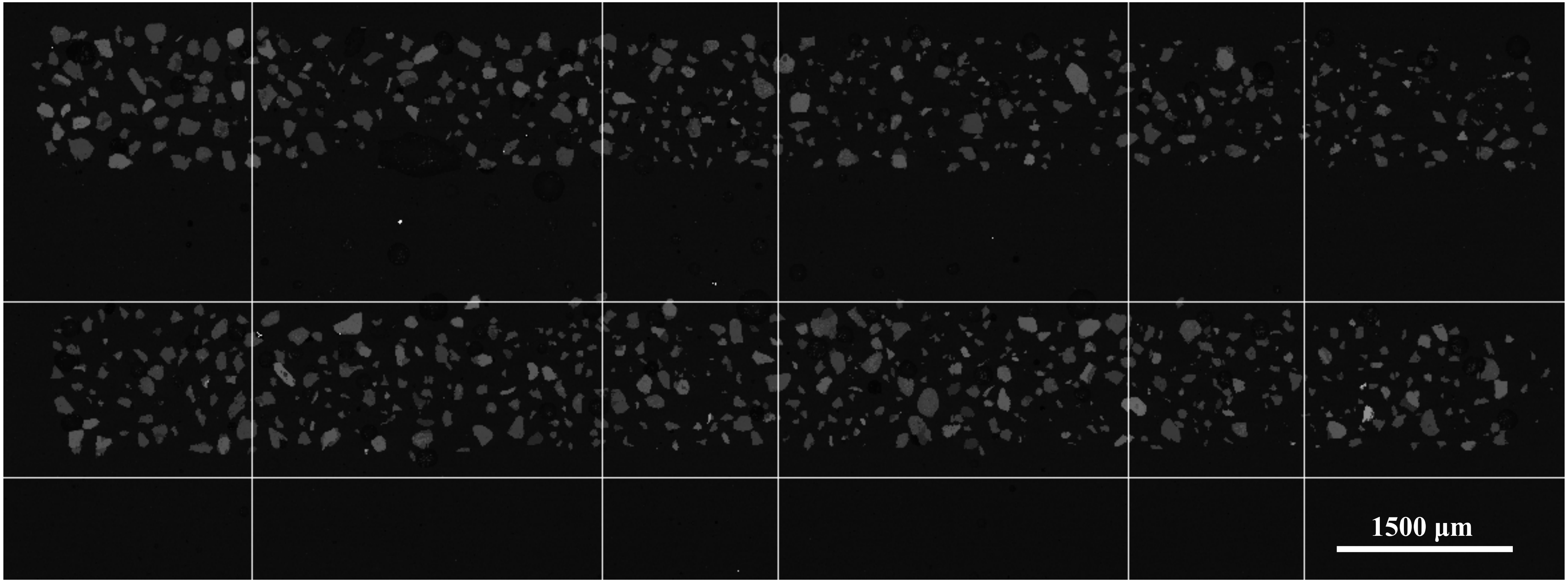

3) 391 Magnetic fraction (processed image)

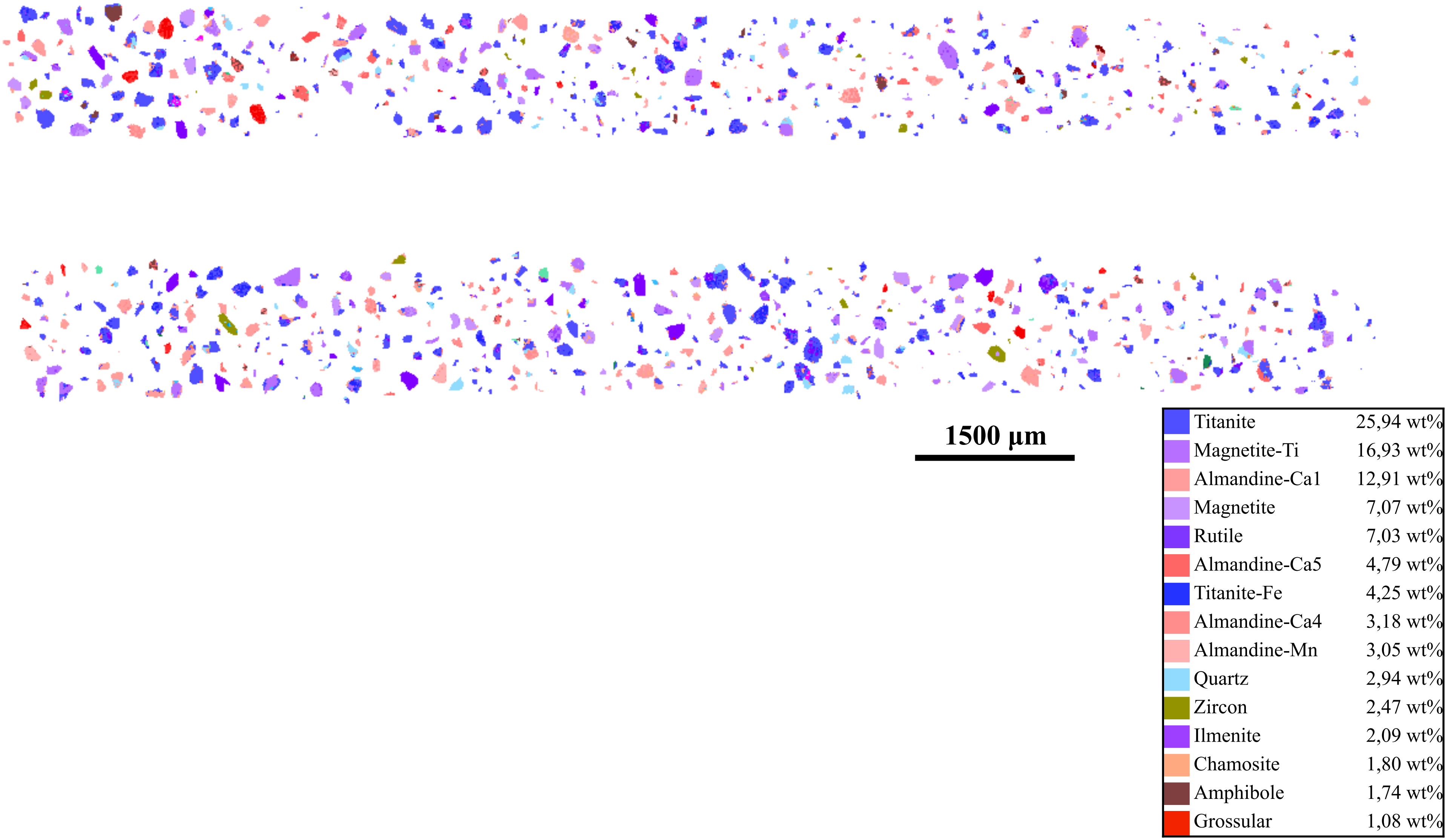

4) 393 Magnetic fraction (BSE-image)

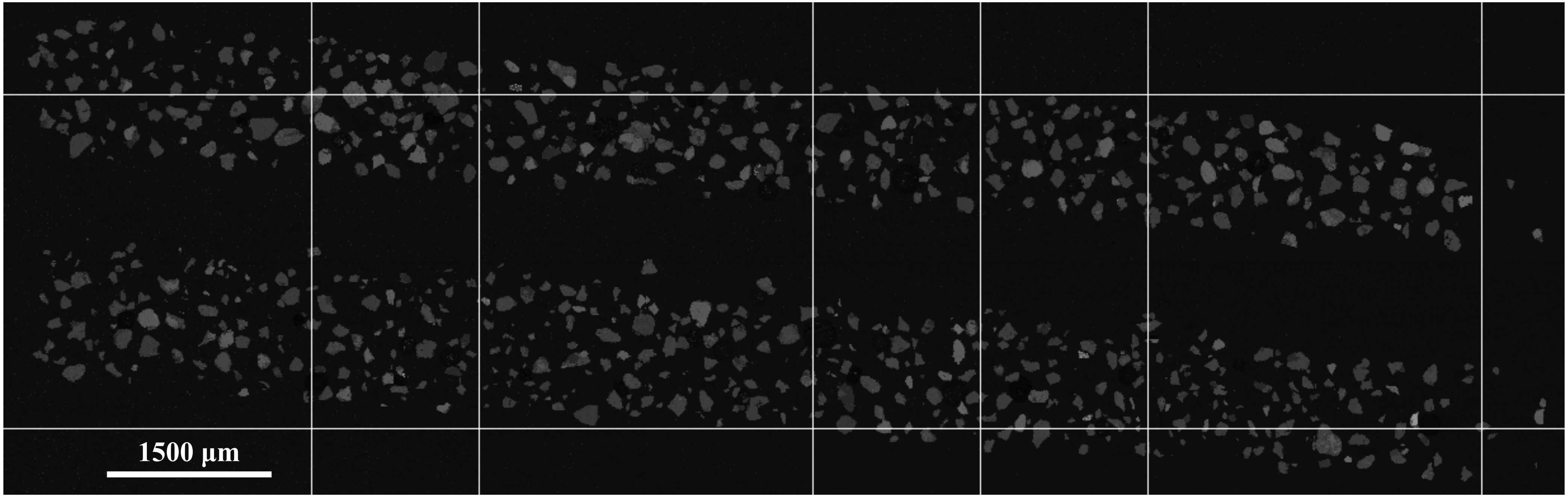

4) 393 Magnetic fraction (processed image)

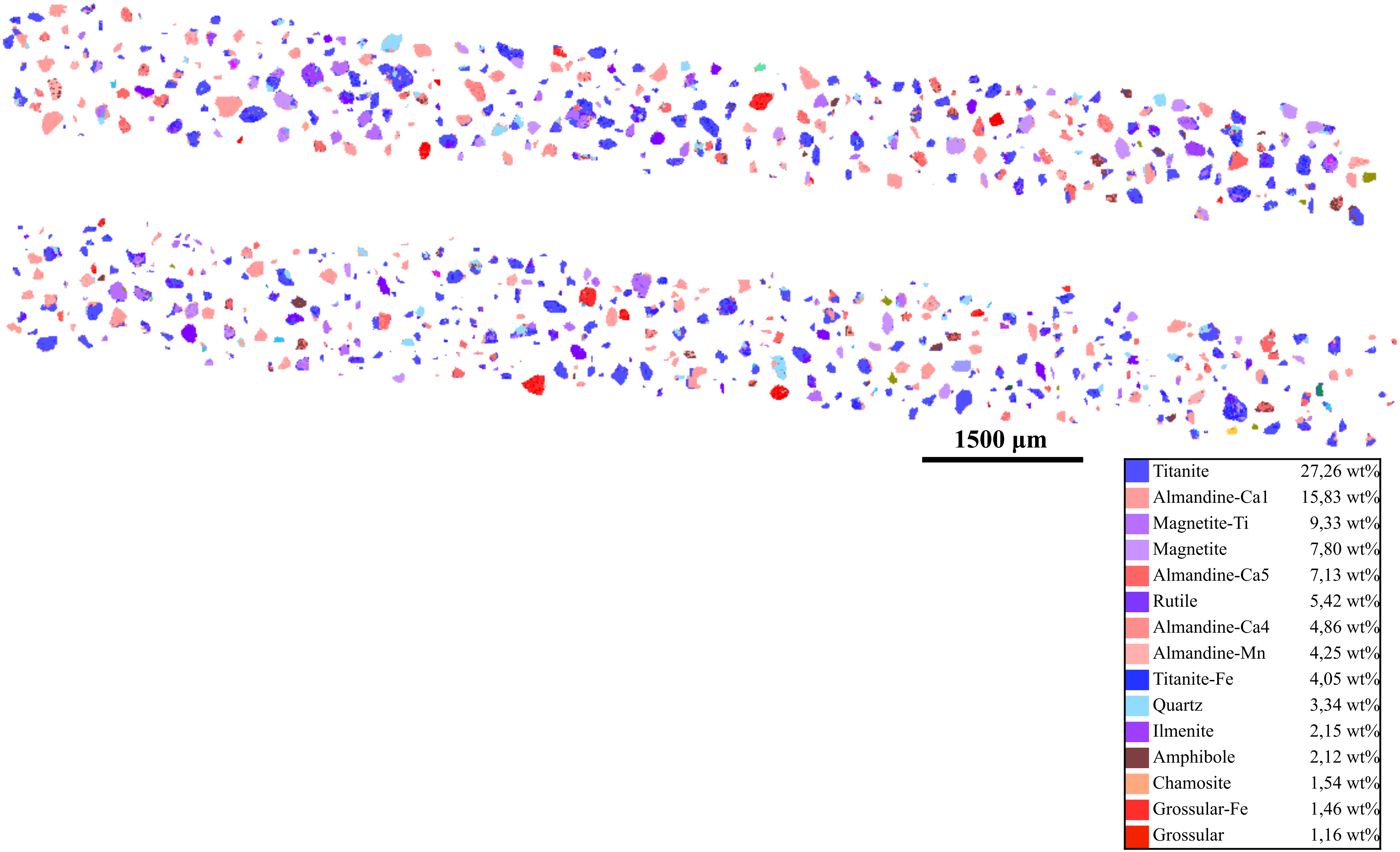

5) BS Magnetic fraction (BSE-image)

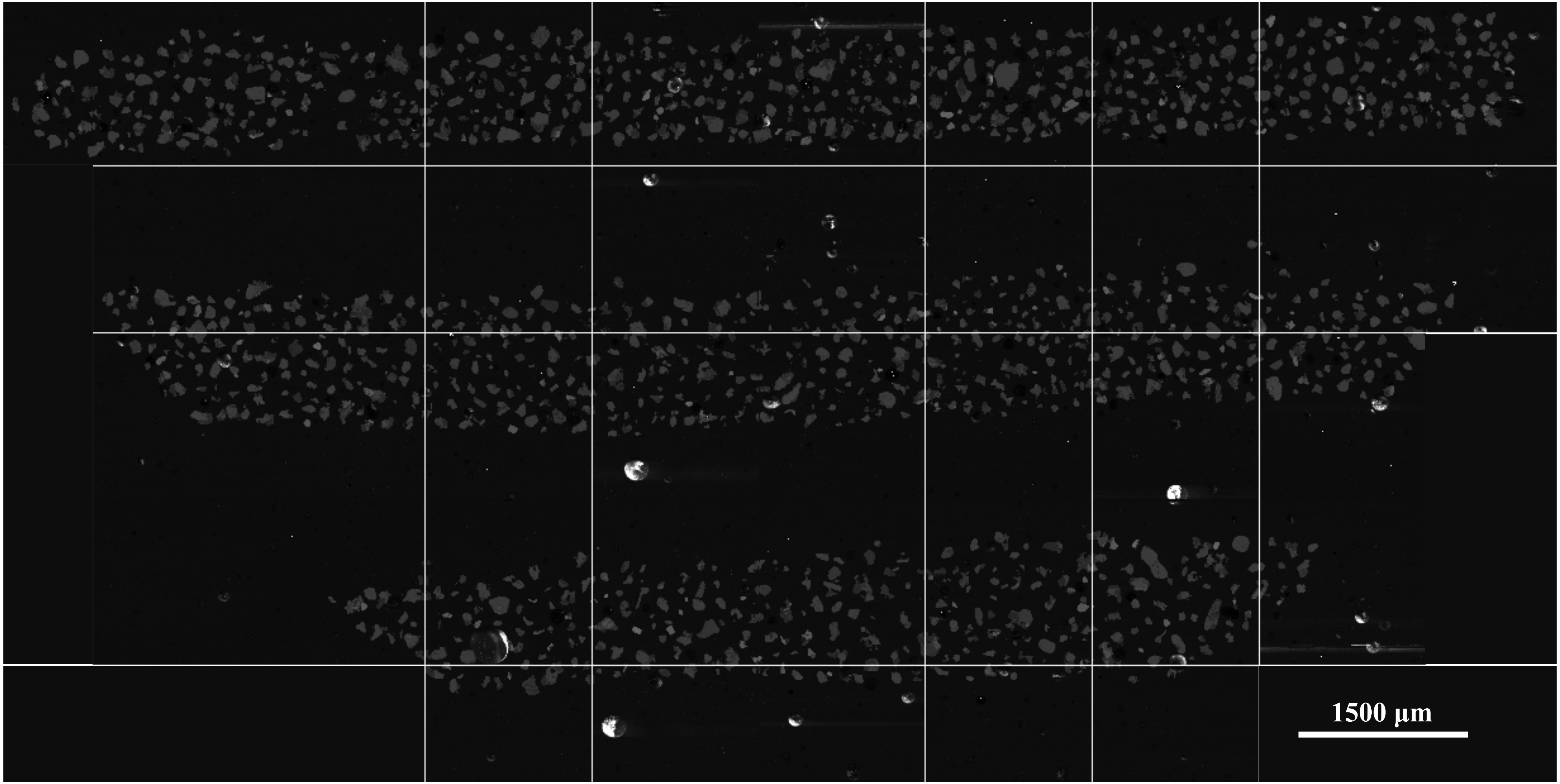

5) BS Magnetic fraction (processed image)

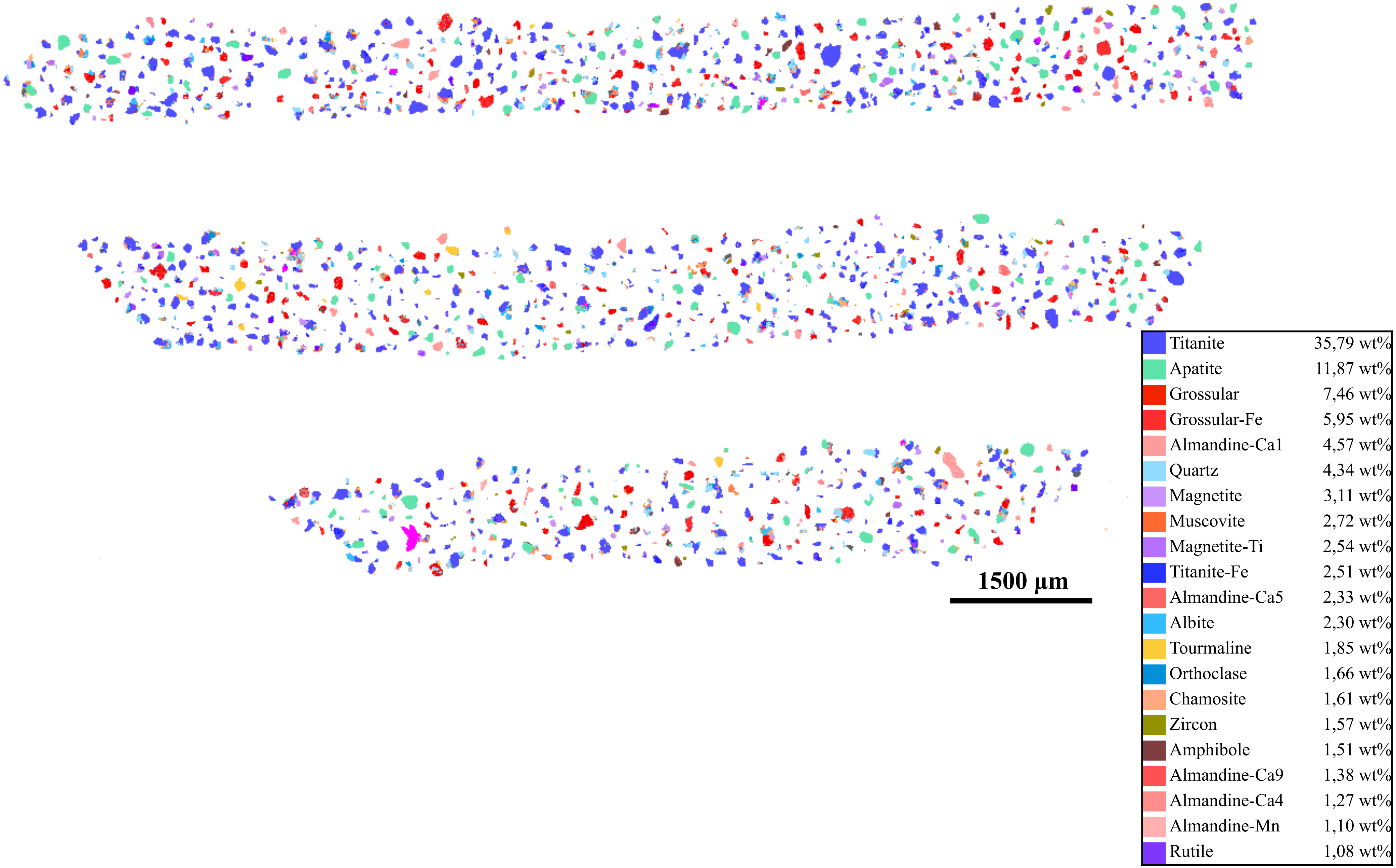

6) 387 Apatite fraction (BSE-image)

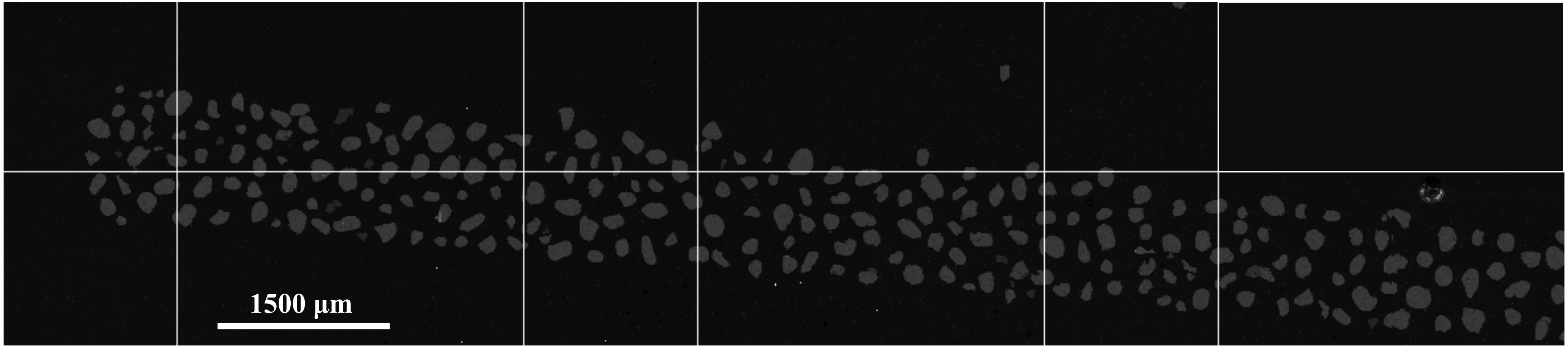

6) 387 Apatite fraction (processed image)

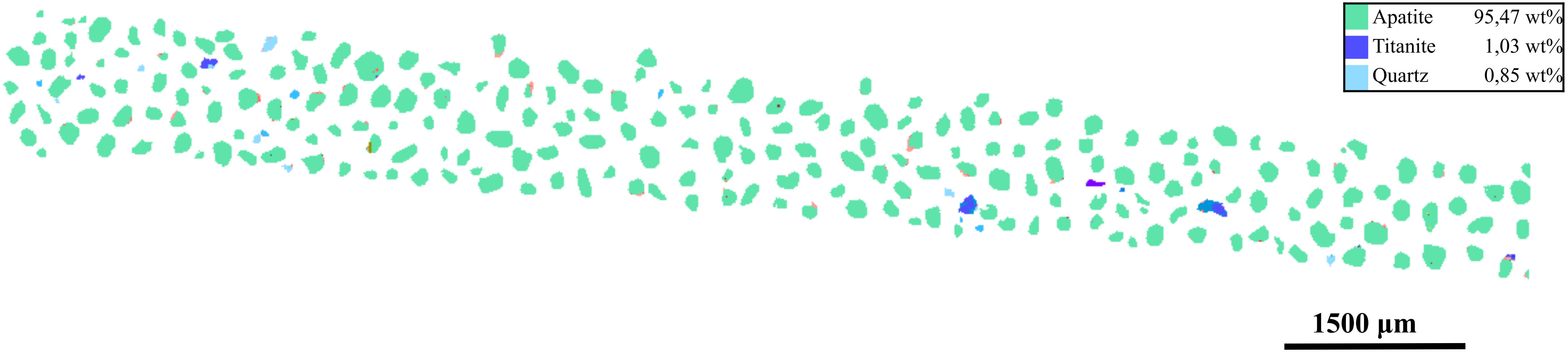

7) 391 Apatite fraction (BSE-image)

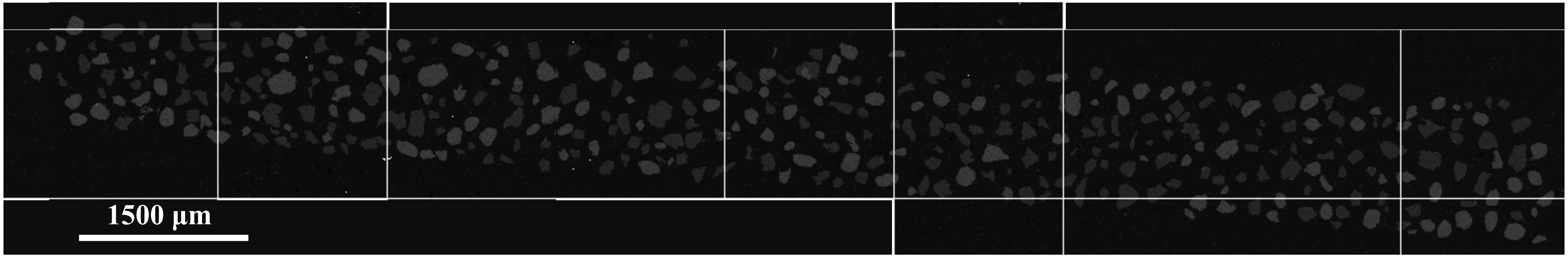

7) 391 Apatite fraction (processed image)

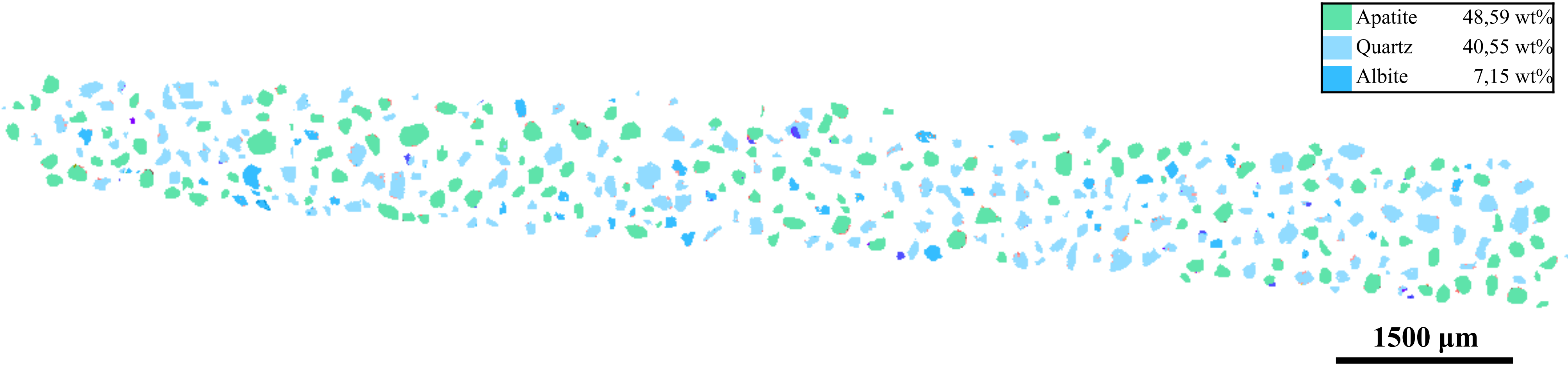

8) BS Apatite fraction (BSE-image)

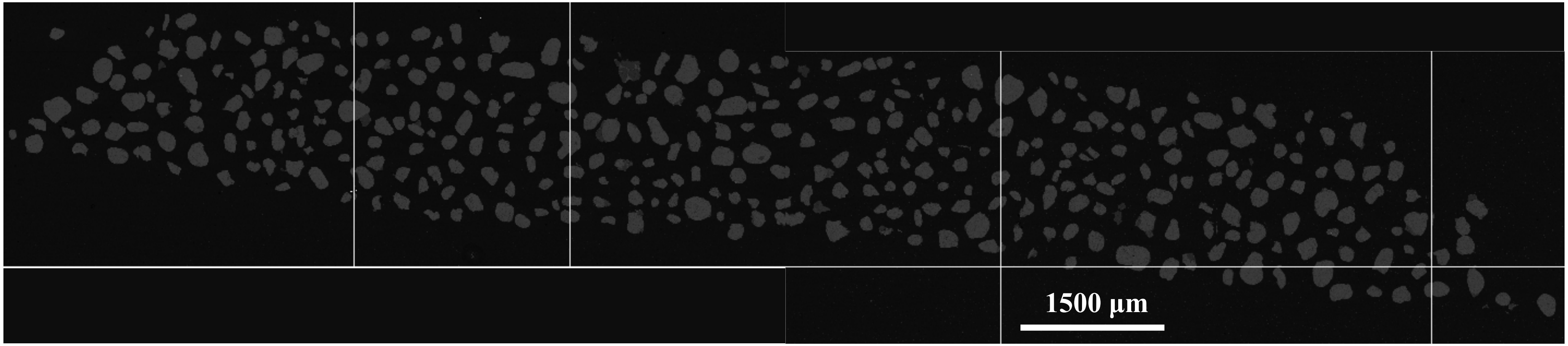

8) BS Apatite fraction (processed image)

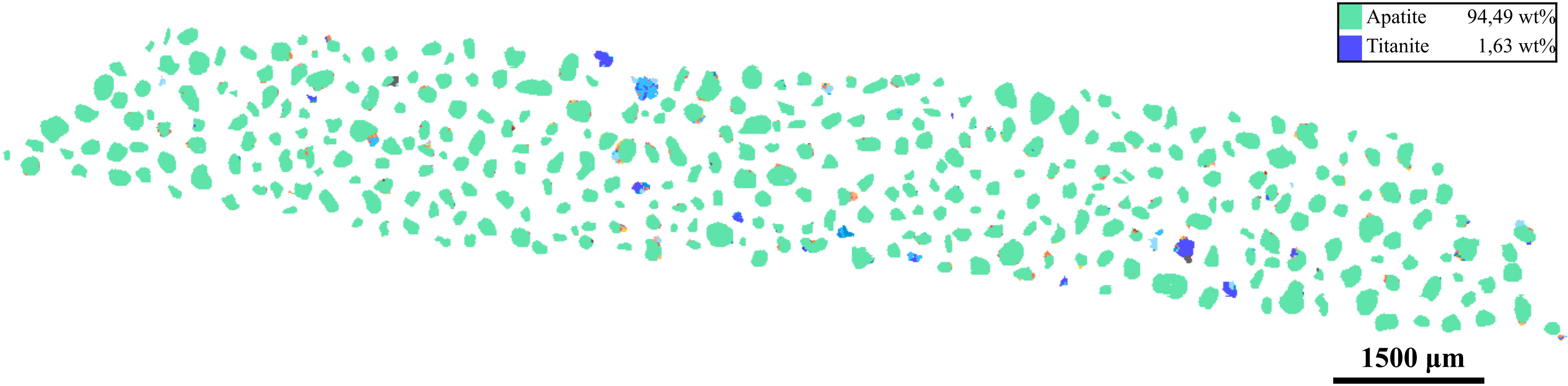

9) 387 Zircon fraction (BSE-image)

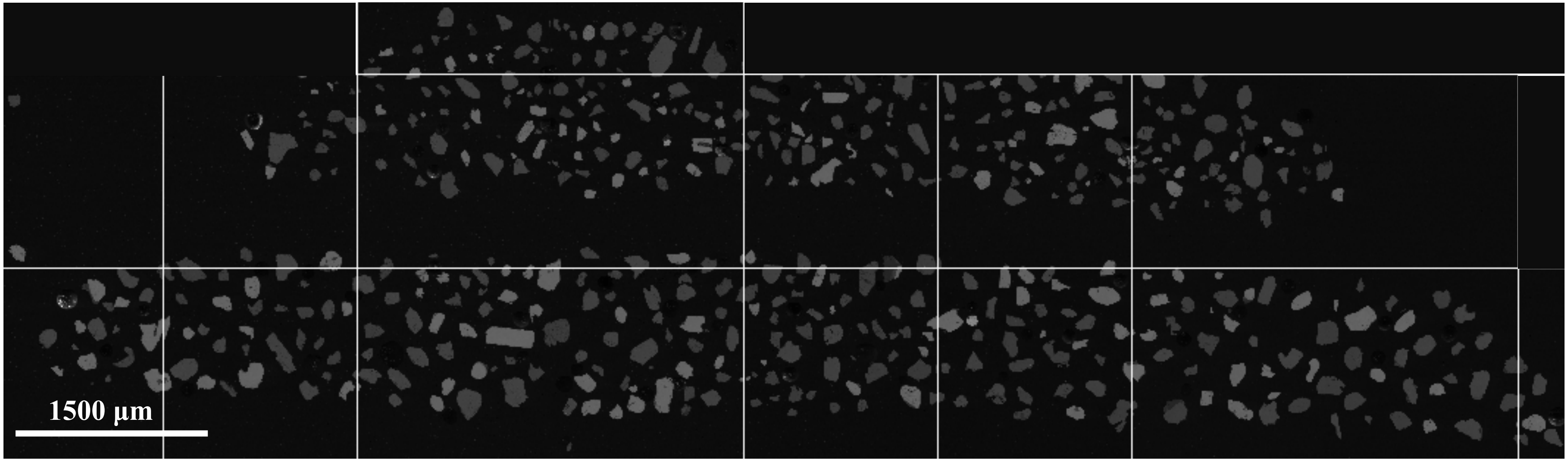

9) 387 Zircon fraction (processed image)

10) 391 Zircon fraction (BSE-image)

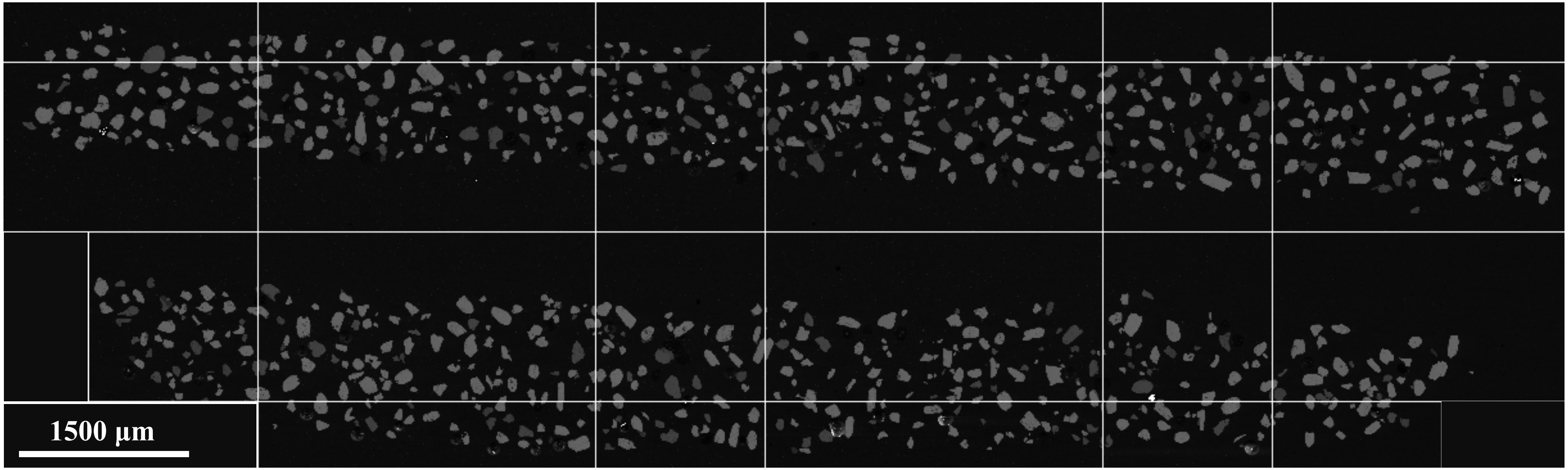

10) 391 Zircon fraction (processed image)

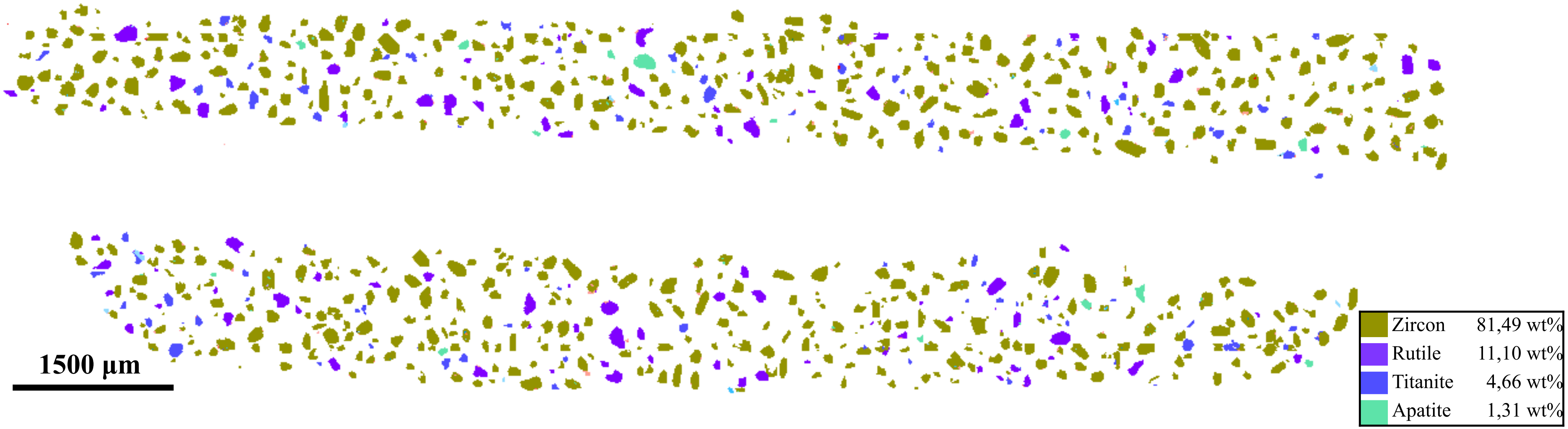

11) BS Zircon fraction (BSE-image)

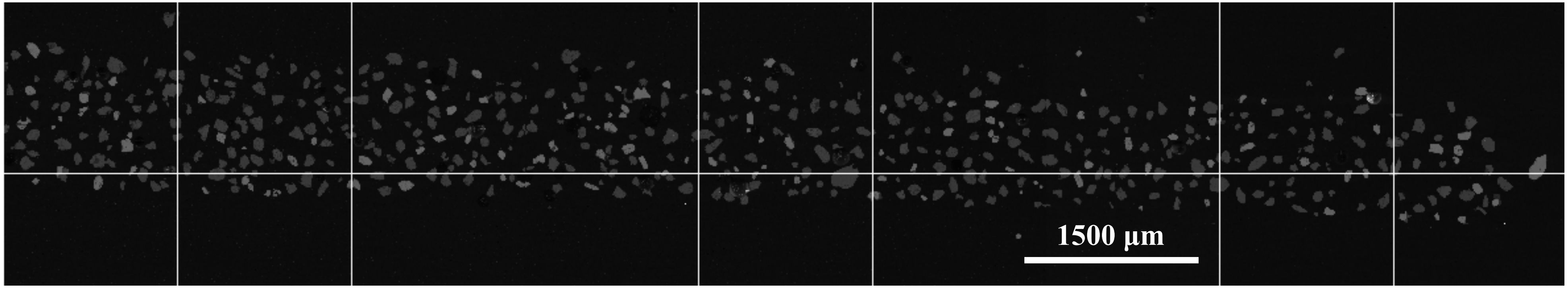

11) BS Zircon fraction (processed image)

Appendix J: Processed images from MLA sorted by particle size

Processed images containing the same grains as in *Appendix I*, but here they are sorted after particle size. Legend with wt% include those minerals >1 wt%. The complete legend can be seen in *Appendix E*.

#	Sample name	Fraction type
1	387	Magnetic fraction
2	389	Magnetic fraction
3	391	Magnetic fraction
4	393	Magnetic fraction
5	BS	Magnetic fraction
6	387	Apatite fraction
7	391	Apatite fraction
8	BS	Apatite fraction
9	387	Zircon fraction
10	391	Zircon fraction
11	BS	Zircon fraction

1) 387 Magnetic fraction

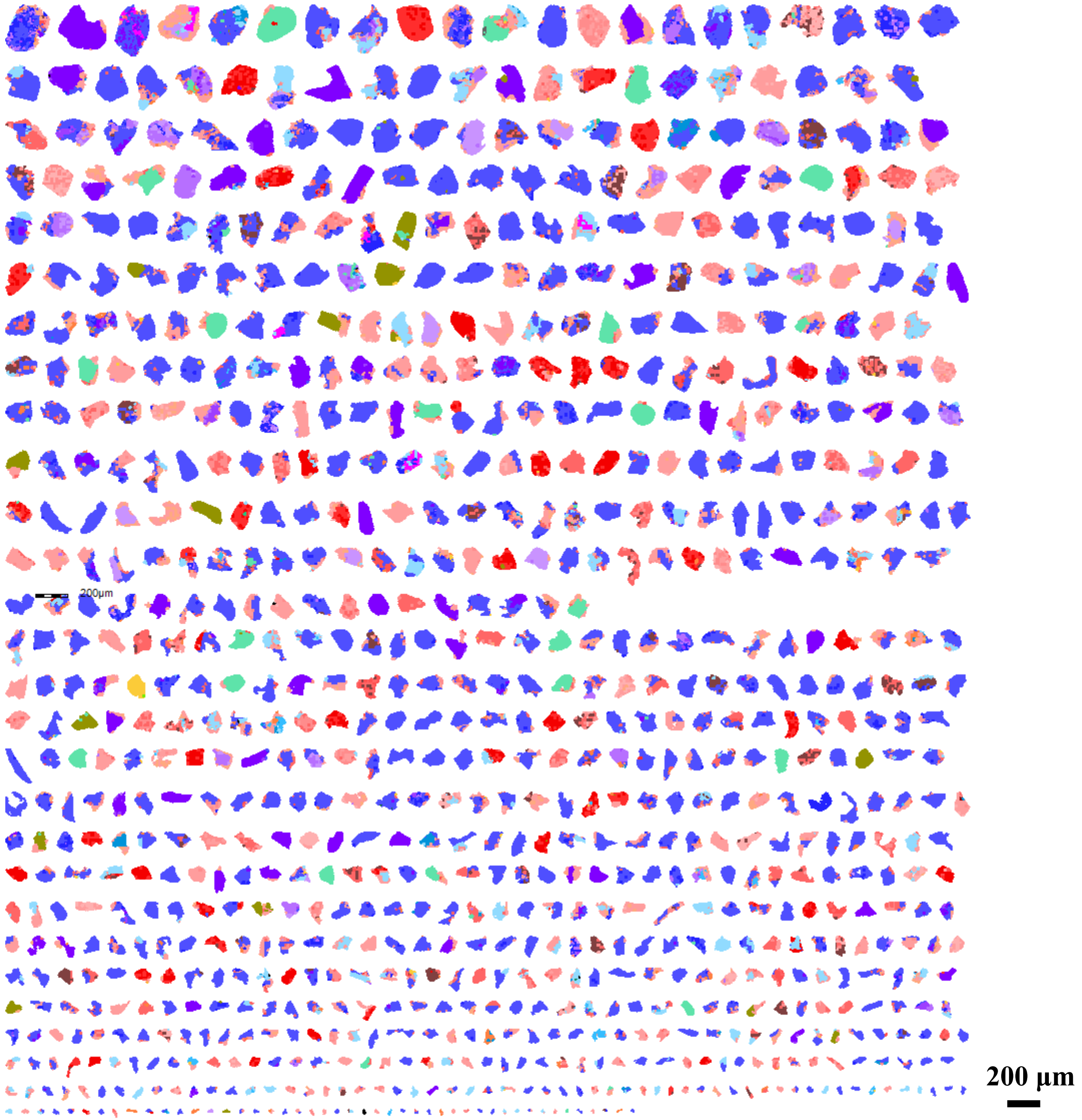

Titanite	41,31 wt%
Almandine-Ca1	13,83 wt%
Rutile	7,97 wt%
Almandine-Ca5	5,89 wt%
Almandine-Ca4	3,68 wt%
Quartz	3,00 wt%
Magnetite-Ti	2,91 wt%
Grossular	2,78 wt%
Apatite	2,70 wt%
Grossular-Fe	2,33 wt%
Magnetite	2,29 wt%
Titanite-Fe	2,07 wt%
Almandine-Mn	1,90 wt%
Amphibole	1,74 wt%
Chamosite	1,71 wt%
Zircon	1,66 wt%

2) 389 Magnetic fraction

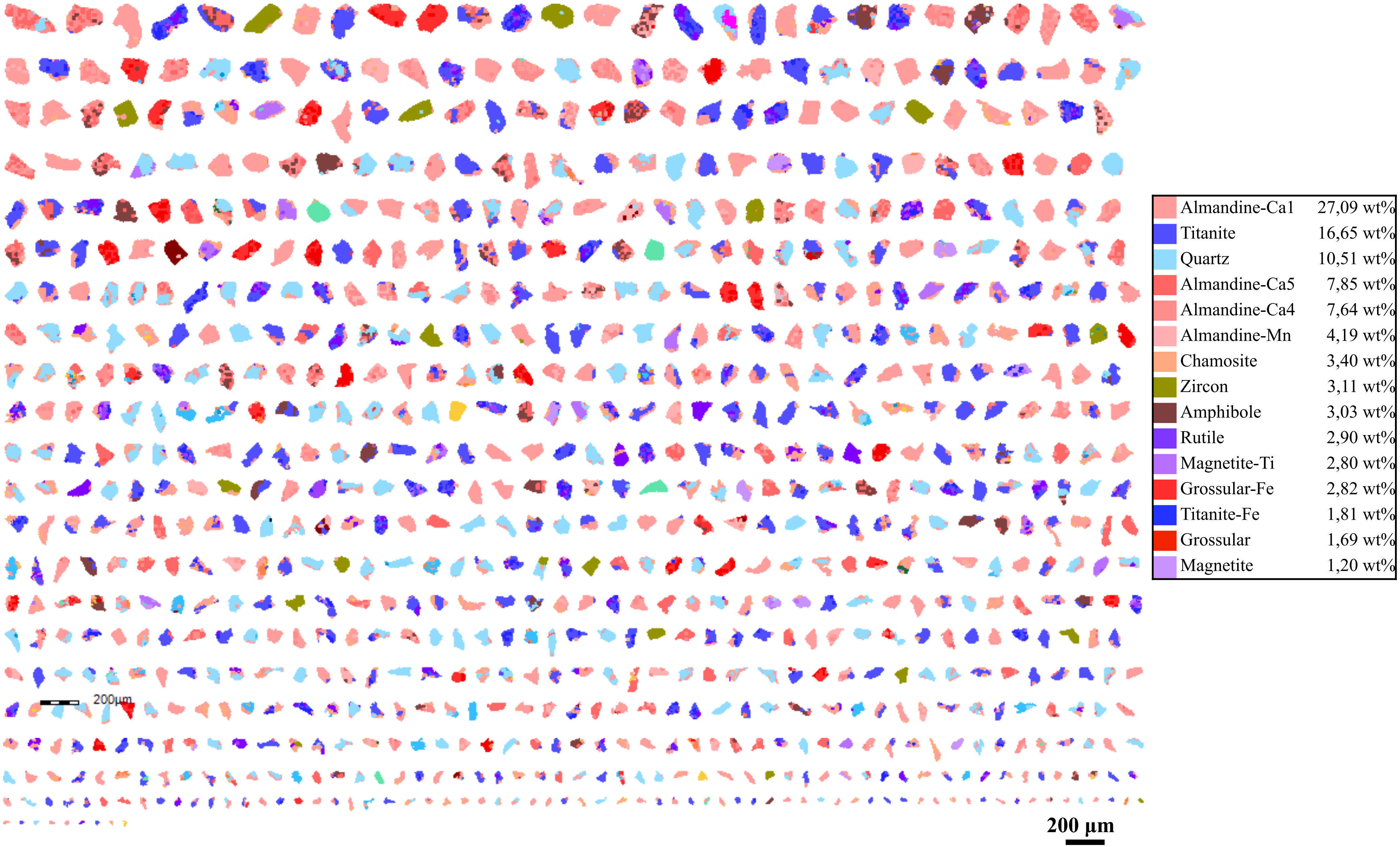

3) 391 Magnetic fraction

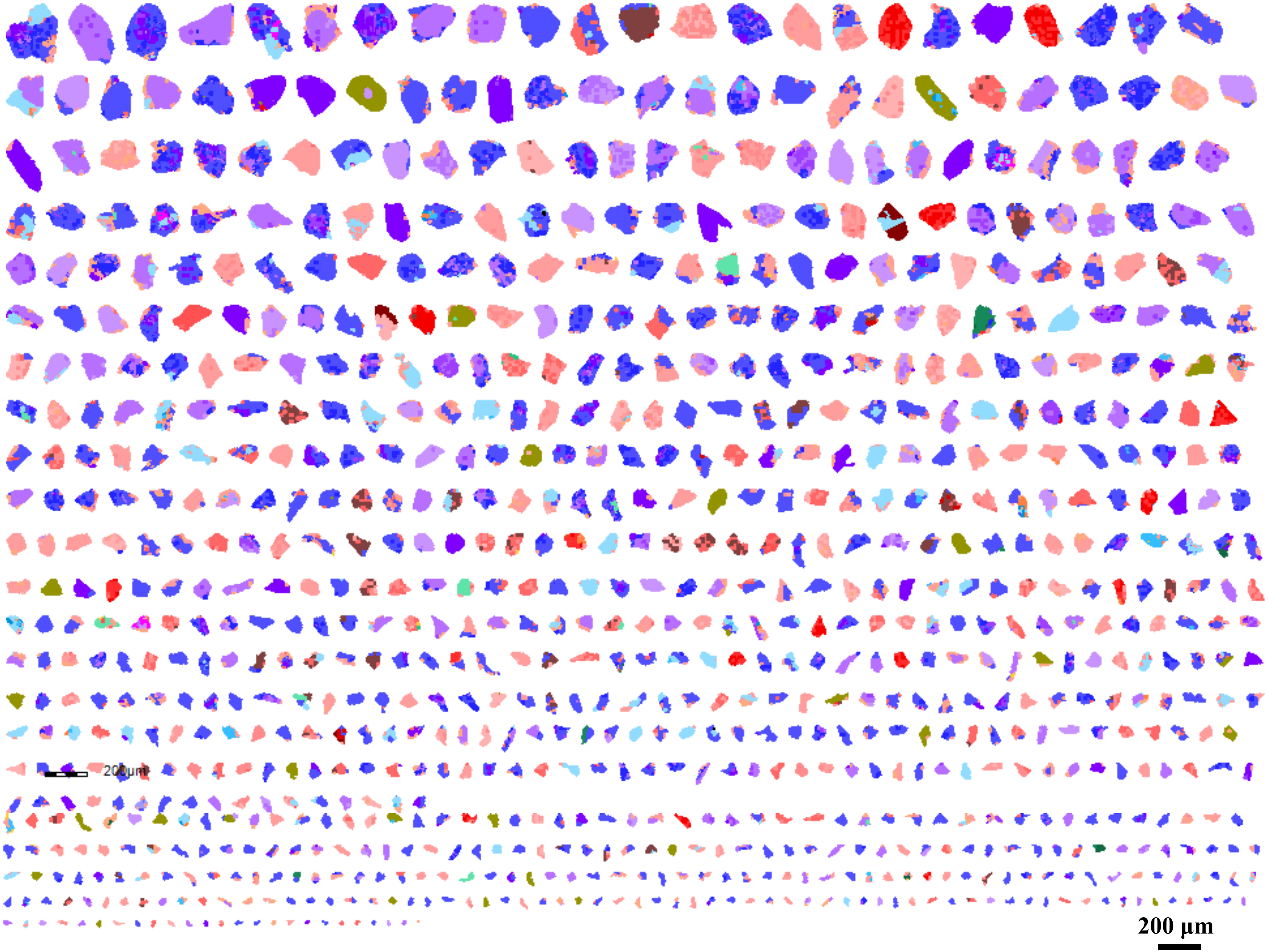

Titanite	25,94 wt%
Magnetite-Ti	16,93 wt%
Almandine-Ca1	12,91 wt%
Magnetite	7,07 wt%
Rutile	7,03 wt%
Almandine-Ca5	4,79 wt%
Titanite-Fe	4,25 wt%
Almandine-Ca4	3,18 wt%
Almandine-Mn	3,05 wt%
Quartz	2,94 wt%
Zircon	2,47 wt%
Ilmenite	2,09 wt%
Chamosite	1,80 wt%
Amphibole	1,74 wt%
Grossular	1,08 wt%

4) 393 Magnetic fraction

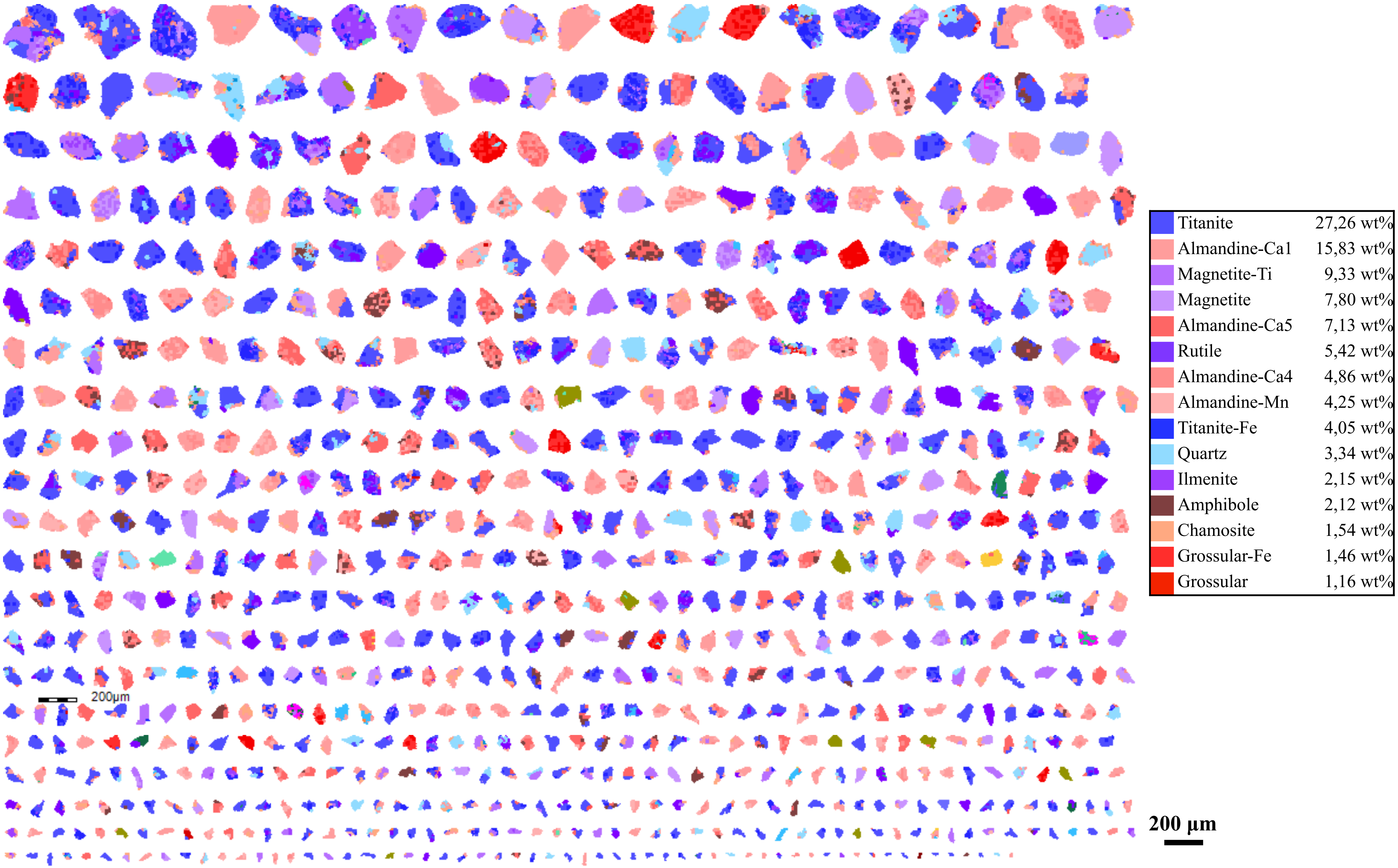

5) BS Magnetic fraction

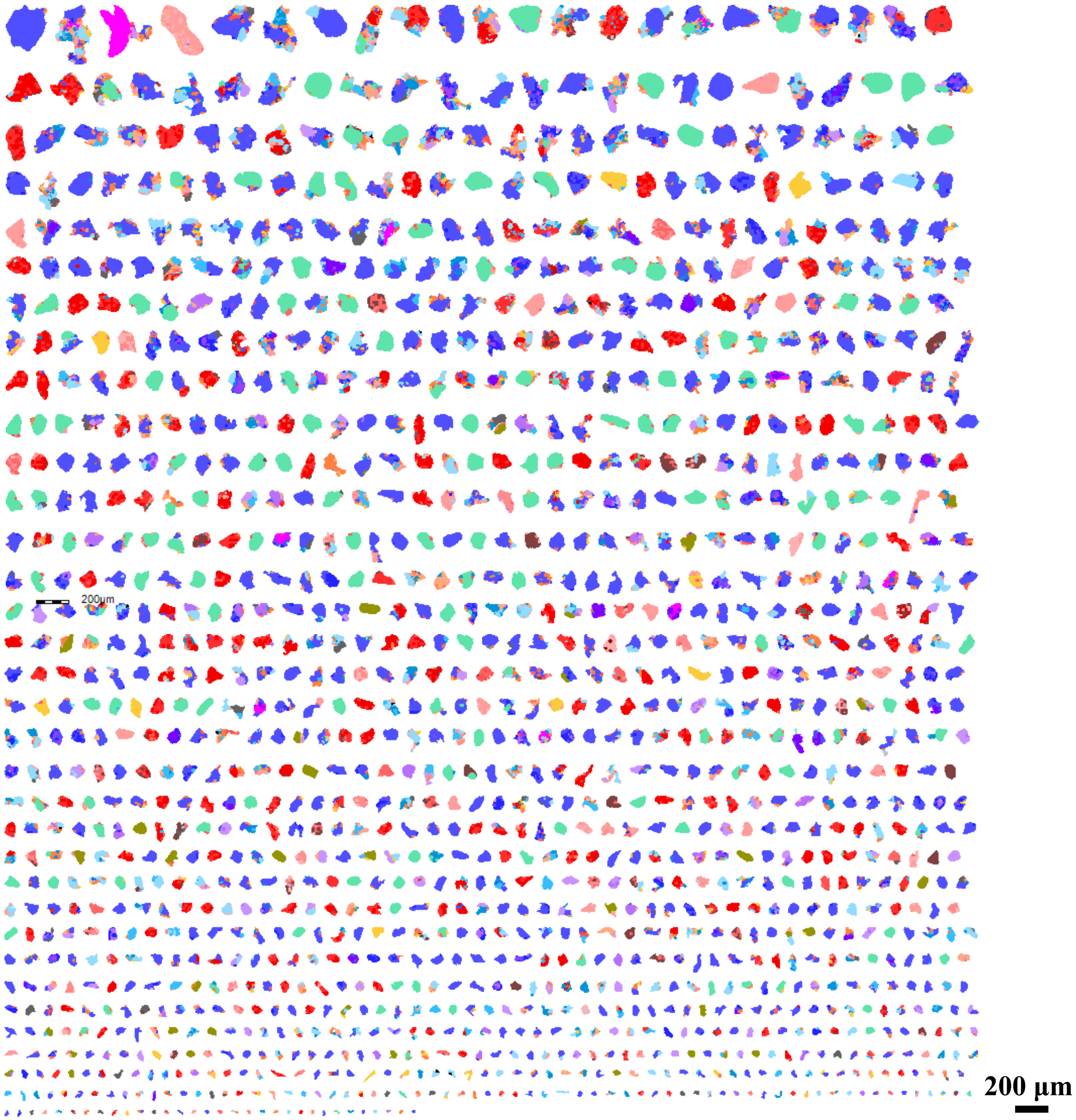

Titanite	35,79 wt%
Apatite	11,87 wt%
Grossular	7,46 wt%
Grossular-Fe	5,95 wt%
Almandine-Ca1	4,57 wt%
Quartz	4,34 wt%
Magnetite	3,11 wt%
Muscovite	2,72 wt%
Magnetite-Ti	2,54 wt%
Titanite-Fe	2,51 wt%
Almandine-Ca5	2,33 wt%
Albite	2,30 wt%
Tourmaline	1,85 wt%
Orthoclase	1,66 wt%
Chamosite	1,61 wt%
Zircon	1,57 wt%
Amphibole	1,51 wt%
Almandine-Ca9	1,38 wt%
Almandine-Ca4	1,27 wt%
Almandine-Mn	1,10 wt%
Rutile	1,08 wt%

6) 387 Apatite fraction

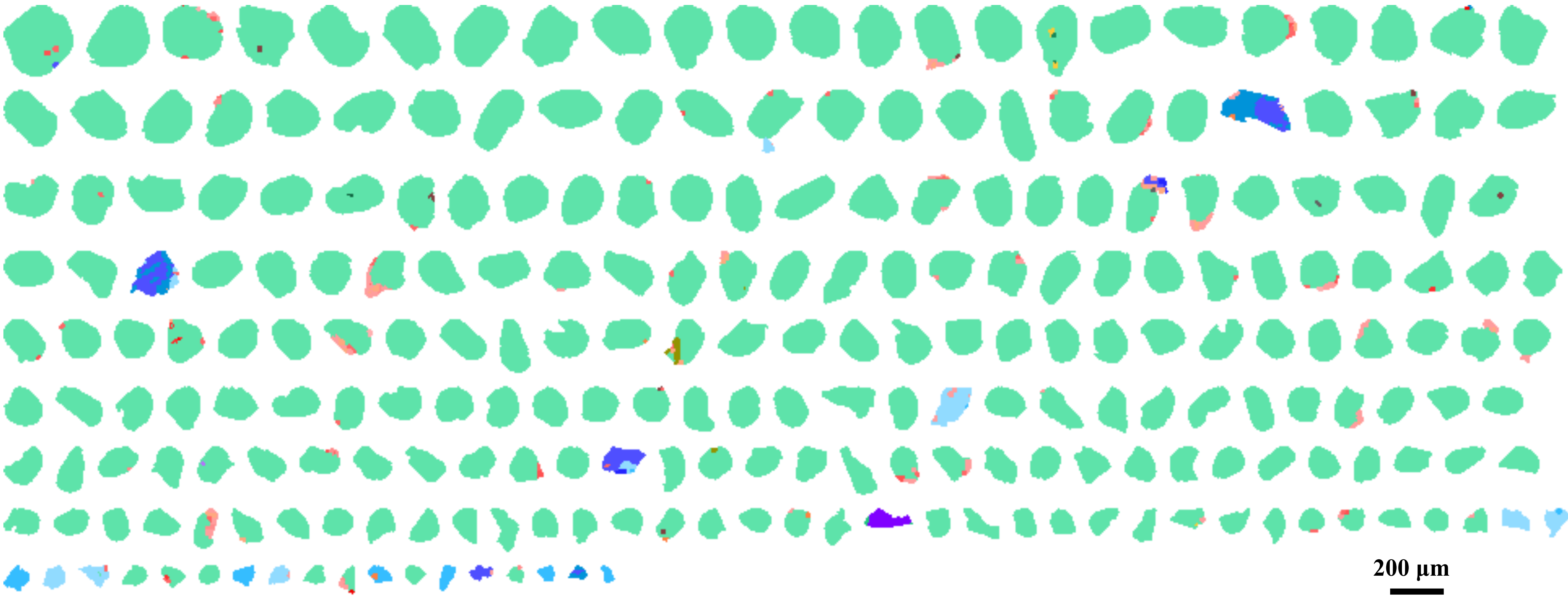

Apatite	95,47 wt%
Titanite	1,03 wt%
Quartz	0,85 wt%

7) 391 Apatite fraction

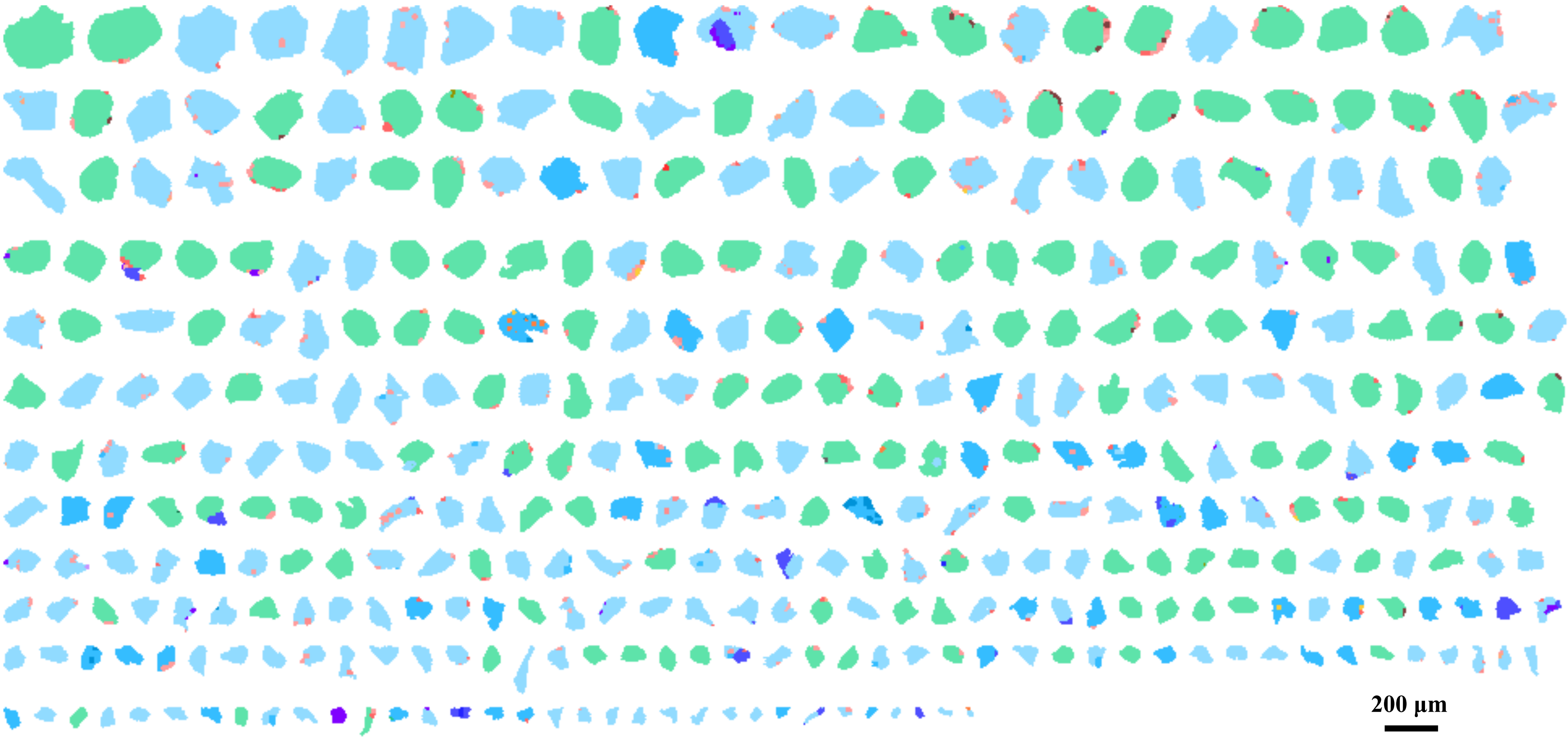

	Apatite	48,59 wt%
	Quartz	40,55 wt%
	Albite	7,15 wt%

8) BS Apatite fraction

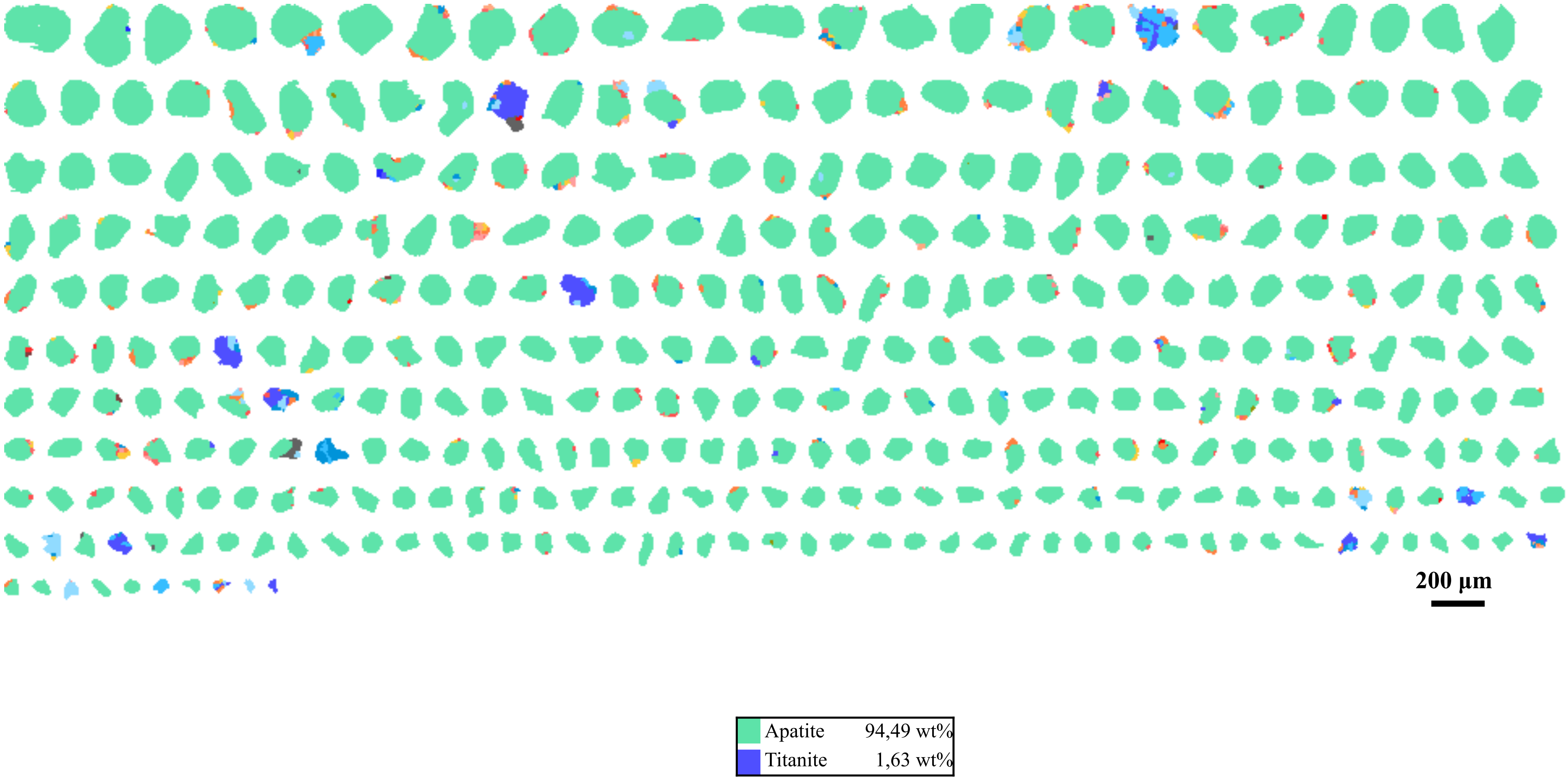

9) 387 Zircon fraction

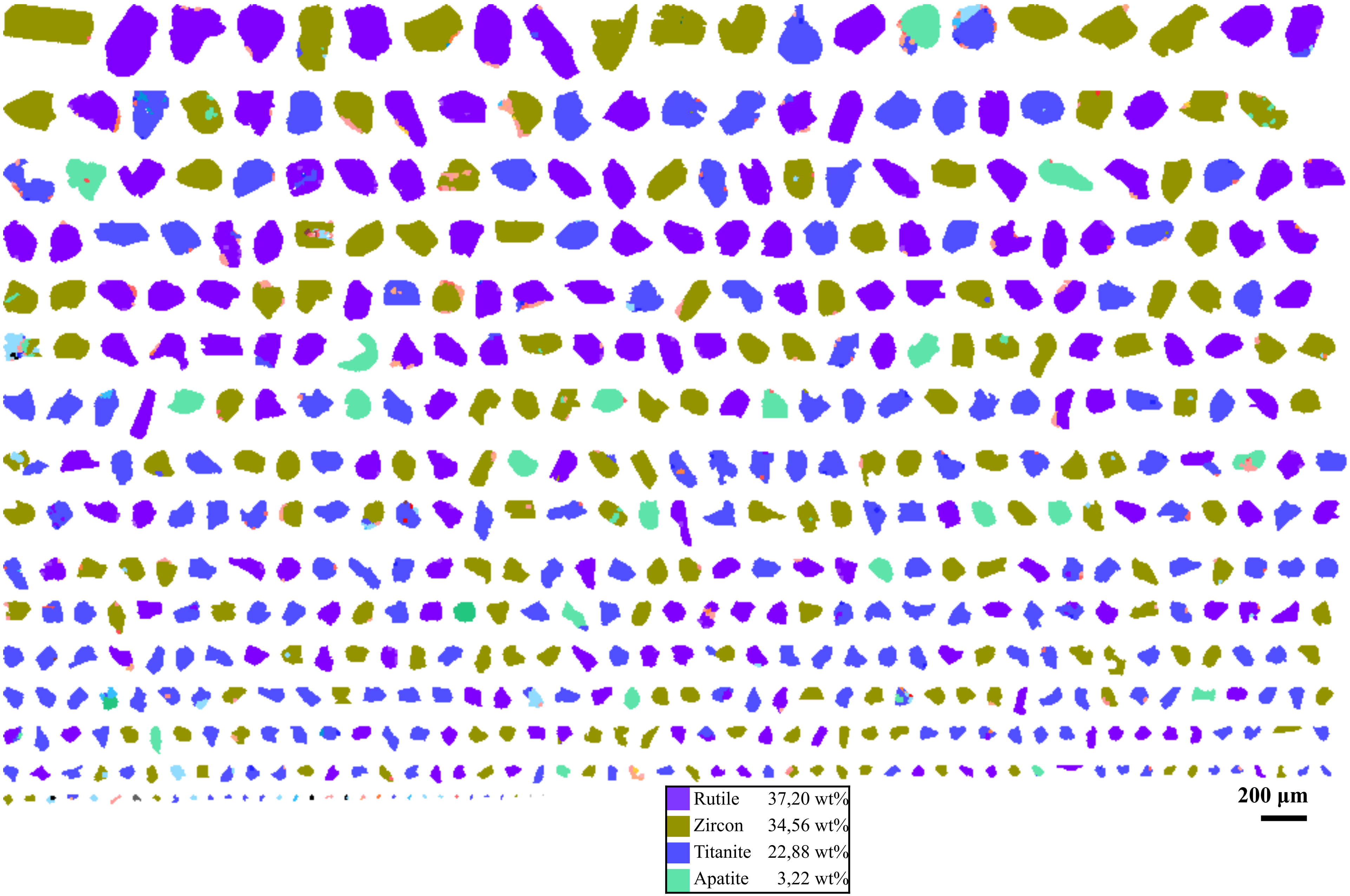

10) 391 Zicron fraction

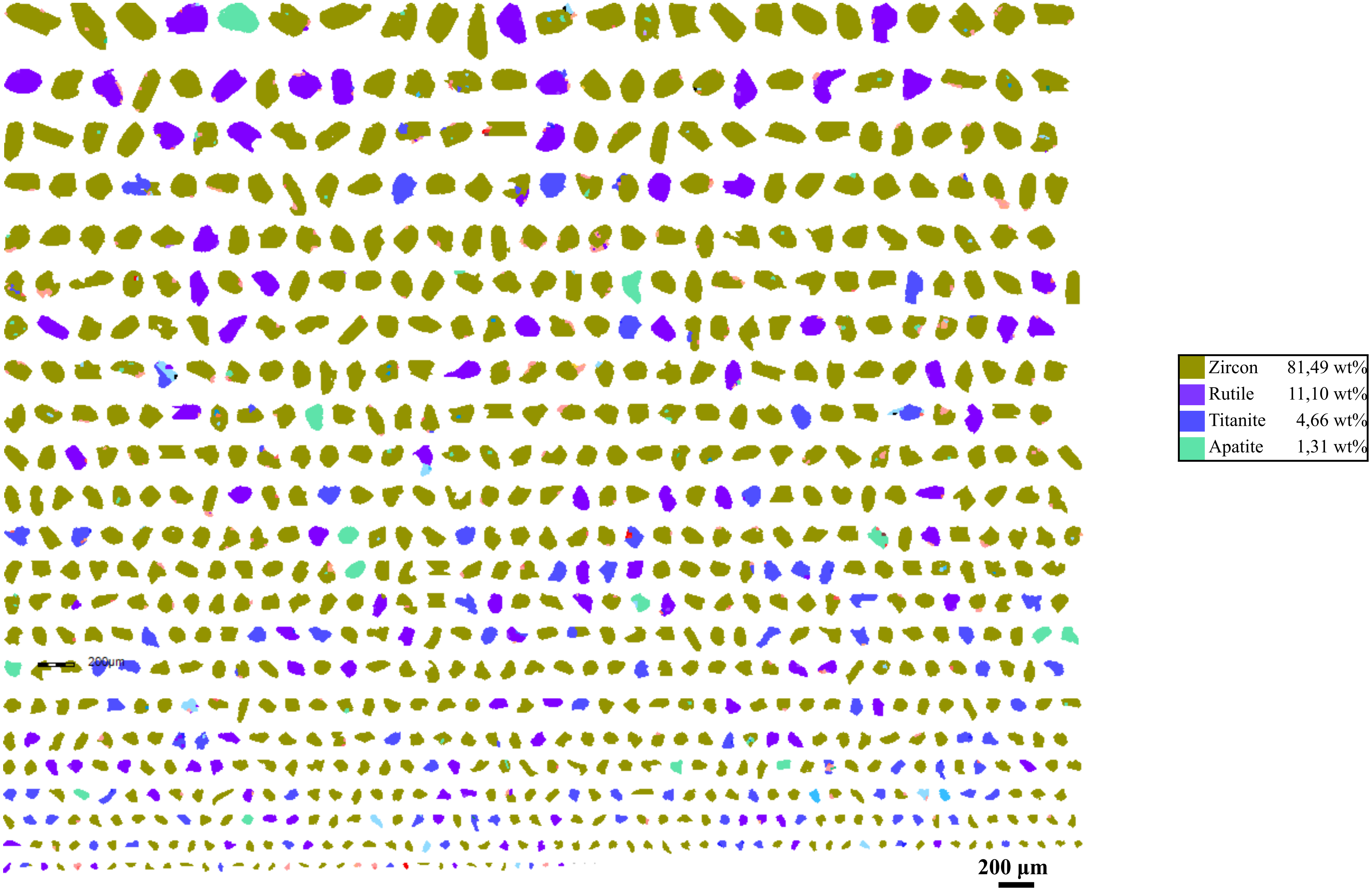

11) BS Zicron fraction

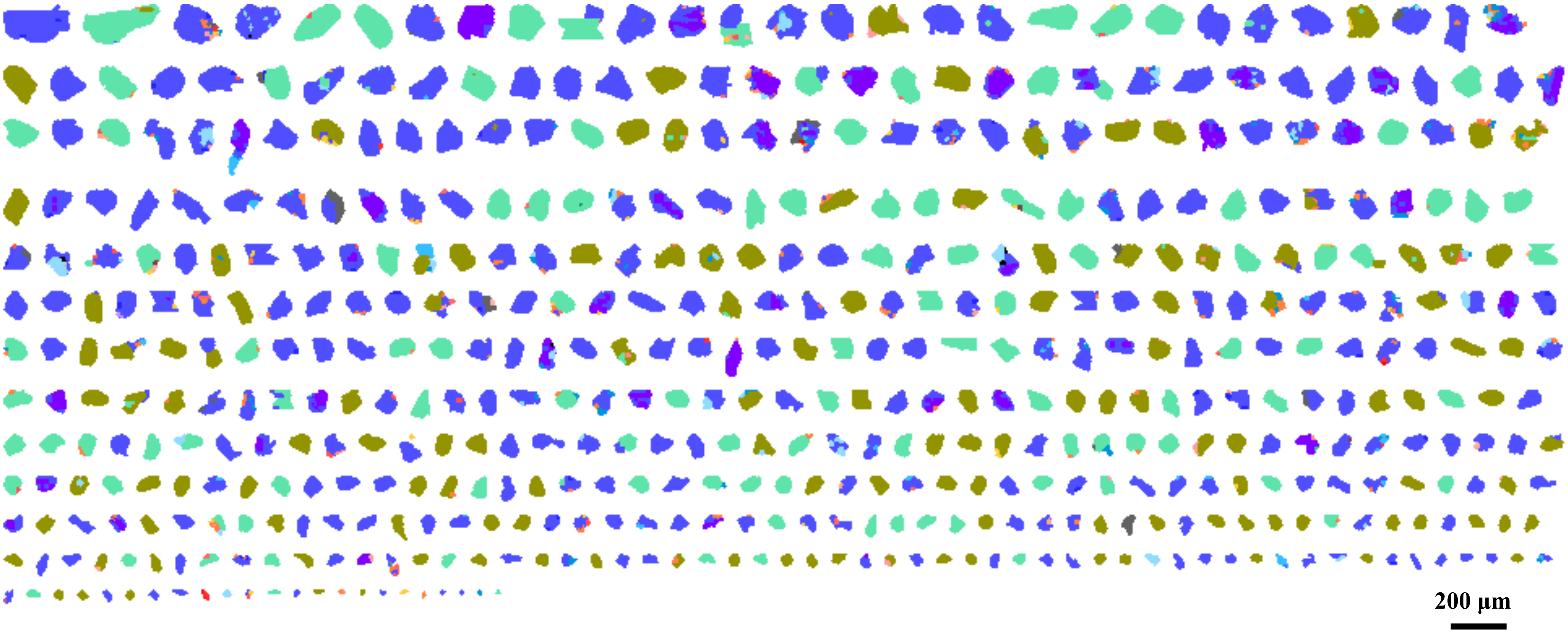

	Titanite	45,59 wt%
	Zircon	25,00 wt%
	Apatite	19,74 wt%
	Rutile	5,94 wt%

Appendix K: Particle size and particle density distributions from MLA

Particle size distribution and particle density distributions from MLA.

1) Particle size distribution (cumulative passing wt%, cumulative retained wt% and retained wt%)

Cumulative passing wt% values are used for particle size distribution plots.
Minimum and maximum sieve sizes for the grey colored areas are used for calculation of settling velocities.

Cumulative passing wt%

	Magnetic fractions					Apatite fractions			Zircon fractions		
Sieve Size (um)	**387**	**389**	**391**	**393**	**BS**	**387**	**391**	**BS**	**387**	**391**	**BS**
300	100,00			100,00					100,00		
250	99,44		100,00	98,18	100,00	100,00	100,00		98,79		
212	96,17		97,76	96,14	98,21	97,73	96,72	100,00	97,03	100,00	
180	85,81	100,00	94,72	86,78	97,04	80,83	91,27	97,36	85,37	98,12	100,00
150	62,23	99,09	76,89	70,10	89,08	48,00	73,62	80,53	70,22	88,60	98,29
125	38,72	90,13	57,07	49,01	77,41	20,95	42,39	59,79	45,19	65,88	92,78
106	22,94	68,57	41,96	31,90	59,87	8,54	26,52	36,65	29,56	41,41	77,68
90	11,56	42,82	30,57	20,10	41,03	3,43	13,59	17,76	17,06	25,00	51,97
75	5,62	20,33	20,06	10,97	23,76	1,27	5,09	6,85	7,94	12,55	27,88
63	2,94	8,39	12,69	6,11	12,32	0,34	2,42	1,59	3,62	6,49	12,01
53	1,39	4,08	6,68	3,21	6,22	0,08	0,81	0,43	1,58	3,22	5,82
45	0,68	2,04	3,44	1,69	3,33	0,03	0,24	0,09	0,73	1,45	2,77
38	0,41	1,23	1,96	0,72	1,43	0,00	0,12	0,04	0,26	0,62	1,12
32	0,24	0,72	0,96	0,32	0,77		0,05	0,04	0,12	0,30	0,27
27	0,15	0,37	0,46	0,15	0,39		0,01	0,00	0,10	0,14	0,15
22	0,06	0,15	0,11	0,07	0,12		0,00		0,06	0,02	0,10
19	0,02	0,05	0,05	0,03	0,04				0,05	0,00	0,06
16	0,00	0,00	0,00	0,00	0,00				0,02		0,04
13,5									0,01		0,00
11,4									0,01		
9,6									0,00		
8,1											

Cumulative retained (wt%)

	Magnetic fractions					Apatite fractions			Zircon fractions		
Sieve Size (um)	**387**	**389**	**391**	**393**	**BS**	**387**	**391**	**BS**	**387**	**391**	**BS**
300	0,00			0,00					0,00		
250	0,56		0,00	1,82	0,00	0,00	0,00		1,21		
212	3,83		2,24	3,86	1,79	2,27	3,28	0,00	2,97	0,00	
180	14,19	0,00	5,28	13,22	2,96	19,17	8,73	2,64	14,63	1,88	0,00
150	37,77	0,91	23,11	29,90	10,92	52,00	26,38	19,47	29,78	11,40	1,71
125	61,28	9,87	42,93	50,99	22,59	79,05	57,61	40,21	54,81	34,12	7,22
106	77,06	31,43	58,04	68,10	40,13	91,46	73,48	63,35	70,44	58,59	22,32
90	88,44	57,18	69,43	79,90	58,97	96,57	86,41	82,24	82,94	75,00	48,03
75	94,38	79,67	79,94	89,03	76,24	98,73	94,91	93,15	92,06	87,45	72,12
63	97,06	91,61	87,31	93,89	87,68	99,66	97,58	98,41	96,38	93,51	87,99
53	98,61	95,92	93,32	96,79	93,78	99,92	99,19	99,57	98,42	96,78	94,18
45	99,32	97,96	96,56	98,31	96,67	99,97	99,76	99,91	99,27	98,55	97,23
38	99,59	98,77	98,04	99,28	98,57	100,00	99,88	99,96	99,74	99,38	98,88
32	99,76	99,28	99,04	99,68	99,23		99,95	99,96	99,88	99,70	99,73
27	99,85	99,63	99,54	99,85	99,61		99,99	100,00	99,90	99,86	99,85
22	99,94	99,85	99,89	99,93	99,88		100,00		99,94	99,98	99,90
19	99,98	99,95	99,95	99,97	99,96				99,95	100,00	99,94
16	100,00	100,00	100,00	100,00	100,00				99,98		99,96
13,5									99,99		100,00
11,4									99,99		
9,6									100,00		
8,1											

Retained (wt%)

	Magnetic fractions					Apatite fractions			Zircon fractions		
Sieve Size (um)	**387**	**389**	**391**	**393**	**BS**	**387**	**391**	**BS**	**387**	**391**	**BS**
300	0,00			0,00					0,00		
250	0,56		0,00	1,82	0,00	0,00	0,00		1,21		
212	3,27		2,24	2,04	1,79	2,27	3,28	0,00	1,76	0,00	
180	10,36	0,00	3,03	9,36	1,16	16,90	5,45	2,64	11,66	1,88	0,00
150	23,58	0,91	17,83	16,68	7,97	32,83	17,64	16,82	15,16	9,53	1,71
125	23,51	8,96	19,82	21,10	11,66	27,04	31,23	20,75	25,02	22,71	5,50
106	15,79	21,57	15,11	17,10	17,54	12,41	15,87	23,14	15,64	24,47	15,10
90	11,37	25,75	11,39	11,80	18,84	5,11	12,93	18,89	12,50	16,41	25,71
75	5,94	22,48	10,51	9,13	17,27	2,16	8,50	10,90	9,12	12,45	24,09
63	2,69	11,94	7,37	4,86	11,44	0,93	2,67	5,26	4,32	6,06	15,87
53	1,54	4,31	6,01	2,90	6,10	0,26	1,61	1,17	2,04	3,27	6,19
45	0,72	2,04	3,24	1,52	2,89	0,05	0,58	0,34	0,84	1,78	3,06
38	0,26	0,81	1,48	0,96	1,90	0,03	0,12	0,04	0,47	0,83	1,64
32	0,17	0,51	1,00	0,41	0,66	0,00	0,07	0,00	0,13	0,32	0,86
27	0,10	0,35	0,50	0,17	0,38		0,04	0,04	0,03	0,15	0,11
22	0,09	0,22	0,35	0,08	0,27		0,01	0,00	0,04	0,12	0,05
19	0,04	0,11	0,06	0,04	0,08		0,00		0,01	0,02	0,04
16	0,02	0,05	0,04	0,03	0,04				0,03	0,00	0,03
13,5	0,00	0,00	0,00	0,00	0,00				0,01		0,04
11,4									0,00		0,00
9,6									0,01		
8,1									0,00		

2) Particle size distribution (retained wt% and Wenworth size class)

Values used for histograms with particle size/grain size (phi), Wenworth size class and retained wt%.

	Retained (wt%)										
	Magnetic fractions					Apatite fractions			Zircon fractions		
Sieve Size (um)	387	389	391	393	BS	387	391	BS	387	391	BS
300	0,00			0,00					0,00		
250	0,56		0,00	1,82	0,00	0,00	0,00		1,21		
212	3,27		2,24	2,04	1,79	2,27	3,28	0,00	1,76	0,00	
180	10,36	0,00	3,03	9,36	1,16	16,90	5,45	2,64	11,66	1,88	0,00
150	23,58	0,91	17,83	16,68	7,97	32,83	17,64	16,82	15,16	9,53	1,71
125	23,51	8,96	19,82	21,10	11,66	27,04	31,23	20,75	25,02	22,71	5,50
106	15,79	21,57	15,11	17,10	17,54	12,41	15,87	23,14	15,64	24,47	15,10
90	11,37	25,75	11,39	11,80	18,84	5,11	12,93	18,89	12,50	16,41	25,71
75	5,94	22,48	10,51	9,13	17,27	2,16	8,50	10,90	9,12	12,45	24,09
63	2,69	11,94	7,37	4,86	11,44	0,93	2,67	5,26	4,32	6,06	15,87
53	1,54	4,31	6,01	2,90	6,10	0,26	1,61	1,17	2,04	3,27	6,19
45	0,72	2,04	3,24	1,52	2,89	0,05	0,58	0,34	0,84	1,78	3,06
38	0,26	0,81	1,48	0,96	1,90	0,03	0,12	0,04	0,47	0,83	1,64
32	0,17	0,51	1,00	0,41	0,66	0,00	0,07	0,00	0,13	0,32	0,86
27	0,10	0,35	0,50	0,17	0,38		0,04	0,04	0,03	0,15	0,11
22	0,09	0,22	0,35	0,08	0,27		0,01	0,00	0,04	0,12	0,05
19	0,04	0,11	0,06	0,04	0,08		0,00		0,01	0,02	0,04
16	0,02	0,05	0,04	0,03	0,04				0,03	0,00	0,03
13,5	0,00	0,00	0,00	0,00	0,00				0,01		0,04
11,4									0,00		0,00
9,6									0,01		
8,1									0,00		

Sieve size (mm)	Particle size (mm)	Phi (ϕ)		Wenworth size class
0,3000	0,3000 -	2 to 1	1,50	Medium sand
0,2500	0,2500 - 0,3000	2 to 1	1,75	Medium sand
0,2120	0,2120 - 0,2500	3 to 2	2,00	Fine sand
0,1800	0,1800 - 0,2120	3 to 2	2,25	Fine sand
0,1500	0,1500 - 0,1800	3 to 2	2,50	Fine sand
0,1250	0,1250 - 0,1500	3 to 2	2,75	Fine sand
0,1060	0,1060 - 0,1250	4 to 3	3,00	Very fine sand
0,0900	0,0900 - 0,1060	4 to 3	3,25	Very fine sand
0,0750	0,0750 - 0,0900	4 to 3	3,50	Very fine sand
0,0630	0,0630 - 0,0750	4 to 3	3,75	Very fine sand
0,0530	0,0530 - 0,0630	5 to 4	4,00	Coarse silt
0,0450	0,0450 - 0,0530	5 to 4	4,25	Coarse silt
0,0380	0,0380 - 0,0450	5 to 4	4,50	Coarse silt
0,0320	0,0320 - 0,0380	5 to 4	4,75	Coarse silt
0,0270	0,0270 - 0,0320	6 to 5	5,00	Medium silt
0,0220	0,0220 - 0,0270	6 to 5	5,25	Medium silt
0,0190	0,0190 - 0,0220	6 to 5	5,50	Medium silt
0,0160	0,0160 - 0,0190	6 to 5	5,75	Medium silt
0,0135	0,0135 - 0,0160	7 to 6	6,00	Fine silt
0,0114	0,0114 - 0,0135	7 to 6	6,25	Fine silt
0,0096	0,0096 - 0,0114	7 to 6	6,50	Fine silt
0,0081	0,0081 - 0,0096	7 to 6	6,75	Fine silt

3) Particle density distribution

Minimum and maximum densities for the grey colored areas are used for calculating settling velocities.

	Weight of particles (%)											Number of particles (%)										
	Magnetic fractions					Apatite fractions			Zircon fractions			Magnetic fractions					Apatite fractions			Zircon fractions		
Density Distribution	**387**	**389**	**391**	**393**	**BS**	**387**	**391**	**BS**	**387**	**391**	**BS**	**387**	**389**	**391**	**393**	**BS**	**387**	**391**	**BS**	**387**	**391**	**BS**
0.0 < D <= 0.1																				0,37	0,35	
0.1 < D <= 0.2																				0,00	0,00	
0.2 < D <= 0.3																				0,00	0,00	
0.3 < D <= 0.4																				0,00	0,00	
0.4 < D <= 0.5																				0,00	0,00	
0.5 < D <= 0.6				0,00	0,00										0,00	0,00				0,00	0,00	
0.6 < D <= 0.7				0,01	0,10										0,13	0,07				0,00	0,00	
0.7 < D <= 0.8				0,00	0,00										0,00	0,00				0,00	0,00	
0.8 < D <= 0.9				0,00	0,00							0,00			0,00	0,00				0,00	0,00	
0.9 < D <= 1.0				0,00	0,00							0,11			0,00	0,00				0,18	0,00	
1.0 < D <= 1.1				0,00	0,03							0,00			0,00	0,07				0,00	0,00	
1.1 < D <= 1.2				0,00	0,00							0,00			0,00	0,00				0,00	0,00	
1.2 < D <= 1.3				0,00	0,02							0,00			0,00	0,07				0,00	0,00	
1.3 < D <= 1.4				0,03	0,03							0,00			0,13	0,07				0,00	0,00	
1.4 < D <= 1.5	0,00			0,00	0,00							0,00			0,00	0,00				0,18	0,00	
1.5 < D <= 1.6	0,07			0,00	0,03							0,11			0,00	0,07				0,00	0,00	
1.6 < D <= 1.7	0,00		0,00	0,00	0,00							0,00		0,00	0,00	0,00				0,00	0,00	
1.7 < D <= 1.8	0,00		0,01	0,00	0,00							0,00		0,11	0,00	0,00				0,00	0,00	
1.8 < D <= 1.9	0,00		0,00	0,00	0,08							0,00		0,00	0,00	0,07				0,00	0,00	
1.9 < D <= 2.0	0,00		0,04	0,00	0,05							0,00		0,11	0,00	0,07				0,00	0,00	
2.0 < D <= 2.1	0,00	0,00	0,00	0,00	0,00							0,00	0,00	0,00	0,00	0,00				0,00	0,00	
2.1 < D <= 2.2	0,00	0,17	0,00	0,00	0,00				0,00			0,00	0,12	0,00	0,00	0,00				0,00	0,00	
2.2 < D <= 2.3	0,00	0,00	0,00	0,03	0,01				0,01			0,00	0,00	0,00	0,13	0,07				0,18	0,00	
2.3 < D <= 2.4	0,14	0,00	0,00	0,00	0,01	0,00	0,00	0,00	0,00			0,11	0,00	0,00	0,00	0,07				0,00	0,00	
2.4 < D <= 2.5	0,00	0,00	0,00	0,00	0,00	0,00	0,00	0,00	0,00			0,00	0,00	0,00	0,00	0,00			0,00	0,00	0,00	0,00
2.5 < D <= 2.6	0,00	0,08	0,19	0,00	0,22	0,00	0,00	0,16	0,00	0,00	0,00	0,00	0,12	0,11	0,00	0,94	0,00	0,00	0,28	0,00	0,00	0,19
2.6 < D <= 2.7	0,21	2,76	0,83	0,43	1,06	1,20	41,86	0,22	0,05	0,11	0,07	1,79	5,41	1,80	1,31	3,63	4,86	51,31	1,11	1,47	0,82	0,58
2.7 < D <= 2.8	0,08	2,79	0,37	0,47	0,90	0,00	6,53	0,66	0,01	0,05	0,06	0,45	3,64	0,67	0,65	2,61	0,00	6,81	0,56	0,18	0,12	0,19
2.8 < D <= 2.9	0,40	2,08	0,21	0,63	1,15	0,05	1,02	0,00	0,06	0,00	0,01	1,12	3,06	0,45	0,65	1,89	0,40	1,05	0,00	0,37	0,00	0,19
2.9 < D <= 3.0	0,57	1,48	0,56	0,29	1,58	0,56	0,15	0,30	0,00	0,00	0,00	1,01	2,12	0,79	0,65	1,82	0,40	0,52	0,56	0,00	0,00	0,00
3.0 < D <= 3.1	0,91	1,88	0,37	0,55	2,30	0,00	0,17	0,04	0,00	0,12	0,79	0,89	2,35	0,67	0,92	2,76	0,00	0,26	0,28	0,00	0,12	1,16
3.1 < D <= 3.2	1,46	1,51	0,75	0,54	13,28	80,13	30,57	81,26	2,19	1,08	15,53	1,90	2,00	0,90	0,79	10,97	76,52	25,92	80,78	2,94	1,52	17,60
3.2 < D <= 3.3	2,82	0,78	1,03	0,39	8,58	14,90	18,86	16,67	1,24	0,08	5,81	2,13	1,18	1,35	0,65	6,68	13,36	12,57	15,32	1,28	0,12	4,84
3.3 < D <= 3.4	4,04	2,80	1,33	2,87	9,63	2,07	0,52	0,34	0,47	0,11	3,54	3,13	3,29	1,23	3,14	7,26	2,43	0,52	0,56	0,18	0,12	3,09
3.4 < D <= 3.5	20,34	5,90	9,23	8,94	22,64	0,77	0,23	0,34	19,91	4,03	37,31	23,38	7,76	16,16	14,53	23,46	1,21	0,79	0,56	28,99	8,89	37,52
3.5 < D <= 3.6	21,66	11,29	13,80	12,61	17,23	0,08	0,00	0,00	2,43	0,16	2,11	22,37	11,28	12,12	12,96	16,12	0,40	0,00	0,00	3,85	0,58	2,51
3.6 < D <= 3.7	6,24	8,43	6,97	8,61	4,74	0,00	0,00		0,31	0,05	0,94	6,60	8,11	8,19	8,25	4,07	0,00	0,00	0,00	0,73	0,12	1,16
3.7 < D <= 3.8	4,07	5,66	3,61	4,52	2,00	0,00	0,00		0,00	0,20	2,45	3,58	5,52	3,93	4,97	2,03	0,00	0,00	0,00	0,00	0,23	1,74
3.8 < D <= 3.9	3,15	5,23	3,50	4,64	1,67	0,00	0,00		0,00	0,16	1,63	3,24	5,29	3,82	4,06	1,31	0,00	0,00	0,00	0,00	0,23	1,35
3.9 < D <= 4.0	4,36	5,12	3,02	3,89	1,00	0,00	0,00		0,27	0,00	1,01	3,47	4,70	3,25	3,14	0,87	0,00	0,00	0,00	0,55	0,00	0,77
4.0 < D <= 4.1	2,40	4,06	2,44	6,40	0,89	0,00	0,00		0,18	0,08	1,13	2,68	3,53	2,92	4,97	1,09	0,00	0,00	0,00	0,18	0,12	0,58
4.1 < D <= 4.2	12,52	28,38	14,96	19,28	5,11	0,00	0,00		2,13	0,15	1,40	12,30	22,80	16,95	18,85	4,87	0,00	0,00	0,00	2,02	0,70	0,97
4.2 < D <= 4.3	8,48	2,20	7,11	6,41	1,03	0,25	0,09		35,54	11,04	2,21	5,59	2,59	4,26	5,10	0,80	0,40	0,26	0,00	26,97	10,88	1,74
4.3 < D <= 4.4	0,53	0,02	0,87	0,96	0,52	0,00	0,00		0,34	0,39	0,75	0,45	0,12	0,56	0,52	0,65	0,00	0,00	0,00	0,55	0,23	0,58
4.4 < D <= 4.5	1,43	0,90	2,14	0,55	0,12				1,17	1,44	2,29	1,01	0,71	1,35	0,39	0,15				0,73	1,05	1,74
4.5 < D <= 4.6	0,81	0,52	2,61	2,01	0,46				5,07	8,03	4,14	0,56	0,35	1,80	1,18	0,44				4,04	6,20	3,29
4.6 < D <= 4.7	1,48	3,54	4,20	2,71	1,18				28,63	72,72	16,83	1,01	2,35	3,48	2,36	1,60				24,04	67,60	18,18
4.7 < D <= 4.8	0,37	0,82	3,23	2,99	0,28				0,00	0,00	0,00	0,22	0,47	2,13	1,83	0,44				0,00	0,00	0,00
4.8 < D <= 4.9	0,82	0,77	5,28	2,85	0,34							0,34	0,47	2,47	1,96	0,44						
4.9 < D <= 5.0	0,19	0,52	4,50	3,38	0,89							0,22	0,35	3,03	2,23	1,23						
5.0 < D <= 5.1	0,10	0,12	5,30	2,05	0,63							0,11	0,12	2,69	1,83	0,73						
5.1 < D <= 5.2	0,35	0,19	1,53	0,97	0,22							0,11	0,24	2,69	1,70	0,51						
5.2 < D <= 5.3	0,00	0,00	0,00	0,00	0,00							0,00	0,00	0,00	0,00	0,00						
Total	100,00	100,00	100,00	100,00	100,00	100,00	100,00	100,00	100,00	100,00	100,00	100,00	100,00	100,00	100,00	100,00	100,00	100,00	100,00	100,00	100,00	100,00

Appendix L: Mineral grain size distributions from MLA

Mineral grain size distributions from MLA. Each table and plot shows the sieve size and the cumulative passing wt%.

#	Sample name	Fraction type
1	387	Magnetic fraction
2	389	Magnetic fraction
3	391	Magnetic fraction
4	393	Magnetic fraction
5	BS	Magnetic fraction
6	387	Apatite fraction
7	391	Apatite fraction
8	BS	Apatite fraction
9	387	Zircon fraction
10	391	Zircon fraction
11	BS	Zircon fraction

1) 387 Magnetic fraction

Cumulative passing (wt%)												
	387											
Sieve size (um)	Chamosite	Amphibole	Tourmaline	Almandine	Grossular	Magnetite	Ilmenite	Rutile	Titanite	Zircon	Apatite	Other
250								100,00				
212				100	100,00			92,51	100,00		100,00	
180				97,12	86,91	100,00		88,17	94,24	100,00	87,71	
150		100,00		89,92	74,49	82,01		63,85	76,79	84,95	71,50	100,00
125		91,33	100,00	71,46	52,93	64,81		46,56	56,79	63,45	45,79	86,63
106		91,33	51,31	60,41	33,09	49,57	100,00	31,48	40,46	37,52	23,16	82,50
90		86,46	51,31	50,38	18,69	32,74	81,80	17,86	25,65	24,79	11,86	70,49
75	100,00	70,55	51,31	42,03	9,78	19,53	81,80	10,80	14,49	16,23	8,59	50,44
63	95,22	52,53	51,31	35,09	6,14	16,37	71,86	8,22	9,53	9,99	7,17	42,08
53	89,23	44,39	51,31	29,11	4,06	14,06	57,65	6,52	5,58	9,99	6,20	34,01
45	87,37	38,88	51,31	23,53	2,77	12,58	57,65	5,69	3,60	5,20	2,73	27,34
38	82,11	34,00	51,31	18,86	2,26	11,16	50,43	4,88	2,70	4,23	2,29	20,89
32	71,29	28,56	51,31	15,43	1,44	8,69	45,32	4,55	1,91	2,37	2,29	17,26
27	61,81	25,53	47,61	12,10	1,00	7,34	39,57	4,00	1,41	2,37	2,29	14,51
22	44,99	18,64	36,25	8,62	0,69	4,93	33,31	3,22	0,94	1,18	1,61	10,32
19	35,59	15,06	30,09	6,63	0,48	4,26	31,43	2,77	0,65	1,18	1,25	7,79
16	16,61	7,63	18,55	4,00	0,34	2,70	15,38	1,51	0,40	0,60	0,38	4,39
13,5	6,24	3,00	10,27	2,47	0,14	1,95	7,30	0,94	0,24	0,60	0,19	2,33
11,4	2,97	0,90	4,83	1,20	0,10	1,38	4,69	0,74	0,14	0,50	0,10	1,13
9,6	2,06	0,59	2,56	0,71	0,04	1,00	3,25	0,41	0,10	0,22	0,04	0,66
8,1	1,61	0,38	1,71	0,40	0,03	0,78	1,87	0,30	0,07	0,16	0,02	0,36
6,8	1,13	0,28	1,30	0,24	0,03	0,50	1,15	0,23	0,05	0,09	0,02	0,20
5,7	0,89	0,13	0,55	0,11	0,01	0,31	0,72	0,13	0,04	0,07	0,02	0,07
4,8	0,65	0,09	0,21	0,07	0,01	0,16	0,65	0,10	0,02	0,05	0,01	0,04
4,1	0,25	0,05	0,21	0,03	0,01	0,07	0,26	0,03	0,01	0,03	0,00	0,02
3,4	0,17	0,03	0,10	0,02	0,00	0,05	0,16	0,02	0,01	0,02		0,01
2,9	0,02	0,01	0,01	0,01		0,01	0,01	0,00	0,00	0,00		0,00
2,4	0,02	0,01	0,01	0,01		0,01	0,01					
2	0,01	0,00	0,01	0,00		0,00	0,01					
1,75	0,01		0,01				0,01					
1,45	0,00		0,00				0,00					
1,2												

2) 389 Magnetic fraction

	Cumulative passing (wt%)											
	389											
Sieve size (um)	Chamosite	Amphibole	Tourmaline	Almandine	Grossular	Magnetite	Ilmenite	Rutile	Titanite	Zircon	Apatite	Other
250												
212												
180												
150				100,00	100,00				100,00	100,00		
125		100,00		92,59	87,36				98,58	74,32		100,00
106		86,37		74,85	73,26	100,00			88,48	47,53	100,00	92,41
90		71,00	100,00	55,25	36,90	72,23	100,00	100,00	74,01	33,88	36,43	76,18
75		67,76	56,26	40,82	20,49	36,97	82,64	85,51	48,32	24,08	16,01	50,95
63	100,00	55,12	56,26	31,04	10,18	25,87	82,64	75,26	31,51	6,62	16,01	32,35
53	97,20	44,20	56,26	24,08	3,82	21,52	74,28	61,94	20,31	3,83	16,01	16,75
45	90,34	39,43	56,26	19,17	2,87	15,43	74,28	53,59	14,01	3,83	16,01	11,37
38	80,58	35,88	46,60	15,84	2,87	14,36	64,63	45,27	10,88	1,28	9,90	8,44
32	73,39	28,85	46,60	12,20	1,33	12,98	61,51	34,56	7,48	1,28	9,90	6,17
27	60,86	24,26	46,60	9,52	0,96	9,25	54,32	25,61	5,55	0,56	7,51	4,93
22	43,32	15,34	36,41	6,64	0,77	6,78	40,53	17,96	3,58	0,56	4,35	3,09
19	35,26	12,80	31,88	5,03	0,77	5,26	30,97	13,26	2,39	0,30	3,04	2,39
16	19,34	3,10	16,31	3,27	0,41	3,73	19,58	7,80	1,23	0,30	2,15	1,60
13,5	10,43	1,05	12,58	1,97	0,18	2,86	13,62	3,76	0,66	0,14	0,59	0,70
11,4	4,80	0,44	5,65	0,93	0,00	1,84	8,28	2,37	0,37	0,04	0,18	0,40
9,6	3,15	0,21	3,29	0,56		1,44	6,49	1,63	0,15	0,04	0,18	0,23
8,1	2,16	0,13	1,36	0,35		1,15	4,47	1,02	0,11	0,04	0,18	0,12
6,8	1,50	0,13	0,73	0,22		0,82	3,23	0,67	0,07	0,04	0,00	0,07
5,7	1,21	0,07	0,25	0,13		0,36	1,95	0,27	0,04	0,04		0,02
4,8	0,99	0,04	0,08	0,07		0,24	1,49	0,17	0,02	0,03		0,01
4,1	0,45	0,02	0,08	0,03		0,12	0,49	0,10	0,01	0,01		0,00
3,4	0,30	0,02	0,08	0,01		0,08	0,32	0,06	0,01	0,00		
2,9	0,01	0,00	0,02	0,00		0,01	0,01	0,02	0,00			
2,4	0,01		0,02			0,01	0,01	0,02				
2	0,00		0,02			0,00	0,01	0,00				
1,75			0,02				0,01					
1,45			0,00				0,00					
1,2												

3) 391 Magnetic fraction

	Cumulative passing (wt%)											
	391											
Sieve size (um)	Chamosite	Amphibole	Tourmaline	Almandine	Grossular	Magnetite	Ilmenite	Rutile	Titanite	Zircon	Apatite	Other
250												
212						100,00			100,00			
180		100,00		100,00	100,00	93,47		100,00	98,46	100,00		
150		80,69		94,51	60,29	85,08		75,98	87,18	82,19		100,00
125		80,69		79,62	47,86	64,70		57,81	76,14	66,60		93,69
106		80,69		69,80	38,43	39,93	100,00	51,38	62,32	57,90	100,00	90,49
90		72,41		56,19	31,55	29,52	83,67	48,89	48,59	44,68	66,43	64,76
75		62,38		42,96	22,20	18,89	83,67	35,99	36,86	29,90	66,43	51,79
63	100,00	49,00		35,32	6,17	14,15	75,52	30,01	28,94	26,97	48,42	42,20
53	95,37	37,12		28,38	6,17	11,10	72,77	26,72	18,91	15,62	35,18	33,14
45	90,60	35,19		23,42	2,79	7,49	58,52	20,77	12,64	8,85	35,18	25,40
38	87,11	30,22		19,38	1,36	6,08	50,83	18,67	8,66	4,22	23,93	16,26
32	81,41	23,32		16,79	1,36	4,46	46,80	13,46	5,28	3,28	14,52	12,25
27	74,16	18,95	100,00	13,71	1,36	3,66	43,70	11,37	3,46	1,52	11,26	10,36
22	59,79	12,16	85,30	9,54	0,84	2,44	36,15	7,38	2,09	0,36	5,32	7,66
19	48,77	9,10	73,13	7,54	0,51	1,77	32,63	6,20	1,52	0,36	5,32	5,30
16	29,19	3,32	54,09	4,86	0,31	1,23	13,34	2,97	0,85	0,36	2,30	3,12
13,5	16,74	1,37	35,22	2,85	0,03	0,91	8,71	1,50	0,48	0,36	1,52	1,44
11,4	7,48	0,40	14,70	1,38	0,03	0,58	5,93	0,99	0,22	0,25	0,00	0,74
9,6	4,59	0,22	7,04	0,72	0,03	0,46	4,25	0,59	0,11	0,25		0,53
8,1	2,93	0,08	1,65	0,38	0,03	0,34	3,34	0,45	0,05	0,15		0,21
6,8	2,22	0,08	1,65	0,22	0,03	0,25	2,38	0,30	0,03	0,15		0,10
5,7	1,44	0,05	0,35	0,09	0,03	0,13	1,63	0,11	0,02	0,09		0,06
4,8	0,93	0,03	0,35	0,06	0,01	0,10	1,20	0,07	0,02	0,09		0,05
4,1	0,46	0,01	0,35	0,02	0,01	0,04	0,46	0,02	0,01	0,02		0,03
3,4	0,25	0,00	0,35	0,01	0,01	0,02	0,26	0,02	0,01	0,00		0,02
2,9	0,03		0,00	0,00	0,00	0,00	0,01	0,00	0,00			0,00
2,4	0,03						0,01					
2	0,01						0,00					
1,75	0,01											
1,45	0,00											
1,2												

4) 393 Magnetic fraction

	Cumulative passing (wt%)											
	393											
Sieve size (um)	Chamosite	Amphibole	Tourmaline	Almandine	Grossular	Magnetite	Ilmenite	Rutile	Titanite	Zircon	Apatite	Other
250				100,00					100,00			
212				97,89	100,00	100,00	100,00		96,27			
180				94,76	68,07	96,50	74,69	100,00	93,71			100,00
150				84,90	45,05	81,13	56,28	93,62	83,91			79,87
125		100,00		64,91	28,97	60,68	56,28	84,29	66,25	100,00		79,87
106		93,35		48,48	23,35	50,61	56,28	65,65	56,17	71,53	100,00	74,13
90		75,32	100,00	37,12	14,85	30,99	49,36	58,15	42,27	52,87	48,30	59,75
75	100,00	75,32	23,68	28,68	12,12	21,73	49,36	52,78	27,95	38,24	48,30	48,70
63	97,17	57,89	23,68	21,56	6,30	14,55	45,49	46,47	18,41	38,24	48,30	38,52
53	95,09	51,61	23,68	16,97	4,97	10,74	43,31	42,98	13,69	14,65	48,30	29,71
45	91,77	41,83	23,68	14,34	3,76	9,01	41,62	33,70	9,29	14,65	48,30	21,43
38	86,82	35,52	23,68	11,66	2,29	6,43	39,27	28,71	5,96	4,09	38,70	17,08
32	83,42	30,65	23,68	9,62	2,29	5,31	33,90	20,58	3,91	4,09	32,20	12,31
27	78,72	26,09	23,68	7,98	1,54	4,30	29,74	15,65	2,67	1,90	21,12	9,19
22	64,88	18,71	17,98	5,81	1,54	3,45	22,42	11,57	1,86	1,90	17,88	6,28
19	51,97	15,23	13,61	4,54	1,54	3,05	20,95	8,72	1,33	1,90	17,88	4,92
16	28,71	6,28	8,24	2,95	0,79	1,89	8,35	3,77	0,77	1,16	7,40	3,03
13,5	15,90	2,39	5,92	1,72	0,37	1,13	4,83	1,96	0,43	1,16	4,87	1,63
11,4	6,74	0,64	2,81	0,67	0,17	0,75	3,79	0,95	0,21	1,16	1,78	0,81
9,6	4,39	0,45	2,81	0,41	0,12	0,57	3,01	0,80	0,11	0,16	0,46	0,53
8,1	2,65	0,21	0,49	0,24	0,08	0,41	2,21	0,50	0,07	0,16	0,00	0,33
6,8	1,97	0,18	0,49	0,13	0,06	0,29	1,31	0,37	0,04	0,16		0,17
5,7	1,58	0,09	0,49	0,09	0,04	0,22	0,94	0,23	0,02	0,16		0,10
4,8	1,22	0,08	0,22	0,05	0,03	0,15	0,59	0,17	0,02	0,04		0,07
4,1	0,53	0,04	0,22	0,03	0,00	0,06	0,20	0,08	0,01	0,00		0,03
3,4	0,34	0,02	0,22	0,02		0,02	0,08	0,04	0,00			0,01
2,9	0,04	0,01	0,00	0,00		0,00	0,01	0,00				0,00
2,4	0,04	0,01					0,01					
2	0,01	0,00					0,00					
1,75	0,01											
1,45	0,00											
1,2												

5) BS Magnetic fraction

	Cumulative passing (wt%)											
	BS											
Sieve size (um)	Chamosite	Amphibole	Tourmaline	Almandine	Grossular	Magnetite	Ilmenite	Rutile	Titanite	Zircon	Apatite	Other
250									100,00			
212				100,00					98,43			
180				94,56	100,00				98,43		100,00	
150				94,56	94,18				95,26		95,67	
125			100,00	91,87	87,59	100,00			85,71		83,05	100,00
106		100,00	77,91	82,16	77,94	96,69		100,00	73,45		64,78	97,46
90	100,00	92,87	77,91	75,64	58,13	96,69		78,02	54,77	100,00	39,75	89,52
75	95,64	78,33	64,89	65,69	37,85	83,63		62,56	36,69	80,93	20,35	78,08
63	90,14	65,59	62,36	58,65	21,59	58,41	100,00	51,03	20,76	59,20	10,30	63,25
53	85,82	56,33	60,53	50,84	13,32	43,18	84,94	31,56	12,72	33,73	5,97	50,39
45	81,27	51,28	60,53	47,66	7,36	28,88	68,67	25,01	8,33	23,12	2,77	39,29
38	74,20	43,55	56,88	41,69	5,08	18,67	58,47	18,15	5,25	10,53	1,93	28,33
32	66,11	38,39	49,72	37,82	2,98	11,82	45,70	11,45	3,41	4,84	1,29	22,10
27	58,18	31,29	43,31	33,78	2,23	8,65	28,60	10,44	2,38	1,77	0,89	17,29
22	48,05	24,85	33,93	26,22	1,39	5,42	21,32	6,71	1,42	1,15	0,43	11,92
19	37,40	22,26	27,58	21,64	0,95	4,12	16,80	5,19	1,13	0,76	0,29	9,06
16	25,76	13,61	17,36	14,03	0,44	2,83	10,87	1,23	0,65	0,48	0,11	5,21
13,5	17,41	7,58	8,49	8,26	0,26	1,45	6,83	0,92	0,36	0,48	0,01	2,68
11,4	11,21	2,60	3,61	3,99	0,19	1,09	3,77	0,71	0,22	0,48	0,01	1,34
9,6	7,05	0,94	1,65	2,26	0,12	0,75	3,05	0,26	0,16	0,39	0,01	0,78
8,1	5,40	0,60	1,10	1,41	0,05	0,44	2,59	0,26	0,10	0,32	0,01	0,42
6,8	3,86	0,45	0,63	0,89	0,05	0,39	1,98	0,20	0,07	0,27	0,01	0,20
5,7	2,80	0,33	0,31	0,52	0,03	0,31	0,87	0,15	0,04	0,16	0,00	0,09
4,8	1,73	0,29	0,19	0,34	0,02	0,14	0,69	0,11	0,02	0,12		0,05
4,1	0,93	0,19	0,08	0,17	0,01	0,03	0,28	0,09	0,01	0,08		0,02
3,4	0,57	0,11	0,06	0,10	0,00	0,01	0,15	0,07	0,00	0,05		0,01
2,9	0,03	0,02	0,02	0,02		0,00	0,01	0,01		0,01		0,00
2,4	0,03	0,02	0,02	0,02			0,01	0,01		0,01		
2	0,02	0,01	0,01	0,01			0,00	0,00		0,01		
1,75	0,02	0,01	0,01	0,01						0,01		
1,45	0,00	0,00	0,00	0,00						0,00		
1,2												

6) 387 Apatite fraction

	Cumulative passing (wt%)											
	387											
Sieve size (um)	Chamosite	Amphibole	Tourmaline	Almandine	Grossular	Magnetite	Ilmenite	Rutile	Titanite	Zircon	Apatite	Other
250											100,00	
212											97,65	
180											80,84	
150											48,72	
125									100,00		20,23	100,00
106									39,75		7,38	70,29
90									16,02		2,58	70,29
75									16,02		0,65	44,85
63				100,00					16,02		0,14	25,99
53				84,09					2,36	100,00	0,07	15,73
45				74,02					2,36	19,44	0,01	11,34
38				57,56					2,36	19,44	0,01	7,66
32	100,00			49,32					2,36	19,44	0,01	5,05
27	88,20		100,00	38,86					0,71	19,44	0,01	5,05
22	79,67		38,93	28,94					0,71	19,44	0,00	4,54
19	60,38	100,00	38,93	22,95					0,71	19,44		4,11
16	19,55	7,60	5,00	14,28	100,00				0,71	8,54		2,27
13,5	2,80	7,60	5,00	6,97	47,94				0,23	0,85		1,10
11,4	2,80	0,00	5,00	2,93	23,17				0,23	0,85		0,47
9,6	2,80		5,00	0,71	5,96				0,00	0,85		0,17
8,1	2,80		5,00	0,54	0,00					0,85		0,14
6,8	1,94		5,00	0,26						0,85		0,08
5,7	1,94		0,00	0,17						0,85		0,00
4,8	1,12			0,17						0,00		
4,1	0,82			0,09								
3,4	0,17			0,05								
2,9	0,00			0,00								
2,4												
2												
1,75												
1,45												
1,2												

7) 391 Apatite fraction

	Cumulative passing (wt%)											
	391											
Sieve size (um)	Chamosite	Amphibole	Tourmaline	Almandine	Grossular	Magnetite	Ilmenite	Rutile	Titanite	Zircon	Apatite	Other
250											100,00	100,00
212											95,15	98,11
180											93,63	89,90
150											74,51	76,81
125											36,34	50,78
106											21,46	33,32
90									100,00		9,46	18,87
75									64,23		2,71	7,62
63								100,00	64,23		0,75	4,05
53								60,70	52,80		0,11	1,56
45				100,00				60,70	24,16		0,01	0,65
38				95,78				60,70	18,94		0,01	0,39
32				89,20				44,01	18,94		0,01	0,17
27		100,00		79,49				44,01	13,55	100,00	0,01	0,06
22	100,00	87,22		62,68				28,41	6,41	3,13	0,01	0,04
19	90,40	77,33	100,00	50,86				22,80	3,69	3,13	0,01	0,04
16	63,87	56,29	50,94	32,33		100,00		19,25	3,69	3,13	0,01	0,03
13,5	32,25	26,13	34,51	17,67		43,97		8,82	3,03	3,13	0,01	0,02
11,4	19,48	0,07	10,56	6,89		0,00		6,97	1,67	3,13	0,00	0,01
9,6	11,71	0,07	0,00	3,12				5,73	1,29	3,13		0,01
8,1	10,02	0,07		2,29				3,47	0,86	3,13		0,01
6,8	8,82	0,07		1,49				2,64	0,48	3,13		0,01
5,7	5,01	0,07		0,94				0,38	0,37	3,13		0,00
4,8	4,30	0,07		0,76				0,00	0,12	3,13		
4,1	3,25	0,07		0,41					0,00	0,00		
3,4	1,13	0,07		0,22								
2,9	0,00	0,07		0,00								
2,4		0,07										
2		0,07										
1,75		0,07										
1,45		0,00										
1,2												

8) BS Apatite fraction

	Cumulative passing (wt%)											
	BS											
Sieve size (um)	Chamosite	Amphibole	Tourmaline	Almandine	Grossular	Magnetite	Ilmenite	Rutile	Titanite	Zircon	Apatite	Other
250												
212											100,00	
180											97,21	
150											82,33	100,00
125									100,00		61,57	81,80
106									75,32		37,46	81,80
90									44,14		18,95	81,80
75									44,14		6,74	75,08
63									29,89		1,31	54,51
53									29,89		0,33	48,69
45									22,43		0,01	40,03
38	00,00			100,00					16,45		0,01	34,38
32	76,67		100,00	96,41					14,31		0,01	27,16
27	61,99		93,71	87,71					11,45		0,01	23,18
22	61,99	100,00	73,20	81,37	100,00				3,95		0,01	16,53
19	48,65	67,51	58,48	73,00	64,22				2,61		0,01	12,67
16	33,72	42,82	32,31	62,36	38,93				1,63		0,01	6,43
13,5	30,52	23,17	21,01	31,51	19,92				0,95	100,00	0,00	3,62
11,4	17,38	10,08	7,14	12,64	19,92				0,68	29,68		1,02
9,6	13,49	0,00	3,94	5,11	0,00				0,34	29,68		0,42
8,1	8,24		1,11	2,40					0,23	14,84		0,29
6,8	6,54		0,72	0,83					0,15	14,84		0,08
5,7	6,54		0,48	0,58					0,09	7,10		0,00
4,8	5,14		0,48	0,58					0,04	7,10		
4,1	2,30		0,32	0,24					0,01	3,23		
3,4	0,80		0,02	0,14					0,01	0,00		
2,9	0,00		0,02	0,02					0,01			
2,4			0,02	0,02					0,01			
2			0,02	0,02					0,00			
1,75			0,02	0,02								
1,45			0,00	0,00								
1,2												

9) 387 Zircon fraction

	Cumulative passing (wt%)											
	387											
Sieve size (um)	Chamosite	Amphibole	Tourmaline	Almandine	Grossular	Magnetite	Ilmenite	Rutile	Titanite	Zircon	Apatite	Other
300										100,00		
250								100,00		96,519		
212								95,28	100,00	96,519		
180								84,59	97,74	80,33	100,00	
150								67,02	79,09	70,61	78,64	
125								35,14	62,70	48,09	63,74	
106								19,49	48,22	30,95	32,52	100,00
90								11,96	30,68	17,01	14,18	87,39
75								5,38	14,61	8,31	11,46	56,99
63								3,40	6,95	4,21	5,77	45,80
53				100,00				1,43	3,97	1,96	5,77	35,47
45				95,70				0,77	2,17	1,03	4,83	35,47
38				83,50				0,35	1,45	0,35	3,44	27,83
32	100,00			72,20				0,17	0,57	0,15	2,03	25,94
27	83,66		100,00	62,72			100,00	0,14	0,52	0,10	1,39	17,79
22	72,64	100,00	69,45	48,92			95,33	0,11	0,26	0,04	1,20	14,21
19	51,12	54,97	17,86	42,06	100,00		91,55	0,09	0,16	0,04	1,02	12,13
16	30,67	22,36	17,86	27,99	61,39		77,48	0,05	0,07	0,03	0,52	5,72
13,5	11,20	22,36	17,86	17,17	27,03	100,00	36,70	0,03	0,06	0,02	0,14	2,73
11,4	4,44	22,36	0,00	3,99	8,88	31,08	2,92	0,02	0,04	0,02	0,14	0,99
9,6	3,48	10,87		0,77	8,88	31,08	1,98	0,01	0,02	0,01	0,05	0,47
8,1	2,07	1,86		0,36	0,00	31,08	1,45	0,01	0,01	0,01	0,02	0,24
6,8	1,16	1,86		0,26		31,08	0,97	0,01	0,00	0,00	0,00	0,16
5,7	0,40	1,86		0,17		31,08	0,35	0,00				0,10
4,8	0,40	1,86		0,12		16,22	0,35					0,05
4,1	0,23	0,00		0,04		6,76	0,02					0,04
3,4	0,10			0,04		0,00	0,02					0,04
2,9	0,00			0,01			0,02					0,00
2,4				0,01			0,02					
2				0,01			0,02					
1,75				0,01			0,02					
1,45				0,00			0,00					
1,2												

10) 391 Zircon fraction

	Cumulative passing (wt%)											
	391											
Sieve size (um)	Chamosite	Amphibole	Tourmaline	Almandine	Grossular	Magnetite	Ilmenite	Rutile	Titanite	Zircon	Apatite	Other
300												
250												
212								100,00		100		
180								96,30		98,23	100,00	
150								85,21	100,00	89,61	77,77	
125								56,66	92,41	67,52	77,77	
106								34,55	81,04	42,05	58,73	
90								25,74	68,67	23,51	40,02	100,00
75								14,81	36,71	11,46	21,12	86,14
63								6,97	26,05	5,64	21,12	75,07
53				100,00				4,41	14,61	2,90	13,44	56,29
45				96,16				2,28	6,70	1,41	11,54	40,12
38	100,00			93,40				1,28	4,08	0,52	11,54	32,58
32	93,75			83,67	100,00			0,86	2,32	0,24	9,87	29,72
27	84,53			80,40	64,06			0,46	1,42	0,12	8,79	25,93
22	70,98		100,00	58,61	16,74	100,00	100,00	0,22	1,05	0,03	6,74	20,84
19	55,10	100,00	31,34	48,17	16,74	63,38	89,91	0,14	0,58	0,01	4,69	17,17
16	38,04	39,50	31,34	35,86	4,08	63,38	77,30	0,07	0,39	0,01	1,64	8,71
13,5	17,32	0,00	31,34	20,68	4,08	25,37	44,96	0,07	0,15	0,01	0,85	5,19
11,4	5,08		0,00	5,08	4,08	25,37	6,24	0,05	0,05	0,01	0,52	2,17
9,6	2,34			1,27	0,00	16,52	6,24	0,02	0,02	0,00	0,13	1,18
8,1	2,34			0,51		3,11	2,65	0,02	0,00		0,00	0,52
6,8	1,69			0,22		3,11	1,58	0,01				0,08
5,7	0,81			0,17		3,11	0,69	0,01				0,08
4,8	0,81			0,11		3,11	0,69	0,00				0,08
4,1	0,58			0,05		1,20	0,25					0,01
3,4	0,18			0,00		0,00	0,25					0,01
2,9	0,05						0,06					0,01
2,4	0,05						0,06					0,01
2	0,02						0,06					0,01
1,75	0,02						0,06					0,01
1,45	0,00						0,00					0,00
1,2												

11) BS Zircon fraction

	Cumulative passing (wt%)											
	BS											
Sieve size (um)	Chamosite	Amphibole	Tourmaline	Almandine	Grossular	Magnetite	Ilmenite	Rutile	Titanite	Zircon	Apatite	Other
300												
250												
212												
180									100,00		100,00	
150									98,03		96,06	
125								100,00	93,62	100,00	89,18	
106								90,41	78,58	89,93	73,40	
90								79,34	56,44	78,31	48,25	
75								43,55	30,51	45,96	27,71	100,00
63								26,01	17,03	21,88	12,50	90,97
53								19,81	8,73	11,56	5,52	76,43
45								15,46	5,55	5,82	2,76	66,01
38								9,91	3,85	2,43	1,31	58,19
32			100,00					6,98	2,32	0,48	0,99	47,20
27	100,00		88,96	100,00	100,00			4,39	1,57	0,33	0,99	41,01
22	78,98		88,96	89,51	67,37			2,77	0,80	0,22	0,61	31,41
19	78,98	100,00	83,49	79,84	48,10			2,05	0,51	0,16	0,49	24,05
16	67,18	59,11	49,78	55,69	21,94			0,62	0,31	0,07	0,12	17,23
13,5	32,59	24,00	25,68	30,12	11,11	100,00		0,19	0,10	0,03	0,03	9,50
11,4	19,24	24,00	5,50	12,40	2,67	31,51		0,19	0,05	0,03	0,00	5,35
9,6	14,29	6,22	2,63	5,55	2,67	31,51		0,19	0,03	0,03		2,42
8,1	8,38	6,22	0,76	2,31	2,67	0,00		0,14	0,02	0,02		0,96
6,8	6,26	6,22	0,04	0,98	0,00			0,07	0,01	0,01		0,34
5,7	4,60	6,22	0,04	0,70				0,05	0,00	0,01		0,12
4,8	3,54	1,78	0,04	0,51			100,00	0,05		0,01		0,07
4,1	1,30	1,78	0,04	0,25			38,46	0,01		0,00		0,03
3,4	0,71	1,78	0,04	0,16			0,00	0,01				0,02
2,9	0,35	0,00	0,04	0,02				0,00				0,01
2,4	0,35		0,04	0,02								0,01
2	0,12		0,04	0,02								0,01
1,75	0,12		0,04	0,02								0,01
1,45	0,00		0,00	0,00								0,00
1,2												

Appendix M: Results from EMPA

Results from analyses with EMPA.

* Tourmaline: Add 10.5 wt% B2O3 to the sum. ** Magnetite: Something is wrong with the wt%-values, since the sum is below 90.0 wt%. According to the scientists performing the analyses with EMPA it might be water and Fe^{2+}, as Fe^{3+} is not considered. The FeO (Fe^{2+}) could be Fe_3O_4 (Fe^{3+}).

Sample/ fraction	Grain name/ measurement number	No.	Wt%												Mineral type
			Na2O	K2O	MnO	TiO2	MgO	CaO	FeO	Cr2O3	Al2O3	V2O3	SiO2	Total	
387 Mf	AMf387-Il1-1	173	0,000	0,006	0,094	12,763	0,000	0,024	77,666	0,061	0,057	0,519	0,000	91,188	
387 Mf	AMf387-Il1-2	174	0,040	0,010	0,134	10,053	0,000	0,001	79,577	0,038	0,000	0,630	0,000	90,483	Ilmenite
387 Mf	AMf387-Il1-3	175	0,000	0,015	0,166	11,712	0,000	0,016	79,704	0,000	0,095	0,584	0,000	92,291	
387 Mf	AMf387-Il1-4	176	0,000	0,000	0,315	12,016	0,000	0,000	77,100	0,000	0,026	0,596	0,051	90,105	
387 Mf	AMf387-T1-1	177	0,002	0,000	0,122	38,572	0,000	27,922	0,911	0,046	0,932	0,827	30,239	99,573	
387 Mf	AMf387-T1-2	178	0,031	0,000	0,080	37,433	0,000	27,892	1,008	0,000	1,197	0,874	30,391	98,906	Titanite
387 Mf	AMf387-T1-3	179	0,011	0,011	0,153	38,131	0,000	27,905	0,880	0,000	1,205	0,879	30,388	99,563	
387 Mf	AMf387-T1-4	180	0,000	0,001	0,123	37,911	0,000	28,172	0,969	0,067	1,026	0,894	30,199	99,362	
387 Mf	AMf387-T2-1	181	0,031	0,021	0,210	35,350	0,008	25,873	1,400	0,000	1,122	0,683	29,943	94,641	
387 Mf	AMf387-T2-2	182	0,000	0,000	0,150	37,181	0,000	27,629	1,031	0,036	1,058	0,777	30,046	97,907	Titanite
387 Mf	AMf387-T2-3	183	0,000	0,000	0,126	37,365	0,000	27,611	1,073	0,000	1,126	0,827	30,019	98,147	
387 Mf	AMf387-T2-4	184	0,004	0,004	0,151	37,265	0,000	27,742	1,122	0,000	1,066	0,847	30,269	98,470	
387 Mf	AMf387-G2-1	189	0,000	0,000	0,206	0,012	8,863	0,962	29,753	0,045	20,998	0,024	38,732	99,594	
387 Mf	AMf387-G2-2	190	0,026	0,000	0,156	0,005	8,787	0,933	29,602	0,000	20,820	0,068	38,802	99,198	Garnet
387 Mf	AMf387-G2-3	191	0,000	0,003	0,182	0,000	8,986	0,891	29,353	0,052	20,817	0,076	38,883	99,244	
387 Mf	AMf387-G2-4	192	0,000	0,005	0,176	0,001	9,055	0,865	29,191	0,120	20,965	0,045	39,269	99,691	
387 Mf	AMf387-G3-1	193	0,000	0,000	1,130	0,113	7,059	5,795	26,374	0,026	20,018	0,043	38,648	99,205	
387 Mf	AMf387-G3-2	194	0,012	0,010	1,109	0,087	7,072	5,846	25,328	0,000	20,090	0,000	38,945	98,499	Garnet
387 Mf	AMf387-G3-3	195	0,019	0,006	1,119	0,046	7,212	5,781	26,105	0,037	20,345	0,000	38,931	99,600	
387 Mf	AMf387-G3-4	196	0,000	0,000	1,112	0,207	7,171	5,821	26,309	0,025	20,186	0,075	39,377	100,283	
387 Mf	AMf387-Rt1-1	197	0,000	0,000	0,009	100,771	0,000	0,017	0,277	0,101	0,014	2,505	0,000	101,188	
387 Mf	AMf387-Rt1-2	198	0,000	0,010	0,000	101,326	0,000	0,018	0,177	0,117	0,046	2,471	0,000	101,694	Rutile
387 Mf	AMf387-Rt1-3	199	0,000	0,000	0,000	100,554	0,000	0,017	0,207	0,127	0,062	2,395	0,032	100,998	
387 Mf	AMf387-Rt1-4	200	0,000	0,008	0,007	100,923	0,000	0,019	0,280	0,170	0,082	2,531	0,000	101,489	
387 Mf	AMf387-G4-1	201	0,033	0,002	0,683	0,039	7,032	2,457	29,246	0,001	20,475	0,011	38,684	98,662	
387 Mf	AMf387-G4-2	202	0,037	0,009	0,697	0,000	7,149	2,466	28,996	0,008	20,554	0,000	38,847	98,762	Garnet
387 Mf	AMf387-G4-3	203	0,000	0,009	0,714	0,038	7,260	2,448	29,606	0,052	20,794	0,065	39,186	100,172	
387 Mf	AMf387-G4-4	204	0,012	0,000	0,722	0,076	7,280	2,576	28,989	0,034	20,660	0,000	39,195	99,544	
387 Mf	AMf387-Rt2-1	205	0,041	0,000	0,000	101,446	0,000	0,039	0,130	0,062	0,041	2,422	0,002	101,760	
387 Mf	AMf387-Rt2-2	206	0,000	0,002	0,025	101,394	0,000	0,009	0,119	0,100	0,036	2,372	0,000	101,683	Rutile
387 Mf	AMf387-Rt2-3	207	0,044	0,001	0,000	100,671	0,024	0,012	0,150	0,068	0,019	2,531	0,000	100,990	
387 Mf	AMf387-Rt2-4	208	0,051	0,001	0,004	100,415	0,000	0,008	0,183	0,066	0,000	2,466	0,000	100,729	

Sample/ fraction	Grain name/ measurement number	No.	Wt%												Mineral type
			Na_2O	K_2O	MnO	TiO_2	MgO	CaO	FeO	Cr_2O_3	Al_2O_3	V_2O_3	SiO_2	Total	
387 Mf	AMf387-Rt3-1	209	0,000	0,005	0,053	99,224	0,000	0,031	0,341	0,023	0,083	2,489	0,000	99,761	
387 Mf	AMf387-Rt3-2	210	0,000	0,000	0,000	99,668	0,000	0,005	0,257	0,026	0,094	2,337	0,055	100,105	Rutile
387 Mf	AMf387-Rt3-3	211	0,000	0,000	0,000	100,206	0,000	0,000	0,290	0,094	0,095	2,402	0,000	100,686	
387 Mf	AMf387-Rt3-4	212	0,036	0,000	0,033	99,021	0,000	0,020	0,334	0,104	0,099	2,408	0,068	99,714	
387 Mf	AMf387-G4-1	213	0,000	0,013	0,272	0,129	0,000	22,840	11,376	0,000	21,673	0,070	38,066	94,440	
387 Mf	AMf387-G4-2	214	0,025	0,000	0,212	0,036	0,000	22,890	12,068	0,000	21,580	0,004	37,809	94,625	Garnet
387 Mf	AMf387-G4-3	215	0,006	0,000	0,191	0,075	0,000	23,144	11,684	0,007	21,821	0,043	37,839	94,809	
387 Mf	AMf387-G4-4	216	0,000	0,000	0,162	0,122	0,000	23,307	11,864	0,000	21,583	0,045	37,849	94,931	
387 Mf	AMf387-T3-1	217	0,000	0,010	0,000	36,623	0,000	26,546	1,243	0,000	1,304	0,710	29,385	95,820	
387 Mf	AMf387-T3-2	218	0,000	0,005	0,063	37,504	0,000	27,554	0,989	0,047	1,065	0,787	30,040	98,053	Titanite
387 Mf	AMf387-T3-3	219	0,027	0,014	0,041	36,499	0,000	26,499	1,214	0,000	1,227	0,698	29,609	95,828	
387 Mf	AMf387-T3-4	220	0,000	0,008	0,000	36,417	0,000	26,342	1,311	0,000	1,293	0,602	29,617	95,588	
387 Mf	AMf387-T4-1	221	0,004	0,018	0,043	42,587	0,000	25,984	1,448	0,049	0,922	0,920	27,582	99,556	
387 Mf	AMf387-T4-2	222	0,028	0,009	0,001	42,560	0,000	26,504	0,911	0,048	0,845	0,802	28,489	100,196	Titanite
387 Mf	AMf387-T4-3	223	0,000	0,002	0,028	40,540	0,000	27,892	1,160	0,040	0,678	0,838	29,915	101,093	
387 Mf	AMf387-T4-4	224	0,000	0,006	0,021	39,973	0,012	27,972	1,173	0,000	0,754	0,730	29,536	100,177	
BS Mf	AMf-BS-T1-1	233	0,026	0,000	0,099	38,656	0,000	27,931	0,602	0,027	1,172	0,844	30,341	99,698	Titanite
BS Mf	AMf-BS-T1-2	234	0,002	0,003	0,091	39,031	0,000	28,278	0,575	0,000	1,145	0,782	30,422	100,329	
BS Mf	AMf-BS-T2-1	235	0,011	0,000	0,094	38,693	0,000	28,431	0,760	0,000	1,153	0,857	30,723	100,722	
BS Mf	AMf-BS-T2-2	236	0,000	0,003	0,103	38,356	0,000	28,464	0,758	0,016	1,158	0,834	30,606	100,298	Titanite
BS Mf	AMf-BS-T2-3	237	0,000	0,008	0,105	38,142	0,000	28,509	0,778	0,067	1,219	0,911	30,607	100,348	
BS Mf	AMf-BS-G2-1	238	0,017	0,000	0,228	0,074	0,081	23,202	10,651	0,000	23,040	0,089	38,012	95,393	
BS Mf	AMf-BS-G2-2	239	0,002	0,003	0,219	0,030	0,079	23,093	10,003	0,032	22,889	0,037	38,011	94,398	Garnet
BS Mf	AMf-BS-G2-3	240	0,020	0,000	0,255	0,068	0,091	23,155	10,609	0,055	22,883	0,024	38,047	95,206	
BS Mf	AMf-BS-G3-1	241	0,003	0,000	0,088	0,067	0,047	23,284	11,076	0,000	22,315	0,000	38,106	94,986	
BS Mf	AMf-BS-G3-2	242	0,000	0,000	0,092	0,120	0,008	22,973	11,684	0,000	21,736	0,011	37,896	94,519	Garnet
BS Mf	AMf-BS-G3-3	243	0,002	0,000	0,051	0,092	0,068	23,204	12,105	0,000	21,565	0,054	37,941	95,082	
BS Mf	AMf-BS-G3-4	244	0,000	0,003	0,039	0,060	0,004	23,144	11,548	0,000	22,012	0,000	38,182	94,991	
BS Mf	AMf-BS-G4-1	245	0,016	0,008	0,246	0,076	8,043	1,093	30,879	0,020	20,490	0,028	38,819	99,719	
BS Mf	AMf-BS-G4-2	246	0,000	0,000	0,293	0,039	8,101	1,062	30,273	0,003	20,715	0,000	39,064	99,550	Garnet
BS Mf	AMf-BS-G4-3	247	0,021	0,000	0,317	0,021	8,273	1,073	30,469	0,004	20,818	0,019	38,755	99,769	
BS Mf	AMf-BS-G4-4	248	0,000	0,000	0,259	0,079	8,351	1,071	30,263	0,066	20,700	0,004	38,922	99,714	
BS Mf	AMf-BS-Tu1-1	249	2,183	0,034	0,011	0,524	7,775	0,982	6,851	0,003	29,294	0,033	36,245	83,934	
BS Mf	AMf-BS-Tu1-2	250	2,150	0,045	0,000	0,519	7,803	1,050	6,837	0,022	29,414	0,000	36,245	84,084	Tourmaline*
BS Mf	AMf-BS-Tu1-3	251	2,218	0,047	0,052	0,533	7,878	0,999	6,843	0,053	29,383	0,014	36,216	84,235	
BS Mf	AMf-BS-Tu1-4	252	2,233	0,022	0,027	0,523	7,783	0,968	6,924	0,114	29,158	0,080	36,102	83,933	
BS Mf	AMf-BS-G5-1	253	0,003	0,000	0,126	0,077	9,145	1,058	29,160	0,008	20,897	0,054	39,488	100,016	
BS Mf	AMf-BS-G5-2	254	0,000	0,018	0,185	0,000	9,166	1,115	29,573	0,060	21,048	0,092	39,340	100,596	Garnet
BS Mf	AMf-BS-G5-3	255	0,016	0,006	0,124	0,033	9,224	0,918	28,885	0,043	21,009	0,000	39,207	99,463	

Sample/ fraction	Grain name/ measurement number	No.	Wt%												Mineral type
			Na2O	K2O	MnO	TiO2	MgO	CaO	FeO	Cr2O3	Al2O3	V2O3	SiO2	Total	
BS Mf	AMf-BS-Tu2-1	256	1,859	0,027	0,000	0,874	7,054	0,778	5,093	0,123	30,937	0,127	36,227	83,098	
BS Mf	AMf-BS-Tu2-2	257	1,845	0,013	0,003	0,929	7,037	0,779	4,992	0,140	31,393	0,114	35,976	83,223	Tourmaline*
BS Mf	AMf-BS-Tu2-3	258	1,815	0,029	0,021	0,797	7,133	0,793	5,231	0,117	31,362	0,088	36,224	83,609	
BS Mf	AMf-BS-Tu2-4	259	1,846	0,018	0,019	0,808	7,147	0,780	5,060	0,018	31,583	0,101	36,614	83,995	
BS Mf	AMf-BS-G6-1	260	0,000	0,019	0,315	0,077	0,025	22,665	10,041	0,049	22,991	0,060	38,137	94,378	Garnet
BS Mf	AMf-BS-G6-2	261	0,006	0,000	0,280	0,208	0,044	22,879	9,843	0,000	23,315	0,045	38,350	94,971	
BS Mf	AMf-BS-Tu3-1	262	1,943	0,041	0,102	0,392	3,034	0,338	12,485	0,021	30,532	0,000	35,375	84,263	
BS Mf	AMf-BS-Tu3-2	263	2,081	0,059	0,141	0,571	3,108	0,466	12,774	0,003	30,175	0,022	35,168	84,567	Tourmaline*
BS Mf	AMf-BS-Tu3-3	264	2,117	0,050	0,144	0,136	3,589	0,468	12,212	0,008	30,318	0,000	35,072	84,114	
BS Mf	AMf-BS-G7-1	265	0,000	0,012	0,039	0,175	0,070	23,303	8,383	0,000	24,861	0,000	38,493	95,335	
BS Mf	AMf-BS-G7-2	266	0,000	0,006	0,071	0,211	0,039	23,283	7,980	0,000	24,670	0,049	38,536	94,844	Garnet
BS Mf	AMf-BS-G7-3	267	0,000	0,015	0,036	0,123	0,060	22,855	8,414	0,000	24,542	0,050	38,681	94,775	
BS Mf	AMf-BS-T3-1	268	0,000	0,000	0,082	38,663	0,000	28,670	0,507	0,000	1,244	0,824	30,517	100,507	
BS Mf	AMf-BS-T3-2	269	0,006	0,000	0,076	37,987	0,000	28,465	0,630	0,023	1,335	0,778	30,529	99,829	Titanite
BS Mf	AMf-BS-T3-3	270	0,000	0,012	0,108	38,175	0,000	28,652	0,553	0,000	1,388	0,807	30,839	100,534	
391 Mf	EMf391-T1-4	209	0,000	0,004	0,025	43,175	0,000	25,526	2,599	0,046	0,733	1,004	27,840	100,950	Titanite
391 Mf	EMf391-A1-2	211	0,115	0,000	3,640	0,083	2,636	8,444	25,526	0,000	20,506	0,052	38,013	99,014	
391 Mf	EMf391-A1-3	212	0,023	0,015	3,647	0,062	2,880	8,313	26,400	0,007	20,446	0,115	37,981	99,888	Garnet
391 Mf	EMf391-A1-4	213	0,075	0,000	3,349	0,064	3,129	8,245	26,143	0,000	20,298	0,066	37,860	99,227	
391 Mf	EMf391-M1-2	215	0,050	0,251	0,906	0,114	10,952	0,256	20,588	0,035	17,973	0,039	27,618	78,783	
391 Mf	EMf391-M1-3	216	0,000	0,000	0,101	5,491	0,000	0,007	84,601	0,060	0,056	0,236	0,125	90,675	Magnetite**
391 Mf	EMf391-M1-4	217	0,009	0,007	0,273	17,221	0,228	0,009	73,527	0,100	0,256	0,868	0,000	92,497	
391 Mf	EMf391-G2-2	219	0,016	0,011	0,415	0,025	7,815	1,596	29,684	0,000	21,366	0,000	38,579	99,507	Garnet
391 Mf	EMf391-G2-3	220	0,007	0,000	0,419	0,031	7,462	1,596	29,659	0,005	21,352	0,000	38,486	99,016	
391 Mf	EMf391-R1-1	221	0,000	0,002	0,055	100,192	0,000	0,049	0,204	0,148	0,069	2,468	0,000	100,720	
391 Mf	EMf391-R1-2	222	0,000	0,013	0,021	100,584	0,000	0,031	0,155	0,039	0,080	2,435	0,020	100,943	Rutile
391 Mf	EMf391-R1-3	223	0,000	0,000	0,003	102,102	0,000	0,017	0,147	0,060	0,093	2,466	0,000	102,422	
391 Mf	EMf391-M2-1	224	0,000	0,000	0,309	45,995	0,050	0,060	44,888	0,078	0,058	1,055	0,949	93,442	
391 Mf	EMf391-M2-2	225	0,007	0,016	0,263	16,832	0,005	0,017	74,523	0,065	0,014	0,661	0,000	92,403	Magnetite**
391 Mf	EMf391-M2-3	226	0,005	0,011	0,033	13,698	0,000	0,035	77,601	0,038	0,085	0,624	0,029	92,159	
391 Mf	EMf391-M2-4	227	0,056	0,000	0,109	47,349	0,051	0,007	44,560	0,000	0,034	1,118	0,000	93,282	
391 Mf	EMf391-G3-2	229	0,012	0,000	1,602	0,000	5,264	3,145	29,810	0,093	20,830	0,021	38,139	98,916	
391 Mf	EMf391-G3-3	230	0,019	0,000	1,592	0,088	5,337	3,125	30,475	0,000	21,059	0,037	38,334	100,065	Garnet
391 Mf	EMf391-G3-4	231	0,000	0,000	1,667	0,000	5,178	3,168	30,497	0,034	21,170	0,000	38,281	99,995	
391 Mf	EMf391-G3-5	232	0,000	0,007	1,637	0,000	5,200	3,187	30,599	0,000	21,073	0,000	38,321	100,023	
391 Mf	EMf391-M3-1	233	0,000	2,136	0,033	15,777	0,308	0,029	64,891	0,018	2,933	0,342	5,454	91,921	
391 Mf	EMf391-M3-2	234	0,000	0,019	0,000	30,131	0,000	0,067	62,453	0,024	0,084	0,632	0,336	93,744	Magnetite**
391 Mf	EMf391-M3-3	235	0,054	0,000	0,004	29,515	0,000	0,056	62,060	0,000	0,437	0,563	0,449	93,137	
391 Mf	EMf391-M3-4	236	0,045	0,011	0,005	20,756	0,000	0,058	70,990	0,071	0,172	0,411	0,262	92,779	

Sample/ fraction	Grain name/ measurement number	No.	Wt%											Mineral type
			Na2O	K2O	MnO	TiO2	MgO	CaO	FeO	Cr2O3	Al2O3	V2O3	SiO2	Total	
391 Mf	EMf391-M4-1	237	0,002	0,026	0,091	14,984	0,000	0,000	75,909	0,000	0,009	0,527	0,000	91,549	Magnetite**
391 Mf	EMf391-M4-2	238	0,000	0,008	0,071	11,476	0,000	0,012	80,215	0,058	0,000	0,357	0,000	92,196	
391 Mf	EMf391-M4-3	239	0,208	0,000	0,028	22,132	0,000	0,036	68,727	0,024	0,004	0,715	0,000	91,875	
391 Mf	EMf391-M4-4	240	0,045	0,000	0,000	9,467	0,000	0,035	81,660	0,105	0,060	0,327	0,000	91,698	
391 Mf	EMf391-M4-5	241	0,024	0,011	0,140	11,892	0,000	0,000	79,803	0,000	0,093	0,412	0,030	92,405	
391 Mf	EMf391-R2-1	242	0,025	0,015	0,000	103,048	0,000	0,022	0,633	0,037	0,021	2,033	0,000	103,801	Rutile
391 Mf	EMf391-R2-2	243	0,009	0,000	0,000	102,867	0,000	0,020	0,401	0,036	0,023	2,142	0,000	103,355	
391 Mf	EMf391-R2-3	244	0,000	0,003	0,037	102,283	0,000	0,024	0,368	0,082	0,000	2,022	0,000	102,797	
391 Mf	EMf391-G4-1	245	0,000	0,002	0,142	0,000	8,687	0,721	30,173	0,001	21,374	0,027	38,821	99,946	Garnet
391 Mf	EMf391-G4-2	246	0,000	0,000	0,185	0,020	8,621	0,678	30,413	0,000	21,572	0,005	39,213	100,706	
391 Mf	EMf391-G4-3	247	0,000	0,003	0,272	0,125	8,781	0,764	30,063	0,000	21,641	0,020	39,092	100,760	
391 Mf	EMf391-G4-4	248	0,009	0,007	0,150	0,023	8,750	0,744	30,297	0,022	21,739	0,027	39,274	101,042	
391 Mf	EMf391-G4-5	249	0,000	0,010	0,209	0,000	8,643	0,772	30,155	0,047	21,751	0,071	39,577	101,235	
391 Mf	EMf391-T2-1	250	0,022	0,000	0,052	42,001	0,000	26,810	1,406	0,051	0,836	0,897	28,419	100,495	Titanite
391 Mf	EMf391-T2-2	251	0,000	0,000	0,047	40,817	0,000	26,846	3,301	0,026	0,943	0,746	28,473	101,200	
391 Mf	EMf391-T2-3	252	0,011	0,002	0,047	49,506	0,000	18,675	11,337	0,000	0,849	1,131	20,484	102,041	
391 Mf	EMf391-T2-4	253	0,000	0,006	0,000	41,659	0,006	27,723	0,543	0,014	0,780	0,955	29,501	101,188	
391 Mf	EMf391-T3-1	254	0,014	0,017	0,060	35,775	0,000	28,791	0,748	0,075	3,076	0,770	30,778	100,104	Titanite
391 Mf	EMf391-T3-2	255	0,037	0,009	0,078	36,080	0,000	28,658	0,756	0,030	3,015	0,784	30,859	100,305	
391 Mf	EMf391-T3-3	256	0,000	0,016	0,043	37,408	0,000	28,122	0,732	0,000	2,823	0,756	30,030	99,930	
391 Mf	EMf391-T3-4	257	0,000	0,004	0,021	35,744	0,000	28,005	0,764	0,000	3,000	0,791	30,940	99,268	
391 Mf	EMf391-G5-1	258	0,000	0,005	0,075	0,129	0,034	23,001	9,286	0,000	24,427	0,014	38,053	95,025	Garnet
391 Mf	EMf391-G5-2	259	0,000	0,000	0,153	0,072	0,014	23,193	9,562	0,000	24,383	0,075	37,915	95,366	
391 Mf	EMf391-G5-3	260	0,000	0,000	0,132	0,125	0,000	23,125	9,601	0,000	24,463	0,068	38,077	95,590	
391 Mf	EMf391-G5-4	261	0,029	0,015	0,111	0,092	0,019	23,541	9,344	0,028	24,592	0,054	38,373	96,197	
391 Mf	EMf391-R3-1	262	0,000	0,007	0,022	102,497	0,000	0,014	0,187	0,157	0,015	2,211	0,000	102,899	Rutile
391 Mf	EMf391-R3-2	263	0,011	0,000	0,027	101,924	0,000	0,023	0,160	0,224	0,041	2,223	0,000	102,411	
391 Mf	EMf391-R3-3	264	0,009	0,021	0,000	101,936	0,000	0,023	0,129	0,169	0,044	2,256	0,000	102,330	
391 Mf	EMf391-A2-1	265	0,014	0,000	6,091	0,053	0,582	9,774	24,806	0,024	19,809	0,059	36,986	98,198	Amphibole
391 Mf	EMf391-A2-2	266	0,086	0,015	6,095	0,050	0,540	10,032	24,884	0,025	19,768	0,000	37,177	98,673	
391 Mf	EMf391-A2-3	267	0,049	0,006	6,065	0,000	0,600	9,974	25,164	0,017	20,009	0,011	37,148	99,043	
391 Mf	EMf391-A2-4	268	0,064	0,000	5,842	0,057	0,554	9,985	24,697	0,102	19,950	0,056	37,377	98,684	
391 Mf	EMf391-A2-5	269	0,064	0,000	5,849	0,063	0,560	10,314	24,569	0,000	20,018	0,031	37,263	98,731	
391 Mf	EMf391-A2-6	270	0,000	0,013	5,873	0,000	0,603	10,273	25,170	0,000	19,556	0,007	37,450	98,944	
391 Mf	EMf391-R4-1	271	0,000	0,007	0,000	101,734	0,000	0,031	0,330	0,059	0,011	2,122	0,000	102,172	Rutile
391 Mf	EMf391-R4-2	272	0,000	0,000	0,012	101,881	0,000	0,025	0,209	0,064	0,032	2,137	0,000	102,222	
391 Mf	EMf391-R4-3	273	0,000	0,000	0,000	101,166	0,000	0,006	0,246	0,031	0,000	2,252	0,000	101,450	

Sample/ fraction	Grain name/ measurement number	No.	Wt%												Mineral type
			Na2O	K2O	MnO	TiO2	MgO	CaO	FeO	Cr2O3	Al2O3	V2O3	SiO2	Total	
391 Mf	EMf391-T4-1	274	0,000	0,011	0,066	36,710	0,000	28,041	1,145	0,024	1,600	0,764	30,032	98,393	
391 Mf	EMf391-T4-2	275	0,000	0,000	0,057	36,839	0,000	27,853	1,155	0,030	1,572	0,796	30,108	98,409	Titanite
391 Mf	EMf391-T4-3	276	0,002	0,010	0,024	37,441	0,000	27,981	0,969	0,000	1,557	0,766	30,143	98,894	
391 Mf	EMf391-T4-4	277	0,000	0,000	0,099	37,097	0,000	28,327	1,041	0,006	1,615	0,826	30,580	99,591	
391 Mf	EMf391-G6-1	278	0,050	0,003	0,353	0,000	6,899	1,352	31,023	0,023	21,361	0,029	38,046	99,138	
391 Mf	EMf391-G6-2	279	0,010	0,006	0,339	0,031	6,889	1,365	31,183	0,056	21,169	0,035	38,169	99,253	
391 Mf	EMf391-G6-3	280	0,050	0,004	0,393	0,019	6,942	1,368	31,369	0,107	21,328	0,000	38,401	99,980	Garnet
391 Mf	EMf391-G6-4	281	0,026	0,011	0,372	0,036	7,065	1,327	31,347	0,071	21,333	0,071	38,472	100,132	
391 Mf	EMf391-G6-5	282	0,011	0,006	0,359	0,005	6,903	1,333	31,057	0,053	21,268	0,006	38,495	99,496	
391 Mf	EMf391-R5-1	283	0,036	0,000	0,041	101,335	0,000	0,022	0,205	0,114	0,071	2,347	0,036	101,858	
391 Mf	EMf391-R5-2	284	0,000	0,002	0,013	101,876	0,000	0,011	0,154	0,060	0,055	2,292	0,000	102,171	Rutile
391 Mf	EMf391-R5-3	285	0,000	0,010	0,024	101,620	0,000	0,014	0,142	0,115	0,056	2,305	0,000	101,981	
391 Mf	EMf391-R5-4	286	0,013	0,012	0,000	102,415	0,000	0,007	0,068	0,056	0,000	2,297	0,000	102,571	
391 Mf	EMf391-M5-1	287	0,028	0,013	0,060	11,703	0,000	0,013	79,336	0,075	0,018	0,565	0,000	91,810	
391 Mf	EMf391-M5-2	288	0,014	0,000	0,114	10,741	0,000	0,004	80,114	0,081	0,000	0,491	0,050	91,610	Magnetite**
391 Mf	EMf391-M5-3	289	0,000	0,000	0,418	12,443	0,000	0,007	78,078	0,058	0,013	0,598	0,000	91,615	
391 Mf	EMf391-M5-4	290	0,000	0,000	0,046	11,424	0,000	0,013	79,963	0,023	0,000	0,438	0,000	91,907	
391 Mf	EMf391-G7-1	291	0,013	0,000	0,553	0,068	8,437	6,942	22,911	0,101	21,251	0,015	39,049	99,340	
391 Mf	EMf391-G7-2	292	0,055	0,011	0,627	0,120	8,463	6,936	22,885	0,046	21,399	0,000	39,167	99,709	Garnet
391 Mf	EMf391-G7-3	293	0,000	0,000	0,524	0,038	8,458	7,050	22,541	0,042	21,458	0,007	39,583	99,700	
391 Mf	EMf391-G7-4	294	0,028	0,000	0,527	0,036	8,324	6,970	23,068	0,066	21,434	0,000	39,689	100,142	
391 Mf	EMf391-T5-1	295	0,025	0,000	0,000	44,121	0,000	24,551	1,809	0,000	1,202	0,930	26,845	99,484	
391 Mf	EMf391-T5-2	296	0,122	0,000	0,103	68,398	0,015	9,579	6,983	0,000	0,611	1,359	10,326	97,497	Titanite
391 Mf	EMf391-T5-3	297	0,000	0,000	0,005	100,408	0,000	0,334	0,402	0,120	0,011	2,090	0,115	103,485	
391 Mf	EMf391-T5-4	298	0,000	0,000	0,026	102,002	0,000	0,406	0,333	0,038	0,038	2,119	0,000	104,961	
391 Mf	EMf391-T5-5	299	0,002	0,000	0,012	37,088	0,000	28,481	0,234	0,000	2,618	0,891	30,750	100,076	
391 Mf	EMf391-R6-1	300	0,000	0,000	0,031	101,165	0,000	0,010	0,478	0,059	0,030	2,196	0,033	101,806	
391 Mf	EMf391-R6-2	301	0,000	0,000	0,000	100,958	0,000	0,003	0,455	0,023	0,004	2,203	0,000	101,443	Rutile
391 Mf	EMf391-R6-3	302	0,009	0,000	0,018	101,366	0,000	0,032	0,504	0,080	0,037	2,236	0,018	102,064	
391 Mf	EMf391-R6-4	303	0,000	0,012	0,013	101,504	0,000	0,013	0,444	0,000	0,035	2,207	0,000	102,021	
391 Mf	EMf391-G8-1	304	0,014	0,006	0,654	0,055	4,433	1,055	34,726	0,040	20,876	0,036	37,589	99,483	
391 Mf	EMf391-G8-2	305	0,000	0,000	0,703	0,008	4,397	1,082	34,684	0,066	20,861	0,000	37,844	99,645	Garnet
391 Mf	EMf391-G8-3	306	0,049	0,000	0,602	0,000	4,429	1,073	34,876	0,000	20,973	0,046	37,980	100,027	
391 Mf	EMf391-G8-4	307	0,000	0,019	0,661	0,069	4,373	1,155	35,140	0,056	21,032	0,000	38,223	100,728	
391 Mf	EMf391-G9-1	308	0,007	0,000	0,560	0,078	8,095	2,624	27,781	0,035	21,448	0,046	38,811	99,484	
391 Mf	EMf391-G9-2	309	0,000	0,018	0,519	0,068	8,207	2,586	27,928	0,028	21,708	0,000	39,100	100,161	Garnet
391 Mf	EMf391-G9-3	310	0,000	0,000	0,520	0,000	8,226	2,562	28,003	0,139	21,609	0,098	39,107	100,263	
391 Mf	EMf391-G9-4	311	0,009	0,006	0,510	0,000	8,181	2,567	27,982	0,046	21,595	0,000	39,241	100,137	
391 Mf	EMf391-G10-1	312	0,009	0,007	3,199	0,007	1,679	2,104	34,898	0,068	20,370	0,047	36,834	99,221	
391 Mf	EMf391-G10-2	313	0,000	0,000	3,237	0,000	1,679	2,112	34,917	0,000	20,680	0,000	37,203	99,828	Garnet
391 Mf	EMf391-G10-3	314	0,019	0,000	3,262	0,000	1,649	2,357	34,782	0,000	20,688	0,031	37,253	100,041	
391 Mf	EMf391-G10-4	315	0,007	0,005	3,363	0,045	1,575	1,749	34,938	0,049	20,503	0,000	37,291	99,526	

Sample/ fraction	Grain name/ measurement number	No.	Wt%												Mineral type
			Na2O	K2O	MnO	TiO2	MgO	CaO	FeO	Cr2O3	Al2O3	V2O3	SiO2	Total	
387 Zf	CZf387-R1-1	389	0,000	0,000	0,000	100,590	0,000	0,010	0,076	0,152	0,017	2,147	0,000	102,992	Rutile
387 Zf	CZf387-R1-2	390	0,036	0,010	0,001	100,031	0,000	0,020	0,082	0,153	0,025	2,206	0,104	102,668	
387 Zf	CZf387-R1-3	391	0,000	0,000	0,000	100,543	0,000	0,029	0,052	0,102	0,040	2,046	0,000	102,813	
387 Zf	CZf387-T1-1	392	0,000	0,000	0,028	39,987	0,000	28,731	0,320	0,000	0,912	0,872	30,364	101,214	Titanite
387 Zf	CZf387-T1-2	393	0,000	0,013	0,003	39,608	0,000	28,666	0,380	0,000	0,840	0,847	30,271	100,627	
387 Zf	CZf387-T1-3	394	0,000	0,006	0,000	38,623	0,000	28,584	0,340	0,020	0,818	0,886	30,395	99,670	
387 Zf	CZf387-R2-1	395	0,029	0,009	0,032	99,996	0,000	0,023	0,253	0,064	0,001	2,219	0,000	102,625	Rutile
387 Zf	CZf387-R2-2	396	0,000	0,009	0,009	101,232	0,000	0,024	0,123	0,247	0,021	2,271	0,000	103,936	
387 Zf	CZf387-R2-3	397	0,000	0,017	0,038	100,850	0,000	0,021	0,226	0,058	0,053	2,138	0,025	103,424	
387 Zf	CZf387-T2-1	398	0,003	0,001	0,064	38,486	0,000	28,660	0,355	0,055	1,340	0,670	30,541	100,175	Titanite
387 Zf	CZf387-T2-2	399	0,000	0,002	0,094	38,903	0,000	28,626	0,310	0,000	1,237	0,607	30,494	100,273	
387 Zf	CZf387-T2-3	400	0,019	0,000	0,089	38,566	0,000	28,699	0,463	0,000	1,358	0,677	30,708	100,578	
387 Zf	CZf387-R3-1	401	0,000	0,018	0,002	101,616	0,000	0,020	0,220	0,000	0,060	1,881	0,000	103,817	Rutile
387 Zf	CZf387-R3-2	402	0,000	0,000	0,012	101,547	0,000	0,027	0,185	0,000	0,021	1,929	0,004	103,725	
387 Zf	CZf387-R3-3	403	0,008	0,003	0,000	101,158	0,000	0,017	0,174	0,041	0,067	1,947	0,000	103,415	
387 Zf	CZf387-T3-1	404	0,009	0,000	0,055	38,725	0,000	28,400	0,253	0,055	1,305	0,686	30,074	99,560	Titanite
387 Zf	CZf387-T3-2	405	0,000	0,008	0,005	38,553	0,000	28,352	0,257	0,000	1,331	0,719	30,233	99,458	
387 Zf	CZf387-T3-3	406	0,000	0,007	0,025	38,716	0,000	28,327	0,153	0,000	1,394	0,773	30,136	99,531	
BS Zf	CZfBS-T1-1	407	0,054	0,010	0,023	31,585	0,000	24,921	0,129	0,000	1,723	0,549	25,251	84,245	Titanite
BS Zf	CZfBS-T1-2	408	0,000	0,000	0,005	36,440	0,000	28,287	0,196	0,028	2,295	0,646	30,154	98,052	
BS Zf	CZfBS-T1-3	409	0,000	0,000	0,000	1,395	0,000	1,373	0,000	0,000	0,039	0,008	92,561	95,376	
BS Zf	CZfBS-T2-1	410	0,000	0,002	0,033	38,431	0,000	28,951	0,402	0,000	1,448	0,732	30,552	100,551	Titanite
BS Zf	CZfBS-T2-2	411	0,000	0,001	0,024	38,549	0,000	28,722	0,309	0,000	1,405	0,707	30,541	100,257	
BS Zf	CZfBS-T2-3	412	0,036	0,000	0,105	39,016	0,000	28,899	0,371	0,000	1,260	0,697	30,502	100,885	
BS Zf	CZfBS-R1-1	413	0,000	0,000	0,011	99,855	0,000	0,033	0,144	0,131	0,055	2,358	0,013	102,599	Rutile
BS Zf	CZfBS-R1-2	414	0,000	0,013	0,031	99,022	0,000	0,093	0,142	0,161	0,047	2,403	0,000	101,911	
BS Zf	CZfBS-R1-3	415	0,000	0,014	0,012	99,696	0,000	0,108	0,069	0,198	0,054	2,491	0,000	102,641	
391 Zf	CZf391-R1-1	416	0,000	0,013	0,010	102,273	0,000	0,011	0,102	0,033	0,030	2,058	0,074	104,602	Rutile
391 Zf	CZf391-R1-2	417	0,000	0,000	0,013	101,600	0,000	0,018	0,151	0,001	0,024	2,101	0,000	103,909	
391 Zf	CZf391-R1-3	418	0,020	0,008	0,000	101,267	0,000	0,011	0,101	0,062	0,073	1,971	0,000	103,513	
391 Zf	CZf391-T1-1	419	0,015	0,000	0,067	37,902	0,000	28,870	0,494	0,000	1,667	0,675	30,457	100,147	Titanite
391 Zf	CZf391-T1-2	420	0,000	0,000	0,048	38,002	0,000	28,699	0,490	0,008	1,584	0,705	30,375	99,911	
391 Zf	CZf391-T1-3	421	0,005	0,000	0,079	37,760	0,000	28,893	0,527	0,025	1,648	0,795	30,613	100,345	
391 Zf	CZf391-R2-1	422	0,000	0,001	0,017	100,382	0,000	0,012	0,011	0,167	0,025	2,351	0,119	103,086	Rutile
391 Zf	CZf391-R2-2	423	0,018	0,000	0,000	100,721	0,000	0,023	0,025	0,133	0,000	2,358	0,000	103,277	
391 Zf	CZf391-R2-3	424	0,014	0,000	0,013	100,977	0,019	0,010	0,000	0,129	0,010	2,387	0,002	103,561	
391 Zf	CZf391-R3-1	425	0,000	0,000	0,000	98,857	0,000	0,000	0,069	0,404	0,049	2,133	0,404	101,915	Rutile
391 Zf	CZf391-R3-2	426	0,024	0,007	0,015	98,335	0,000	0,073	0,043	0,444	0,048	2,138	0,000	101,126	
391 Zf	CZf391-R3-3	427	0,000	0,005	0,000	99,012	0,000	0,047	0,012	0,392	0,023	2,079	0,000	101,568	
391 Zf	CZf391-R4-1	428	0,000	0,000	0,016	100,884	0,000	0,029	0,139	0,067	0,000	2,121	0,013	103,268	Rutile
391 Zf	CZf391-R4-2	429	0,004	0,000	0,000	101,801	0,000	0,023	0,088	0,085	0,000	2,062	0,000	104,063	
391 Zf	CZf391-R4-3	430	0,039	0,017	0,036	101,161	0,000	0,021	0,163	0,113	0,058	2,091	0,000	103,698	
391 Zf	CZf391-R4-4	431	0,000	0,003	0,000	100,775	0,000	0,013	0,161	0,117	0,027	2,096	0,000	103,193	

Appendix N: Titanite, tourmaline and garnet values from EMPA

Chemical compositions of titanite, tourmaline and garnet from analyses with EMPA. Values are used for ternary plots.

Titanites identified with EMPA

Sample/ fraction	Grain name/ measurement number	No.	Wt%											
			Na2O	K2O	MnO	TiO2	MgO	CaO	FeO	Cr2O3	Al2O3	V2O3	SiO2	Total
387 Mf	AMf387-T2-1	181	0,03	0,02	0,21	35,35	0,01	25,87	1,40	0,00	1,12	0,68	29,94	94,63
387 Mf	AMf387-T3-1	217	0,00	0,01	0,00	36,62	0,00	26,55	1,24	0,00	1,30	0,71	29,39	95,82
387 Mf	AMf387-T4-1	221	0,00	0,02	0,04	42,59	0,00	25,98	1,45	0,05	0,92	0,92	27,58	99,55
BS Mf	AMf-BS-T1-1	233	0,03	0,00	0,10	38,66	0,00	27,93	0,60	0,03	1,17	0,84	30,34	99,70
BS Mf	AMf-BS-T2-1	235	0,01	0,00	0,09	38,69	0,00	28,43	0,76	0,00	1,15	0,86	30,72	100,71
BS Mf	AMf-BS-T3-1	268	0,00	0,00	0,08	38,66	0,00	28,67	0,51	0,00	1,24	0,82	30,52	100,50
391 Mf	EMf391-T1-4	209	0,00	0,00	0,02	43,17	0,00	25,53	2,60	0,05	0,73	1,00	27,84	100,94
391 Mf	EMf391-T2-1	250	0,02	0,00	0,05	42,00	0,00	26,81	1,41	0,05	0,84	0,90	28,42	100,50
391 Mf	EMf391-T3-3	256	0,00	0,02	0,04	37,41	0,00	28,12	0,73	0,00	2,82	0,76	30,03	99,93
391 Mf	EMf391-T4-1	274	0,00	0,01	0,07	36,71	0,00	28,04	1,15	0,02	1,60	0,76	30,03	98,39
391 Mf	EMf391-T5-1	295	0,03	0,00	0,00	44,12	0,00	24,55	1,81	0,00	1,20	0,93	26,85	99,49

Sample/ fraction	Grain name/ measurement number	No.	Wt%												
			Na	K	Mn	Ti	Mg	Ca	Fe	Cr	Al	V	Si	O	Total
387 Mf	AMf387-T2-1	181	0,02	0,02	0,16	21,19	0,01	18,49	1,09	0,00	0,59	0,42	13,99	44,02	100,00
387 Mf	AMf387-T3-1	217	0,00	0,01	0,00	21,95	0,00	18,98	0,96	0,00	0,69	0,44	13,74	43,24	100,00
387 Mf	AMf387-T4-1	221	0,00	0,02	0,03	25,53	0,00	18,57	1,13	0,03	0,49	0,57	12,89	40,75	100,00
BS Mf	AMf-BS-T1-1	233	0,02	0,00	0,08	23,18	0,00	19,96	0,47	0,02	0,62	0,52	14,18	40,96	100,00
BS Mf	AMf-BS-T2-1	235	0,01	0,00	0,07	23,20	0,00	20,32	0,59	0,00	0,61	0,53	14,36	40,32	100,00
BS Mf	AMf-BS-T3-1	268	0,00	0,00	0,06	23,18	0,00	20,49	0,40	0,00	0,66	0,50	14,27	40,45	100,00
391 Mf	EMf391-T1-4	209	0,00	0,00	0,02	25,88	0,00	18,25	2,02	0,03	0,39	0,61	13,01	39,79	100,00
391 Mf	EMf391-T2-1	250	0,01	0,00	0,04	25,18	0,00	19,16	1,10	0,03	0,44	0,55	13,28	40,19	100,00
391 Mf	EMf391-T3-3	254	0,00	0,01	0,03	22,43	0,00	20,10	0,57	0,00	1,49	0,46	14,04	40,87	100,00
391 Mf	EMf391-T4-1	274	0,00	0,01	0,05	22,01	0,00	20,04	0,89	0,01	0,85	0,47	14,04	41,63	100,00
391 Mf	EMf391-T5-1	295	0,02	0,00	0,00	26,45	0,00	17,55	1,41	0,00	0,64	0,57	12,55	40,82	100,00

Numbers for the ternary plot

Al	Fe	Ti
2,5914525	4,757524906	92,6510226
2,9146274	4,083092127	93,0022805
1,7935969	4,151765473	94,0546377
2,5521626	1,922213052	95,5256244
2,4949858	2,42165143	95,0833628
2,7085298	1,636100276	95,6553699
1,3657737	7,144256213	91,4899701
1,6638109	4,101772819	94,2344162
6,1007105	2,323081634	91,5762079
3,5656678	3,763973324	92,6703589
2,2290159	4,937854608	92,8331295

Tourmalines identified with EMPA

Sample/ fraction	Grain name/ measurement number	No.	Wt%												
			Na2O	K2O	MnO	TiO2	MgO	CaO	FeO	Cr2O3	Al2O3	V2O3	SiO2	B2O3	Total
BS Mf	AMf-BS-Tu1-1	249	2,18	0,03	0,01	0,52	7,77	0,98	6,85	0,00	29,29	0,03	36,24	10,50	94,43
BS Mf	AMf-BS-Tu1-2	250	2,15	0,05	0,00	0,52	7,80	1,05	6,84	0,02	29,41	0,00	36,25	10,50	94,58
BS Mf	AMf-BS-Tu1-3	251	2,22	0,05	0,05	0,53	7,88	1,00	6,84	0,05	29,38	0,01	36,22	10,50	94,73
BS Mf	AMf-BS-Tu1-4	252	2,23	0,02	0,03	0,52	7,78	0,97	6,92	0,11	29,16	0,08	36,10	10,50	94,43
BS Mf	AMf-BS-Tu2-1	256	1,86	0,03	0,00	0,87	7,05	0,78	5,09	0,12	30,94	0,13	36,23	10,50	93,60
BS Mf	AMf-BS-Tu2-2	257	1,84	0,01	0,00	0,93	7,04	0,78	4,99	0,14	31,39	0,11	35,98	10,50	93,72
BS Mf	AMf-BS-Tu2-3	258	1,82	0,03	0,02	0,80	7,13	0,79	5,23	0,12	31,36	0,09	36,22	10,50	94,11
BS Mf	AMf-BS-Tu2-4	259	1,85	0,02	0,02	0,81	7,15	0,78	5,06	0,02	31,58	0,10	36,61	10,50	94,49
BS Mf	AMf-BS-Tu3-1	262	1,94	0,04	0,10	0,39	3,03	0,34	12,49	0,02	30,53	0,00	35,37	10,50	94,76
BS Mf	AMf-BS-Tu3-2	263	2,08	0,06	0,14	0,57	3,11	0,47	12,77	0,00	30,18	0,02	35,17	10,50	95,07
BS Mf	AMf-BS-Tu3-3	264	2,12	0,05	0,14	0,14	3,59	0,47	12,21	0,01	30,32	0,00	35,07	10,50	94,61

Sample/ fraction	Grain name/ measurement number	No.	Wt%													
			Na	K	Mn	Ti	Mg	Ca	Fe	Cr	Al	V	Si	B	O	Total
BS Mf	AMf-BS-Tu1-1	249	1,62	0,03	0,01	0,31	4,69	0,70	5,33	0,00	15,51	0,02	16,94	3,26	51,58	100,00
BS Mf	AMf-BS-Tu1-2	250	1,59	0,04	0,00	0,31	4,71	0,75	5,31	0,02	15,57	0,00	16,94	3,26	51,50	100,00
BS Mf	AMf-BS-Tu1-3	251	1,65	0,04	0,04	0,32	4,75	0,72	5,32	0,04	15,55	0,01	16,93	3,26	51,38	100,00
BS Mf	AMf-BS-Tu1-4	252	1,66	0,02	0,02	0,31	4,69	0,69	5,38	0,08	15,43	0,05	16,87	3,26	51,52	100,00
BS Mf	AMf-BS-Tu2-1	256	1,38	0,02	0,00	0,52	4,25	0,56	3,96	0,08	16,37	0,08	16,93	3,26	52,57	100,00
BS Mf	AMf-BS-Tu2-2	257	1,37	0,01	0,00	0,56	4,24	0,56	3,88	0,10	16,62	0,07	16,82	3,26	52,52	100,00
BS Mf	AMf-BS-Tu2-3	258	1,35	0,02	0,02	0,48	4,30	0,57	4,07	0,08	16,60	0,05	16,93	3,26	52,27	100,00
BS Mf	AMf-BS-Tu2-4	259	1,37	0,02	0,01	0,48	4,31	0,56	3,93	0,01	16,72	0,06	17,11	3,26	52,15	100,00
BS Mf	AMf-BS-Tu3-1	262	1,44	0,03	0,08	0,24	1,83	0,24	9,70	0,01	16,16	0,00	16,53	3,26	50,46	100,00
BS Mf	AMf-BS-Tu3-2	263	1,54	0,05	0,11	0,34	1,87	0,33	9,93	0,00	15,97	0,01	16,44	3,26	50,13	100,00
BS Mf	AMf-BS-Tu3-3	264	1,57	0,04	0,11	0,08	2,16	0,34	9,49	0,01	16,05	0,00	16,39	3,26	50,50	100,00

Numbers for the ternary plot

Al	Al50Mg50	Al50Fe50
43,05	28,03	28,92
43,07	28,04	28,89
43,03	28,09	28,88
42,98	28,03	28,99
44,43	27,99	27,59
44,55	27,97	27,48
44,40	27,96	27,64
44,51	27,99	27,49
42,43	23,62	33,95
42,20	23,58	34,22
42,32	24,01	33,67

Sample/ fraction	Grain name/ measurement number	No.	Wt%													
			Na	K	Mn	Ti	Mg	Ca	Fe	Cr	Al	V	Si	B	O	Total
BS Mf	AMf-BS-Tu1-1	249	1,62	0,03	0,01	0,31	4,69	0,70	5,33	0,00	15,51	0,02	16,94	3,26	51,58	100,00
BS Mf	AMf-BS-Tu1-2	250	1,59	0,04	0,00	0,31	4,71	0,75	5,31	0,02	15,57	0,00	16,94	3,26	51,50	100,00
BS Mf	AMf-BS-Tu1-3	251	1,65	0,04	0,04	0,32	4,75	0,72	5,32	0,04	15,55	0,01	16,93	3,26	51,38	100,00
BS Mf	AMf-BS-Tu1-4	252	1,66	0,02	0,02	0,31	4,69	0,69	5,38	0,08	15,43	0,05	16,87	3,26	51,52	100,00
BS Mf	AMf-BS-Tu2-1	256	1,38	0,02	0,00	0,52	4,25	0,56	3,96	0,08	16,37	0,08	16,93	3,26	52,57	100,00
BS Mf	AMf-BS-Tu2-2	257	1,37	0,01	0,00	0,56	4,24	0,56	3,88	0,10	16,62	0,07	16,82	3,26	52,52	100,00
BS Mf	AMf-BS-Tu2-3	258	1,35	0,02	0,02	0,48	4,30	0,57	4,07	0,08	16,60	0,05	16,93	3,26	52,27	100,00
BS Mf	AMf-BS-Tu2-4	259	1,37	0,02	0,01	0,48	4,31	0,56	3,93	0,01	16,72	0,06	17,11	3,26	52,15	100,00
BS Mf	AMf-BS-Tu3-1	262	1,44	0,03	0,08	0,24	1,83	0,24	9,70	0,01	16,16	0,00	16,53	3,26	50,46	100,00
BS Mf	AMf-BS-Tu3-2	263	1,54	0,05	0,11	0,34	1,87	0,33	9,93	0,00	15,97	0,01	16,44	3,26	50,13	100,00
BS Mf	AMf-BS-Tu3-3	264	1,57	0,04	0,11	0,08	2,16	0,34	9,49	0,01	16,05	0,00	16,39	3,26	50,50	100,00

Numbers for the ternary plot

Ca	Mg	Fe
6,58	43,74	49,68
7,00	43,68	49,32
6,65	44,04	49,30
6,45	43,58	49,97
6,37	48,50	45,13
6,44	48,87	44,68
6,38	48,13	45,49
6,36	48,96	44,68
2,06	15,54	82,40
2,76	15,44	81,80
2,80	18,05	79,15

Garnets identified with EMPA

Sample/ fraction	Grain name/ measurement number	No.	Wt%											
			Na2O	K2O	MnO	TiO2	MgO	CaO	FeO	Cr2O3	Al2O3	V2O3	SiO2	Total
387 Mf	AMf387-G2-1	189	0,00	0,00	0,21	0,01	8,86	0,96	29,75	0,04	21,00	0,02	38,73	99,59
387 Mf	AMf387-G3-1	193	0,00	0,00	1,13	0,11	7,06	5,80	26,37	0,03	20,02	0,04	38,65	99,21
387 Mf	AMf387-G4-1	201	0,03	0,00	0,68	0,04	7,03	2,46	29,25	0,00	20,48	0,01	38,68	98,66
387 Mf	AMf387-G4-1	213	0,00	0,01	0,27	0,13	0,00	22,84	11,38	0,00	21,67	0,07	38,07	94,44
BS Mf	AMf-BS-G2-1	238	0,02	0,00	0,23	0,07	0,08	23,20	10,65	0,00	23,04	0,09	38,01	95,39
BS Mf	AMf-BS-G3-1	241	0,00	0,00	0,09	0,07	0,05	23,28	11,08	0,00	22,32	0,00	38,11	94,99
BS Mf	AMf-BS-G4-1	245	0,02	0,01	0,25	0,08	8,04	1,09	30,88	0,02	20,49	0,03	38,82	99,72
BS Mf	AMf-BS-G5-1	253	0,00	0,00	0,13	0,08	9,15	1,06	29,16	0,01	20,90	0,05	39,49	100,02
BS Mf	AMf-BS-G6-1	260	0,00	0,02	0,32	0,08	0,03	22,67	10,04	0,05	22,99	0,06	38,14	94,38
BS Mf	AMf-BS-G7-1	265	0,00	0,01	0,04	0,17	0,07	23,30	8,38	0,00	24,86	0,00	38,49	95,34
391 Mf	EMf391-A1-2	211	0,12	0,00	3,64	0,08	2,64	8,44	25,53	0,00	20,51	0,05	38,01	99,01
391 Mf	EMf391-G2-2	219	0,02	0,01	0,42	0,02	7,81	1,60	29,68	0,00	21,37	0,00	38,58	99,51
391 Mf	EMf391-G3-2	229	0,01	0,00	1,60	0,00	5,26	3,14	29,81	0,09	20,83	0,02	38,14	98,92
391 Mf	EMf391-G4-1	245	0,00	0,00	0,14	0,00	8,69	0,72	30,17	0,00	21,37	0,03	38,82	99,95
391 Mf	EMf391-G5-1	258	0,00	0,01	0,07	0,13	0,03	23,00	9,29	0,00	24,43	0,01	38,05	95,02
391 Mf	EMf391-G6-1	278	0,05	0,00	0,35	0,00	6,90	1,35	31,02	0,02	21,36	0,03	38,05	99,14
391 Mf	EMf391-G7-1	291	0,01	0,00	0,55	0,07	8,44	6,94	22,91	0,10	21,25	0,02	39,05	99,34
391 Mf	EMf391-G8-1	304	0,01	0,01	0,65	0,05	4,43	1,06	34,73	0,04	20,88	0,04	37,59	99,48
391 Mf	EMf391-G9-1	308	0,01	0,00	0,56	0,08	8,09	2,62	27,78	0,04	21,45	0,05	38,81	99,48
391 Mf	EMf391-G10-1	312	0,01	0,01	3,20	0,01	1,68	2,10	34,90	0,07	20,37	0,05	36,83	99,22

Sample/ fraction	Grain name/ measurement number	No.	Wt%												
			Na	K	Mn	Ti	Mg	Ca	Fe	Cr	Al	V	Si	O	Total
387 Mf	AMf387-G2-1	189	0,00	0,00	0,16	0,01	5,35	0,69	23,13	0,03	11,11	0,01	18,10	41,41	100,00
387 Mf	AMf387-G3-1	193	0,00	0,00	0,87	0,07	4,26	4,14	20,50	0,02	10,59	0,03	18,06	41,46	100,00
387 Mf	AMf387-G4-1	201	0,02	0,00	0,53	0,02	4,24	1,76	22,73	0,00	10,84	0,01	18,08	41,77	100,00
387 Mf	AMf387-G4-1	213	0,00	0,01	0,21	0,08	0,00	16,32	8,84	0,00	11,47	0,04	17,79	45,23	100,00
BS Mf	AMf-BS-G2-1	238	0,01	0,00	0,18	0,04	0,05	16,58	8,28	0,00	12,19	0,05	17,77	44,84	100,00
BS Mf	AMf-BS-G3-1	241	0,00	0,00	0,07	0,04	0,03	16,64	8,61	0,00	11,81	0,00	17,81	44,99	100,00
BS Mf	AMf-BS-G4-1	245	0,01	0,01	0,19	0,05	4,85	0,78	24,00	0,01	10,84	0,02	18,14	41,09	100,00
BS Mf	AMf-BS-G5-1	253	0,00	0,00	0,10	0,05	5,52	0,76	22,67	0,01	11,06	0,03	18,46	41,36	100,00
BS Mf	AMf-BS-G6-1	260	0,00	0,02	0,24	0,05	0,02	16,20	7,80	0,03	12,17	0,04	17,83	45,61	100,00
BS Mf	AMf-BS-G7-1	265	0,00	0,01	0,03	0,10	0,04	16,65	6,52	0,00	13,16	0,00	17,99	45,49	100,00
391 Mf	EMf391-A1-2	211	0,09	0,00	2,82	0,05	1,59	6,03	19,84	0,00	10,85	0,03	17,77	40,93	100,00
391 Mf	EMf391-G2-2	219	0,01	0,01	0,32	0,01	4,71	1,14	23,07	0,00	11,31	0,00	18,03	41,38	100,00
391 Mf	EMf391-G3-2	229	0,01	0,00	1,24	0,00	3,17	2,25	23,17	0,06	11,02	0,01	17,83	41,23	100,00
391 Mf	EMf391-G4-1	245	0,00	0,00	0,11	0,00	5,24	0,52	23,45	0,00	11,31	0,02	18,14	41,21	100,00
391 Mf	EMf391-G5-1	258	0,00	0,00	0,06	0,08	0,02	16,44	7,22	0,00	12,93	0,01	17,79	45,46	100,00
391 Mf	EMf391-G6-1	278	0,04	0,00	0,27	0,00	4,16	0,97	24,11	0,02	11,31	0,02	17,78	41,32	100,00
391 Mf	EMf391-G7-1	291	0,01	0,00	0,43	0,04	5,09	4,96	17,81	0,07	11,25	0,01	18,25	42,09	100,00
391 Mf	EMf391-G8-1	304	0,01	0,00	0,51	0,03	2,67	0,75	26,99	0,03	11,05	0,02	17,57	40,36	100,00
391 Mf	EMf391-G9-1	308	0,01	0,00	0,43	0,05	4,88	1,88	21,59	0,02	11,35	0,03	18,14	41,62	100,00
391 Mf	EMf391-G10-1	312	0,01	0,01	2,48	0,00	1,01	1,50	27,13	0,05	10,78	0,03	17,22	39,79	100,00

Numbers for the ternary plot

Mg	Ca	Fe+Mn
18,23	2,34	79,43
14,30	13,91	71,79
14,49	6,00	79,50
0,00	64,32	35,68
0,20	66,10	33,71
0,11	65,65	34,24
16,26	2,62	81,12
19,00	2,60	78,40
0,06	66,76	33,17
0,18	71,65	28,16
5,25	19,93	74,82
16,11	3,90	79,99
10,64	7,53	81,83
17,87	1,76	80,37
0,09	69,26	30,66
14,10	3,27	82,63
17,99	17,54	64,47
8,64	2,44	88,92
16,96	6,51	76,53
3,15	4,68	92,17